# Site U1383[1]

Expedition 336 Scientists[2]

## Chapter contents



## Site summary

Integrated Ocean Drilling Program (IODP) Expedition 336 Site U1383 (prospectus Site NP-2) is located 5.9 km northeast of IODP Site U1382 in an area of elevated conductive heat flow in 4414 m water depth. The primary objective at Site U1383 was to install a multilevel subseafloor borehole observatory (CORK) for long-term coupled microbiological, biogeochemical, and hydrological experiments in uppermost basaltic crust. Basement coring, downhole logging, and hydrologic experiments were also planned.

Hole U1383B (22°48.1328′N, 46°03.1556′W) was prepared for drilling 500 m into basement by installing a reentry cone with 20 inch casing extending to 35 meters below seafloor (mbsf). We then prepared the hole for 16 inch casing by drilling an 18½ inch hole to 68 mbsf; the sediment/basement interface is at 53 mbsf. After installing and cementing the 16 inch casing to 54 mbsf, we started to prepare the hole for 10¾ inch casing by drilling a hole into basement with a 14¾ inch tricone bit. We decided to abandon Hole U1383B after this tricone bit failed at 89.8 mbsf, resulting in large parts of the bit being left in the hole. Although we did not choose to deepen this hole, it remains a viable CORK hole because it has a completely functional reentry cone and casing system with ~35 m of accessible basement. A remotely operated vehicle (ROV) landing platform was therefore installed in the reentry cone to facilitate future ROV operations, which will include installation of an instrumented plug in Hole U1383B.

Hole U1383C (22°48.1241′N, 46°03.1662′W) was started at the site of the original jet-in test, 25 m southwest of Hole U1383B. The primary objective was installing a multilevel CORK in the uppermost ~300 m of basement. The ultimate configuration of the CORK in Hole U1383C was to be determined by the depth of basement penetration and the downhole logging results. A reentry cone with 16 inch casing was installed to 34.8 mbsf, and a 14¾ inch hole was drilled to 69.5 mbsf for the 10¾ inch casing string. The sediment/basement interface was encountered at 38.3 mbsf. After cementing the 10¾ inch casing at 60.4 mbsf, drilling in Hole U1383C proceeded with a rotary core barrel (RCB) bit from 69.5 to 331.5 mbsf. From this 262 m long interval, 50.3 m of core was recovered (19.2%). Rocks are glassy to fine-grained basalts with variable phenocryst (plagioclase and olivine) contents. Three major lithologic units were distinguished on the basis of primary texture and phenocryst abundance. From 69.5 to 127 mbsf, the core consists of microcrystalline to fine-grained,

[1] Expedition 336 Scientists, 2012. Site U1383. *In* Edwards, K.J., Bach, W., Klaus, A., and the Expedition 336 Scientists, *Proc. IODP,* 336: Tokyo (Integrated Ocean Drilling Program Management International, Inc.). doi:10.2204/iodp.proc.336.105.2012
[2] **Expedition 336 Scientists' addresses.**


doi:10.2204/iodp.proc.336.105.2012

sparsely plagioclase-phyric basalt with abundant glassy margins and numerous intervals of hard interflow limestone. From 127 to 164 mbsf, massive plagioclase-olivine-phyric basalts occur, occasionally hosting limestone (with and without basalt clasts) as fracture fill. Below 164 mbsf, glassy to variolitic to cryptocrystalline basalts (most likely pillow flows) predominate, and limestone is largely missing. Each of these three main lithologic units is divided into numerous subunits on the basis of hyaloclastite layers and rare tectonic breccias. The overall abundance of glass is noticeably greater than that in Hole U1382A, and the extent of palagonitization ranges from weak to moderate. Basalts are avesicular to sparsely vesicular and show vesicle fills of clay, zeolite (mainly phillipsite), calcium carbonate, and Fe oxyhydroxide. Brownish alteration halos commonly track veins filled with clay or carbonate and zeolite. Within Unit 3, a gradational change from glassy, to variolitic with abundant hyaloclastite layers, to more massive microcrystalline, to fine-grained basalt with rare glassy margins can be observed.

Although the hyaloclastites are noticeably palagonitized throughout the hole, the extent of background alteration appears to decrease downsection. Vein densities average 33 veins/m and increase somewhat downsection to 50 veins/m. Zeolite veins are abundant in the upper section of the drilled interval, whereas carbonate veins predominate in the lowermost part. Sparse vesicles are filled with zeolite and clay.

Physical properties measurements reveal tight correlations between sonic velocity, density, and porosity of the basalt. These correlations reflect changes in physical properties as a result of low-temperature alteration. In basalts with up to 40% alteration, *P*-wave velocities and bulk densities as low as 4750 m/s and 2.43 g/cm$^3$ were recorded. These most altered basalts also show exceptionally high porosities (up to 16.6%). Despite the locally high alteration intensity, natural gamma radiation (NGR) core scanning revealed fairly low average potassium and uranium concentrations (e.g., 0.19 ± 0.05 wt% K). Fresh basalts show physical properties and K concentrations typical for mid-ocean-ridge basalt.

Whole-rock geochemical data show that basalts from Units 1 and 2 systematically differ in Zr/Y and Zr/Ti ratios from basalts from Unit 3. The compositional variability in the different units is primarily due to fractionation of olivine, but some trends (gain of K, loss of Mg) are also related to increased alteration intensity. The porphyritic basalts do not show the distinct plagioclase accumulation signature revealed in similar basalts from Hole U1382A and Deep Sea Drilling Project (DSDP) Hole 395A. Correlations between Site U1383 and Sites U1382 and 395 based on geochemical composition cannot be made for individual flow units, indicating that the sites belong to different volcanic centers that were fed by mantle sources with variable compositions.

Hard rock samples for microbiological analysis were collected from every RCB core from Hole U1383C. Roughly 12% (6.11 m total) of core recovered from Hole U1383C was taken as whole-round samples from the core splitting room and dedicated to microbiological analysis. The 79 hard rock microbiology samples span a range of lithologic units, alteration states, and presence of chilled margins, and some contain at least one vein or fracture. Additionally, a few background contamination samples were collected for shore-based DNA analysis, including recovered plastic bags that held the fluorescent microsphere solutions in the core catcher.

Samples recovered were preserved for shore-based DNA and RNA analysis, shore-based fluorescence in situ hybridization (FISH) and cell counting, ship-based culturing and enrichments, shore-based isotopic analysis, and ship-based fluorescent microsphere analysis. Microspheres were used during all coring operations to help in evaluating core contamination. The enrichment and cultivation experiments initiated include carbon fixation incubations; carbon and nitrogen cycling experiments; enrichments for methanogens, sulfate reducers, sulfide oxidizers, and nitrate-reducing iron-oxidizing bacteria; and enrichments for heterotrophic metabolisms. Deep ultraviolet (UV) (<250 nm) scanning of hard rock materials was used to identify sample regions with concentrations of biomass and organic material.

Wireline logging data include natural total and spectral gamma radiation, density, compressional velocity, electrical images, and deep UV–induced fluorescence (acquired with the new Deep Exploration Biosphere Investigative tool [DEBI-t]) of a 274.5 m section of open hole. Lithologic Unit 1 is characterized by variable caliper, density, and sonic velocity values. Gamma ray intensities are generally low but increase in the bottom part of the unit. Lithologic Unit 2 has a uniform caliper and high densities and apparent sonic velocities and shows high-resistivity massive flows with fractures in the Formation MicroScanner (FMS) images. The upper section of lithologic Unit 3 (153–166 mbsf) is characterized by decreases in density, apparent resistivity, and velocity and an increase in gamma ray intensity. This interval corresponds to thin flows with interpillow/flow sediments and tectonic breccia. From 166 mbsf to the bottom of the hole, the logging data reveal fairly uniform values for density, velocity, and apparent resistivity. Areas with peaks in gamma ray intensity correspond to intervals

with abundant hyaloclastite in the recovered core (in particular around 175 mbsf and from 220 to 250 mbsf).

Drill string packer experiments were attempted in Hole U1383C to assess the transmissivity and average permeability of open-hole zones bounded by the bottom of the hole at 331.5 mbsf and three different packer inflation seats at 53, 141, and 197 mbsf. The packer experiments were not successful.

In preparation for the CORK observatory, Hole U1383C was cased through the 38.3 m thick sediment section with 10¾ inch casing to 60.4 mbsf and through a 14¾ inch rathole to 69.5 mbsf. After the hole was RCB cored to 331.5 mbsf and cleaned in five wiper trips, there was no noticeable fill, which was verified during logging. The CORK screens and downhole instrument string targeted three zones, selected mainly on the basis of recovered core and the caliper log. An upper zone extends from the combination packer and landing seat at 58.4 mbsf in the casing to the first open-hole packer and landing seat at 145.7 mbsf. Within this section the miniscreens are centered at 100 mbsf, with the slotted portion of the casing extending from 76 to 129 mbsf. The middle zone extends to an open-hole packer and landing seat at 199.9 mbsf. Within this section the screens are centered at 162 mbsf, with the slotted casing extending from 146 to 181 mbsf. The deep zone reaches to the bottom of the hole (331.5 mbsf) with miniscreens centered at 203 mbsf. The miniscreens are connected to the wellhead by five umbilicals with stainless steel or Tefzel internal tubing that are strapped to the outside of the casing. The downhole tool string consists of six different OsmoSampler packages, two dissolved oxygen sensors and recorders (one in the shallow zone and one in the middle zone), two miniature temperature recorders, sinker bars, sealing plugs, and interspersed sections of ⅜ inch (0.95 cm) Spectra line. The wellhead is instrumented with a pressure logger monitoring each of the three horizons and bottom seawater and a fast-flow OsmoSampler with both standard and microbiological sampling packages. The CORK extends to 247.6 mbsf, yet leaves the bottom portion of the hole open for future logging and access (247.6–331.5 mbsf).

## Operations

Our objective at Site U1383 was to install a multilevel CORK to perform long-term coupled microbiological, biogeochemical, and hydrological experiments in deeper portions of the oceanic crust. The operational tasks conducted at Site U1383 are given in Table **T1.** A summary of each of the three holes occupied at Site U1383 is presented in Table **T2.** Our first step was to use an 18½ inch tricone drill bit to perform a jet-in test to determine the length of 20 inch casing to install with the reentry cone. While we assembled this bottom-hole assembly (BHA) and lowered to the seafloor, we retrieved the seafloor beacon used for Hole 395A and transited ~5.8 km to Site U1383 in dynamic positioning mode. After arriving at Site U1383, we dropped a positioning beacon at 1812 h on 12 October 2011 (all times are local ship time, Universal Time Coordinated [UTC] – 3 h). The jet-in test in Hole U1383A began at 2240 h on 12 October and reached 36 mbsf at 0200 h on 13 October. The penetration rate during the last 2 m was very slow. The 18½ inch bit was back on board at 0930 h, ending Hole U1383A.

On the basis of the jet-in test, we deployed 34.84 m of 20 inch casing for Hole U1383B. The casing and reentry cone were run to the bottom, but our initial attempt jetted in the casing to only 29 mbsf. After trying to advance the casing for over 3 h with no progress, we pulled the string out of the seafloor and moved 50 m to the northeast. Our second attempt to start Hole U1383B began at 0810 h on 14 October. This time, we were able to fully land the reentry system and casing at 1015 h. We released the running tool at 1035 h and retrieved the drill string, with the bit arriving on the rig floor at 1915 h.

Our next job was to drill an 18½ inch hole into uppermost basement for the 16 inch casing. After both drill collar pup joints and the casing running tool were laid out, the 18½ inch bit was removed, the nozzles were changed, and the BHA was made up and run back to the bottom. During the trip into the hole we had to pause to slip and cut 115 ft of drill line and to start lowering the camera system for reentry. We reentered Hole U1383B at 0518 h on 15 October, began drilling at 0704 h, and encountered basement at 0723 h at 53 mbsf. Drilling continued to 68 mbsf at a penetration rate of ~2 m/h. We drilled to this depth to allow ~9 m of rathole for the 16 inch casing. Once 68 mbsf was reached, the hole was reamed and conditioned and the bit was retrieved.

After the bit was back on the rig floor at 0450 h on 16 October, the casing running tool was picked up and made up to the BHA and set back in the derrick. A total of 58.82 m of 16 inch casing, including the casing hanger, was assembled. The running tool was made up to the casing, and the casing was then run to the bottom, pausing only to deploy the camera system. Hole U1383B was reentered at 1524 h after ~20 min of maneuvering. The casing was then lowered into the open hole until the casing shoe contacted the sediment/basement interface. The casing shoe would not pass the interface after 1 h of attempts, even with rotation. The ship was offset, and repeated attempts were made until the shoe passed

the basement contact. Unfortunately, the casing was unable to advance enough to successfully land the casing hanger in the reentry cone. The final position of the casing shoe was ~3 m short of landing. The 16 inch casing was retrieved at 1945 h on 16 October, arriving back on the rig floor at 0315 h on 17 October. The top two joints of casing were removed, and the length of the casing shoe joint was shortened by 5 m. A new casing shoe was welded onto the shoe joint, and at 0800 h the casing was lowered back into the hole. The running tool was reattached, and the casing was once again run back to the bottom. The camera system was installed 70 stands into the trip to the bottom. At 1537 h, Hole U1383B was reentered with the 16 inch casing for the second time. The casing was successfully landed at 1630 h and cemented into place with 20 bbl of cement with lost-circulation material (LCM; Cello-Flake). The casing running tool was released at 1745 h, and the drill string was circulated out to remove any excess cement from the string. At 1845 h on 17 October, the drill string was pulled back to the surface, stopping only so that the camera system could be removed. The running tool cleared the rotary table at 0130 h on 18 October and then was detorqued and laid out.

The next stage of operations was to drill ~100 m of basement to install 10¾ inch casing. A new 14¾ inch bit was made up to the BHA, and the drill string was tripped to the bottom. At 90 stands into the trip, the camera system was installed and run to the bottom behind the bit. The trip was suspended just above the seafloor to slip and cut 115 ft of drilling line from the drawworks winch. Hole U1383B was reentered at 1210 h on 18 October after 15 min of maneuvering. The bit was tripped to near the bottom, the top drive was picked up, and cement was tagged at 49 mbsf (5 m above the casing shoe). After 45 min of drilling, the bit reached the bottom of the cement at 57 mbsf (3 m below the casing shoe). From 1500 h on 18 October through 0515 h on 19 October, drilling proceeded to 89.8 mbsf. At this depth, torque increased, revolutions per minute became erratic, and penetration rates dropped to zero. A wiper trip was performed from 89.8 mbsf to the 16 inch casing shoe at 54 mbsf and back to the bottom. Attempts to resume drilling were unsuccessful. At 1000 h, we decided to pull the bit and inspect it at the surface. The top drive was set back, and the drill string was pulled from the hole. The bit cleared the rotary table at 1750 h on 19 October. Inspection of the bit revealed that two of the three rotary cones and both shanks, including bearings and nozzles, had broken off the body of the bit. Only one cone remained on the bit, and it too had all the inserts broken off. After discussions with all of the operations staff on board, we decided that we would have a greater chance of achieving the expedition objectives by starting a new hole rather than trying to salvage Hole U1383B. The final configuration of reentry cone, casing, and hole depth is shown in Figure **F1.** Subsequently, we deployed a ROV platform on top of the reentry cone (see below).

At 1830 h, construction began on a reentry cone for Hole U1383C. Because of several factors, we decided to start the new reentry system with 16 inch casing jetted in to 34.58 mbsf at the same location as the original jet-in test in Hole U1383A. Assembly of the Hole U1383C reentry cone was completed at 0630 h on 20 October. The reentry cone was moved to the moonpool and positioned on the moonpool doors, and then 35 m of 16 inch casing was picked up, landed, and latched into the reentry cone. The running tool was then released, and the stand was set back in the derrick. The stand with the 14¾ inch drill bit was then picked up, followed by another 5 m of 8¼ inch drill collar pup joints to space the bit out to the 16 inch casing shoe. The drill collar stand with the casing running tool was picked up and made up to the BHA and lowered and latched into the 16 inch casing hanger. The remainder of the BHA was assembled, and the reentry system and casing were lowered to just above the seafloor, stopping every 30 stands to fill the drill string. The camera system was installed 90 stands in and run to just above the reentry system. Hole U1383C was spudded at 1900 h on 20 October. The reentry system was jetted in ~35 m, and the casing running tool was released at 2130 h. The camera system and drill string were then pulled back to the surface, and the 14¾ inch bit cleared the rotary table at 0545 h on 21 October. After the nozzles on the bit were changed, the drilling BHA was assembled and run back to the bottom. The camera system was installed at Stand 70 and run to the bottom, following the bit to the seafloor. At 1130 h, the vessel began maneuvering, and Hole U1383C was reentered at 1444 h. After the top drive was picked up, drilling began at 1635 h on 21 October. Contact was made with basement at 38.3 mbsf, just 3.6 m below the 16 inch casing shoe, after only 10 min of drilling. Basement drilling continued with slow penetration rates (0.5–2.5 m/h), reaching a total depth of 69.5 mbsf at 1840 h on 22 October.

We assembled 60.41 m of 10¾ inch casing with a swellable packer just below the casing hanger and lowered it to just above the seafloor, pausing about halfway to deploy the camera system. After ~30 min of maneuvering, we reentered Hole U1383C at 1626 h on 23 October. The casing string was landed at 1720 h, and we confirmed it was latched in with a 20,000 lb overpull. The casing was secured in place by pumping 25 bbl of cement with LCM (Cello-Flake). The casing running tool was released at

1940 h, the drill string was flushed clear of any remaining cement, and we started pulling out of the hole. With the casing running tool at 2336 meters below rig floor (mbrf), the trip was halted so we could slip and cut 115 ft of drill line. We also spent 2 h replacing a spool valve and repairing a hydraulic line on the 5 inch pipe racker. We then continued retrieving the casing running tool, which was back on board at 0825 h on 24 October.

We assembled a RCB bit and BHA, verified the core barrel space out, and lowered it to the seafloor. About halfway down, we paused to deploy the camera system. This reentry took us only ~10 min of maneuvering. After we retrieved the camera system, installed the top drive, and spaced out for drilling, we tagged the top of the cement at 43.8 mbsf (~16.6 m above the casing shoe). Once we drilled out the cement and cleaned out the rathole, we recovered the center bit. We dropped an RCB core barrel and started coring at 0000 h on 25 October. A summary of the cores recovered in Hole U1383C is presented in Table **T2.** We cut Cores 336-U1383C-2R through 18R from 69.5 to 211.6 mbsf. After Core 15R had been cut, we performed a wiper trip back up to the casing shoe and encountered 20 m of fill while getting back to the bottom of the hole. Hole cleaning remained a priority, with mud sweeps being performed on average twice during each cored interval. A total of 142.1 m was cored, and 28.55 m was recovered (20%). Just as Core 18R began to be cut (with 45.8 h on the bit), the vessel began experiencing high heave. This heave made it almost impossible to keep sufficient weight on the bit to keep it on the bottom, so we circulated cuttings out of the hole with a final mud sweep and pulled the bit out of the hole. The RCB bit was back on board at 1720 h on 28 October. It was fortunate that we did not continue coring with this bit because it had experienced bearing failures on all four roller cones.

We conducted routine rig maintenance while we assembled a new C-7 RCB bit and inspected the float valve and support bearing assemblies. This maintenance identified a faulty air cylinder for the locking pin on the motion compensator that had to be repaired, which resulted in 9.25 h of rig downtime. During the repair, we assembled the previous BHA and added three more drill collars. We installed a center bit so that the float valve would remain open during the trip, allowing the drill string to fill with seawater. At 0630 on 29 October, we started tripping the BHA to the seafloor. The reentry cone was visible as soon as the camera system reached the seafloor, and the bit was almost directly over the cone. We reentered Hole U1383C in several minutes at 1231 h on 29 October. We retrieved the camera system and the center bit and lowered the bit to the bottom of the hole to check for tight spots and to circulate out any fill at the bottom before changing bits.

We assembled a second RCB bit to continue coring in Hole U1383C. After the bit was lowered to the bottom of the hole, it was circulated clean. An RCB core barrel was dropped, and coring resumed with Core 336-U1383C-19R. We decided to core with drilling knobbies because of high vessel motion and operating in deep water. RCB coring continued through Core 336-U1383C-23R, at which point we made a short wiper trip to both clean a short section of hole and to replace three drilling knobbies with a stand of 5½ inch drill pipe. Once the bit was back on the bottom, we circulated a mud sweep and resumed coring. Two 20 bbl sweeps were pumped on every core to keep the hole clean. We decided to stop RCB coring at 4756.7 mbrf (331.5 mbsf) because of accumulating bit hours, minimal time left in the expedition, and because a sufficient depth was reached to achieve the CORK objectives. Thirty-one cores recovered 50.31 m of rocks from a 262.0 m interval. Overall recovery was 19%, varying from 8% to a maximum of 43%.

We conducted three wiper trips to prepare the hole for downhole logging, packer experiments, and CORK installation. At 1400 h on 1 November, the first wiper trip began, and hole cleaning continued until the following day. Three wiper trips were made from total depth to the 10¾ inch casing shoe and back. Tight spots were recorded at 4692, 4703, 4708, 4716, 4724, 4743, 4751, and 4752 mbrf (266.8, 277.8, 282.8, 290.8, 298.8, 317.8, 325.8, and 326.8 mbsf). These spots were reamed and rechecked during the first wiper trip. At the end of the first wiper trip, 4 m of fill was found on the bottom and cleaned out. We circulated a 70 bbl sweep of high-viscosity mud, and then the hole was displaced with salt water. The subsequent two wiper trips did not detect tight spots or fill on the bottom. At 0545 h on 2 November, we started to pull the string out of Hole U1383C, and it cleared the seafloor at 0625 h. The RCB bit was back on the rig floor at 1315 h.

Before we started assembling the logging/packer BHA, we picked up and assembled six 6¾ inch perforated drill collars into a stand. The exterior of the stand was then completely coated with an epoxy paint and set back in the derrick to cure. This stand is the lowermost portion of the CORK completion string.

The logging and drill string packer BHA was then assembled and lowered to the seafloor. After ~3 min of maneuvering, we reentered Hole U1383C at 2342 h on 2 November. The logging bit was positioned ~5 m from the base of the 10¾ inch casing shoe.

The logging equipment was rigged up to run the adapted microbiology combination II (AMC II) tool

string, which included the DEBI-t deep UV–induced fluorescence, density/caliper (Hostile Environment Litho-Density Sonde [HLDS]), and spectral gamma ray (Hostile Environment Natural Gamma Ray Sonde [HNGS]) tools. During assembly, the resistivity tool failed and had to be removed from the string. The tool string was run into the hole, and two full passes were conducted, tagging bottom and confirming drill pipe depth and lack of fill in the hole. After this first tool string was back on board, the FMS-sonic tool string was rigged up. This tool string included the spectral natural gamma ray, Dipole Shear Sonic Imager (DSI), and FMS tools. This second string also completed two successful passes; it was pulled out of the hole and rigged down at 2315 h on 3 November.

Following logging, we picked up the top drive and prepared for the first of three scheduled packer tests. We were unable to set the packer in the casing, and the test at this level was abandoned. The packer was then moved to 4566 mbrf (140.8 mbsf) in open hole. The packer was inflated, and flow tests were completed as scheduled. The packer was then moved to the final position but was unable to hold pressure. The packer experiment was concluded, the top drive was set back, and the drill string was pulled out of the hole to just above the seafloor.

Before beginning CORK installation in Hole U1383C, we decided to deploy an ROV platform in Hole U1383B to facilitate a future borehole observatory installation by ROV. We moved to Hole U1383B, deployed the camera system, and reentered the hole at 1350 h on 4 November. We retrieved the camera system, assembled a modified ROV platform around the drill pipe, and let it free fall down onto the reentry cone at the seafloor. The platform had been modified to self-center on the reentry cone because there was no CORK wellhead to help it center as designed. The camera was deployed, and the platform was observed to be sitting in the cone—although perhaps just slightly off-center. The bit was pulled out of the hole at 1818 h. After pulling the bit well above the seafloor, we paused operations to slip and cut the drill line. At 2015 h, the trip out of the hole resumed, and the logging bit arrived back on the rig floor at 0300 h on 5 November. We observed that the drill string packer element had experienced a blowout. After we had the drill collars stored in the derrick, we began assembling the Hole U1383C CORK.

A schematic of the installed observatory is shown in Figures **F2** and **F3.** The individual CORK pieces assembled are listed in Table **T3.** The observatory assembly started with lowering the preassembled 6¾ inch perforated drill collar stand below the rig floor. We picked up, assembled, and painted with epoxy four additional 15 ft long perforated drill collars, which we added to the top of the first stand to provide additional weight to the bottom of the CORK to hopefully ease the string past a ledge encountered during hole cleaning. We then started assembling the various pieces of the CORK, including (1) external umbilicals terminated at screens, (2) coated and perforated steel and slotted fiberglass tubing, (3) landing seats, (4) packers, and (5) a variety of required crossovers. Five external umbilicals allow access to these three zones for microbiological, geochemical, and pressure sampling. The CORK tubing (coated steel and fiberglass) extends to 247.6 mbsf and includes perforated and slotted intervals (76.3–129.4, 145.9–181.1, and 203.7–246.6 mbsf) that provide access to the three isolated intervals but leave the bottom portion of the hole open for future logging and access (247.6–331.5 mbsf). An internal OsmoSampler string extends the full length of the CORK and includes seals isolating the three zones and microbiological, geochemical, pressure, and temperature experiments.

At just after 1700 h on 5 November, we finished assembling the 247.6 m long CORK observatory and picked up the CORK head and attached it to the casing string. The last umbilical connections were made to the bottom of the CORK head. The CORK was lowered to the moonpool and landed on the moonpool doors. The CORK running tool was removed, and the OsmoSampler instrument string was assembled and lowered inside the CORK and casing. The CORK running tool was reinstalled, and the packer inflation line was connected. The CORK was then lowered below the keel to flood the umbilicals to remove air from the pressure lines. The CORK was then raised to the moonpool, and the seafloor fast-flow OsmoSampler was installed. All valves except the geochemistry bay upper Zone 2 valve (which was connected to the seafloor fast-flow OsmoSampler) were closed and secured. The CORK was lowered to ~100 meters below sea level (mbsl), and the camera frame was test fit over the CORK head. At 0000 h on 6 November 2011, after ~21 h of assembly, we started lowering the CORK assembly to the seafloor. During the trip in the hole, the drill pipe was filled with seawater every six stands, which lengthened the trip to a total of 8.25 h. At 0915 h, the vessel began maneuvering to reenter Hole U1383C. The hole was reentered at 0941 h. After reentry, the CORK was slowly lowered into the hole while drill string weight was carefully monitored and the procedure was observed with the camera. Approximately 35 m above the landing point, the top drive was picked up, and the CORK was fully landed at 1127 h on 6 November. Afterward, the mud pumps were brought online to pump up the packers. We applied pressure to the packers for 30 min but were unable to get them to

hold a sustained pressure. It was evident there was a small leak somewhere in the system between the standpipe on the rig floor and the bottom packer. We were unable to detect where the leak might be, and there are many possibilities or combinations depending on where the leak is—from all packers pressurized and sealing to only the top swellable packer sealing. After the camera was recovered, the ROV platform was assembled, hung from the camera frame, and run to the bottom. The platform was released at 1630 h without incident. The camera was pulled back to the surface, the slings and releasing tool were removed, and the camera was lowered back to the bottom to monitor the release of the running tool from the CORK head. The running tool was released at 2015 h on 6 November, ending the Hole U1383C CORK deployment. When the CORK running tool was released, the CORK wellhead also appeared to rotate. Several possibilities could account for this action, but it is likely the result of tightening the upper casing in excess of the manual tightening on the rig floor. A similar occurrence was noted with the Juan de Fuca CORKs. The camera and drill string were retrieved, with the CORK running tool arriving back on the rig floor at 0315 h on 7 November, ending Hole U1383C.

## CORK observatory

Hole U1383C was cased through the 38.3 m thick sediment section with 10¾ inch casing to 60.4 mbsf and a 14¾ inch rathole to 69.5 mbsf. The casing was cemented in place with cement that included Cello-Flake LCM. When it was drilled out, the cement extended 16.6 m uphole from the casing shoe inside the casing. The hole was then RCB cored to 331.5 mbsf. After cleaning, a lack of fill was verified during logging.

The CORK screens and downhole instrument string targeted three zones selected on the basis of drilling rate, core recovery, and caliper log. The upper zone is defined by a combination packer and landing seat (58.4 mbsf) in the casing and the first open-hole packer and landing seat at 145.7 mbsf. Within this section the miniscreens are centered at 100 mbsf, with the slotted portion of the casing extending from 76 to 129 mbsf. The middle zone is isolated by the two open-hole packers and landing seats, with the bottom landing seat at 199.9 mbsf. Within this section the screens are centered at 162 mbsf, with the slotted casing extending from 146 to 181 mbsf. The deep zone is defined as the bottom of the deepest landing seat (199.9 mbsf) to the bottom of the hole (331.5 mbsf), with miniscreens beginning at 203 mbsf.

Because of the need to keep the CORK in tension and potential issues regarding a ledge within the borehole, additional heavy, perforated, resin-coated drill collars were used at the bottom of the CORK assembly. The monitoring section of the CORK comprises (from the bottom up) a bullnose that is not restricted (terminates at 247.6 mbsf, leaving 83.9 m of open borehole for future open-hole logging), 10 perforated 6¼ inch diameter drill collars, a crossover, a shortened 3.12 m long section of perforated 5½ inch diameter casing to maximize the amount of open borehole below, a crossover to fiberglass, a landing seat (2⅞ inch), and an inflatable packer (see Figs. **F2, F3;** Table **T3**).

All steel portions are coated with either Xylan, TK-34XT, or Amerlock to reduce reactivity (**Edwards et al.,** 2012; **Orcutt et al.,** 2012). However, due to handling operations, some steel was exposed. The bullnose and the first drill collars were connected, painted with an epoxy, and hung in the derrick several days prior to use. The additional four drill collars were added to this string and painted before being lowered to the moonpool area, where all of the collars were inspected. Grease (pipe dope) was wiped with 10% ethanol, and scratches in the epoxy were painted with a fast-drying epoxy paint (Alocit 28) that also dries in water. The perforated 5½ inch casing section was connected, cleaned, and painted as it was lowered past the moonpool. Both ends of the inflatable packers were painted with fast-drying epoxy paint (Alocit 28), as were any scratches in the steel landing seats and crossovers. Some grease was wiped from the fiberglass casing. Above the combination packer is more steel casing, which is untreated because none of this section is exposed to the formation of interest.

Umbilicals with internal stainless steel or Tefzel tubing were strapped to the outside of the casing and connected to miniscreens located at ~100, 162, and 203 mbsf (see Fig. **F2;** Table **T3**). Four miniscreens were deployed at 203 mbsf. Three of these screens were attached to ½ inch diameter Tefzel tubing, ⅛ inch diameter stainless steel tubing, and ¼ inch diameter tubing, ending at the base of the 5½ inch casing. The ¼ inch stainless steel tubing and miniscreen for pressure monitoring were attached directly to the packer, ~3 m shallower than the other miniscreens. Miniscreen locations for the other two depths (100 and 162 mbsf) were staggered. The ½ inch diameter Tefzel tubing was positioned at the prescribed depth, which is ~1 m deeper than the ⅛ inch diameter stainless steel tubing and ¼ inch diameter tubing for geochemistry. These miniscreens were ~1 m deeper than the ¼ inch stainless steel tubing for pressure monitoring. A single ½ inch diameter stainless steel

tube was used to inflate all three packers in series, and each has a check valve that opens at 25 psi (172 kPa).

The wellhead was a standard lateral CORK (L-CORK) with a 4 inch diameter ball valve.

### Downhole samplers and experiments

The downhole tool string consists of six OsmoSampler packages, a dissolved-oxygen sensor and recorder, two miniature temperature recorders, sinker bars, sealing plugs, and interspersed sections of ⅜ inch (0.95 cm) Spectra rope (Table **T4**). In addition, the wellhead was populated with a pressure logger capable of monitoring each of the three horizons and bottom seawater and a fast-flow OsmoSampler that included standard and MBIO OsmoSampler packages. Complete details of this deployment are provided in **Edwards et al.** (2012) and are summarized in the "CORK observatory" sections of the other site chapters in this volume. More information on the various OsmoSampler packages is provided in detail in Wheat et al. (2011).

### Scientific and operational implications

The CORK plumbing was finished before the CORK head was landed on the moonpool doors. The CORK running tool was removed, exposing the top of the wellhead at the rig floor, and the bushings were installed to stabilize the CORK. The instrument string was deployed as designed. Lastly, the top plug was deployed and latched properly. A new hydraulic hose was made to connect to the packer inflation line, and the CORK was lowered ~5 m below the ship with all the valves open for 10 min. The wellhead was brought back to the moonpool, where the valves (including the pressure purge valves) were closed, the cap to the underwater mateable connector was removed, the ball valve was closed with the cap in place, and the fast-flow OsmoSampler package was installed. During this 10 min dunking of the wellhead, seawater was at the level of the open ball valves (the lowest open port of the wellhead plumbing), which indicates that the shallowest borehole plug sealed as planned. The CORK and ROV platform were landed, and the CORK running tool unlatched as planned.

## Petrology and hard rock geochemistry

Basement in Hole U1383C was cored from 69.5 to 331.5 mbsf with an overall recovery of 19.2%. The recovered core material was divided into three major lithologic units on the basis of changes in rock lithologies and contacts between pillow lavas and sheets or more massive flows (Fig. **F4;** Table **T5**). Each unit was further divided into subunits on the basis of sedimentary and brecciated contacts, including interflow sediments, tectonic or sedimentary breccias, and hyaloclastites. In contrast to Hole U1382A, subunits were not defined on the basis of chilled margins because of the large number of pillow margins recovered.

The basalts comprise three distinct petrologic types: (1) sparsely plagioclase-olivine-phyric basalt (Unit 1), (2) highly plagioclase-olivine-phyric basalt (Unit 2), and (3) aphyric cryptocrystalline to fine-grained basalt (Unit 3). The units consist of pillow sequences (Units 1 and 3) and perhaps a sheet or massive flow (Unit 2). They range in thickness from 37 m (Unit 2) to 57 m (Unit 1) to 161 m (Unit 3). The core sequence comprises 247 chilled margins and several brecciated glassy zones, featuring spectacular hyaloclastites with variably palagonitized glass clasts. Interflow sediments and sedimentary breccias were recovered in 12 different intervals representing a total of 1% of recovered basement rocks. Interflow materials are present in Units 1 and 2 (to 165 mbsf) and are classified as limestone on the basis of micritic calcite filling. They lack sedimentary structure and well-preserved micro- or nannofossils. Each major lava flow unit consists of several cooling units, which are recognized by glassy or variolitic margins or marked changes in groundmass grain size. Initial results from thin section studies reveal a range of groundmass grain size, from glassy to fine grained with aphanitic, hyalophytic to intersertal textures. Trace amounts of primary sulfides were observed in thin sections of fine-grained basalts.

Basalts of Unit 1 are either aphyric or sparsely plagioclase-olivine-phyric and have <3% vesicles. Basalts of Unit 2 are highly plagioclase-olivine-phyric, with phenocryst contents ranging up to 13% and plagioclase being more abundant than olivine. The phyric basalts in Unit 2 are petrographically similar to the plagioclase-olivine-phyric basalts cored in Hole U1382A (Unit 6), although geochemical analysis suggests that these basalts formed from different parental magma sources. The aphyric pillow basalts in Unit 3 are petrologically and geochemically similar to each other and include several discrete intervals of hyaloclastites. These intervals are most abundant between Cores 336-U1383C-20R and 24R and probably represent different successive cooling units. Unit 3, although much thicker, is also petrographically similar to the pillow lava units in Hole U1382A, but the bulk rock chemical data indicate different magma sources.

In all units, the extent of alteration ranges from fresh (<1%) to 60%, with brown to dark green clay followed

by iddingsite being the most abundant secondary phases replacing primary minerals and mesostasis. Vesicles and veins, representing <2% of the recovered core material, are variably filled by the following assemblages: (1) smectite (e.g., nontronite and saponite) and celadonite; (2) reddish-brown iddingsite, generally logged as mixed Fe oxyhydroxides and smectite assemblages; (3) zeolite, identified as mainly phillipsite; (4) carbonate, identified as mainly calcite; and (5) micritic limestone similar to the calcareous interflow sediment. The volcanic basement in Hole U1383C has an average vein density of 33 veins/m (Fig. F5), which is significantly higher than in Hole U1382A (average of 20 veins/m) but is similar to other sections from the upper volcanic basement (Alt et al., 1996).

## Lithologic units

### Unit 1

Depth: 69.5–126.7 mbsf

Lithology: nonvesicular to sparsely vesicular aphyric to sparsely phyric pillow lava

Unit 1 is composed of 11 subunits that are distinguished mostly on the basis of brecciated contacts such as interflow sediments and sedimentary breccia. The basalts are nonvesicular (<1% vesicles) to sparsely vesicular (maximum of 4% vesicles) and sparsely plagioclase-olivine-phyric, with plagioclase phenocrysts (1%–3%) being more abundant than olivine phenocrysts (<0.1%–1%). Plagioclase phenocrysts range from <0.1 to 2 mm in size and are generally fresh. Only pervasively altered pieces show slight plagioclase alteration (<10%). Olivine phenocrysts are <1 mm in size and are moderately to completely altered to an assemblage of secondary brown clay (smectite) and Fe oxyhydroxides (± iddingsite) in grayish-brown alteration patches.

Groundmass grain size ranges from cryptocrystalline to microcrystalline and is rarely fine grained; glass is encountered only within chilled margins. Groundmass alteration is generally slight to moderate (5%–20%) but reaches 40% in pervasively altered basalts (Fig. F6). The average extent of alteration in Unit 1 is ~8%. Altered basalts generally display well-developed alteration patches and halos along veins and broken surfaces of pieces (Fig. F7). Vesicles remain mostly unfilled, with only 25% vesicle filling, on average, composed of mixed smectite (possibly celadonite) and Fe oxyhydroxide (possibly iddingsite) mineral assemblages (Fig. F6).

Unit 1 features five subunits of interflow sediments composed of micritic limestone (Fig. F8). In some cases, interflow sediments are defined as sedimentary breccias because of the occurrence of angular basaltic clasts (mainly altered glass) in the matrix. Glassy margins are variably palagonitized (up to 80%) with a reddish-brown alteration color and are occasionally in direct contact with interflow sediments (e.g., Section 336-U1383C-3R-2 [Piece 2]). The sharp and irregular contact between the limestone and altered glassy margin is indicative of direct contact with soft sediment, presumably nannofossil ooze, during lava emplacement.

The average vein density in Unit 1 is ~20 veins/m, and vein width ranges from 0.1 to 5 mm. The larger veins, typically >1 mm, are composed of carbonate (micrite) of sedimentary origin (i.e., from interflow limestone). Thinner veins are filled with a mixed mineral assemblage of smectite, iddingsite (± Fe oxyhydroxides), and zeolite. Microcrystalline carbonate occurrence in this assemblage is considered to form from micritic carbonate dissolution and recrystallization. Grayish-brown halos, and more rarely dark green halos, line veins, with larger halos lining veins exposed at the outer surface or side of a piece.

### Unit 2

Depth: 126.7–163.7 mbsf

Lithology: sparsely vesicular phyric basalt sheet to massive flow

This unit of plagioclase-olivine-phyric basalt is composed of nine subunits distinguished from each other on the basis of sedimentary breccias and interflow sediments. About 25 chilled glassy margins with planar glassy contacts were recovered, together with limestone intervals, suggesting that this unit represents several sheet flow cooling units (Fig. F9).

The basalts are sparsely vesicular (<5% vesicles), show dominantly glomerophyritic texture, and have a cryptocrystalline to fine-grained groundmass. Tabular to elongated euhedral plagioclase phenocrysts have an overall abundance between 4% and 7% on average, with crystal sizes ranging from <1 to 2.5 mm. Olivine phenocrysts are less abundant (~1% modal abundance) and smaller in size (<1.4 mm). Euhedral olivine phenocrysts are partly altered (~40% alteration) to brown clay (smectite ± iddingsite) in the alteration patches, whereas plagioclase remains fresh or is merely tainted with Fe oxides. Glass from chilled margins is extensively devitrified and altered to palagonite (up to 95%), whereas groundmass alteration averages 7%–15% and is always <25%. Note that the highly altered aphyric chilled margin (up to 70% alteration) in Section 336-U1383C-9R-1 (Piece 1), together with basalt in Section 9R-1 (Piece 2), is possibly derived from borehole wall breakouts from Unit 1 above.

Vesicles are filled with abundant Fe oxyhydroxides (± iddingsite), smectite (± celadonite), and minor

zeolite (phillipsite) and calcite. Some vesicles remain unfilled (50% on average), with only thin coatings of dark green clay (e.g., nontronite). The grayish-brown alteration halos have more unfilled or iddingsite-rich vesicles than the freshest dark gray groundmass. In many cases, patchy alteration cannot be attributed to haloed veins on the basis of recovered specimens (Fig. F10). Pervasive grayish-brown alteration was also encountered in several pieces and is the result of the complete alteration of olivine phenocrysts and slight plagioclase alteration. Sedimentary breccias were recovered in four intervals (Sections 336-U1383C-10R-1 [Piece 8], 10R-2 [Pieces 9 and 19], and 12R-1 [Piece 11]) and are composed of >80%–95% micritic carbonate matrix with minor angular and highly altered glass clasts ranging from <0.1 to 8 mm (Fig. F8).

### Unit 3

Depth: 163.7–324.8 mbsf
Lithology: nonvesicular aphyric pillow lava

This unit of aphyric basalt is composed of 30 subunits that were identified on the basis of hyaloclastites (13 subunits) and tectonic breccias (2 subunits). A total of 173 glassy or variolitic chilled pillow margins were recovered (Fig. F4), suggesting that Unit 3 is composed of multiple pillow lava sequences. The basalts are generally nonvesicular (<0.5% vesicle abundance), with the exception of irregular vugs as wide as 5 mm encountered in Sections 336-U1383C-20R-1 (Pieces 25 and 26) (Subunit 3-14; see "Core descriptions"). In Core 336-U1383C-28R, vesicle abundance increases substantially, up to 3%, also because of the occurrence of irregular vugs. Basalt groundmass generally ranges from glassy to cryptocrystalline, although microcrystalline to fine-grained groundmass with intersertal texture is not uncommon. Fine-grained basalts feature plagioclase laths up to 1 mm, with olivine <0.3 mm.

Recovered basalts are mostly fresh (<1%) to moderately altered (up to 15% alteration), with a common blotchy alteration texture of devitrified variolitic glass in pillow margins (Fig. F11). Alteration halos are also common and feature mixed Fe oxyhydroxides, brown to green clay (smectite), and minor carbonate replacing olivine and interstitial glass in the groundmass and filling vesicles. The cryptocrystalline groundmass has numerous microphenocrysts of olivine that are variably altered (~60% alteration on average).

Volcanic breccias (hyaloclastite) were recovered throughout Unit 3 but are most abundant in Cores 336-U1383C-20R and 22R (Fig. F4). The hyaloclastite subunits are rather similar to each other, and all display poorly sorted angular clasts of glass ranging in size from 0.1 to 15 mm (Fig. F12). Clasts are essentially composed of glassy basalt fragments covering the whole spectrum of alteration intensity from fresh obsidian-like glass to completely palagonitized and devitrified glass. In some cases, the contact of hyaloclastite with a cryptocrystalline basalt margin was recovered. In other cases, highly fractured chilled margins grade into hyaloclastite in the outer rim (Fig. F12). The matrix of hyaloclastites is often lacking, leading to numerous open vugs partly filled by reddish Fe-rich clays and zeolite. Zeolite generally constitutes the cement between basalt clasts.

The top of Unit 3 features a remarkable tectonic breccia (Section 336-U1383C-11R-1 [Piece 9]) showing a sharp contact between two different basalt lithologies from Unit 3 (microcrystalline and fine-grained aphyric basalt) separated by micritic sedimentary filling (Fig. F13). This interval is considered to represent a fault or large fissure that was filled by debris from overlying sediment and basalts. Several contacts with tectonic breccias were also recovered on the outside of basalt pieces (e.g., Cores 336-U1383C-26R and 32R; Fig. F13). These breccias are composed of poorly sorted angular clasts of altered basalts and light to dark brown clay filling.

## Igneous petrology

### Sparsely plagioclase-olivine-phyric basalt (Unit 1)

The uppermost part of Hole U1383C (Unit 1) is composed of sparsely (~3%) plagioclase-olivine-phyric basalt. Plagioclase phenocrysts (up to ~1 mm) in Unit 1 basalts are euhedral to subhedral and typically well elongated. Some of the phenocrysts have hollow cores parallel to an elongated direction filled by glass or cryptocrystalline groundmass material (Fig. F14). About 30% of the phenocrysts occur as glomerocrysts in which tabular plagioclase crystals form an assemblage with olivine. Olivine phenocrysts are present throughout as euhedral to subhedral crystals and are generally polyhedral to granular in shape. Most of them are <0.2 mm in size, although crystals as large as 1 mm were observed.

The groundmass texture of microcrystalline to fine-grained basalts in Unit 1 is intersertal, although glassy to cryptocrystalline chilled margin samples (e.g., Sections 336-U1383C-2R-2 [Piece 3] and 6R-1 [Pieces 7 and 17]) have hyalophitic to aphanitic textures. In the microcrystalline to fine-grained basalts, groundmass mainly consists of ~40% lath-shaped plagioclase (as large as 2 mm), ~30% anhedral to subhedral pyroxene, and 2% equant or elongate opaque Fe-Ti oxide minerals (as large as 0.04 mm). Plagioclase crystals are skeletal, showing "swallow-tail" and rectangular "belt-buckle" forms. In the microcrystalline

mesostasis that typically makes up 20%–40% of the rock, plumoselike intergrowth between acicular plagioclase needles and interstitial anhedral clinopyroxene were also commonly observed with Fe-Ti oxide mineral grains.

In the chilled margin samples, a variety of quench crystallization textures were observed, including spherulitic textures with glassy groundmass and plagioclase sheaves with or without plumose clinopyroxene. From the glassy margin to the more crystallized interior, three zones showing different quench crystallization textures were typically recognized in the samples: (1) a glassy spherulite zone consisting of a glass matrix in which tiny and skeletal acicular plagioclase, tabular plagioclase phenocrysts, and granular olivine microphenocrysts form the interior of dark spherules (Fig. **F14B**); (2) a dense spherulite zone with only a few acicular plagioclase in dark groundmass; and (3) a crystallized zone composed of well-developed plagioclase fan-spherulites with interstitial cryptocrystalline mesostasis (Fig. **F14C**). Very fine equant to elongate titanomagnetite crystals in mesostasis and in interstices between plagioclase were also observed in the crystalline zone (Fig. **F14C**).

### Highly plagioclase-olivine-phyric basalt (Unit 2)

The basalts from Unit 2 are characterized by abundant (up to 10%), large (up to 6 mm) euhedral plagioclase phenocrysts (some of which can be regarded as "megacrysts"), with ~3% of olivine up to 0.5 mm. The plagioclase phenocrysts often contain glass inclusions as blebs in their cores (Fig. **F14D**), and some parts of the phenocrysts also show internal skeletal structures with irregularly shaped inclusions of groundmass or glass (Fig. **F14E**). The edges of phenocrysts often exhibit dendritic overgrowth (Fig. **F14F**), reflecting undercooling upon extrusion. Euhedral to subhedral olivine phenocrysts were also observed throughout Unit 2 basalts as polyhedral to granular crystals. Most are <0.3 mm in size, although crystals as large as 1 mm also occur. Between 30% and 50% of the plagioclase phenocrysts are glomerocrysts, in which tabular plagioclase crystals form single-phase glomerocrysts or mixed-phase glomerocrysts with olivine.

The groundmass grain size of Unit 2 basalts is microcrystalline to fine grained. In the microcrystalline basalts, plagioclase laths are skeletal and elongated, and swallow-tail and belt-buckle forms were commonly observed. The microcrystalline groundmass also contains quench-textured mesostasis composed mainly of sheaves of acicular plagioclase needles and anhedral clinopyroxene forming plumose intergrowth. Equant or elongate tiny opaque Fe-Ti oxides (as large as 0.02 mm) occur in interstices between plagioclase laths and needles with clinopyroxene. Plagioclase laths in the fine-grained basalts exhibit a tabular shape and less skeletal intergrowth with anhedral prismatic clinopyroxene crystals. Fe-Ti oxide mineral grains are coarser (>0.06 mm) than those in the microcrystalline basalts and occur in interstices between plagioclase lath as equant to elongate grains.

### Aphyric cryptocrystalline basalt (Unit 3)

The pillow basalts in Unit 3 are aphyric with a glassy to fine-grained groundmass. In altered samples, small olivine crystals (equant to elongate, skeletal, and up to 1 mm) are pseudomorphed by brownish clay minerals. The groundmass is composed of olivine, plagioclase, clinopyroxene, Fe-Ti oxide, and cryptocrystalline to microcrystalline mesostasis. The groundmass grain size of the basalts generally ranges from glassy/cryptocrystalline to microcrystalline/fine grained, which corresponds to chilled margins and the interior of pillow lobes, respectively.

In microcrystalline basalts, plagioclase is present as skeletal laths or acicular sheaves (<1 mm in size). The skeletal plagioclase laths often exhibit rectangular belt-buckle and swallow-tailed forms (Fig. **F15A**), depending on the cut directions of the crystals. Several samples contain radiating acicular plagioclase bundles enclosing tiny clinopyroxene and titanomagnetite (Fig. **F15B**). On the other hand, plagioclase crystals in fine-grained samples exhibit tabular shapes and are as large as 2 mm. Olivine crystals in Unit 3 basalts show a variety of quench crystal morphologies. In finer grained samples, characteristic olivine morphologies of the skeletal and elongated olivine crystals were commonly observed, including hopperlike (Fig. **F15C**), lanternlike (Fig. **F15D**), and swallow-tailed (Fig. **F15E**) forms. Clinopyroxene crystals are generally intergrown with plagioclase. In microcrystalline samples, plumose intergrowth of acicular plagioclase needles and anhedral clinopyroxene was commonly observed in the groundmass. In fine-grained samples, on the other hand, coarser grained prismatic clinopyroxene crystals are intergrown with tabular plagioclase laths. Fe-Ti oxide mineral grains in the samples are very tiny (generally <0.01 mm) and equant or elongated in shape. These minerals occur in the mesostasis and interstices between acicular plagioclase needles.

Unit 3 is characterized by well-recognizable variolitic-textured chilled margins with or without fresh volcanic glass. Thin sections made from variolitic-textured chilled margin samples (e.g., Sections 336-U1383C-16R-1 [Piece 14], 16R-2 [Piece 6], and 19R-1 [Piece 6]) are mainly composed of a glassy outer zone and variolitic inner zone. The glassy zone is composed of

"linked chain" and "lantern and chain" olivine crystals (Fig. F15F) and devitrified glassy to cryptocrystalline matrix. Acicular plagioclase sheaves or swirls occur in the center of each variole, together with intergrown clinopyroxene and Fe-Ti oxide. The frequency of varioles increases from the glassy part to the variolitic zone, which suggests that the variolitic texture (or the variole itself) occurs at the transition from glass solidification to mineral crystallization.

## Interflow sediments and sedimentary breccias

The lithology of interflow sediments recovered in Hole U1383C is essentially micritic limestone (i.e., very fine calcite crystals) with light brown-beige color. The limestones also contain poorly sorted volcanic clasts of different sizes, from silt to sand size and gravel. Thin section observations of Section 336-U1383C-7R-2 (Piece 13), Thin Section 37, show that the limestones are made of very fine calcite crystals with two domains separated by a layer of palagonitized glass clasts. These domains are differentiated on the basis of clay concentration, which resulted in slightly different colors. No sedimentary structure or micro- to nannofossils were identified in thin section. According to the classification of Dunham (1962) for limestone, interflow sediments represent mudstone with very rare nannofossils and clasts. Smear slides allowed identification of some very rare nannofossils such as *Discoaster* spp.

Some contacts between chilled margins and limestone show that lava emplacement occurred after deposition of the limestones or its ooze precursor. The limestone described above may represent a highly lithified version of the nannofossil ooze and chalk described in the sedimentary section of Hole U1383E. The unconsolidated ooze could have undergone high-temperature dissolution and recrystallization during the emplacement of overlying lava flows. This possibility would explain the highly lithified state of the limestone, which is unusual for young (<10 Ma) sediments overlying basaltic oceanic crust.

## Volcanic rock alteration

All basement volcanic rocks recovered from Hole U1383C are affected only by low-temperature alteration by seawater. Dark gray rocks with grayish-brown alteration patches are the most abundant type and are present throughout the basaltic section. These rocks are the least altered, generally containing <3% by volume of secondary minerals such as dark green clays (saponite and celadonite) and Fe oxyhydroxides (iddingsite) replacing olivine phenocrysts, groundmass, and filling vesicles. In addition, glass from pillow margins and hyaloclastite is variably replaced by palagonite. Zeolite, identified as phillipsite in thin section and by X-ray diffraction (XRD), is a common secondary mineral filling vesicles and veins and forming hyaloclastite cement. Carbonate (calcite) was also encountered throughout all units, although Units 1 and 2 contain mostly micritic carbonate of sedimentary origin as vein fill and breccia cement. Carbonate precipitate was mostly encountered in the lower part of Unit 3 as vein and vug filling. Alteration intensity of the basalts is variable and ranges from fresh to moderate (up to 20%), manifested as replacement of groundmass and phenocrysts, vesicle filling, glassy margin replacement, and vein formation with adjacent alteration halos. Highly altered rocks with up to 50% alteration were also recovered, but such high extents of alteration were found only in pervasively altered basalt and resulted in extensive replacement of interstitial glass and cryptocrystalline groundmass by smectitic clay minerals. Thin section estimation of groundmass alteration is generally consistent with results from visual core description, except in chilled pillow margins where microscopic observations suggest a lower extent of alteration, with both cryptocrystalline and olivine microphenocrysts often remaining unaltered (Table T6). Throughout the following sections we refer to volume percentages of alteration types, breccias, vesicles, and veins by assuming that the surface areas of these features on the cut faces of the core, when converted to area percent, are equivalent to volume percent of the core. In Figures F6 and F5 we report a summary of calculated averages per core of abundance, volume, width, and mineralogy of vesicles, veins, and halos.

### Secondary minerals

In basaltic rocks from Hole U1383C, secondary minerals have developed as replacement of primary phenocrysts, disseminated in the groundmass as replacement of mesostasis, and as vesicle and vein filling. The identification of secondary minerals was primarily made in hand specimen on the basis of color, habit, and texture, with subsequent verification by thin section observations and XRD (Table T6). The most abundant secondary minerals in Hole U1383C are clay minerals, which are present in all types of alteration. Specific secondary clay minerals (e.g., saponite, nontronite, and celadonite) were characterized for a few examples during logging of alteration and veins, but they were generally referred to as "smectite" or "dark green" or "brown" clays. A distinction was made between micritic carbonate derived from interflow sediments (limestone) and veins of sparry carbonate away from palagonitized glass clasts.

Saponite is the dominant clay mineral and is present throughout the cores. In hand specimen, saponite

occurs in black, dark green, and greenish-brown colors. When brown color was observed, the mineral composition was recorded as mixed smectite–Fe oxyhydroxide assemblages. In thin section, saponite is characterized by pale to dark brown and pale green colors and a mottled or fibrous form with variable pleochroism. Saponite generally replaces groundmass and olivine (micro)phenocrysts uniformly, preserving the primary igneous textures. In the case of variolitic pillow margins, saponite replacement is pervasive across the mesostasis and groundmass, leading to the formation of mottled replacement or blotches and revealing the original variolitic texture (Fig. F15). Commonly, saponite lines or fills vesicles (in association with other secondary formations such as iddingsite, Fe oxyhydroxide, carbonate, and zeolite) and forms a lining along thin (0.1 mm) veins.

Celadonite is the only other clay mineral identified in hand specimen and thin section, and it appears bright green to blue in hand specimen. Celadonite is also present in all four types of alteration but is less abundant than saponite. In hand specimen, celadonite (mainly in vesicles) is green-blue, whereas in thin section it is pale green (see **"Vesicle filling"**).

Zeolite is the next most abundant secondary phase and is found as a major mineral filling vesicles, vugs, and veins and as hyaloclastite cement (Fig. F16). It is often associated with other secondary minerals such as calcite and smectite. Phillipsite was identified by XRD analysis in bulk rock powder (Table T6). In general, zeolite-filled vesicles and veins are more common in Unit 3 in aphyric fine-grained and cryptocrystalline basalts. Zeolite occurs as either fibrous aggregates in druses (sometimes overgrown by carbonate), as radiating or colloform aggregates showing fan-shaped extinction (under cross-polarized light), or as microcrystalline euhedral granular filling.

Fe oxyhydroxide mainly occurs as a discrete phase or mixed with saponite and other smectitic clay phases. In many cases, the mixed assemblage of Fe oxyhydroxide and clays was described as "iddingsite," which was previously reported for Hole 395A (Juteau et al., 1979). Fe oxyhydroxides were identified in thin section by their deep red color to nearly opaque appearance, whereas iddingsite (showing weak pleochroism) was identified by its bright orange to red color. When present as replacement of microphenocrysts (mainly olivine) and groundmass, Fe oxyhydroxides (± iddingsite) are mixed with saponite and preserve the intersertal to hyalophitic textures. In veins and vesicles, iddingsite is bright orange to reddish brown and occurs with or without intergrown clays and may contain aggregates of Fe oxyhydroxides. Staining of plagioclase phenocrysts and replacement of olivine with Fe oxyhydroxides is a common feature in the grayish-brown halos in all recovered units.

Carbonate is present principally as vug, vesicle, and vein filling (Fig. F17). Within the upper part of Unit 1, carbonate (calcite) occurs mainly as crypto- to microcrystalline aggregates hosting clay minerals and fine palagonitized glass shards. This type of carbonate filling was interpreted to result from interflow sediment (limestone) infill. In the lower part of Unit 1 and in Unit 2, calcite is generally recrystallized to coarser aggregates, usually anhedral to acicular, with much less clay material. In the lower part of Unit 3, calcite (with possibly minor aragonite) veins are also common, either as pure carbonate veins or associated with zeolite, forming acicular to granular crystal aggregates. As for zeolite-filled vesicles, calcite was found essentially within grayish-brown alteration halos or pervasively altered sparsely vesicular variolitic basalts. XRD analysis of bulk rock powder did not allow unambiguous identification of carbonate minerals.

Ultratraces of secondary sulfide (pyrite) were identified in thin section or under the binocular microscope. They occur as <10 µm crystals along cracks in plagioclase or disseminated in the groundmass of the fine-grained aphyric basalt of Unit 3. They also occur in vesicles and voids associated with other secondary minerals such as pale green saponite or celadonite (e.g., Section 336-U1383C-13R-1 [Piece 5], Thin Section 44). In Section 336-U1383C-28R-1 (Piece 7), Thin Section 54, spherical secondary pyrite (<10 µm grain size) extensively oxidized to Fe oxyhydroxide was identified along a thin saponite vein.

## Phenocryst alteration

### *Plagioclase*

Plagioclase phenocrysts and microphenocrysts are fresh, except in pervasively altered grayish-brown basalt (alteration <10%). In the only transformations observed, plagioclases of aphyric basalt samples in the immediate vicinity of veinlets filled with smectite have been partially replaced by clay or tainted by Fe oxyhydroxides.

### *Pyroxene*

The augitic clinopyroxene remains essentially unaltered. When pyroxene occurs as microliths or plumose in microcrystalline groundmass, extensive brown staining suggests incipient pyroxene alteration. However, the exact extent of clinopyroxene alteration is difficult to estimate on the basis of thin section observation (e.g., Section 336-U1383C-10R-1 [Piece 1], Thin Section 41).

### *Olivine*

Olivine phenocrysts and microcrysts are the minerals most sensitive to alteration. Olivine is partially or completely replaced by reddish-brown iddingsite (a mixture of smectite and Fe oxyhydroxide) in the alteration halos (Section 336-U1383C-31R-2 [Piece 6], Thin Section 57). In grayish-brown alteration halos, olivine pseudomorphs are revealed as a result of replacement by iddingsite. In fresh dark gray basalts and devitrified chilled margins, olivine is remarkably fresh.

## Groundmass alteration

In crypto- to microcrystalline groundmass, plagioclase microliths (e.g., sheaves) are quite fresh, although the extent of alteration of clinopyroxene plumose is difficult to estimate. In thin section, the highest alteration intensity of the groundmass is observed in pervasively altered basalts. For example, Section 336-U1383C-3R-1 (Piece 2), Thin Section 30, in Unit 1 displays up to 40% groundmass alteration from extensive replacement of microcrystalline mesostasis by brown clay. The pervasively altered phyric basalt of Unit 2 generally shows more modest alteration (15%; Section 336-U1383C-10R-1 [Piece 7], Thin Section 41) because of less abundant mesostasis. In Unit 3, several pieces of pervasively altered crypto- to microcrystalline basalt display groundmass alteration as high as 25% (e.g., Sections 336-U1383C-16R-2 [Piece 7], Thin Section 48, 20R-1 [Piece 9], Thin Section 51, and 31R-2 [Piece 6], Thin Section 57). Microscopic observation of fine-grained aphyric avesicular basalt at the bottom of Unit 3 (e.g., Sections 336-U1383C-23R-1 [Piece 10], Thin Section 52, and 32R-2 [Piece 9], Thin Section 59) shows an overall alteration of 6%–8% that is attributed to alteration of interstitial mesostasis and olivine. Microscopic and XRD observations (as well as geochemical studies; see **"Hard rock geochemistry"**) of several fresh/altered pairs were undertaken to examine mineralogical changes with varying extents of alteration. Although not systematic, results show that olivine is readily altered (i.e., olivine was barely identified by XRD) in most altered samples.

## Glass and chilled margins

Chilled margins often show advanced palagonitization, which develops as an irregular alteration front. Glass devitrification developing as a spherulitic texture is generally more abundant in palagonite alteration rinds but is also not uncommon in fresh glass around plagioclase and olivine microliths (Fig. **F18;** Section 336-U1383C-2R-2 [Piece 3], Thin Section 28). The cryptocrystalline mesostasis of chilled margins commonly consists of coalesced spherules. In fresh glass, the spherules show weak birefringence. Altered glass is revealed by a zone of typically yellowish-brown material commonly referred to as palagonite (Honnorez, 1972). The boundary between spherules or palagonite and fresh glass is generally characterized by a granular texture and also develops channel-like or branchlike structures. Such microtubules have been suggested to form by microbial process (Fisk et al., 1998) and appear to be widespread in glassy margins.

Microscopic investigation of the blotchy alteration texture in pillow margins allowed identification of several domains that are generally similar to the alteration of variolitic texture reported for Hole U1382A (see the **"Site U1382"** chapter [Expedition 336 Scientists, 2012b]) and Hole 395A (Natland, 1979).

## Vesicle filling

All basalts recovered are sparsely vesicular to nonvesicular, and vesicle abundances per core are <1% (Fig. **F6**). The following filling associations were found in the vesicles: (1) dark brown to dark green smectite (nontronite and smectite); (2) reddish-brown iddingsite, generally logged as mixed Fe oxyhydroxides and smectite assemblages; (3) zeolite, mainly phillipsite; and (4) carbonate (calcite). No clear trend with depth was found, but dark green clay (saponite and celadonite) mixed with variable proportions of Fe oxyhydroxides forms the vast majority of vesicle filling material in the upper section of Hole U1383C (Cores 336-U1383C-2R through 20R), whereas zeolite- and carbonate-filled vesicles are more abundant in the lower section.

Interestingly, vesicle filling in all units is very limited (25% on average), and larger vesicles are mainly void except in the phyric basalt of Unit 2. Vesicle filling colors range from blue-green in the freshest grayish diabase to dark brown and white in the brown alteration halos, which suggests different stages of vesicle filling during rock alteration. An example of a composite mineral filling of vesicles is illustrated in Figure **F19,** showing (1) mixed saponite and possible celadonite vesicle filling in gray groundmass, (2) smectite stained with Fe oxyhydroxide in dark brown alteration, and (3) mixed iddingsite smectite zeolite-filled vesicles in grayish-brown halos. An example of thin section observation of vesicle filling is illustrated in Figures **F15** and **F16.** In variolitic, sparsely vesicular pillow basalt from Unit 3 (e.g., Section 336-U1383C-16R-2 [Piece 6], Thin Section 47), vesicles often display bimodal filling (i.e., carbonate or zeolite filling), although most vesicles remain unfilled.

Cores 336-U1383C-23R and 24R feature several pieces with 1–3 mm vugs filled by carbonate. In rare cases, pyrite is found as euhedral crystals associated with saponite or other secondary minerals in vugs of microcrystalline to fine-grained basalt.

### Veins and halos

The following filling associations are found in veins: (1) Fe-rich dark green smectite (nontronite and smectite); (2) reddish-brown iddingsite, generally logged as mixed Fe oxyhydroxides and smectite assemblages; (3) zeolite, mainly phillipsite; (4) carbonate; and (5) micritic sediment, possibly from interflow limestone filling (Fig. F5). As with Hole U1382A, the volume percent of veins for each core was estimated by calculating the volume of veins relative to the volume of core recovered. Approximately 780 veins, including 500 haloed veins, were logged during core description of Hole U1383C (Fig. F17). The average vein abundance is ~1%, which is three times higher than the vein abundance in Hole U1382A, reflecting in most part the occurrence of carbonate(micrite)-filled veins wider than 1 mm. We also logged 203 halos in both pillow lava and massive flows that have highly variable widths and are not always clearly associated with a vein. For this reason, we logged nonveined halos as having 0 mm vein thickness. Both veins (with or without halos) and nonveined halos were logged for the total vein count, which gives an estimation of the minimum and maximum vein abundance per core. Using this approach, we estimated that the recovered section in Hole U1383C has between 22 and 50 veins/m, averaging 33 veins/m for the entire drilled section. This estimate is higher than that for Hole U1382A (average of 20 veins/m) and similar to that for sections of other upper volcanic basement (e.g., 27 veins/m in Ocean Drilling Program [ODP] Hole 896A, 24 veins/m in ODP Hole 801C, and 31 veins/m in DSDP Hole 504B; Alt et al., 1996; Plank, Ludden, Escutia, et al., 2000). Veins range in thickness from ~0.1 to ~6 mm, but vein thickness of <0.2 mm is by far the most common. Mixed smectite and iddingsite (Fe oxyhydroxide) veins are the most abundant. Carbonate and zeolite veins also represent a significant fraction of veins greater than that in Hole U1382A.

In Unit 1, zeolite veins are often associated with micritic and recrystallized calcite, as confirmed by thin section observations and XRD analysis of a vein filling Section 336-U1383C-2R-1 (Piece 7) (Table T6). An example of a composite zeolite-carbonate vein is illustrated in Figure F17A, which shows three domains: (1) micritic carbonate filling mixed with altered glass shards, (2) later stage recrystallized calcite lacking glass shards, and (3) cryptocrystalline zeolite mixed with clay with low birefringence. Pure zeolite veins were also observed in thin (<0.2 mm) veins, especially in association with glassy margins, as illustrated in Figure F16.

In Unit 3, mixed carbonate and zeolite veins were also commonly identified, but they lack micritic fillings. As shown in Figure F17A, mineral habit and paragenesis suggest the following sequence: (1) zeolite first crystallized in open vein fractures, forming radiated acicular to fibrous clusters; (2) calcite partly replaced zeolite or form pseudomorphic overgrowth; and (3) granular calcite, showing radial extinction, finally filled the remaining vein space. Pure zeolite veins were commonly observed throughout Unit 3, as shown in Sections 336-U1383C-16R-1 (Piece 14), Thin Section 47, 29R-1 (Piece 14), Thin Section 55, and 31R-2 (Piece 6), Thin Section 57, and phillipsite was identified in bulk rock powders by XRD analysis (Table T6).

Grayish-brown alteration halos, and to a lesser extent dark (green) halos, were identified in all volcanic units in Hole U1383C (Fig. F5). Brown halos are characterized by the presence of abundant iddingsite disseminated in the groundmass, staining smectite-filled pores, and replacing olivine and mesostasis. Dark green halos are characterized by higher green clay (e.g., celadonite) abundance in the groundmass relative to iddingsite. In most cases, grayish to dark brown alteration halos develop after, or are superimposed onto, dark green halos (Fig. F8B). In Unit 1, brown halos represent ~20% of the recovered material, whereas dark halos represent >8%. In the highly phyric basalt of Unit 2, alteration halos are even more abundant (27% of brown halos and 14% of dark halos). Aphyric pillow basalts from Unit 3 also display mixed dark and brown halos (15% and 7%, respectively) but differ from other units in by the abundant occurrence of blotchy alteration textures making up as much as 33% of the recovered material.

A representative piece of microcrystalline aphyric avesicular basalt with alteration halos was investigated by thin section (Section 336-U1383C-28R-1 [Piece 7], Thin Section 54). The margins are more altered (~20% alteration) with abundant Fe-rich clay (smectite) replacement of skeletal olivine sheaves and mesostasis. Iddingsite is also common throughout the groundmass and as vesicle filling. The less altered gray core (<1% alteration) is devoid of iddingsite, and only olivine (10% alteration) is replaced by dark green smectite.

### Hyaloclastite

Hyaloclastites were recovered in all units in Hole U1383C and represent ~2.5% of the total basement recovered (Fig. F4). Cores 336-U1383C-20R and 22R feature the highest amount of hyaloclastite intervals, representing ~17% and 10%, respectively, of these cores. The glassy fragments in hyaloclastic breccias have typical concentric alteration rims surrounding fresh glass preserved in the central part of the fragments (Fig. F12). In all of the hyaloclastite recovered, glass clasts are variably altered to palagonite, forming

layered, bright reddish-brown to yellowish-brown alteration fronts (Fig. F20). In the single thin section of hyaloclastite investigated (Section 336-U1383C-20R-1 [Piece 28], Thin Section 50), the transition between palagonite and fresh glass lacks granular or fibrous textures, contrasting remarkably with the pillow margin textures (Fig. F18) and showing ubiquitous microtubules extending into the fresh glass. The fresh glass also displays more limited spherulites associated with glass devitrification. The hyaloclastite cement is mainly zeolite (phillipsite) forming an external rind around glass clasts. Numerous open vugs between glass clasts feature drusy euhedral to fibrous phillipsite druses. The matrix of the hyaloclastites is often missing and is mostly composed of mixed zeolite and palagonite to smectitic clay without carbonate.

## Hard rock geochemistry

Concentrations of major element oxides and several trace elements, together with weight loss on ignition (LOI), were determined for 25 whole-rock samples from Hole U1383C. The results are presented in Table T7, where major element oxide concentrations were normalized to 100% and total iron was recalculated as $Fe_2O_3$ ($Fe_2O_3^T$).

Basalts from Hole U1383C are typical depleted mid-ocean-ridge tholeiites with low K/Ti ratios and Mg numbers between 35 and 63. Whole-rock compositions do not show any systematic downhole trends (Fig. F21). The relationship between $Al_2O_3$ and CaO concentrations (Fig. F22) suggests that the accumulation of plagioclase could affect the composition of plagioclase-phyric basalts in Units 1 and 2. CaO concentrations also correlate with Sr and Ba contents, which is consistent with plagioclase accumulation. Compositional variations in MgO, $Al_2O_3$, $Fe_2O_3^T$, and $TiO_2$ suggest, however, that the effect of plagioclase accumulation on bulk-rock chemistry of the plagioclase-phyric basalts from Units 1 and 2 is quite limited (Fig. F23), which contrasts significantly with the same type of basalt from Holes U1382A (see the "Site U1382" chapter [Expedition 336 Scientists, 2012b]) and 395A (Bougault et al., 1979; Rhodes et al., 1979). Negative correlations in the MgO vs. $Al_2O_3$ and MgO vs. CaO plots suggest a lack of clinopyroxene and plagioclase fractionation (i.e., only olivine fractionation was involved) on the magma evolution of Hole U1383C basalts (Fig. F23).

### Differences in magmatic geochemical signatures

In order to determine if there are differences in the composition of primitive magmas unaffected by crystal fractionation and mineral accumulation, the correlation between Zr, Y, and $TiO_2$ was examined. Figure F24 shows two separate trends with different Zr/Y and Zr/$TiO_2$ ratios. Rocks from Units 1 and 2 show generally higher Zr/Y and Zr/$TiO_2$ ratios than those from Unit 3 (except one sample in the Y/Zr panel). These results imply that, despite the petrographic difference, both the sparsely plagioclase-olivine-phyric basalts in Unit 1 and the highly plagioclase-olivine-phyric basalts in Unit 2 are derived from the same parental magma. In contrast, the aphyric basalts from Unit 3 may be derived from a different magma source.

Given the Zr-Y-$TiO_2$ systematics, it is interesting to note that the highly plagioclase-phyric basalt unit in Hole U1383C (Unit 2) belongs to the shallower unit, whereas the same type of basalt in Unit 6 in Hole U1382A belongs to the deeper unit. Moreover, in Hole U1382A the values of Zr/Y and Zr/$TiO_2$ in shallower units are lower than those in deeper units (including the porphyritic basalt unit) (Fig. F25). In contrast, shallower units in Hole U1383C (including the porphyritic basalt unit) have higher Zr/Y and Zr/$TiO_2$ ratios than the deeper unit (Fig. F25). These facts lead us to consider that the two sequences of basalt units in Holes U1382A and U1383C are chemically different, despite the striking similarities in petrographic features.

### Alteration

LOI values of Hole U1383C basalts are as high as 3.66 wt%, with an average of 1.63 wt%. The values are generally higher than those observed in Hole U1382A (2.69 wt%; 0.90 wt% on average). High extents of groundmass alteration, observed by macroscopic and microscopic observations in Hole U1383C basalts, are consistent with the higher LOI values, although generally low LOI values indicate that the degree of bulk-rock alteration is still relatively small. Downhole variation of LOI values suggests that the degree of alteration is significantly higher in the shallower (<200 mbsf) part than in the deeper part (Fig. F21), which is similar to the pattern observed in Hole U1382A. However, unlike Hole U1382A, there is no correlation between LOI and $K_2O$ contents (Fig. F26), suggesting a lack of K enrichment during alteration of Hole U1383C basalts. On the other hand, CaO and Ba concentrations are weakly correlated with LOI values. It is likely that the presence of secondary minerals (possibly carbonate minerals or zeolite) also affects the bulk-rock compositions of CaO and Ba in some degree, although a significant amount of variation in these elements is attributed to igneous processes, as shown above. In addition, there is also a weak negative correlation between LOI and MgO (Fig. F26), suggesting that depletion of MgO is associated with alteration.

Macroscopic and microscopic observations indicate selective replacement of olivine by Fe oxyhydroxide in the Hole U1383C basalts. It is thus possible that alteration of olivine causes the depletion of MgO in bulk-rock chemistry of altered basalt samples.

## Microbiology

Hard rock samples were collected for microbiological studies from every interval cored with the RCB in Hole U1383C. Roughly 12% (6.11 m total) of core recovered from Hole U1383C was taken as whole-round samples from the core splitting room and dedicated to microbiological analysis. The 79 hard rock microbiology samples span a range of lithologic units, alteration states, and presence of chilled margins, and some contain at least one vein or fracture. Table **T8** provides a description of the collected samples, and appendix Figures AF1–AF79 provide photographs of the whole-round samples taken (see the **"Appendix"**). Additionally, a few background contamination samples were collected for shore-based DNA analysis, including any recovered plastic bags that held the fluorescent microsphere solutions in the core catcher.

In accordance with protocols described in **"Microbiology"** in the "Methods" chapter (Expedition 336 Scientists, 2012a), samples were selected in the core splitting room as quickly as possible after core recovery, following initial discussion with petrologists on sample representation and photographing the sample before it was removed from the core liner. When sample volume permitted, samples were preserved for shore-based DNA and RNA analysis, FISH, cell counting analysis, isotopic analysis, and fluorescent microsphere analysis as well as ship-based culturing and enrichment experiments. Microspheres were used during all coring operations to help in evaluating core contamination. Microsphere density was evaluated in all samples following iterative washing of the exterior of the whole-round samples with sterile seawater. Table **T8** summarizes the results of the microsphere contamination survey, listing whether the microspheres were detected in the first or last of 3–4 total washes with sterilized seawater. Of the 79 hard rock samples collected from Hole U1383C, 30 had microspheres in the first wash but none in the final wash, 19 did not have any detectable microspheres in any wash, and 30 had microspheres in all washes.

Several enrichment and cultivation experiments were started with rock samples collected from Hole U1383C (see **"Microbiology"** in the "Methods" chapter [Expedition 336 Scientists, 2012a]). Carbon-fixation incubations were initiated with several glassy basalt samples: 336-U1383C-13R-2-MBIOB, 19R-1-MBIOA, 20R-1-MBIOA, and 22R-1-MBIOA. Enrichments for carbon- and nitrogen-cycling (carbon fixation, methane oxidation, and nitrate reduction) microorganisms were conducted with samples from 18 different basalt samples. Enrichments for methanogens, sulfate reducers, sulfide oxidizers, and nitrate-reducing iron-oxidizing bacteria were conducted with rocks from several horizons: Samples 336-U1383C-6R-1-MBIOA, 9R-3-MBIOD, 10R-2-MBIOC, 16R-2-MBIOB, 20R-2-MBIOB, 30R-2-MBIOB, and 32R-2-MBIOA. Enrichments for heterotrophic metabolisms will be set up with material from Samples 336-U1383C-13R-2-MBIOB, 19R-1-MBIOA, 20R-1-MBIOA, and 22R-1-MBIOA.

Forty-one samples from Hole U1383C were scanned with the Deep Exploration Biosphere Investigative portable tool (DEBI-pt) deep UV fluorescence instrument for evaluation of microbial and organic carbon, mineral composition, and the presence of fluorescent microsphere contamination controls on the surfaces of rock fragments. Laboratory tests revealed that the fluorescent microspheres (made of polystyrene) used as contamination checks during coring have a distinct fluorescence pattern (Fig. **F27**) when excited by deep UV light. During subsampling of rocks collected from Hole U1383C, care was taken to document the orientation (i.e., exterior and interior) of fragments used for DEBI-pt scanning to enable evaluation of whether microsphere contamination tracers were found on either the exterior or interior of the samples. Of the samples scanned, only two exterior pieces (Samples 336-U1383C-2R-2-MBIOE and 8R-2-MBIOB) showed unequivocal fluorescence patterns consistent with those of microspheres. Other samples contained spectral signatures that had some resemblance to microspheres; however, suspect regions also contained fluorescence from a variety of other sources, precluding definitive identification at that time. All other samples showed varying degrees of microbial and organic carbon abundance. Some samples contained very little microbial fluorescence (e.g., Sample 336-U1383C-6R-1-MBIOA; Fig. **F28**), whereas others had a higher concentration of biomass (e.g., Sample 336-U1383C-26R-1-MBIOA; Fig. **F29**). The majority of fluorescence in the low-biomass Sample 336-U1383C-6R-1-MBIOA (Fig. **F28**) had spectral characteristics consistent with calcium, potassium, and magnesium silicates. A small amount of biomass and other low molecular–weight aromatic hydrocarbons occurred in some of the areas with altered basalt, whereas very little signal was detected in the areas with ochre alteration. In contrast, Sample 336-U1383C-26R-1-MBIOA had a higher degree of organic and microbial fluorescence distributed throughout the scanned region (Fig. **F29**).

# Physical properties

The igneous rocks recovered from Hole U1383C were characterized for physical properties as described in the "Methods" chapter (Expedition 336 Scientists, 2012a). All recovered cores were processed with the Whole-Round Multisensor Logger (WRMSL) for measurements of gamma ray attenuation (GRA) density and magnetic susceptibility (MS). All basement rocks were analyzed for NGR total counts to derive potassium weight percentage. Cores 336-U1383C-15R and 18R were shorter than 50 cm, so no NGR measurements were performed on them. All archive core halves were analyzed for color reflectance and point magnetic susceptibility (MSP).

Twenty-three discrete cube-shaped samples were cut from the working core halves for *P*-wave compressional velocities and moisture and density (MAD) measurements. Discrete samples were taken from sections of the core showing marked differences in alteration intensity. For each sample, we tried to take subsamples with uniform alteration; fractures and veins were avoided as much as possible. For each main lithology, a sample of altered rock and an unaltered specimen were taken, when available.

## Gamma ray attenuation and bulk density

The WRMSL was used to measure magnetic susceptibility and bulk density on the whole-round cores. The GRA measurements are sensitive to gaps and cracks in the material, as well as to underfilled liners and unsaturated samples. Raw data from the WRMSL were filtered to remove underestimated data as described in the "Methods" chapter (Expedition 336 Scientists, 2012a). Briefly, the filter eliminates measurements with a variation in density >0.15 g/cm$^3$ in four consecutive measurements. Hard rock cores generally have a smaller diameter (~58 mm) than the internal diameter of the core liner (66 mm) considered by the instrument. This discrepancy can be corrected by multiplying the system output by $^{66}/_{58}$ = 1.138 (Jarrard and Kerneklian, 2007). The pieces recovered from Hole U1383C were generally smaller in diameter than the ones recovered from Hole U1382A. This is reflected in the reduced number of data points left after filtering. The basalt recovered from Hole U1383C also exhibits a higher extent and more variable alteration than basalt from Hole U1382A. These differences are reflected in the GRA measurements, which present a larger range than those for Hole U1382A. The GRA bulk density values range from 1.55 to 3.15 g/cm$^3$, however, both extremes of this range should be used with caution because values for rocks having a diameter smaller than 58 mm are underestimated and those for rocks with an uncommonly large diameter may be overestimated. All MAD bulk density values lie within the range obtained by GRA density (Fig. F30). The average value obtained for GRA bulk density is 2.71 ± 0.02 g/cm$^3$.

## Magnetic susceptibility

The raw MS data obtained from the WRMSL were filtered on the basis of the GRA data because both sensors are installed on the same track and have a similar range of detection (Fig. F31). The filtering helps ensure that unrepresentative values from piece ends and cracks are eliminated from the final data. MS data were also corrected for the diameter of the core (58 mm for hard rock and 66 mm for sediment) based on the equation given by the manufacturer (see MS2 Magnetic Susceptibility System operation manual, www.bartington.com/operation-manuals.html). The correction factor applied for the igneous sections was 1.012. However, this measurement assumes that the core liner is filled and does not take into consideration the gaps between samples; because this assumption is rarely correct for hard rock cores, the values measured need to be considered as minimums.

The MSP sensor is installed on the same track as the color reflectance spectroscopy sensor, and MSP data were filtered using the same criteria as those for color reflectance as explained in the "Methods" chapter (Expedition 336 Scientists, 2012a). No correction was applied after filtering the measured data. Both whole-round and point magnetic susceptibility measurements present similar peaks, with a maximum (MSP = 1391 × 10$^{-5}$ SI, MS = 905 × 10$^{-5}$ SI) located at ~145.4 mbsf in lithologic Unit 2, corresponding to a massive basalt flow (Fig. F31). A second and subordinate peak (MS = 669 × 10$^{-5}$ SI, MSP = 980 × 10$^{-5}$ SI) was found at ~139.4 mbsf, corresponding to another basalt flow in lithologic Subunit 2-1. Numerous smaller peaks were identified on the basis of MSP data. The magnetic susceptibility sensor in the whole-round track did not detect all of these peaks.

## Natural gamma radiation

NGR total counts and potassium concentration data obtained from the Natural Gamma Radiation Logger (NGRL) are summarized in Figure F32. Count time for each core section (2 h) was maximized to increase the resolution of the data obtained. The total counts per second represent all of the radioactive elements detected by the system. Spectral data were recorded, and the counts per second for each channel indicate the abundance of a particular element. When these values are related to a radioactive standard with known composition, the concentration of the element in the core section can be calculated. The total

counts from the whole rounds range from 0.65 to 4.63 cps once the background is subtracted (Fig. F32). Potassium concentration was calculated by using GRA bulk density as the effective density for the corrections.

Shipboard analyses of bulk rock composition by inductively coupled plasma–atomic emission spectrometry (ICP-AES) obtained potassium concentrations similar to the NGR data collected (Fig. F32). NGR potassium concentrations are in the range of 0.1–0.46 wt%, with an average of 0.19 ± 0.05 wt%. Potassium concentrations from ICP-AES range from 0.11 to 0.25 wt%, with an average of 0.16 ± 0.05 wt%. These results document a marked variability in potassium concentrations for all samples from Hole U1383C. In general, uranium and thorium concentrations detected by NGR are very low in basalt (Fig. F32), but they are higher than those detected in rocks from Hole U1382A. The main contributor to total gamma ray counts is $^{40}$K.

NGR potassium concentrations and total counts per second do not show any major trends or differences with depth. This was also observed by the downhole logging tools (Fig. F33). However, potassium concentrations measured in the cores are lower than those obtained from downhole logging.

## Moisture and density

Results of measurements of bulk density, dry density, grain density, void ratio, and porosity on 23 discrete samples are presented in Table T9. These values were determined using Method C (see "Physical properties" in the "Methods" chapter [Expedition 336 Scientists, 2012a]). Samples were chosen to be representative of the different levels of alteration in the lithologic units. Thin sections were taken in areas adjacent to the areas used for physical properties measurements in order to identify relationships with petrographic properties. The extent of alteration estimated for thin sections (thin section number indicated, see "Petrology, alteration, structural geology, and hard rock geochemistry" in the "Methods" chapter [Expedition 336 Scientists, 2012a] for more information) from adjacent pieces is presented in Table T9. This wide range is in agreement with the large spread in density data. Average bulk density from discrete samples ranges from 2.43 to 2.90 g/cm$^3$ (Fig. F30). Dry density values range from 2.26 to 2.87 g/cm$^3$, and grain densities vary between 2.71 and 2.96 g/cm$^3$. Porosity ranges from 1.87% for to 16.61%, and the void ratio varies between 0.02 and 0.20. Strong correlations were found between porosity and bulk density and *P*-wave velocity (Fig. F34). The relationships between porosity, alteration intensity, and LOI data are shown in Figure F35. The presence of particular secondary minerals (e.g., carbonates) may explain some of the scatter in the relationship between porosity and LOI and alteration degree, but further studies are needed to resolve this. The percentage of vesicles in basalt from Hole U1383C is low and is not considered to play a major role on porosity for these rocks (see "Petrology and hard rock geochemistry" for values on vesicularity). The MAD values obtained are within the range of values found in the literature for basalt from the Mid-Atlantic Ridge near 37°N (Hyndman and Drury, 1976).

## Compressional *P*-wave velocity

All of the discrete samples were used to determine the compressional *P*-wave velocity of the main lithologic units. *P*-wave velocities were measured along the three axes (*x, y,* and *z*) in oriented cube-shaped samples. In nonoriented samples, only *x*-axis velocities were measured. All samples were measured three times. Measurements were done as quickly as possible for each saturated sample to avoid desiccation of the sample, which would affect the measured *P*-wave velocity. A summary of these measurements is presented in Figure F36. *P*-wave velocity shows a good direct correlation with bulk density and an inverse correlation with porosity determined by MAD measurements (Fig. F34).

The mean value for *P*-wave velocity measurements ranges from 4741 to 7631 m/s along the *x*-axis. Along the *y*-axis, the measurements range from 4749 to 7064 m/s, and along the *z*-axis, the *P*-wave measurements range from 4825 to 6983 m/s. A summary of all averaged values for each sample is presented in Table T9. The mean *P*-wave velocity values correlate strongly with porosity and bulk density values (Fig. F34). Low values seem to be consistent with an elevated degree of alteration of the samples. The values obtained for *P*-wave velocities of Hole U1383C fresh basalt samples are within the range of values found in the literature for basalt of the Mid-Atlantic Ridge (Hyndman and Drury, 1976; Miller and Christensen, 1997; Johnson and Semyan, 1994).

Two samples (336-U1383C-10R-2W, 10–12 cm, and 28R-1W, 40–42 cm) seem to present some anisotropy (standard deviation = 498 and 119 m/s, respectively) when *P*-wave tests were done on three axes. These samples correspond to avesicular plagioclase-olivine-phyric basalt and aphyric basalt, respectively.

## Thermal conductivity

Thirty measurements were taken on archive pieces longer than 6 cm (Fig. F37). The uneven distribution of samples within the recovered section is the result

of the limited availability of samples of the right size. Most of the samples have similar values (1.680 ± 0.056 W/[m·K]). Three samples, located at ~78.11, ~87.65, and ~313.15 mbsf, have lower thermal conductivity values (1.410 ± 0.004 W/[m·K] for the first two depths and 1.435 ± 0.003 W/[m·K] for the last depth). The samples with lower thermal conductivity correspond to pieces with high presence of veins.

### Color reflectance spectroscopy

Color reflectance L* for Hole U1383C varies between 11.90% and 66.50%, with a mean of 37.48% ± 4.49% (Table **T10;** Fig. **F38**). In general, basalt reflectance values are homogeneous, without pronounced differences between cores (Fig. **F38**). The values of a* and b* close to zero reflect the dark color of the basalt. The higher values obtained for L* (>50) and the outliers represented in the tristimulus scale indicate the presence of sedimentary breccia. Color reflectance was not measured in small pieces and fragments because of the lack of flat surfaces (see **"Physical properties"** in the "Methods" chapter [Expedition 336 Scientists, 2012a]). Altered pieces have positive b* values, contrasting with the negative b* values obtained in fresh basalt pieces (Fig. **F39**).

## Downhole logging

Downhole logging measurements obtained from Hole U1383C include total and spectral natural gamma ray, density, compressional velocity, electrical images, and deep UV–induced fluorescence. An open-hole section of 274.47 m was logged with two tool strings (Figs. **F40, F41**) over a period of ~22.5 h. The borehole remained in good condition throughout logging, and no obvious tight spots were encountered in open hole.

### Logging operations

Downhole logging of Hole U1383C started on 3 November 2011 at 0025 h (all times are ship local, UTC – 3 h) after RCB coring ended at a total depth of 331.5 m core depth below seafloor (CSF). A summary of logging operations is presented in Table **T11;** see **"Operations"** for full operational details on hole preparation for logging.

Two tool strings were deployed in Hole U1383C: (1) the AMC II and (2) the FMS-DSI (FMS-sonic). The AMC II tool string included the standard logging equipment head-q tension (LEH-QT) (cablehead), the Enhanced Digital Telemetry Cartridge (EDTC; with total gamma ray measurement), the HLDS, the Lamont Multifunction Telemetry Module (MFTM), and the DEBI-t (for tool string details, see **"Downhole logging"** in the "Methods" chapter [Expedition 336 Scientists, 2012a]) (Fig. **F40**). The AMC II was lowered into the borehole at 0255 h on 3 November. The wireline heave compensator (WHC) was optimized with the AMC II in open hole at 4510.1 m wireline log depth below rig floor (WRF). The AMC II completed a downlog to a total depth of 4750.1 m WRF (~7 m above the bottom of the hole [drillers depth]; note that we deliberately did not tag bottom with the DEBI-t), an uplog to 4486.5 m WRF, a second downlog to 4751.4 (tagged bottom), and a final uplog that terminated at 4412.8 m WRF after logging the seafloor. The AMC II tool string was rigged down by 1310 h.

The second tool string deployed was the standard FMS-sonic tool string, which was composed of the HNGS, the DSI, the General Purpose Inclinometry Tool (GPIT), and the FMS (Fig. **F41**). The FMS-sonic tool string was lowered into the hole at 1410 h on 3 November and reached the bottom of the borehole (4757.1 m WRF) at 1746 h, following logging down from the seafloor. The FMS-sonic tool string performed two successful full passes of the hole and was returned to the surface and rigged down at 2245 h on 3 November, at which time logging operations in Hole U1383C were completed.

### Data processing and quality assessment

The logging data were recorded on board the R/V *JOIDES Resolution* by Schlumberger and archived in Digital Log Interchange Standard (DLIS) format. Data were sent via satellite transfer to shore, processed, and transferred back to the ship for archiving in the shipboard database. Processing and data quality notes are given below. The DEBI-t data recorded to SD memory card (video and full systems and fluorescence data in binary format) were also sent via satellite for archiving; however, data conversion and depth matching of the DEBI-t to the other standard final depth-matched log data were done on board (see **"Downhole logging"** in the "Methods" chapter [Expedition 336 Scientists, 2012a]).

Depth shifts were applied to the logging data by selecting a reference (base) log (usually the total gamma ray log from the run with the greatest vertical extent and no sudden changes in cable speed) and aligning features in equivalent logs from other tool string passes by eye. In the case of Hole U1383C, the base log was the gamma ray profile from the second uplog of the AMC II tool string. The original logs were first shifted to the seafloor (4421.5 m WRF), which was determined by the step in gamma ray values. This depth did not differ markedly from the seafloor depth given by the drillers (4 m difference).

Proper depth shifting of wireline logging depths relative to core depths was essential to correlate the downhole logging data with all other measurements and observations made on core recovered from Hole U1383C. The seafloor was the only target that offered a potential wireline logging depth reference. However, note that data acquired through the seafloor resulted from logging through the BHA and casing, so data from this interval are of poor quality and highly attenuated and should be used only qualitatively. However, the data are adequate to help pick the seafloor. The quality of wireline logging data was assessed by evaluating whether logged values are reasonable for the lithologies encountered and by checking consistency between different passes of the same tool. Specific details of the depth adjustments required to match logging runs/data are available in the logging processing notes in the log database for Hole U1383C (**iodp.ldeo.columbia.edu/DATA/**).

A wide (>30.5 cm) or irregular borehole can affect most log data, particularly measurements taken with tools like the HLDS (bulk density) that require decentralization and good contact with the borehole wall. The density log correlates well with the velocity and apparent resistivity logs but is largely affected by hole conditions. Hole diameter was recorded by the hydraulic caliper on the HLDS tool (LCAL) and by the FMS calipers (C1 and C2) (Fig. **F42**). Both calipers showed a very reasonable hole with a diameter ranging from 23.3 to 48.2 cm and averaging 31.5 cm (LCAL data). The main breakouts were observed in the upper portion of the hole at ~60–130 and ~154–165 m wireline log matched depth below seafloor (WMSF); however, only certain sections in the uppermost depth range were out of the range of the FMS caliper arms (38.1 cm diameter). Good repeatability was observed between the two downlogs and two uplogs of the AMC II and the two passes of the FMS-sonic, particularly for measurements of compressional velocity and bulk density.

Bulk density (HLDS) data were recorded with a sampling rate of 197 measurements per minute (2.54 cm at 300 m/h), in addition to the standard sampling rate of 32 measurements per minute (15.24 cm at 300 m/h). The enhanced bulk density curve is the result of the Schlumberger enhanced processing technique performed on the MAXIS system on board the *JOIDES Resolution*. In normal processing, short-spaced data are smoothed to match long-spaced data (depth and resolution matched). In enhanced processing, the raw detail obtained from the short-spaced data is added to the standard compensated density (Flaum et al., 1987). In a situation where there is good contact between the HLDS pad and the borehole wall (low density correction), the results are improved because the short spacing has better vertical resolution (i.e., it has the capability to resolve thinner beds/units).

The DSI was operated in the following modes: P&S monopole, upper and lower dipole, and Stoneley for both Pass 1 and Pass 2 (all with standard frequency). The slowness data from DTCO and DTSM (Table **T6** in the "Methods" chapter [Expedition 336 Scientists, 2012a]) are of good quality for these passes and were thus converted to acoustic velocities (VELP and VELS, respectively) (for a full list of acronyms, see **"Downhole logging"** in the "Methods" chapter [Expedition 336 Scientists, 2012a]). Postexpedition reprocessing of the original sonic waveforms is highly recommended to obtain more reliable velocity results.

The FMS images are of good quality over the majority of the hole; the only images that should be treated with caution are those taken where the main borehole breakouts are located (see above) because the pad may not have maintained good contact with the borehole wall.

## Preliminary results

Downhole logging measurements obtained from Hole U1383C include natural total and spectral gamma ray, density, apparent electrical resistivity, and deep UV–induced fluorescence. The results are summarized below.

### Density

Density ranges from 1.10 to 3.12 g/cm$^3$ (average = 2.40 g/cm$^3$) in Hole U1383C (Fig. **F42**). A comparison between discrete physical properties samples and the downhole density log shows relatively good agreement (average values measured on the cores range between 2.43 and 2.90 g/cm$^3$). Low density values correspond to intervals with larger borehole dimensions and sections that exhibit much lower acoustic velocities (Fig. **F42**). Considerably variable density values in the upper portion of the open hole (~60–130 m WMSF) occur where the borehole is much more irregular (log Units I and II; see **"Log units"**) and correspond to nonvesicular to sparsely vesicular aphyric to sparsely phyric basalt pillow lava in lithologic Unit 1. Bulk density values vary throughout Hole U1383C; however, density generally increases with depth.

### Gamma ray measurements

Standard, computed, and individual spectral contributions from $^{40}$K, $^{238}$U, and $^{232}$Th were part of the gamma ray measurements obtained in Hole U1383C with the HNGS and the EDTC (total gamma ray only) (see Table **T6** in the "Methods" chapter [Expedition 336 Scientists, 2012a]). The total gamma ray

measurements through the BHA (pipe to ~52 mbsf) and casing show two main anomalies from the seafloor to ~59 m WMSF (where casing was set) (Figs. F42, F33).

Basaltic oceanic crust typically has low gamma ray intensities (e.g., Bartetzko et al., 2001; Barr et al., 2002), and the lithologic units penetrated and logged in Hole U1383C follow this trend. Total spectral gamma ray (HSGR) values obtained in Hole U1383C range from 0.01 to 20.21 gAPI and average 6.55 gAPI. Potassium values are relatively low and range from 0 to 0.66 wt%, with an average value of 0.26 wt% (Fig. F33). These values agree well with NGR measured on the whole-round cores (0.1–0.46 wt%; average = 0.19 wt%; see "Physical properties") and values obtained using geochemical analysis (0.11–0.25 wt%) (see "Hard rock geochemistry"). Uranium concentrations average 0.16 ppm and have a maximum value of 1.02 ppm. Thorium concentrations average 0.16 ppm and reach a maximum value of 1.40 ppm.

The gamma ray data collected in Hole U1383C do not exhibit any particular trends, in contrast to Holes 395A and U1382A, which are eruptive sequences that exhibit distinctive uphole-increasing gamma ray intensity. The overall trend in the gamma ray data from Hole U1383C seems be dominated by the influence of potassium.

## Elastic wave velocity

Compressional wave velocity ($V_P$) ranges from 2.62 to 6.45 km/s, with data collected downhole generally exhibiting much lower velocities than those collected on discrete physical properties cubes (Fig. F42). There is a clear relationship between $V_P$ and density (and apparent resistivity); $V_P$ is higher where density (and apparent resistivity) is higher. The lowest $V_P$ values can be related to the pillow basalts in lithologic Unit 1 (log Unit II; see "Log units"), whereas the highest $V_P$ values correspond to a section of more massive basalt units (visible in FMS data) associated with lithologic Unit 2 (log Unit III). Compressional wave velocity measured on discrete samples taken from the core (values range from 4.74 to 7.63 km/s) does not correlate that well with downhole logging data. However, velocity values obtained by downhole logging give an overall value for the formation measured, including fractures and basalt and matrix (e.g., hyaloclastite) mixtures, and are therefore generally lower.

## Fluorescence

The fluorescence spectrum for Hole U1383C is uniform throughout the borehole except below ~290 m WMSF, where it was likely influenced by drilling mud (sepiolite). The structure of the fluorescence pattern is much different from the spectra collected in the previous holes and is not consistent with bacterial signatures, although there does appear to be a spectral feature consistent with a sporelike signal. The 455 nm band showed the highest degree of variability, particularly during the uplogs, when the calipers were deployed. This may reflect changing lithology as the upper fluorescence bands in DEBI-t will respond to aluminosilicates with high amounts of K, Na, and Mg. Additionally, in the lowermost 50 m of the hole, signal intensities for Hole U1383C are lower than those observed in the previous two holes measured (Fig. F43).

At ~40 m above the base of the borehole (~290 m WMSF), the signal intensity of the 455 nm band increases significantly (Fig. F44), most likely because of the presence of sepiolite at the bottom of Hole U1383C. It may be that the high signal count is due to both the fluorescence intensity and the reflectivity of the sepiolite. This possibility is corroborated by video data from the DEBI-t, which shows the instrument going from a cleaner environment into a very cloudy, highly reflective environment. As the tool string ascended, the high intensity of the 455 nm band decreased after the 280 m WMSF mark (Fig. F45). The video log also indicates that the hole was not as clean as Hole U1382A because particulates consistent with sepiolite and cement were present throughout the hole. Additionally, uplog video data show an increase in the amount of large particulates in the water compared to the downlog video data. This finding can most easily be explained by the fact that the caliper arm was extended during the uplog, causing it to scrape and break up the cement.

## Apparent electrical resistivity measurements

No resistivity sonde was run on the AMC II tool string; however, in order to obtain a qualitative idea of electrical resistivity or apparent electrical resistivity, an average value of very shallow penetrating conductivity from the four FMS pads was obtained during log processing, and the reciprocal of this value was plotted (Fig. F42). Normally, to make a resistivity measurement, a logging tool (e.g., the Dual Induction Tool) creates a voltage between a pair of electrodes and measures the current flowing between them. Provided that the current path is controlled (usually by focusing electrodes), the conductance measured (current/applied voltage) can be converted to a measure of the average conductivity or resistivity of the formation through which the current flows. The microresistivity buttons are not designed to measure resistivity because the button current is not focused or calibrated. However, the response of a

microresistivity button, albeit uncalibrated, normally moves in the same direction as formation conductivity. The data calculated from the FMS pad averages, referred to here as apparent resistivity, agree well with both density and compressional velocity. In regions of high velocity and density, high apparent resistivity (log Unit III; see "Log units") is also present, and there is an overall subtle trend of increasing apparent resistivity with depth.

## Log units

Preliminary interpretation of the downhole log data divided Hole U1383C into a number of log units (Fig. F42). Log units were defined only below the casing (~60 m WMSF) in the open-hole section and were characterized using gamma ray, density, compressional velocity, and apparent resistivity.

Five main log units were qualitatively identified in the open-hole section of Hole U1383C (Fig. F42):

Log Unit I (~60–94 m WMSF) exhibits some of the lowest gamma ray intensities, with a subtle decrease downhole. Some small zones of higher gamma ray may correspond to more altered formations. Gamma ray values range between 4 and 12 gAPI. Bulk density values are highly variable throughout this unit, ranging between 1.25 and 2.75 g/cm$^3$. Borehole diameter is also highly variable, with some areas of washout present where there is a transition from the end of the rathole into a fractured formation. Apparent resistivity values follow a very similar trend as density but show three main areas of increased resistivity at ~80, 88, and 93 m WMSF. Compressional velocity shows an arching trend, with upper unit values of ~4 km/s (~60 m WMSF), moving to lower values of ~3.5 km/s (~75 m WMSF), and then finally increasing to ~4.5 km/s at the base of log Unit I. This log unit correlates to lithologic Unit 1 and relates to nonvesicular to sparsely vesicular aphyric to sparsely phyric pillow lava with intercalated limestone.

Log Unit II (~94–132 m WMSF) exhibits slightly higher, though relatively constant, gamma ray values. Values cluster around 7 gAPI, with the exception of a peak at ~121 m WMSF (which relates to a very conductive section in the FMS electrical images). The borehole caliper is highly variable over the entirety of this log unit, and, in keeping, so are the density values. Just as in the preceding log unit, density values have a wide range between 1.1 and 2.8 g/cm$^3$; however, there is a shift to lower density values at the top of this unit. There is an overall trend of increasing density with depth downhole in this log unit. Apparent resistivity shows a similar trend as density in that there is a decrease in values at the top of the log unit compared to the previous unit and a very slight increase with depth throughout. Acoustic velocity values also show a shift to lower values at the top of the unit. Values range between 3 and 5.5 km/s and, like density and apparent resistivity, show a slight downhole-increasing trend. Log Unit II corresponds to the lower portion of lithologic Unit 1, which is nonvesicular to sparsely vesicular aphyric to sparsely phyric pillow lava. However, FMS imagery shows more frequent conductive zones in the upper portion of this log unit compared to log Unit I (relating to fractured and altered materials) and hence slightly higher gamma ray values and lower density, apparent resistivity, and velocity values. The conductive zones in this unit become slightly less pervasive with depth downhole, which is reflected in the subtle increasing trend in density, apparent resistivity, and velocity.

Log Unit III (~132–153 m WMSF) has relatively stable values for gamma ray intensities (centered around 6.5 gAPI) compared to log Units I and II. It also features some of the highest density (3.2 g/cm$^3$), resistivity, and acoustic velocity (6.25 km/s) values measured in this hole. This interval represents a section of sparely vesicular plagioclase-olivine-phyric basalt sheet to massive flow (lithologic Unit II). Additionally, the borehole is in gauge in this region and therefore has excellent FMS imagery that shows a zone of high resistivity and a fracture pattern indicative of a massive flow unit.

Log Unit IV (~153–166 m WMSF) is characterized by a significant drop in density (values around 2.4 g/cm$^3$), apparent resistivity, and velocity (values around 3.5 km/s) and an increase in gamma ray intensity. Additionally, gamma ray intensities are marginally higher than in log Unit III and show a slight increase in intensity with depth. It is possible that this log unit reflects the interpillow/flow sediments and tectonic breccias that were observed in core from this interval (see "Petrology and hard rock geochemistry"). FMS electrical imagery shows an area of very conductive material containing a low proportion of high-resistivity layers and clasts.

Log Unit V (~166–327 m WMSF) exhibits relatively uniform values for density, apparent resistivity, and velocity. Gamma ray intensities have much more structure downhole in this unit, particularly in log Unit V Zones A and B, where higher intensities are present. Log Unit V Zone C shows an area of decreased density, apparent resistivity, and acoustic velocity. There is an overall trend, albeit very subtle, of increasing density, apparent resistivity, and acoustic velocity with depth. Lithologic Unit 3, comprising nonvesicular aphyric pillow lava, relates to this log unit. FMS imagery shows a slight increase in resistive formation with depth. Additionally, electrical images show Zone A to be associated with a very conductive

band that may be a large empty fracture or a unit of material with elevated alteration and higher porosity. Zone B also shows a number of thin bands of high conductivity that may relate to empty or filled fractures within more resistive material. Zone C relates to a highly conductive region with relatively small clasts of resistive material (likely basalt). Zones A and B correspond to intervals of high abundance of hyaloclastite in the core. The hyaloclastites are more altered than the basalt flows, and this variability may account for the increased range in gamma ray intensities in this interval.

### Electrical images

In Hole U1383C, we also acquired FMS electrical resistivity images (Figs. **F46**). The quality of electrical resistivity image measurements depends on close contact between the measuring pads on the tool and the borehole wall. The FMS borehole images collected in Hole U1383C are of very good quality; however, sections of the borehole were not in gauge, and in these sections (~60–77, ~71–76, ~96–102, ~108–115, ~118–130, and ~153–166 m WMSF) the quality of the images is diminished.

FMS imagery provides essential information—especially because core recovery in Hole U1383C was only 19%. Using FMS imagery and other log data, we can fill the data gap in the core record, providing a continuous record downhole. Figure **F42** shows divisions of units based on FMS images over the entire section. It is not possible to determine the petrology of the lithology, but the structural and textural make-up is clear.

The FMS images highlight some of the key units observed in core recovered from Hole U1383C (Fig. **F46**), including more massive flow units, pillow basalts, fractured sections, and potential sedimentary horizons. However, perhaps more importantly, the FMS images help refine lithologic boundaries when contacts were not recovered in the core. Another strength of FMS imagery is the fact that the images are oriented to geographic north (using the GPIT), and by picking sinusoidal traces on the images one can obtain important oriented structural information for key boundaries, fractures, and other features of interest. It is possible to differentiate between picked fractures (be they conductive or resistive) and boundaries or pronounced fractures in the lava flows. Structural studies are a key part of postexpedition research. Such structural picks can aid overall interpretation of the lithologic sequence observed in the core and be used to orient observed structures and produce a stress regime model for the drilled formation.

One of our key scientific aims is to integrate core and log measurements, observations, and interpretations. The FMS data permit integration of core observations and images by constraining the location of recovered core pieces when recovery is low; depth uncertainty for core pieces in low recovery can be as high as 9.6 m. Before the cores were split, images of the external surfaces of the whole-round cores were taken on the line-scan imager. These images were mosaicked together so that an attempt could be made to find the piece in the FMS images. Additional time will be spent postexpedition trying to line up some of these core images from formations recovered from Hole U1383C; however, compared to those from Hole U1382A, the recovered pieces are of much shorter length and hence likely more difficult and time consuming to place.

## Packer experiments

Drill string packer experiments were attempted in Hole U1383C with the intent of assessing the transmissivity and average permeability of open-hole zones bounded by the bottom of the hole at 331.5 mbsf and three different packer inflation seats: (1) in casing about 7 m above the casing shoe at 60.4 mbsf; (2) at 141 mbsf, centered in the massive flow boundary between lithologic Units 1 and 2, and (3) at 197 mbsf, near the top of lithologic Unit 3. The open-hole packer seats were chosen primarily on the basis of caliper log data that were quite consistent with the lithologic division into major units. At each packer seat, the plan was to inflate the single-element packer, monitor the difference between hydrostatic pressure and sealed hole pressure, and then conduct two constant-rate injection tests of 1 h duration each. However, the experiments failed at all three seats. At the seat within casing, the packer would not hold inflation because of the effect of heave and the slick inner diameter of the casing, as occurred in Hole 1382A (see **"Packer experiments"** in the "Site U1382" chapter [Expedition 336 Scientists, 2012b]). At the first open-hole seat (141 mbsf), the packer apparently seated and the injection test sequence was performed, but when the go-devil was recovered hours later, the downhole pressure data showed almost no response (Fig. **F47**). When the packer was moved to the second open-hole seat (197 mbsf), it would not hold inflation pressure or seat against the borehole wall, so the packer experiments were terminated.

When the BHA was recovered, the upper end of the inflation element was observed to have been peeled back around nearly the full circumference; in this condition it was incapable of holding inflation pressure or sealing the zone beneath the packer, which explains the inability to hold inflation pressure at

the second open-hole seat, as well as the lack of apparent formation response during the test sequence at the first open-hole seat. The damage probably happened during the move from the seat in casing to the first open-hole seat, possibly when the packer hung up on a ledge at ~100 mbsf (see **"Operations"**).

## References


Alt, J.C., Teagle, D.A.H., Laverne, C., Vanko, D.A., Bach, W., Honnorez, J., Becker, K., Ayadi, M., and Pezard, P.A., 1996. Ridge-flank alteration of upper ocean crust in the eastern Pacific: synthesis of results for volcanic rocks of Holes 504B and 896A. *In* Alt, J.C., Kinoshita, H., Stokking, L.B., and Michael, P.J. (Eds.), *Proc. ODP, Sci. Results,* 148: College Station, TX (Ocean Drilling Program), 435–450. **doi:10.2973/odp.proc.sr.148.150.1996**

Barr, S.R., Révillon, S., Brewer, T.S., Harvey, P.K., and Tarney, J., 2002. Determining the inputs to the Mariana Subduction Factory: using core-log integration to reconstruct basement lithology at ODP Hole 801C. *Geochem., Geophys., Geosyst.,* 3(11):8901–8925. **doi:10.1029/2001GC000255**

Bartetzko, A., Pezard, P., Goldberg, D., Sun, Y.-F., and Becker, K., 2001. Volcanic stratigraphy of DSDP/ODP Hole 395A: an interpretation using well-logging data. *Mar. Geophys. Res.,* 22(2):111–127. **doi:10.1023/A:1010359128574**

Bougault, H., Treuil, M., and Joron J.L., 1979. Trace elements in basalts from 23°N and 36°N in the Atlantic Ocean: fractional crystallization, partial melting, and heterogeneity of the upper mantle. *In* Melson, W. G., Rabinowitz, P. D., et al., *Init. Repts. DSDP,* 45: Washington, DC (U.S. Govt. Printing Office), 493–506. **doi:10.2973/dsdp.proc.45.122.1979**

Brewer, T.S., Bach, W., and Furnes, H., 1996. Geochemistry of lavas from Hole 896A. *In* Alt, J.C., Kinoshita, H., Stokking, L.B., and Michael, P.J. (Eds.), *Proc. ODP, Sci. Results,* 148: College Station, TX (Ocean Drilling Program), 9–19. **doi:10.2973/odp.proc.sr.148.101.1996**

Dunham, R.J., 1962. Classification of carbonate rocks according to depositional texture. *In* Ham, W.E. (Ed.), *Classification of Carbonate Rocks.* AAPG Mem., 1:108–121.

Edwards, K.J., Wheat, C.G., Orcutt, B.N., Hulme, S., Becker, K., Jannasch, H., Haddad, A., Pettigrew, T., Rhinehart, W., Grigar, K., Bach, W., Kirkwood, W., and Klaus, A., 2012. Design and deployment of borehole observatories and experiments during IODP Expedition 336, Mid-Atlantic Ridge flank at North Pond. *In* Edwards, K.J., Bach, W., Klaus, A., and the Expedition 336 Scientists, *Proc. IODP,* 336: Tokyo (Integrated Ocean Drilling Program Management International, Inc.). **doi:10.2204/iodp.proc.336.109.2012**

Expedition 336 Scientists, 2012a. Methods. *In* Edwards, K.J., Bach, W., Klaus, A., and the Expedition 336 Scientists, *Proc. IODP,* 336: Tokyo (Integrated Ocean Drilling Program Management International, Inc.). **doi:10.2204/iodp.proc.336.102.2012**

Expedition 336 Scientists, 2012b. Site U1382. *In* Edwards, K.J., Bach, W., Klaus, A., and the Expedition 336 Scientists, *Proc. IODP,* 336: Tokyo (Integrated Ocean Drilling Program Management International, Inc.). **doi:10.2204/iodp.proc.336.104.2012**

Fisk, M.R., Giovannoni, S.J., and Thorseth, I.H., 1998. Alteration of oceanic volcanic glass: textural evidence of microbial activity. *Science,* 281(5379):978–980. **doi:10.1126/science.281.5379.978**

Flaum, C., Galford, J.E., and Hastings, A., 1987. Enhanced vertical resolution processing of dual detector gamma-gamma density logs. *Trans. SPWLA Annu. Logging Symp.,* 28.

Honnorez, J., 1972. La palagonitisation: l'alteration sous-marine du verre volcanique basique de Palagonia (Sicile) [Palagonitization: the submarine alteration of basic volcanic glass in Palagonia, Sicily]. *Publ. Vulkaninst. Immanuel Friedlaender,* 9.

Hyndman, R.D., and Drury, M.J., 1976. The physical properties of oceanic basement rocks from deep drilling on the Mid-Atlantic Ridge. *J. Geophys. Res., [Solid Earth],* 81(23):4042–4052. **doi:10.1029/JB081i023p04042**

Jarrard, R.D., and Kerneklian, M.J., 2007. Data report: physical properties of the upper oceanic crust of ODP Site 1256: multisensor track and moisture and density measurements. *In* Teagle, D.A.H., Wilson, D.S., Acton, G.D., and Vanko, D.A. (Eds.), *Proc. ODP, Sci. Results,* 206: College Station, TX (Ocean Drilling Program), 1–11. **doi:10.2973/odp.proc.sr.206.011.2007**

Johnson, H.P., and Semyan, S.W., 1994. Age variation in the physical properties of oceanic basalts: implications for crustal formation and evolution. *J. Geophys. Res., [Solid Earth],* 99(B2):3123–3134. **doi:10.1029/93JB00717**

Juteau, T., Bingöl, F., Noack, Y., Whitechurch, H., Hoffert, M., Wirrmann, D., and Courtois, C., 1979. Preliminary results: mineralogy and geochemistry of alteration products in Leg 45 basement samples. *In* Melson, W.G., Rabinowitz, P.D., et al., *Init. Repts. DSDP,* 45: Washington, DC (U.S. Govt. Printing Office), 613–645. **doi:10.2973/dsdp.proc.45.138.1979**

Miller, D.J., and Christensen, N.I., 1997. Seismic velocities of lower crustal and upper mantle rocks from the slow-spreading Mid-Atlantic Ridge, south of the Kane Transform Zone (MARK). *In* Karson, J.A., Cannat, M., Miller, D.J., and Elthon, D. (Eds.), *Proc. ODP, Sci. Results,* 153: College Station, TX (Ocean Drilling Program), 437–454. **doi:10.2973/odp.proc.sr.153.043.1997**

Natland, J.H., 1979. Crystal morphologies in basalts from DSDP Site 395, 23°N, 46°W, Mid-Atlantic Ridge. *In* Melson, W.G., Rabinowitz, P.D., et al., *Init. Repts. DSDP,* 45: Washington, DC (U.S. Govt. Printing Office), 423–445. **doi:10.2973/dsdp.proc.45.118.1979**

Orcutt, B.N., Barco, R.A., Joye, S.B., and Edwards, K.J., 2012. Summary of carbon, nitrogen, and iron leaching characteristics and fluorescence properties of materials considered for subseafloor observatory assembly. *In* Edwards, K.J., Bach, W., Klaus, A., and the Expedition 336 Scientists, *Proc. IODP,* 336: Tokyo (Integrated Ocean Drilling Program Management International, Inc.). **doi:10.2204/iodp.proc.336.108.2012**

Plank, T., Ludden, J.N., Escutia, C., et al., 2000. *Proc. ODP, Init. Repts.,* 185: College Station, TX (Ocean Drilling Program). **doi:10.2973/odp.proc.ir.185.2000**

Rhodes, J.M., Blanchard, D.P., Dungan, M.A., Rodgers, K.V., and Brannon, J.C., 1979. Chemistry of Leg 45 basalts. *In* Melson, W.G., Rabinowitz, P.D., et al., *Init. Repts. DSDP,* 45: Washington, DC (U.S. Govt. Printing Office), 447–459. **doi:10.2973/dsdp.proc.45.119.1979**

Wheat, C.G., Jannasch, H.W., Kastner, M., Hulme, S., Cowen, J., Edwards, K.J., Orcutt, B.N., and Glazer, B., 2011. Fluid sampling from oceanic borehole observatories: design and methods for CORK activities (1990–2010). *In* Fisher, A.T., Tsuji, T., Petronotis, K., and the Expedition 327 Scientists, *Proc. IODP,* 327: Tokyo (Integrated Ocean Drilling Program Management International, Inc.). **doi:10.2204/iodp.proc.327.109.2011**

**Publication:** 16 November 2012
**MS 336-105**

**Figure F1.** Schematic of reentry cone and casing installed in Hole U1383B. CORK = subseafloor borehole observatory. csg = casing.

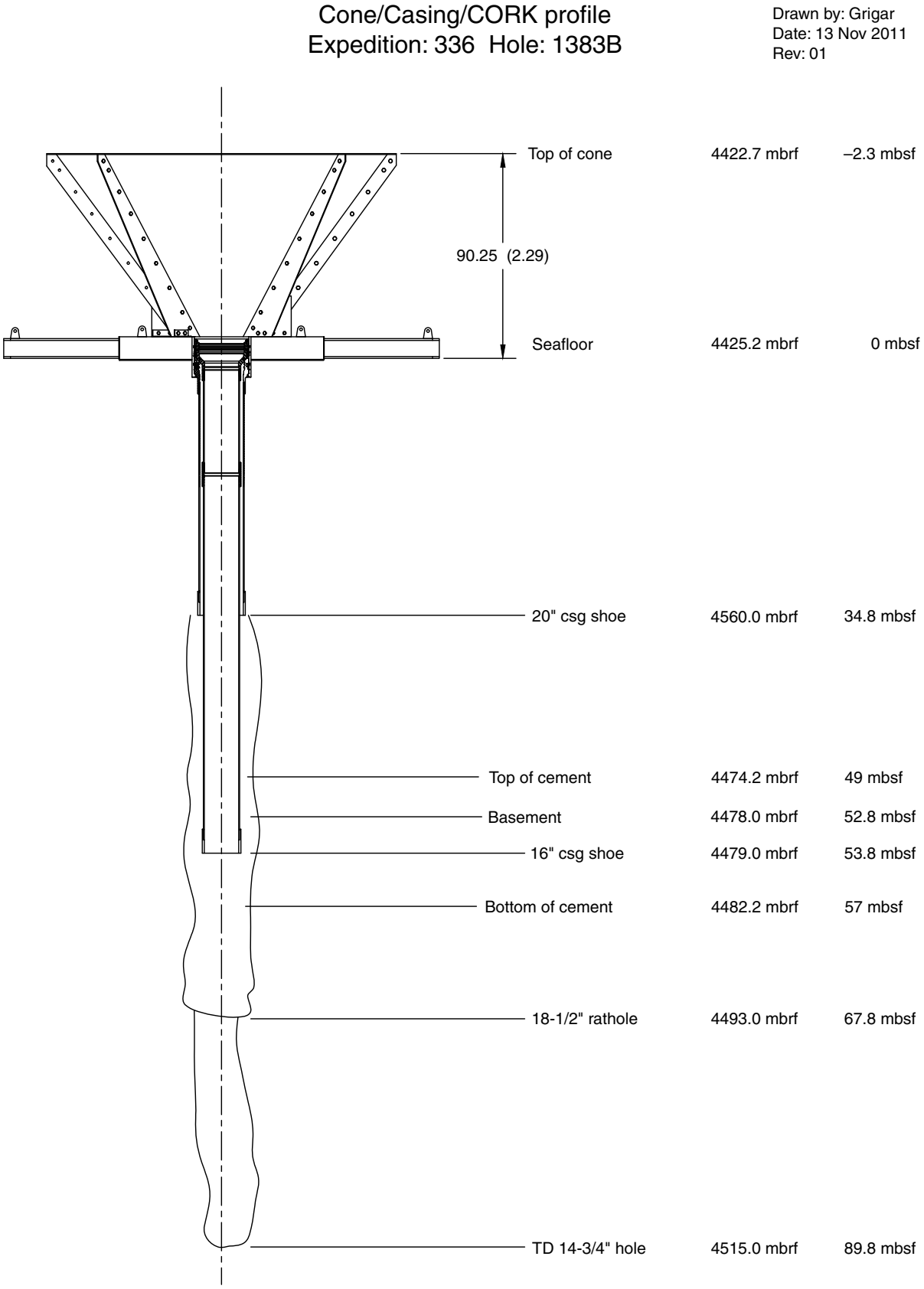

**Figure F2.** Hole U1383C subseafloor borehole observatory (CORK) configuration.

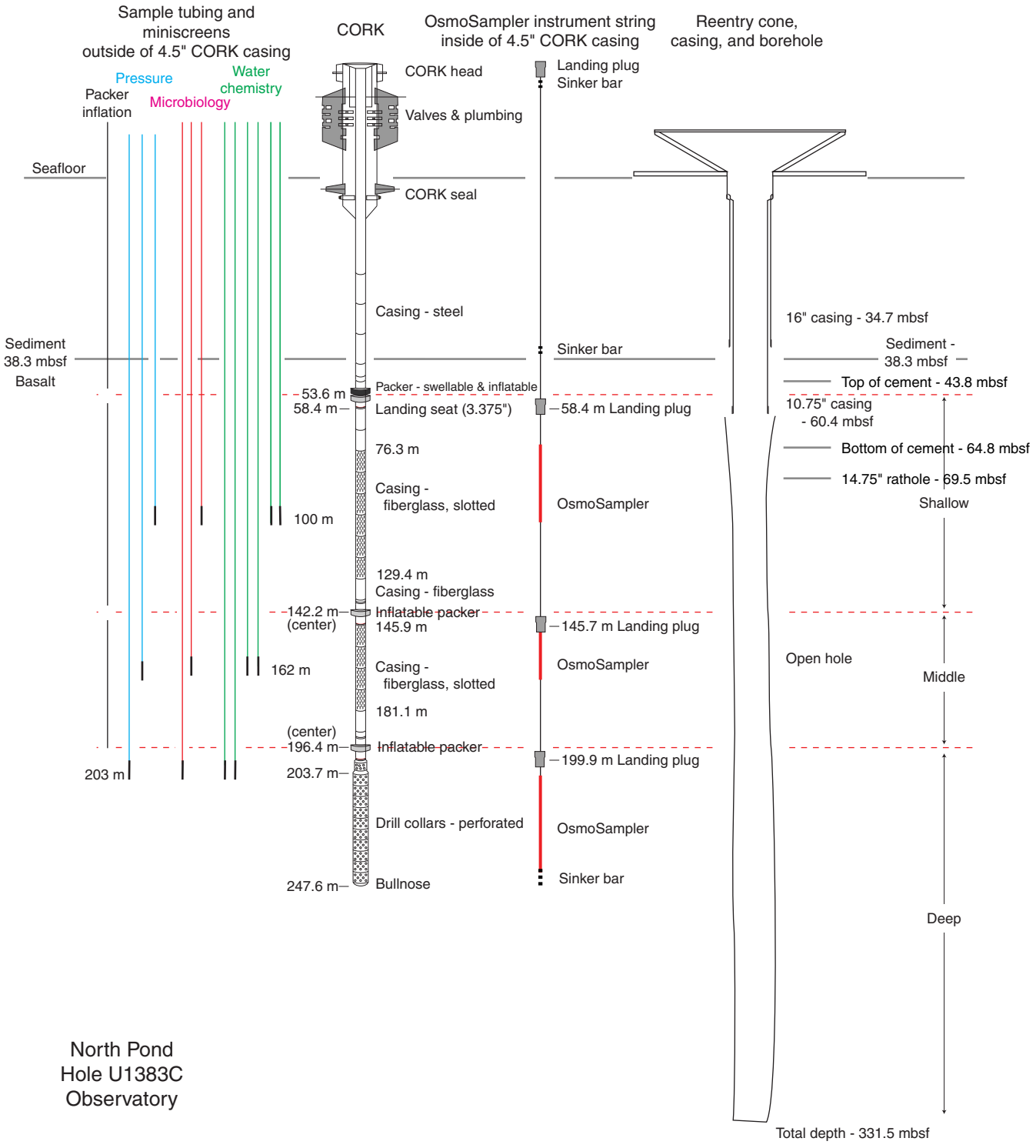

**Figure F3.** Schematic of subseafloor borehole observatory (CORK) installed in Hole U1383C. csg = casing, stl = steel. MBIO = microbiology.

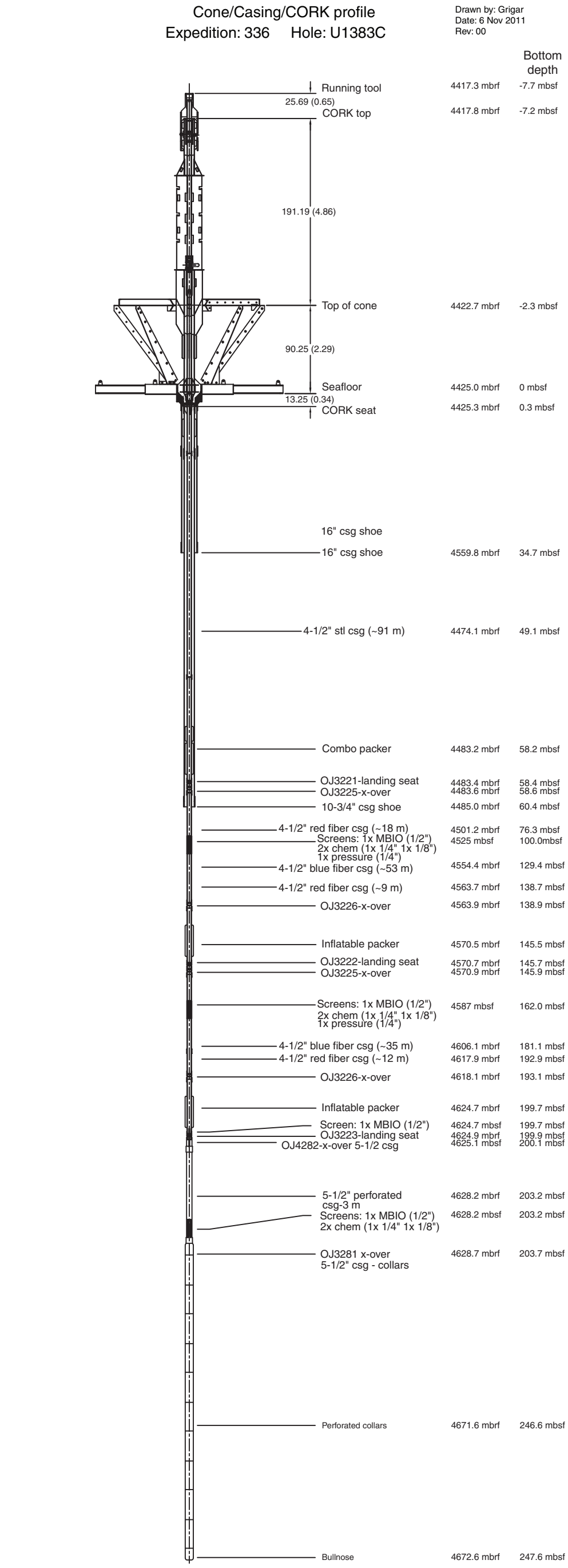

**Figure F4.** Hole U1383D lithologic summary, including major basalt lithologies, lava flows, and abundances of chilled margins, interflow sediments, hyaloclastites, and tectonic breccias. Broad changes in lithology or primary igneous structure are illustrated with different colors in the sequence column.

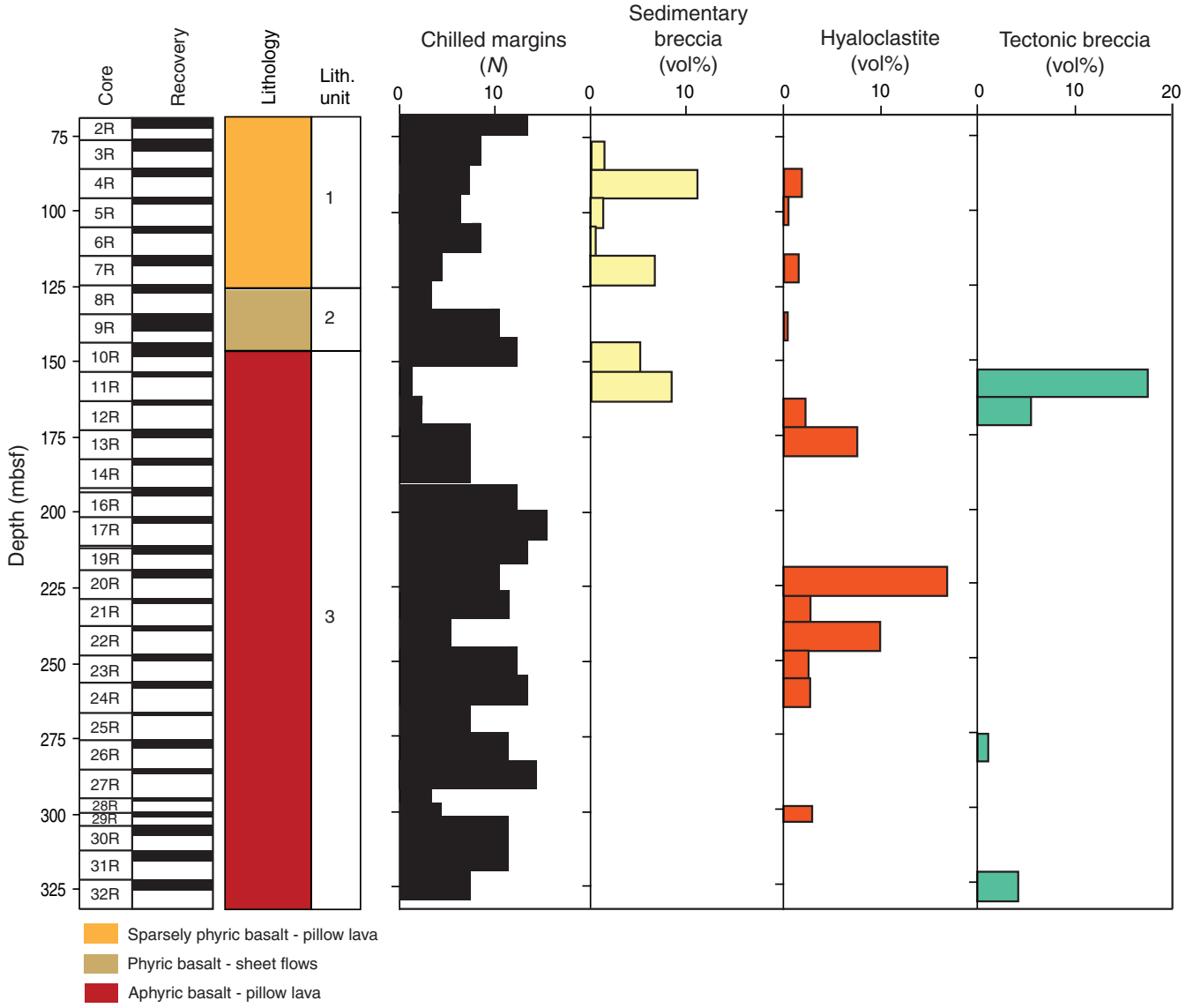

**Figure F5.** Plots of abundance, composition, and distribution of veins (average per core), Hole U1383C.

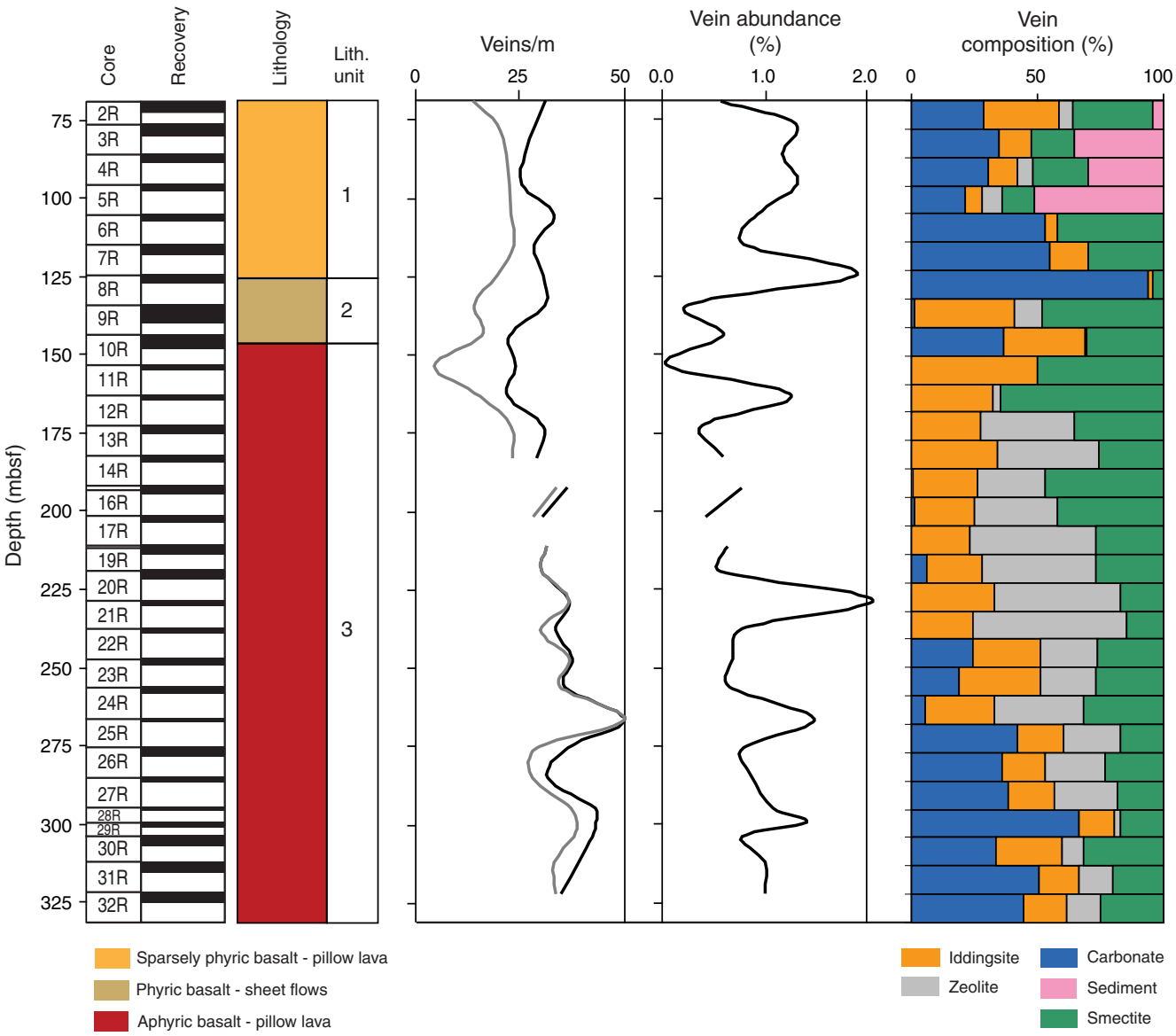

**Figure F6.** Plots of abundance, composition, and distribution of vesicles (average per core) and alteration features, Hole U1383C.

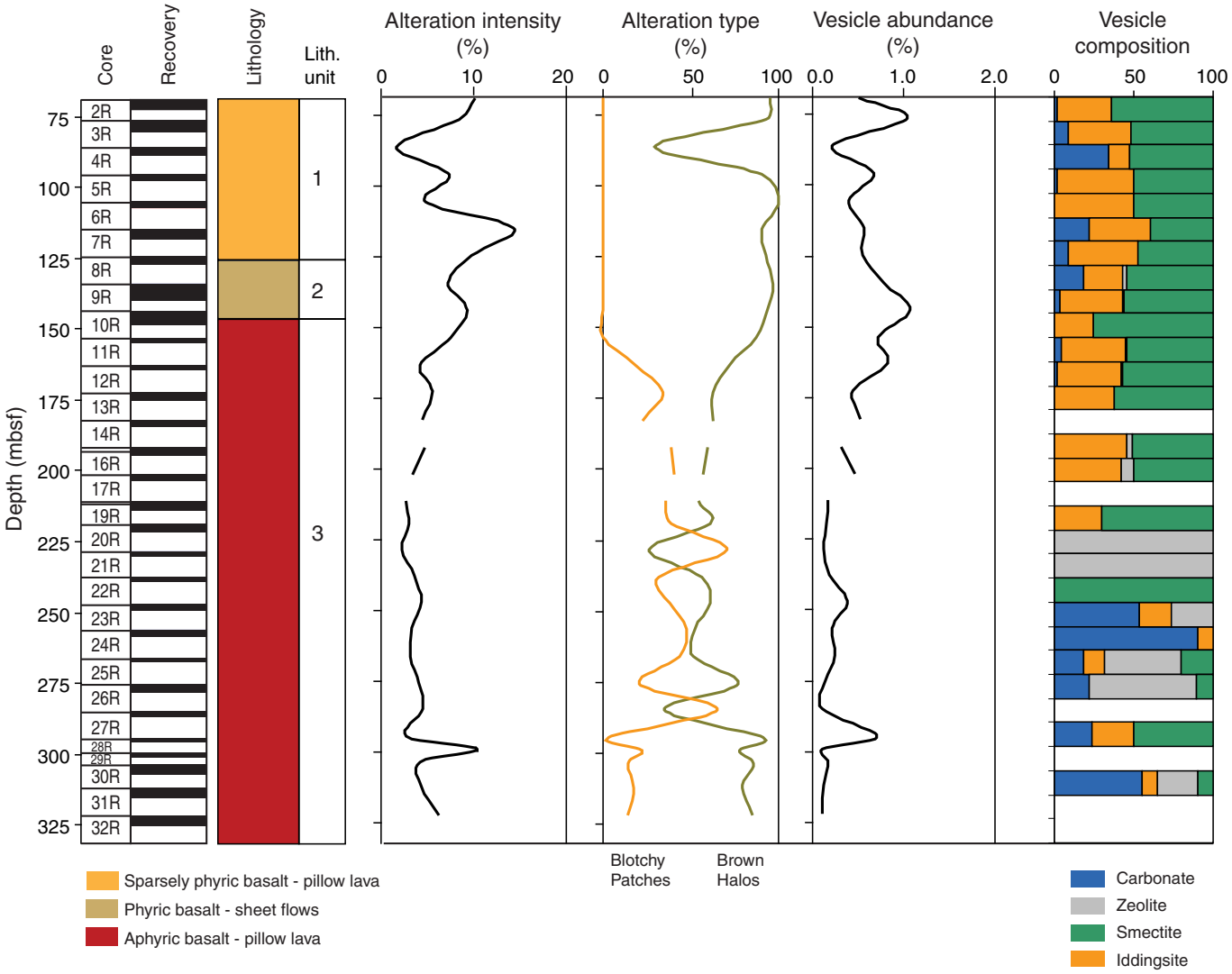

**Figure F7.** Half-round and whole-round core scanner images illustrating different kinds of alteration features, Unit 1 (interval 336-U1383C-4R-1, 93–111 cm). **A.** Grayish-brown alteration halos in sparsely phyric basalt with microcrystalline groundmass. Both subhorizontal and vertical veins are composed of micritic carbonate with minor smectite and iddingsite. **B.** Pervasively altered sparsely plagioclase-phyric basalt with microcrystalline groundmass (interval 336-U1383C-3R-3, 55–62 cm [Piece 10]). Groundmass contains microphenocrysts of plagioclase laths (<1 mm) and olivine (<0.3 mm) altered to iddingsite. Note the inclined irregular veinlet in the center, filled with dark green clay, and the larger carbonate (micritic) vein on the left.

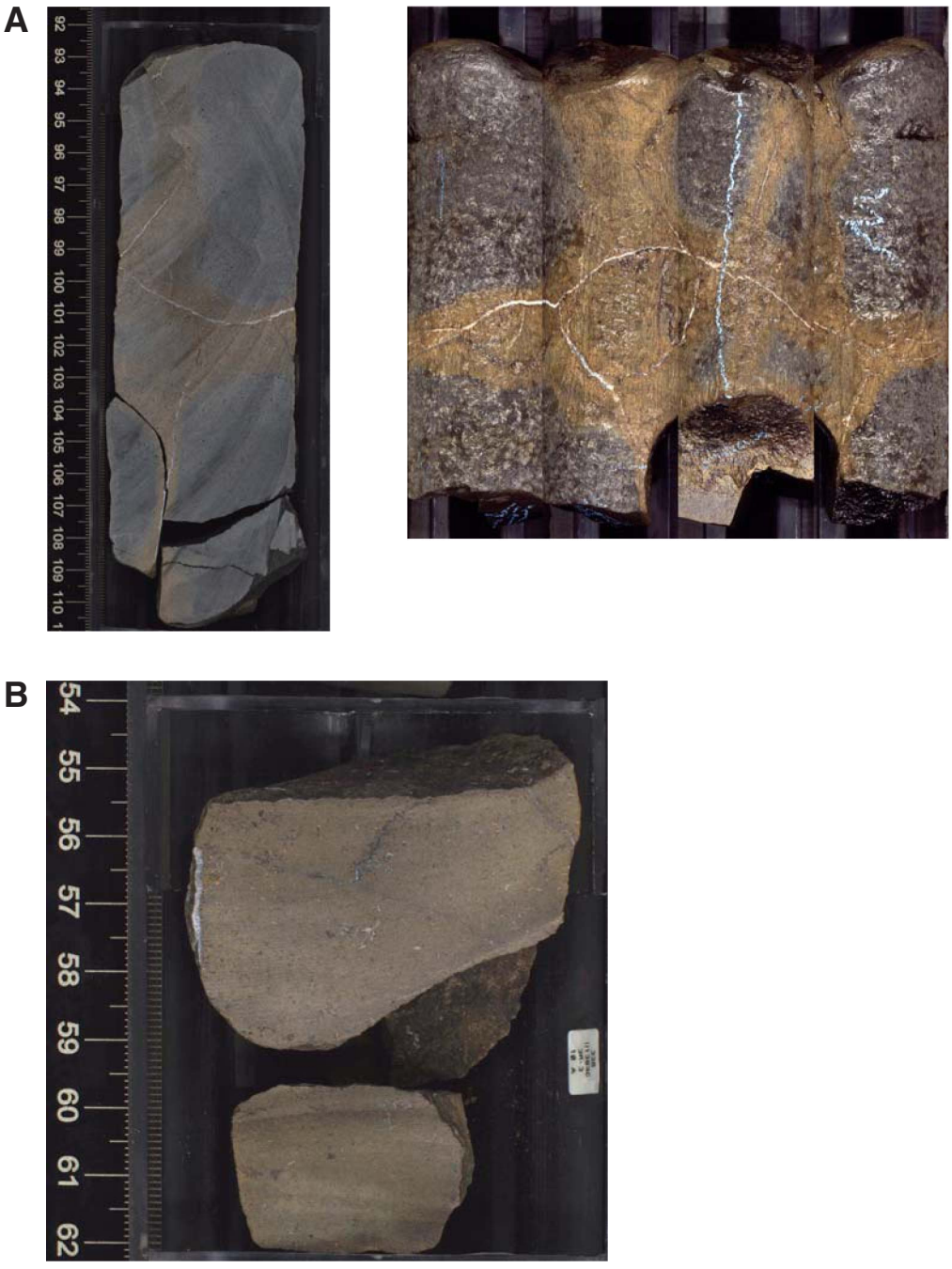

**Figure F8.** Close-up photograph of interflow sediments and sedimentary breccia, Units 1 and 2. **A.** Interflow limestone with beige color composed of nearly 100% micritic calcite and sand- to silt-sized basaltic black spots (interval 336-U1383C-10R-2, 64–70 cm [Piece 10]). Color change from light brown to darker brown is attributed to grain size and an increased amount of clay. **B.** Brecciated sparsely phyric basalt showing jigsaw-puzzle clasts cemented by a micritic matrix identical to interflow sediments (interval 336-U1383C-6R-1, 128–132 cm [Piece 21]). Note also the brown alteration halos superimposed onto dark halos from both sides of the thin (0.2 mm) vertical vein in the center of the piece.

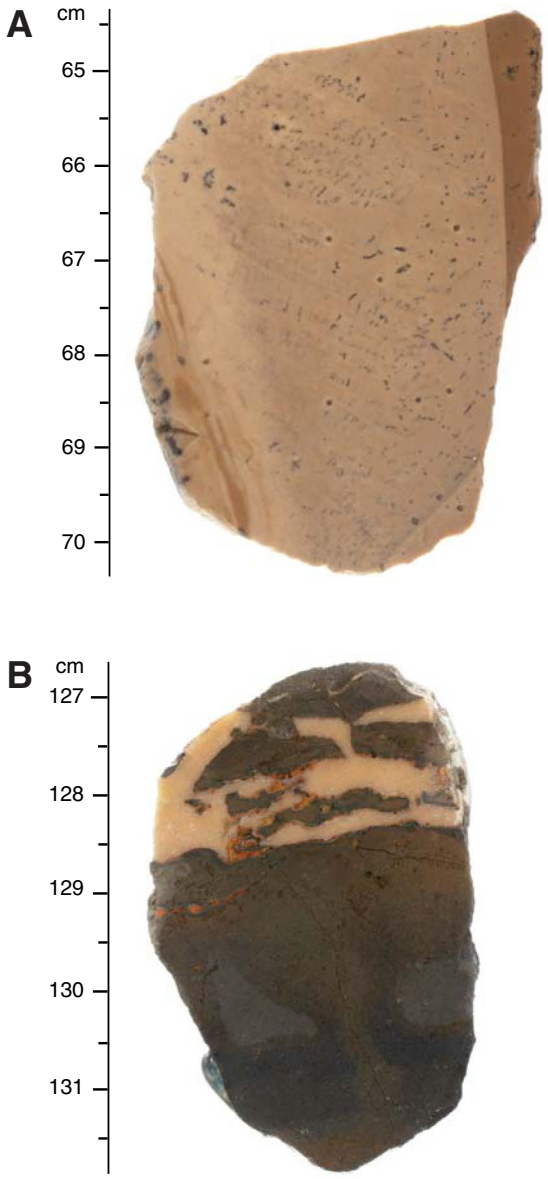

**Figure F9.** Binocular microscope photomicrographs and close-up photographs of select chilled margins, Hole U1383C. **A.** Planar chilled margin of phyric basalt from Unit 2, interpreted as representing the margin of a sheet flow (interval 336-U1383C-9R-1, 49–54 cm [Piece 8]). The crypto- to microcrystalline groundmass hosts euhedral tabular plagioclase phenocrysts with minor and partly altered olivine. **B.** Glassy margin showing translucent red palagonitized glass with spherulitic devitrification textures surrounding plagioclase laths (interval 336-U1383C-9R-3, 65–71 cm [Piece 9]). Note the zeolite-rich veinlet crosscutting a plagioclase phenocryst. Field of view = 2 cm.

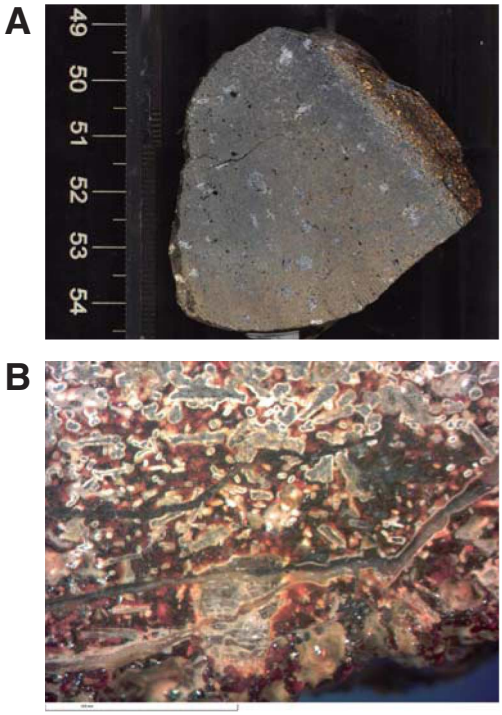

**Figure F10.** Whole-round and half-round core scanner images illustrating different kinds of alteration features, Unit 2. **A.** Pervasively altered phyric basalt with microcrystalline groundmass (interval 336-U1383C-9R-3, 71–80 cm [Piece 10]). Olivine is extensively altered to iddingsite throughout the groundmass. **B.** Patchy alteration of sparsely phyric basalt with microcrystalline groundmass (interval 336-U1383C-9R-3, 81–93 cm [Piece 11]). Note that the grayish-brown alteration halos are related to exposed fractures on both sides of the piece.

**Figure F11.** Half-round and whole-round core scanner images illustrating different kinds of alteration features, Unit 3. **A.** Pervasively altered aphyric basalt with crypto- to microcrystalline groundmass (interval 336-U1383C-31R-2, 44–58 cm [Piece 7]). Note numerous isolated and irregular veins composed of mixed calcite and zeolite assemblages. **B.** Alteration halos in aphyric basalt with cryptocrystalline groundmass (interval 336-U1383C-31R-2, 59–71 cm [Piece 8]). **C.** Variolitic pillow margin showing a typical blotchy alteration texture caused by various extents of alteration of mesostasis and interstitial glass (interval 336-U1383C-16R-2, 29–34 cm [Piece 6]). **D.** Fine-grained aphyric basalt from the bottom of Unit 3 (interval 336-U1383C-32R-1, 124–133 cm [Piece 6]).

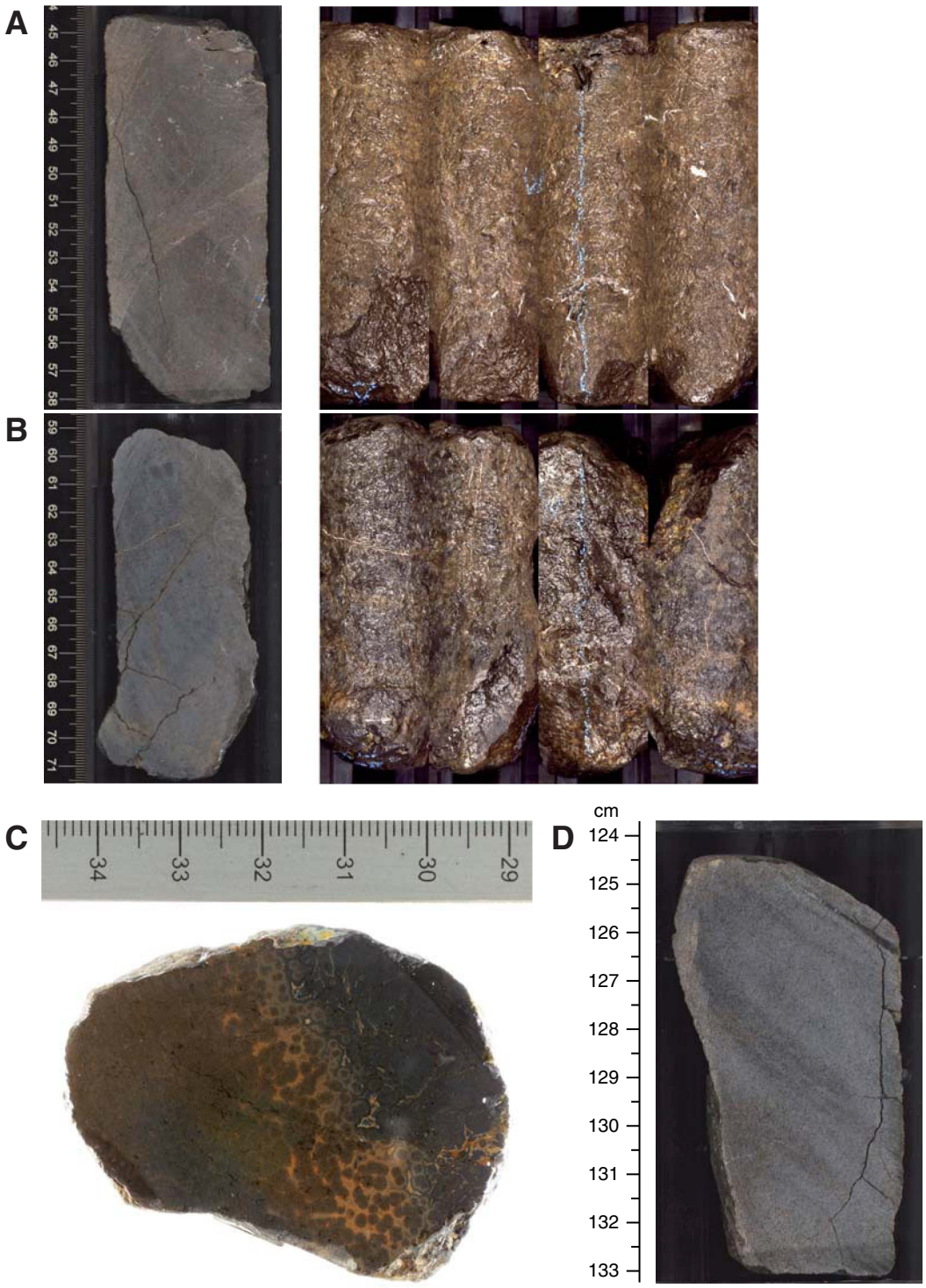

**Figure F12.** Close-up photographs of hyaloclastites, Hole U1383C. **A, B.** Hyaloclastite with angular and poorly sorted cryptocrystalline and glassy clasts (interval 336-U1383C-13R-1, 58–61 cm [Piece 12]): (A) the most altered glass shards are typically replaced by reddish- to yellowish-brown palagonite, (B) concentric alteration rinds in larger basaltic clasts. The white cement around the clasts is essentially composed of zeolite. Field of view (FOV) = 1.5 cm. **C, D.** Interval 336-U1383C-9R-3, 49–54 cm (Piece 7): (C) chilled margin of phyric basalt with crypto- to microcrystalline groundmass grading into hyaloclastite, (D) internal structures of basalt clasts assembled with a jigsaw-puzzle fit and cemented by zeolite. Open vugs have a higher abundance of Fe oxyhydroxides with zeolite cement. Hairline veinlet network in cryptocrystalline to glassy clasts has incipient light gray alteration halos attributed to mesostasis alteration. FOV = 1.2 cm. Red box shows orientation of photograph relative to C.

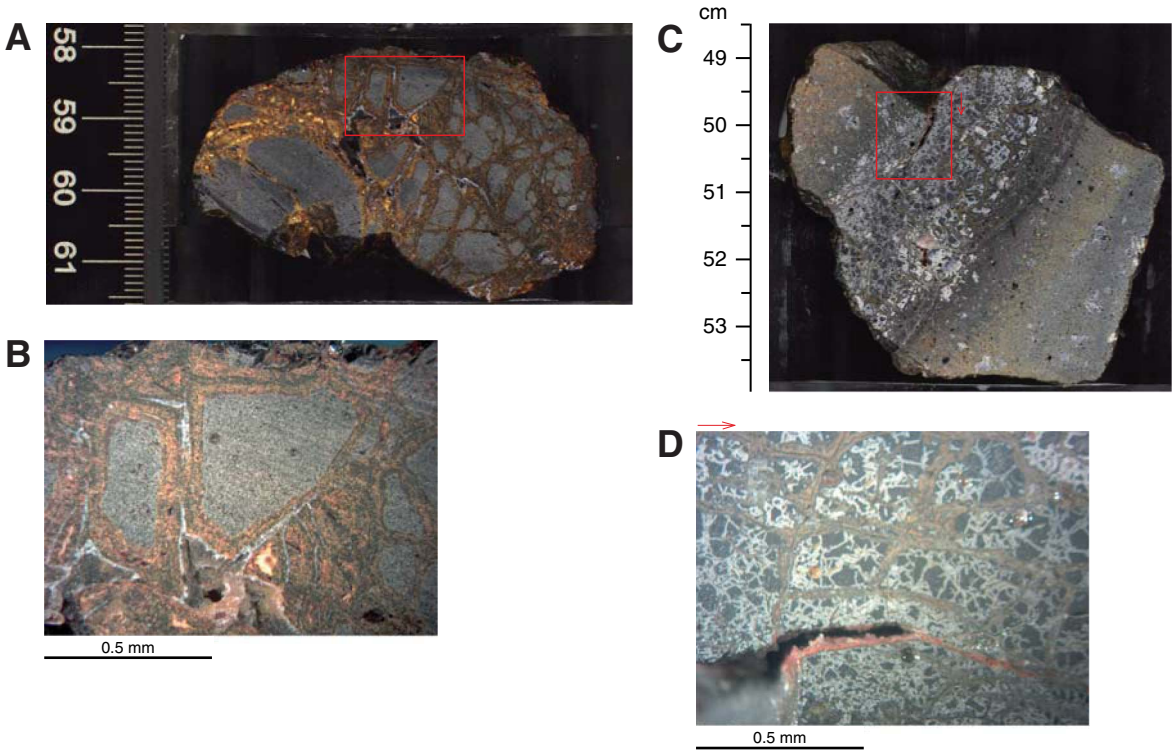

**Figure F13.** Close-up photographs of different breccia types, Hole U1383C. **A.** Whole-round and half-round close-up photographs of tectonic breccia in Unit 3 (interval 336-U1383C-11R-1, 46–54 cm [Piece 9]). Bottom photograph shows microcrystalline aphyric basalt (left) and fine-grained aphyric basalt (right) separated by light brown cryptocrystalline micritic sediment. **B.** Composite breccia with two domains (interval 336-U1383C-32R-3, 0–4 cm [Piece 1]). The top left piece margin is breccia with small (<1 mm) angular basaltic clasts cemented by a light brown to green clay matrix. The rest of the piece is possibly pseudobreccia with gray basaltic domains that are less altered than the remaining basaltic groundmass, which is composed essentially of grayish-brown clay.

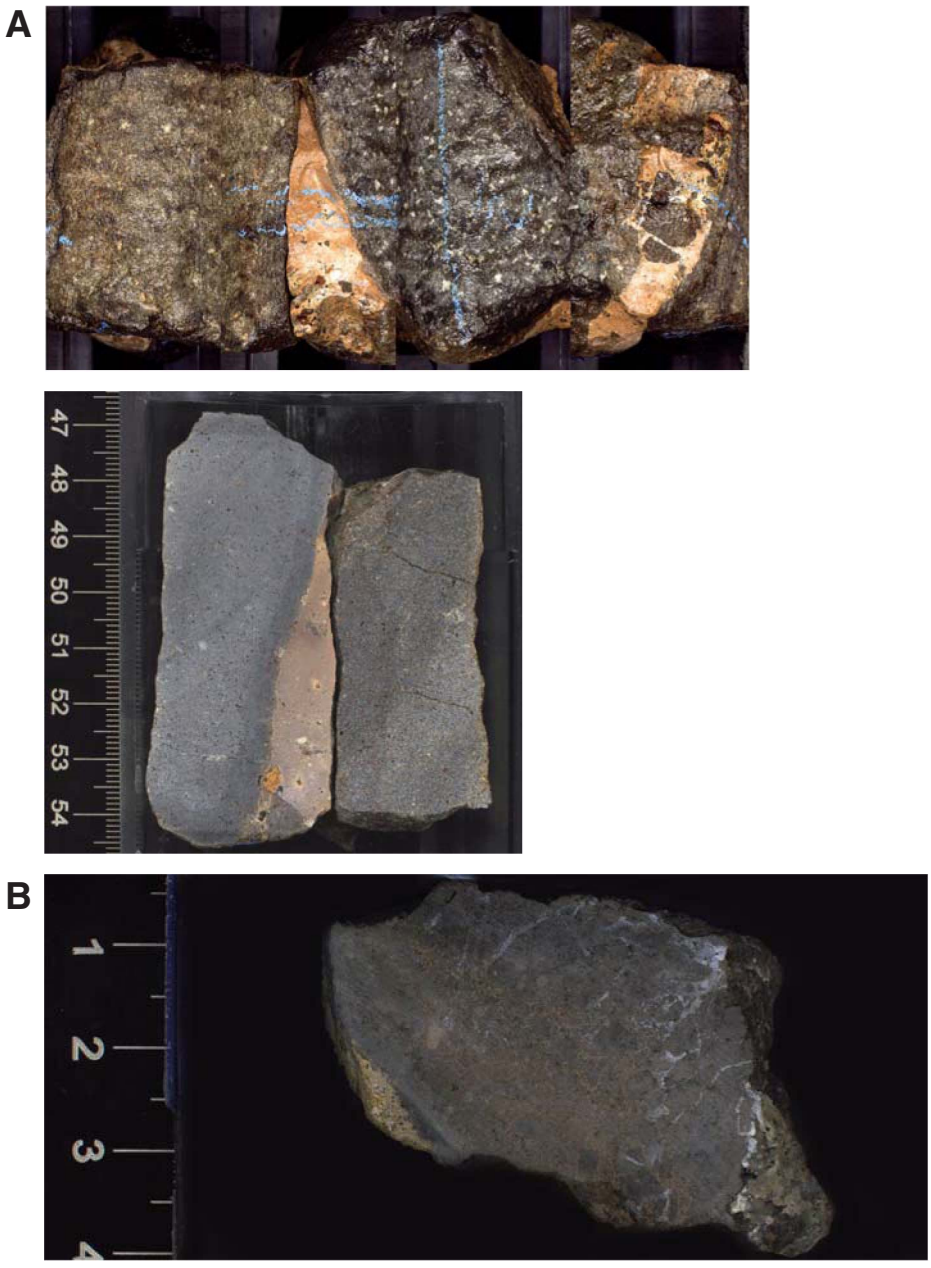

**Figure F14.** Photomicrographs of sparsely to highly plagioclase-olivine phyric basalt, Units 1 and 2. **A.** Plagioclase phenocryst in Unit 1 with hollow cores parallel to an elongated direction and filled with glass or cryptocrystalline groundmass material (Sample 336-U1383C-3R-1, 3–6 cm [Piece 2], Thin Section 30). **B, C.** Sample 336-U1383C-6R-1, 39–42 cm (Piece 7), Thin Section 35: (B) spherulites in glass matrix growing out from tiny acicular plagioclase, skeletal plagioclase laths, tabular plagioclase phenocrysts, and granular olivine microphenocrysts, (C) well-developed plagioclase fan-spherulites composed of plumose plagioclase-clinopyroxene intergrowth and interstitial titanomagnetite. **D.** Plagioclase phenocryst containing glass inclusions as blebs in the core (Sample 336-U1383C-9R-4, 78–80 cm [Piece 9], Thin Section 40). **E.** Plagioclase phenocryst showing sieve texture with irregularly shaped inclusions of groundmass or glass (Sample 336-U1383C-9R-4, 78–80 cm [Piece 9], Thin Section 40). **F.** Crystal edge of a plagioclase phenocryst exhibiting dendritic overgrowth in a sharply zoned rim (Sample 336-U1383C-9R-3, 77–80 cm [Piece 10], Thin Section 39).

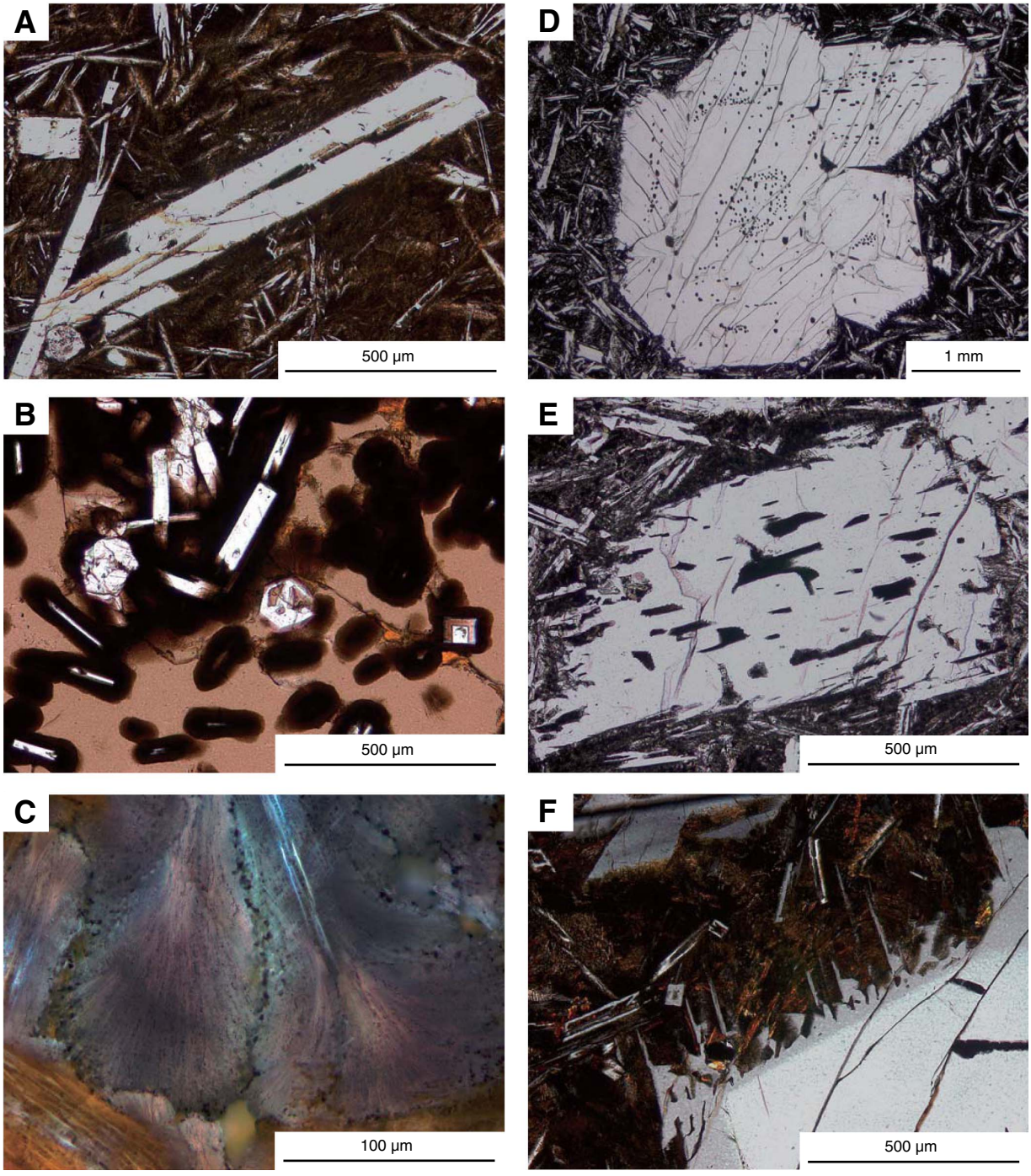

**Figure F15.** Photomicrographs of aphyric basalts, Unit 3. **A.** Skeletal plagioclase laths exhibiting belt-buckle and swallow-tailed forms (Sample 336-U1383C-16R-2, 39–43 cm [Piece 7], Thin Section 48). **B.** Radiating acicular plagioclase bundles shown in microcrystalline basalt (Sample 336-U1383C-31R-2, 5–8 cm [Piece 1], Thin Section 56). **C–E.** Sample 336-U1383C-23R-1, 57–61 cm (Piece 10), Thin Section 52: (C) hopperlike olivine crystal in microcrystalline basalt, (D) lanternlike olivine crystal in microcrystalline basalt, (E) swallow-tailed olivine crystal in microcrystalline basalt. **F.** Linked-chain and lantern-and-chain olivine crystals shown in variolitic chilled margin (Sample 336-U1383C-16R-2, 30–33 cm [Piece 6], Thin Section 47).

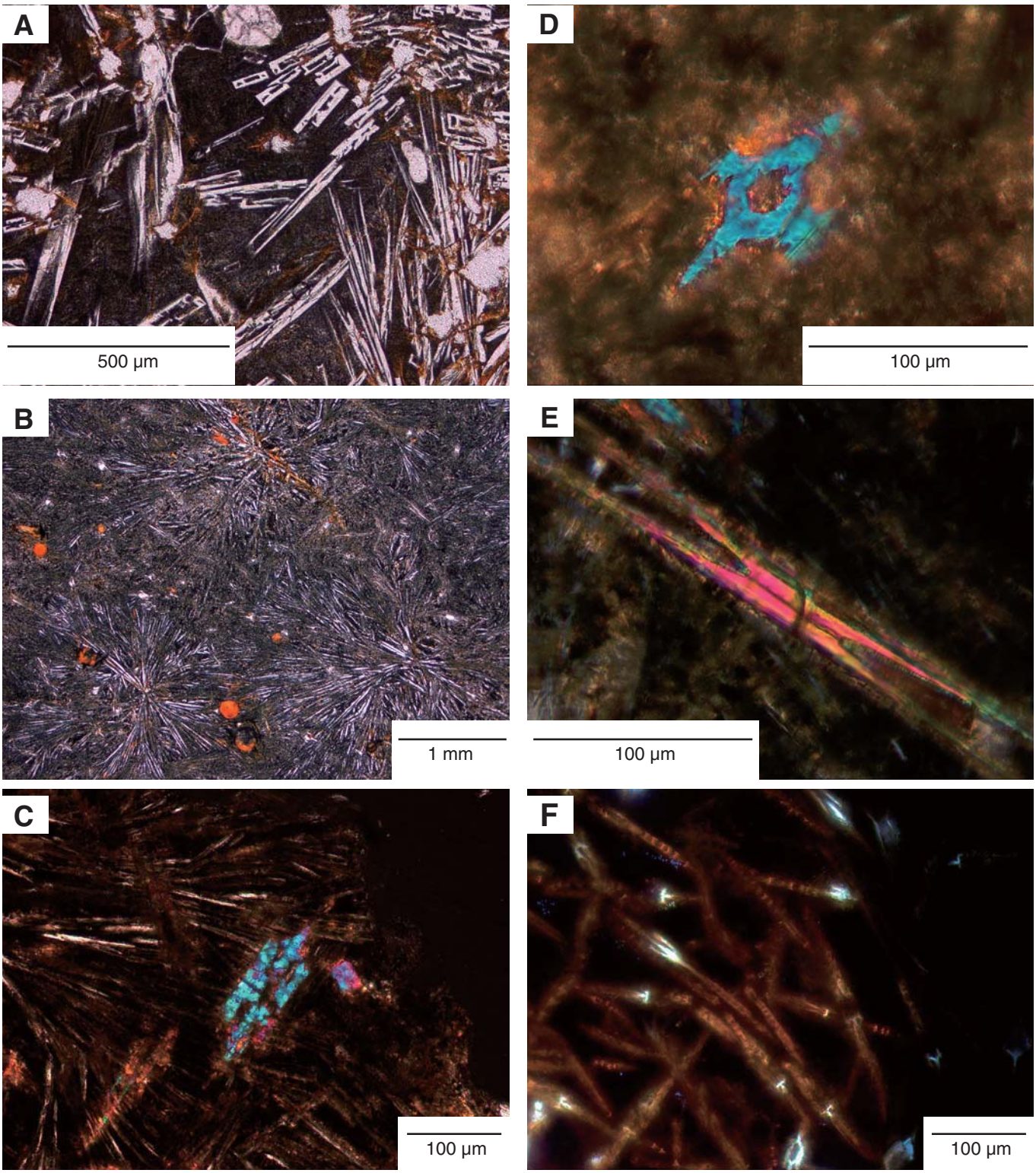

**Figure F16.** Photomicrographs of zeolite occurrence in veins and vesicles. **A.** Zeolite-filled vesicle in pervasively altered microcrystalline basalt showing radial acicular aggregates (Sample 336-U1383C-7R-2, 95–96 cm [Piece 16], Thin Section 38). Field of view (FOV) = 1.2 mm; cross-polarized light. **B.** Thin (0.1 mm) zeolite veinlets in variolitic cryptocrystalline basalt with interconnected hairline veinlets lined by incipient alteration halos (Sample 336-U1383C-16R-2, 30–33 cm [Piece 6], Thin Section 47). Euhedral olivine (top) remains unaltered thorough the mesostasis. FOV = 5 mm; cross-polarized light. **C.** Vein filled by acicular zeolite with low birefringence (Sample 336-U1383C-6R-1, 100–104 cm [Piece 17], Thin Section 34). Left image under single-polarized light; right image under cross-polarized light. FOV = 5 mm.

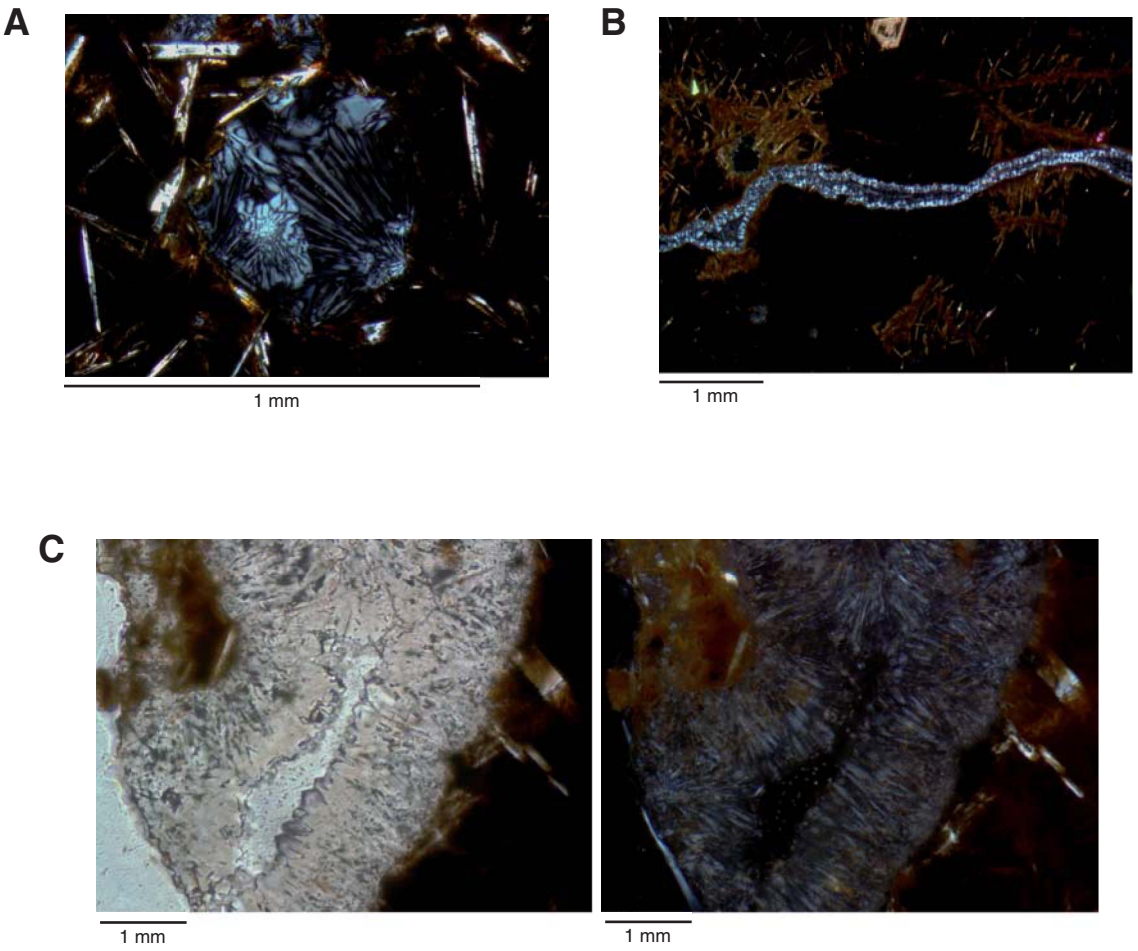

**Figure F17.** Photomicrographs of composite zeolite and carbonate veins. Left images are under single-polarized light; right images are under cross-polarized light. **A.** Photomicrograph of 1 mm wide vein with three domains (Sample 336-U1383C-2R-2, 15–18 cm [Piece 3], Thin Section 28). From right to left: (1) recrystallized calcite rim (50 µm across), (2) zeolite filling with very low birefringence and mixed with altered glass shards and Fe oxyhydroxides, and (3) micritic filling with altered glass and zeolite clasts. Field of view (FOV) = 1.2 mm. **B.** Photomicrograph of 0.1 mm composite vein with drusy acicular to fibrous zeolite druses with very low birefringence overgrowth by fibrous calcite (Sample 336-U1383C-29R-1, 58–64 cm [Piece 14], Thin Section 55). Later stage granular calcite showing radial extinction fills the remaining open space. FOV = 1.1 mm.

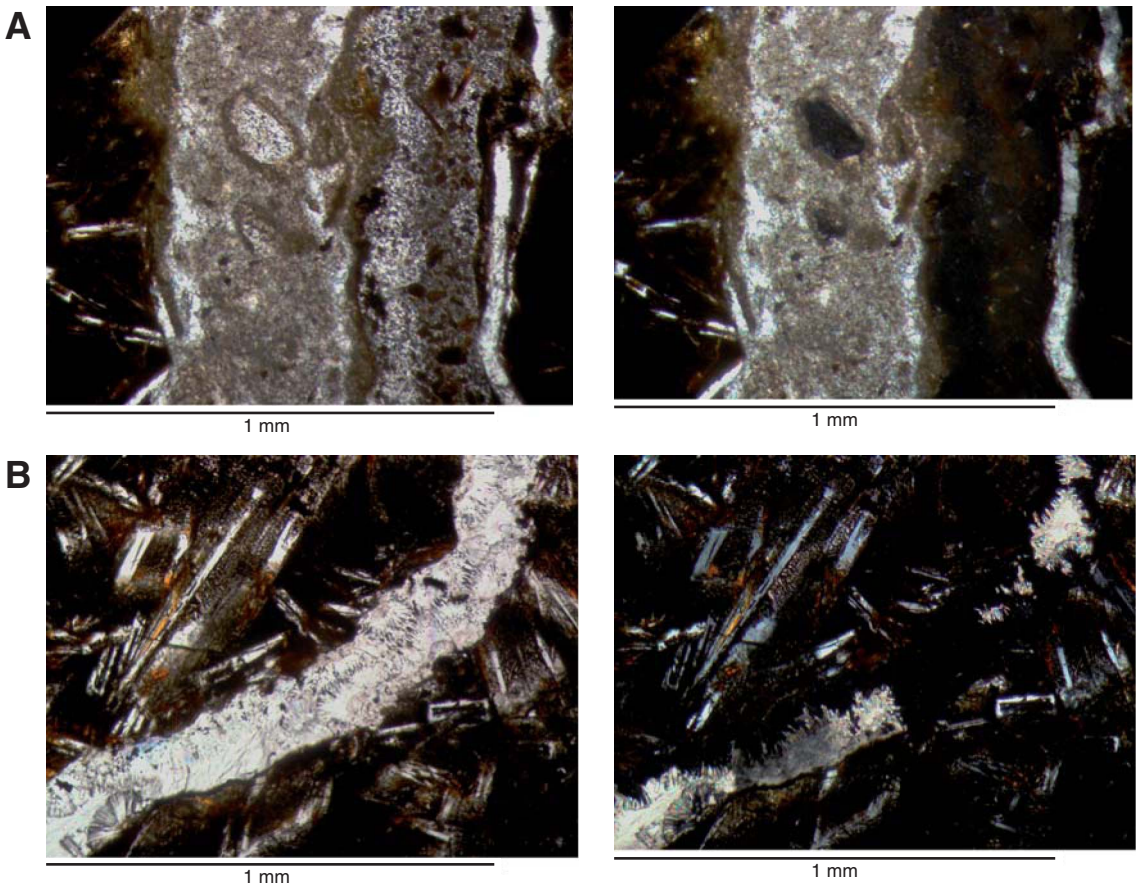

**Figure F18.** Photomicrographs of a chilled margin of sparsely phyric nonvesicular basalt, Unit 1 (Sample 336-U1383C-2R-2, 15–18 cm [Piece 3], Thin Section 28). **A.** Whole thin section photomicrograph showing three domains across the chilled margin. From right to left: (1) fresh glass with euhedral plagioclase and olivine crystals surrounded by spherulitic rim, resulting in glass devitrification; (2) bright yellowish-brown palagonite with higher intensity of spherulitic texture; and (3) cryptocrystalline mesostasis formed by coalescent spherulites. Field of view (FOV) = 5 mm; single-polarized light. **B.** Photomicrograph of area in A, showing contact between spherulite, palagonite, and fresh glass. Microtubules extending from alteration patches into fresh glass are common. FOV = 0.5 mm; single-polarized light. **C.** Photomicrograph of palagonite/fresh glass interface with sharp contact, gradual alteration bands, and absence of microtubules. FOV = 0.25 mm; single-polarized light.

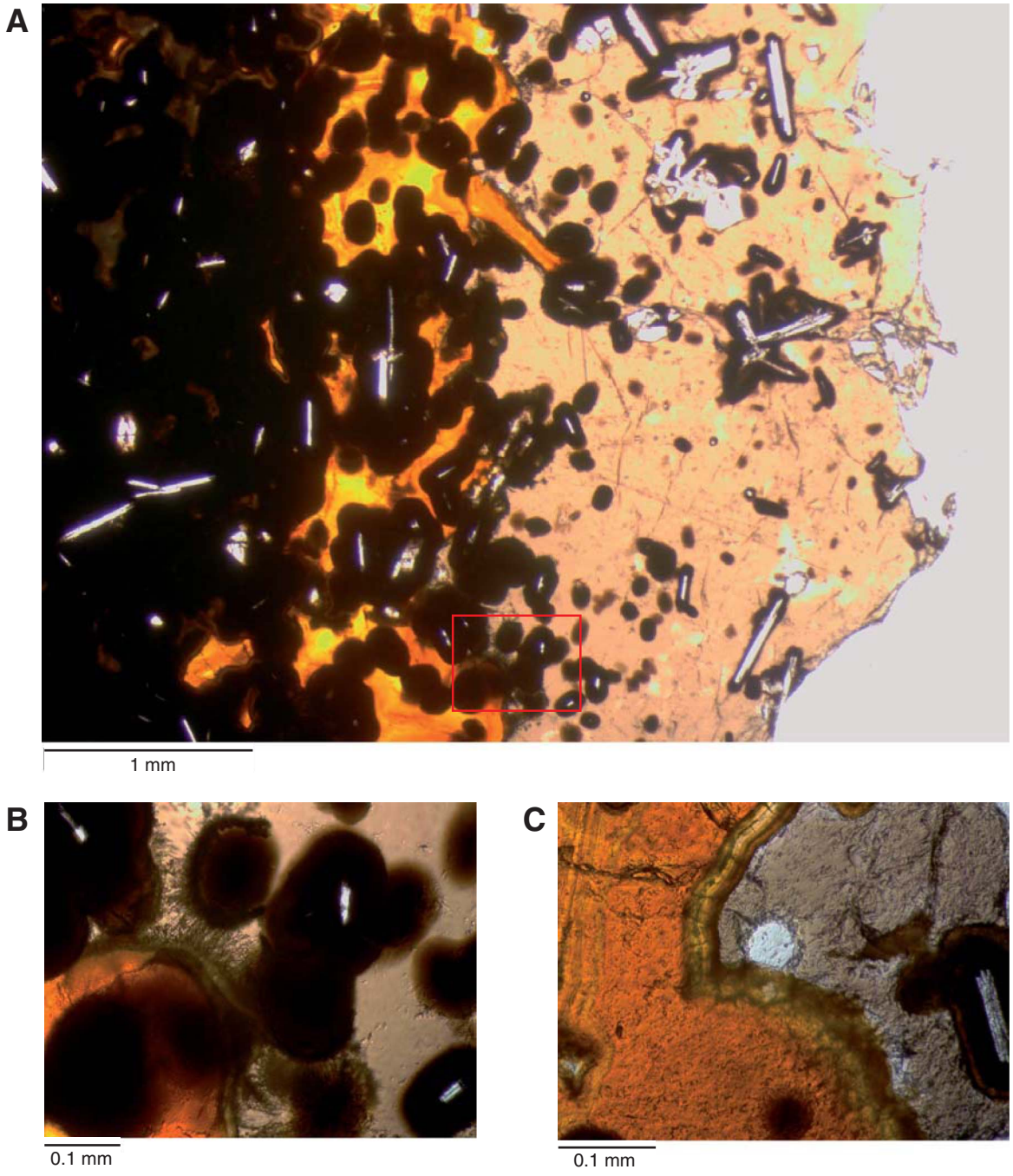

**Figure F19.** Binocular microscope photomicrographs and close-up photographs of sparsely vesicular phyric basalt, Unit 2 (interval 336-U1383C-10R-1, 71–86 cm [Piece 15]). **A.** Half-round core photograph with a grayish-brown alteration halo surrounding a fresher gray interior. Red lines separate domains with different vesicle filling colors. **B.** Vesicle filling in the freshest gray groundmass composed mostly of bluish-green clay (celadonite). Field of view (FOV) = 1 cm. **C.** Composite vesicle filling at alteration halo boundary, with more abundant smectite and iddingsite assemblages. FOV = 1 cm. **D.** Vesicle filling further away from the freshest groundmass, with increased zeolite filling. FOV = 1 cm. **E.** Composite vesicle filling in the alteration halos, showing green clay and Fe oxyhydroxide fillings (note that Fe oxyhydroxide may either form the center or rims of the vesicles). FOV = 2 cm.

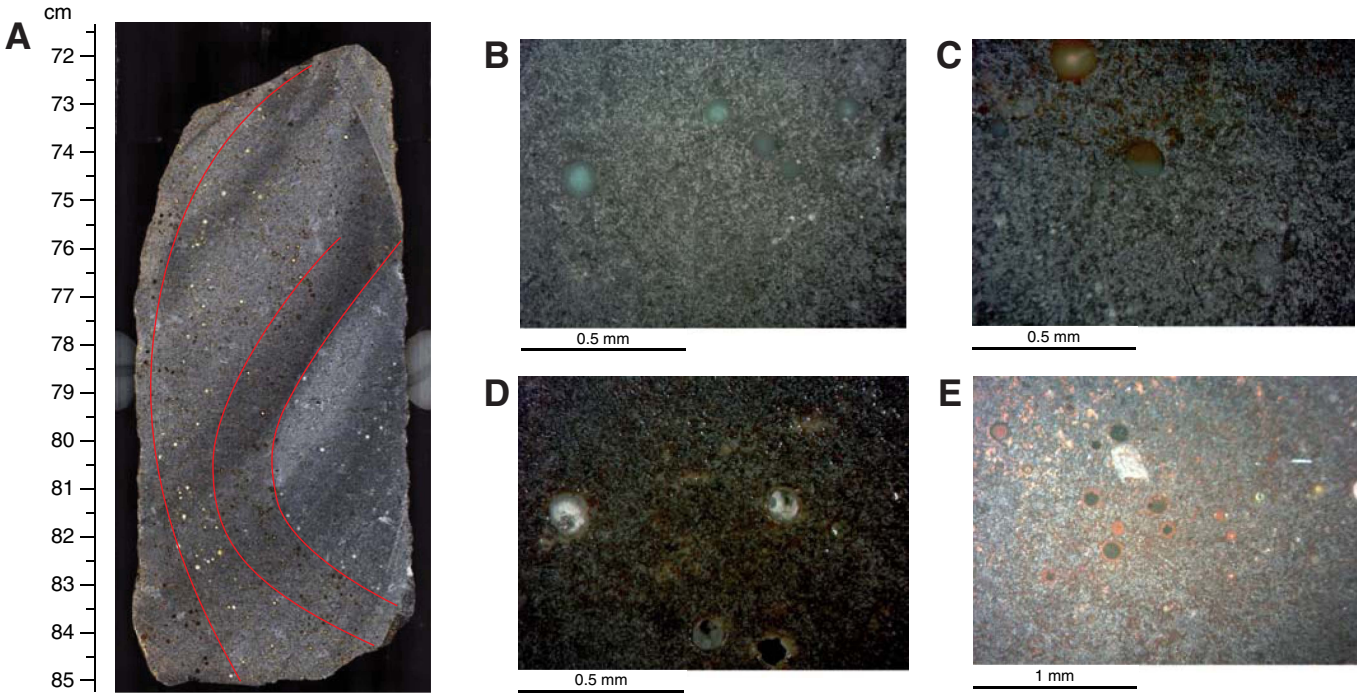

**Figure F20.** Photomicrographs of hyaloclastite, Unit 3 (Sample 336-U1383C-20R-1, 39–42 cm [Piece 28], Thin Section 50). **A.** Whole thin section photomicrograph showing partly palagonitized glass clasts with minor devitrification spherulites and microliths. **B.** Large red box in A: Concentric alteration rim of palagonite (yellowish brown) extending into fresh glass (light brown). A zeolite cement forms a thin (<100 µm) coating along palagonitized glass clasts, whereas the matrix is composed of a mixed assemblage of clay, palagonite, and zeolite. Left image is in single-polarized light, right image is under cross-polarized light. Cross-polarized image shows concentric palagonite bands with bright birefringence. Field of view (FOV) = 4 mm. **C.** Small red box in A: sharp transition between palagonite and fresh glass, which contrasts with chilled margin glass alteration (Fig. F18). The alteration front in this hyaloclastite remarkably lacks composite alteration halos and microtubules extending into the fresh glass. Note the thin external rim of zeolite at the bottom of the photograph with acicular to fibrous crystallization. Left image is under single-polarized light; right image is under cross-polarized light. FOV = 1.1 mm.

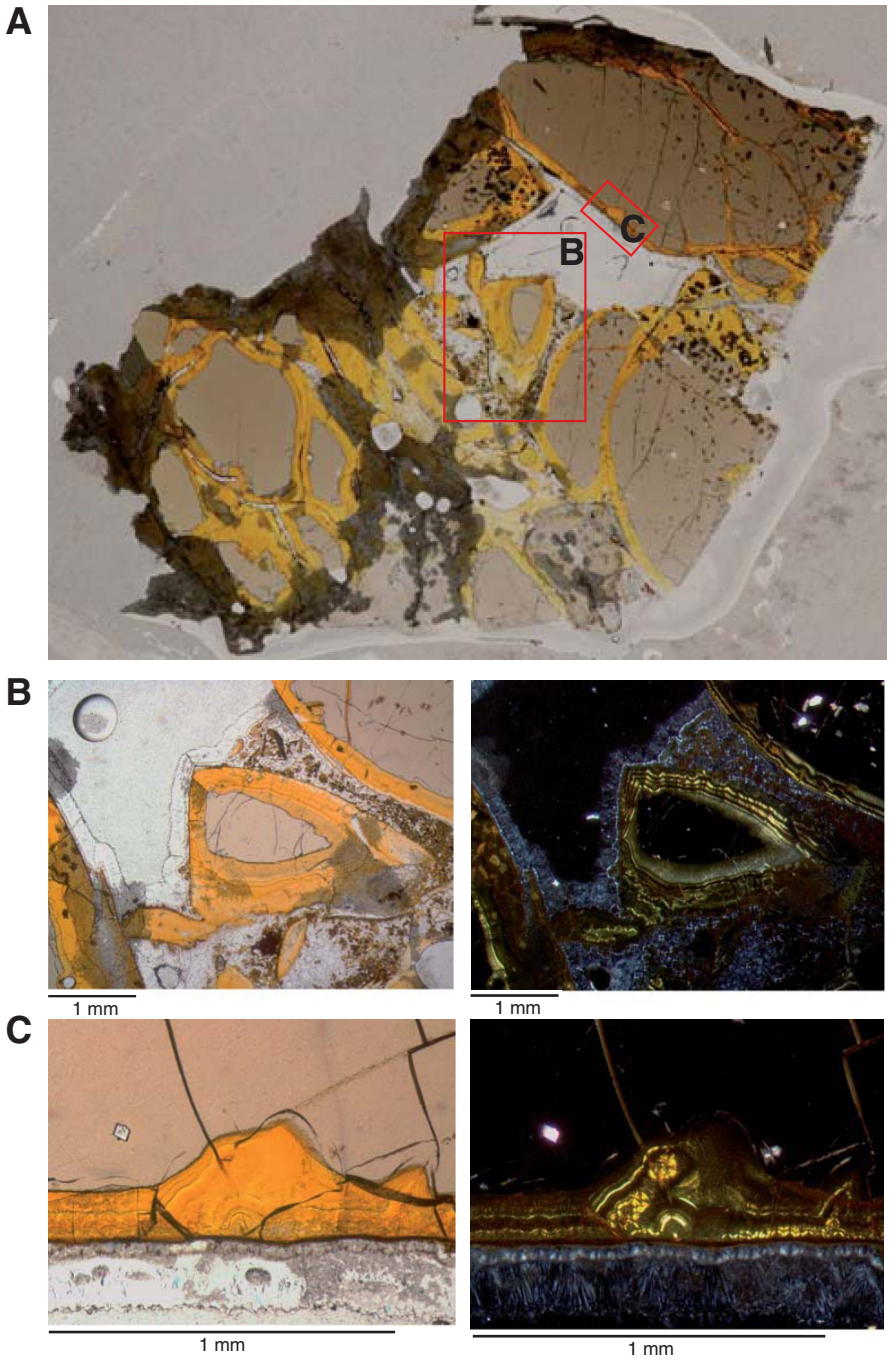

**Figure F21.** Downhole variations of MgO, CaO, Zr/Y, Zr/$TiO_2$, and weight loss on ignition (LOI), Hole U1383C. Black horizontal dashed lines indicate unit boundaries. Red and blue vertical dashed lines represent average value of shallower units (1 and 2) and deeper unit (3), respectively.

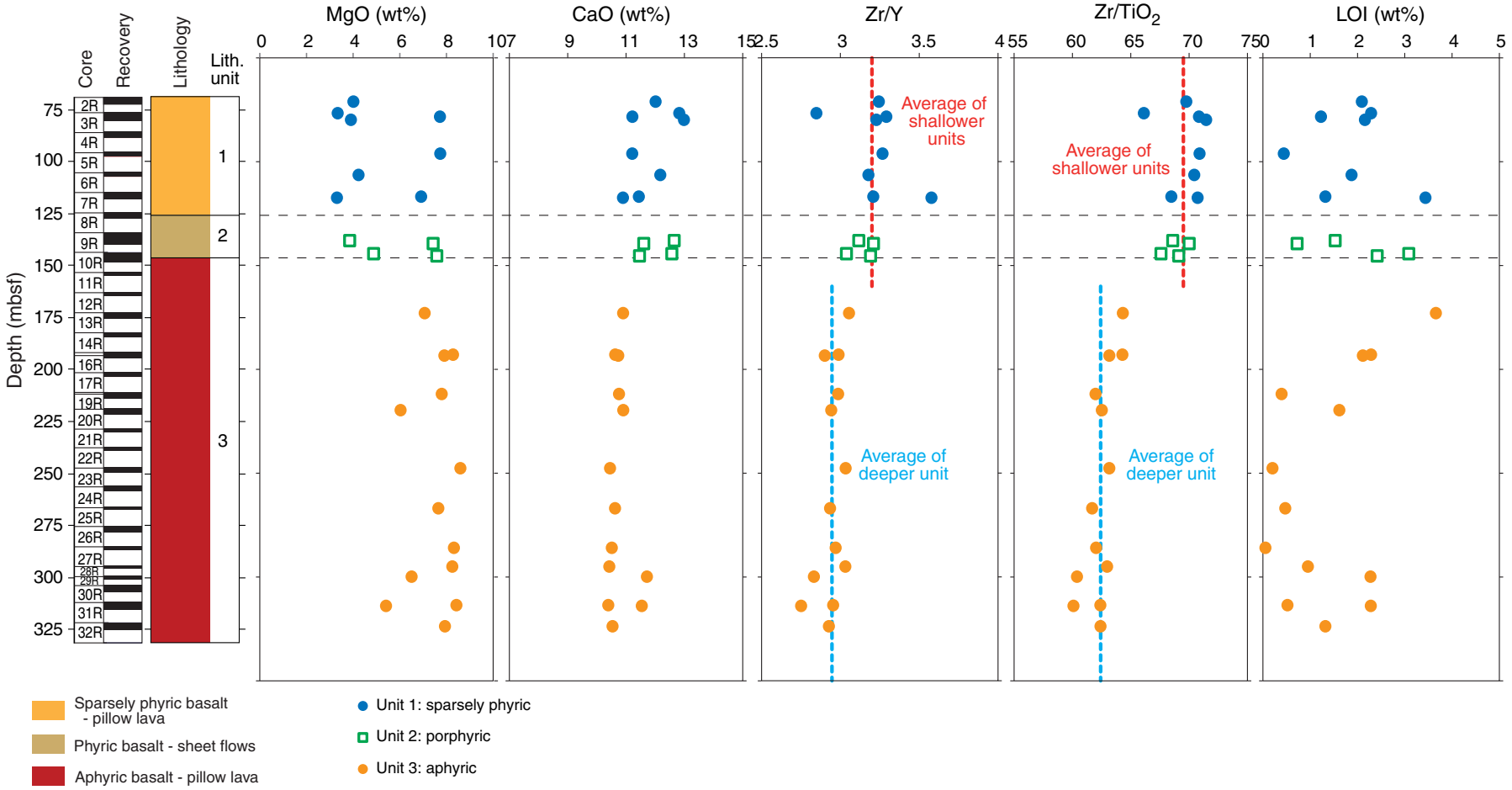

**Figure F22.** Plots of $Al_2O_3$ vs. CaO, CaO vs. Sr, and CaO vs. Ba for basaltic rock samples, Hole U1383C. Data ranges for aphyric and phyric basalts from corresponding depths in Deep Sea Drilling Project (DSDP) Hole 395A (Bougault et al., 1979; Rhodes et al., 1979) are also shown in $Al_2O_3$ vs. CaO and CaO vs. Sr plots for comparison.

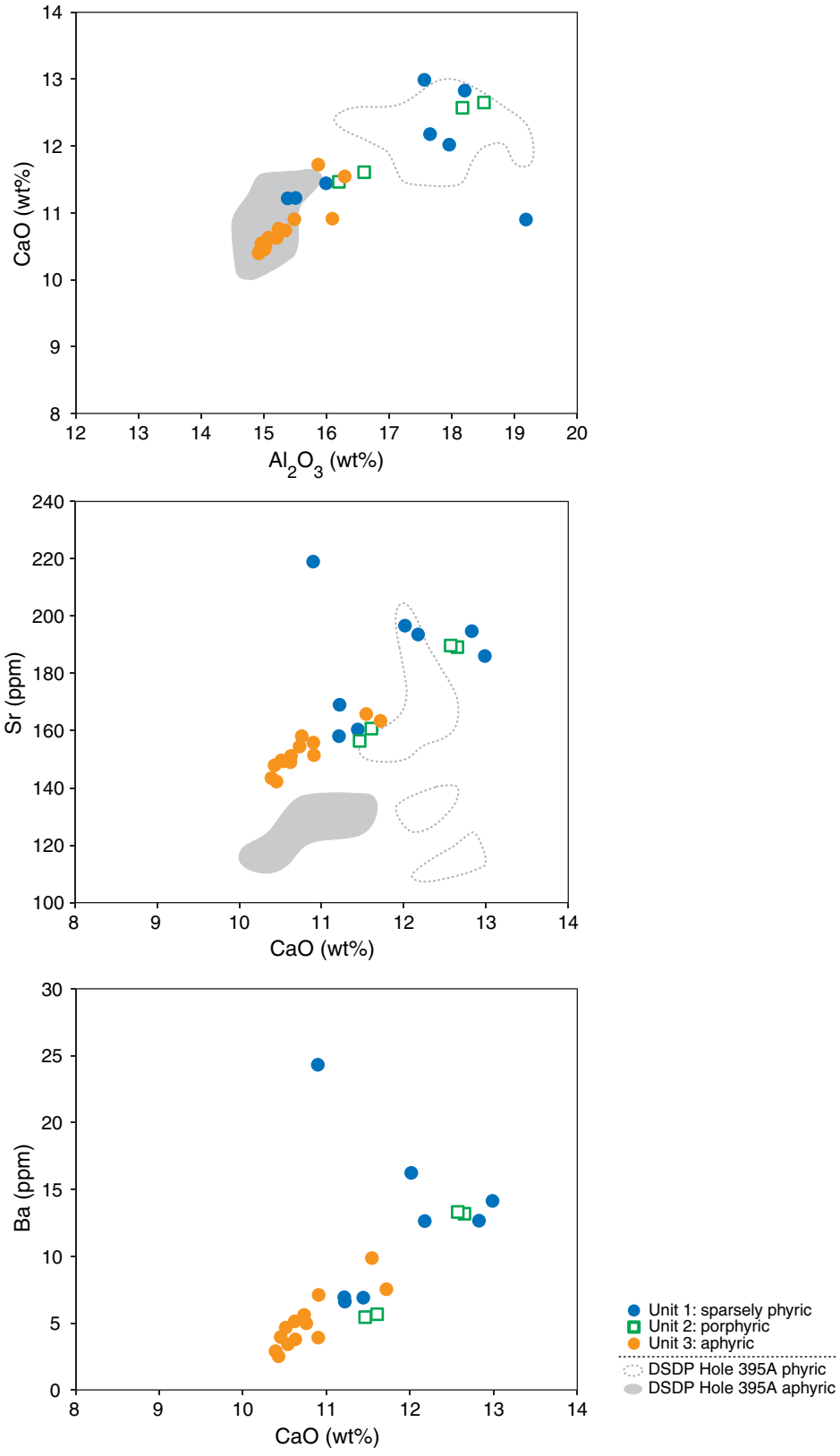

**Figure F23.** Plots of MgO vs. $Al_2O_3$, $Fe_2O_3^T$, and $TiO_2$ for basaltic rock samples, Hole U1383C. Data ranges for aphyric and phyric basalts from corresponding depths in Deep Sea Drilling Project (DSDP) Hole 395A (Bougault et al., 1979; Rhodes et al., 1979) are also shown for comparison. Possible olivine, clinopyroxene, and plagioclase fractionation lines and plagioclase accumulation trends are not based on the chemistry of observed minerals in the Hole U1383C basalts but are simply inferred from published mineral chemistry data of mid-ocean-ridge basalt (e.g., Brewer et al., 1996). $Fe_2O_3^T$ = total iron as $Fe_2O_3$.

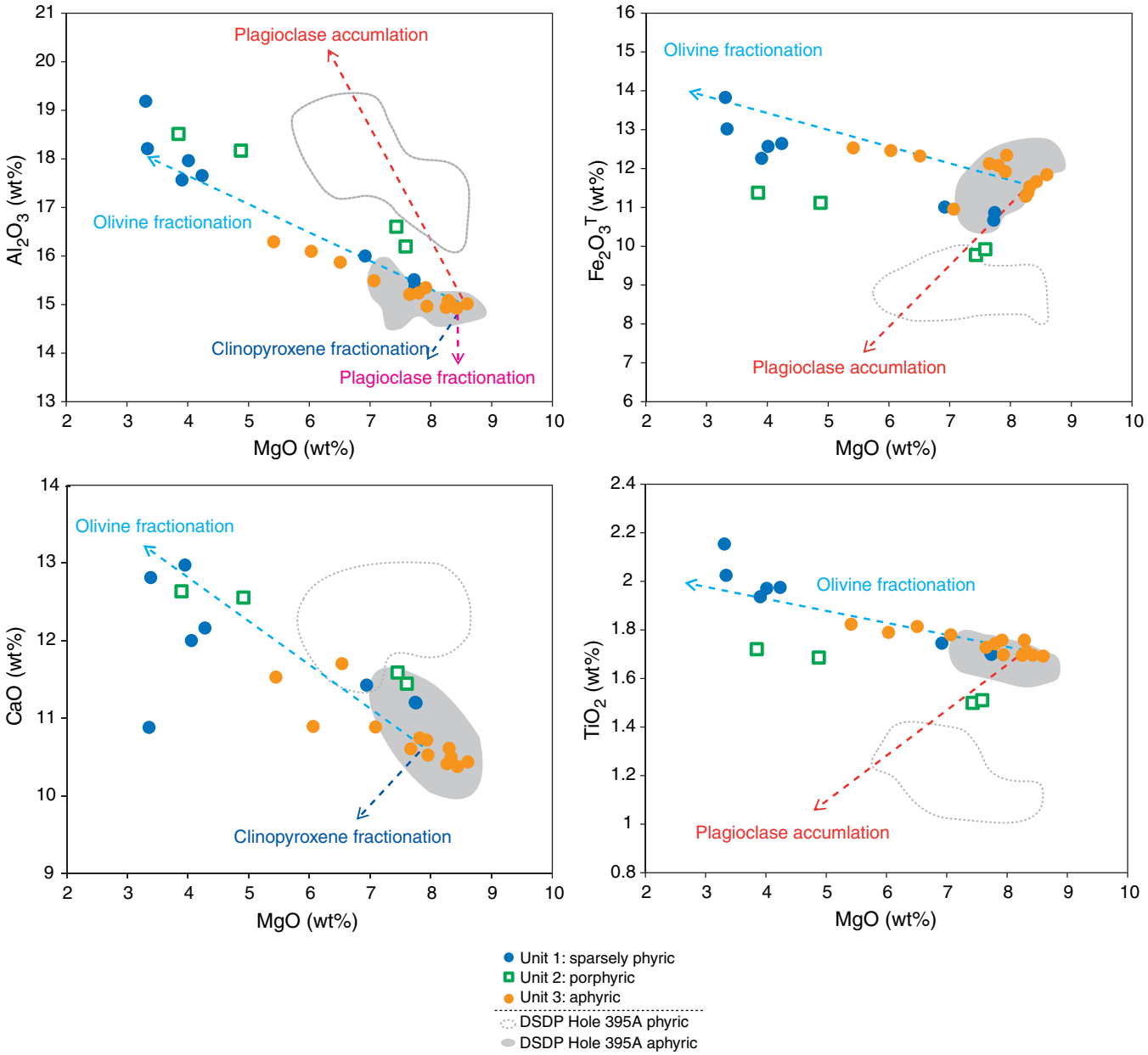

**Figure F24.** Plots of Zr vs. Y and $TiO_2$ for basaltic rock samples, Hole U1383C. Different trends for shallower and deeper units, shown as red and blue solid lines, suggest the difference of parental magmas between these units. The shallower and deeper trends observed in Hole U1382A are also shown as red and blue dashed lines for comparison.

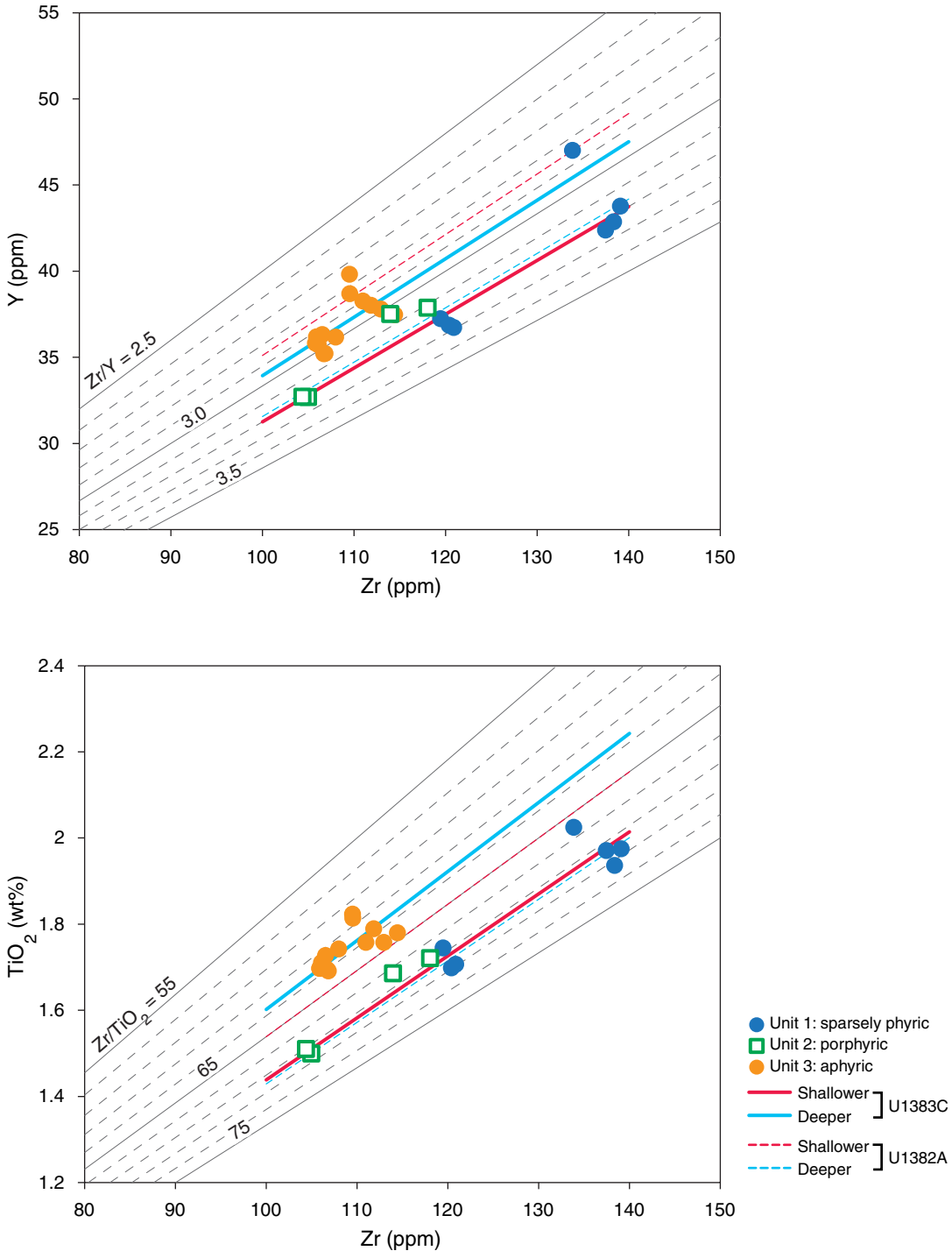

**Figure F25.** Plot of Zr/Y vs. $Zr/TiO_2$ for basaltic rock samples, Hole U1383C. Data ranges for shallower and deeper units in Hole U1382A are also shown for comparison. Note that the porphyritic unit in Hole U1382A belongs to a deeper unit, which has higher Zr/Y and $Zr/TiO_2$ values than shallower units, whereas that in U1383C belongs to a shallower unit, which has higher values than deeper units. This difference implies that the two petrographically similar basalts from Holes U1382A and U1383C were derived from different magma sources.

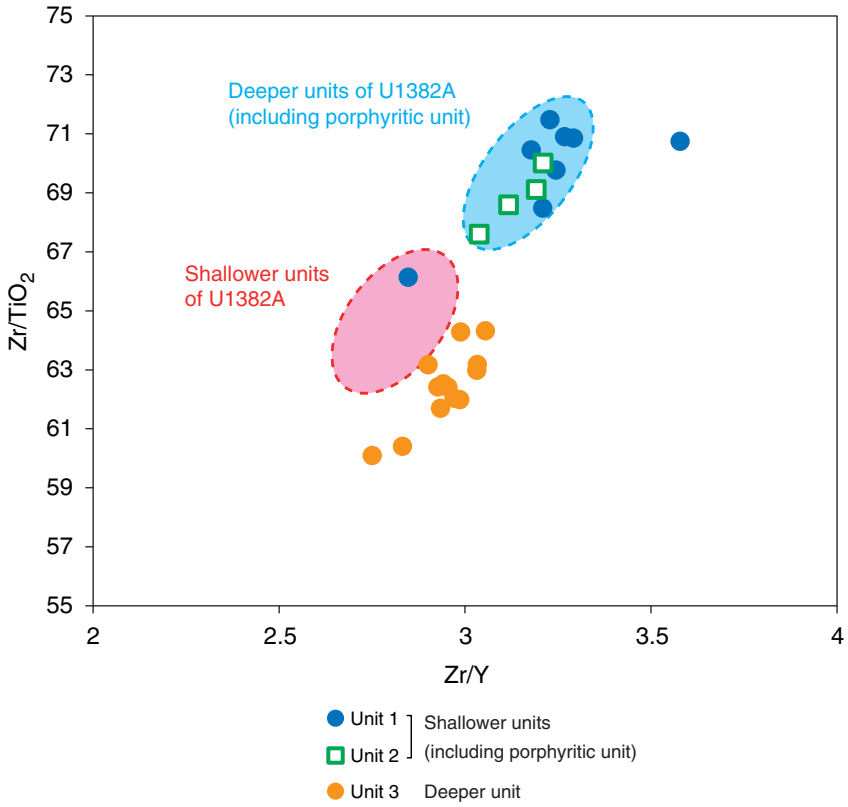

**Figure F26.** Plots of weight loss on ignition (LOI) vs. $K_2O$, CaO, Ba, and MgO for basaltic rock samples, Hole U1383C.

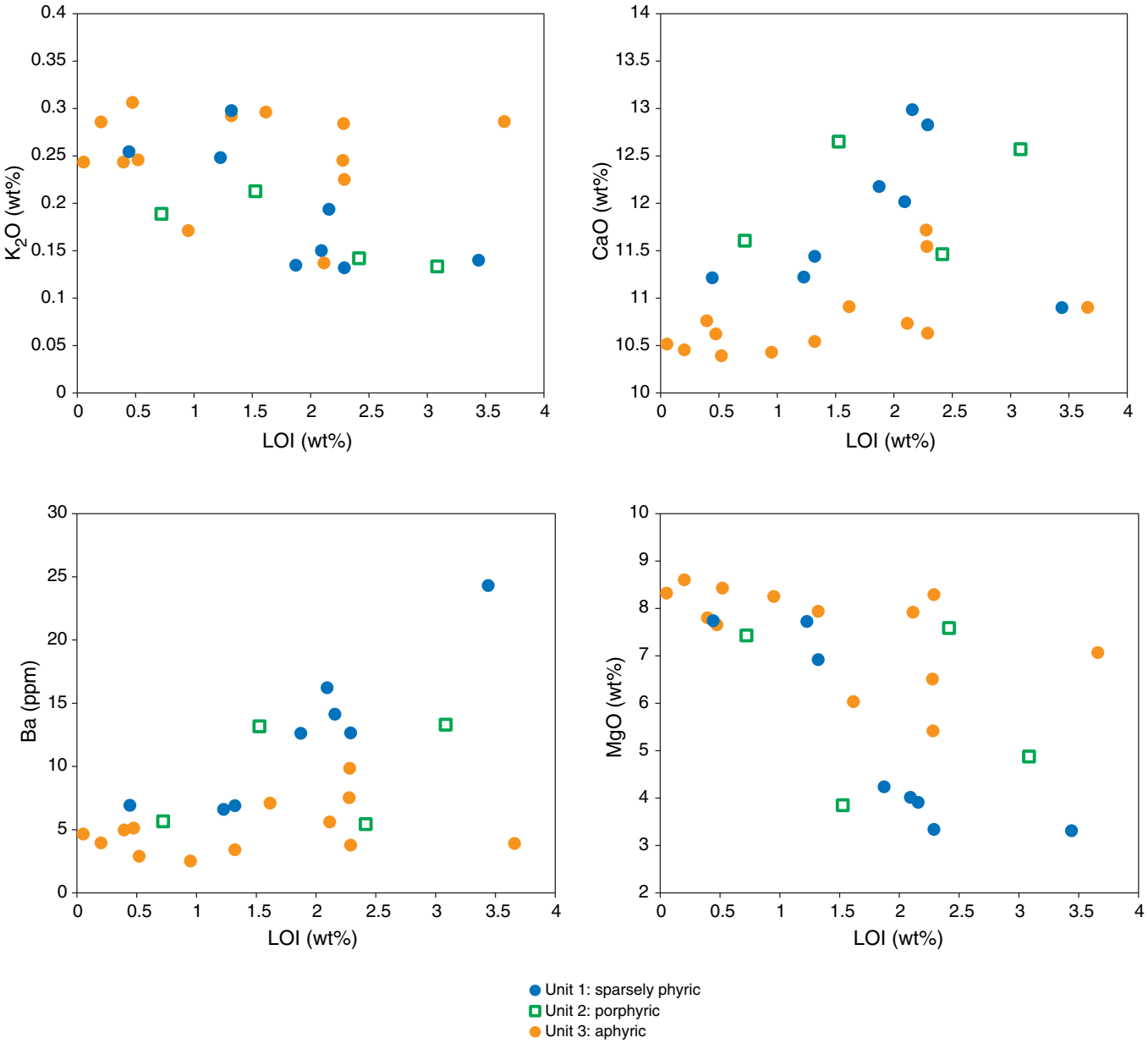

**Figure F27**. Fluorescence profile for pure microspheres. Each band (data not shown) represents a region of the fluorescence spectrum used by the DEBI-pt to characterize organic samples. Microspheres produce a unique fluorescence spectra with a peak emission at 320 nm when excited at 224 nm.

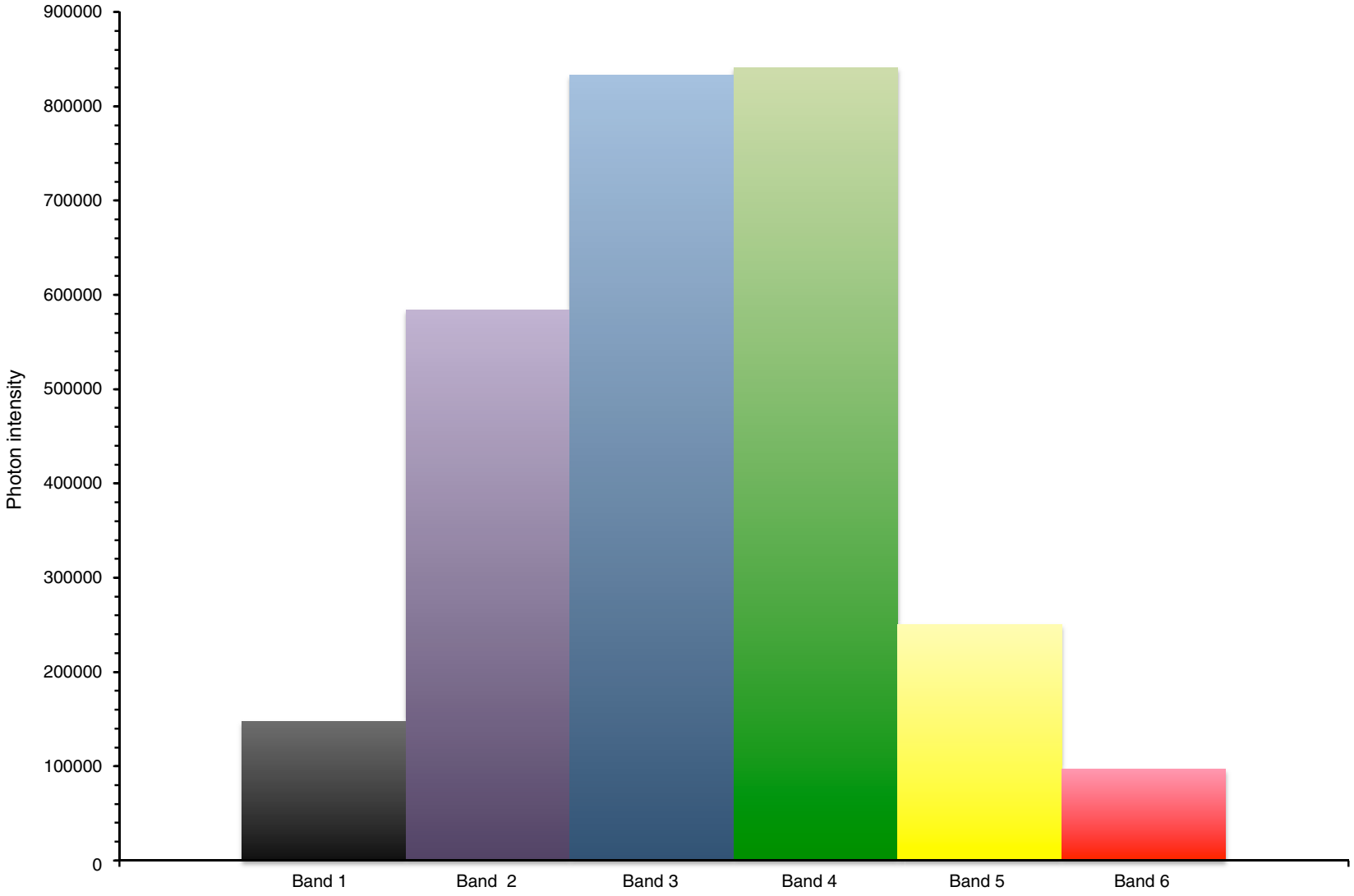

**Figure F28. A, B.** DEBI-pt scanning results for altered basalt from whole-round Sample 336-U1383C-6R-1-MBIOA. The sample shows heterogeneous regions of fluorescence from both mineralogical and biological signals. The maroon and pink fluorescence is indicative of silicates containing potassium, calcium, and magnesium. Regions of yellow and orange fluorescence indicate areas of the sample with detectable levels of organic carbon. Green areas indicate the presence of biomass. However, these regions tend to be found in the periphery.

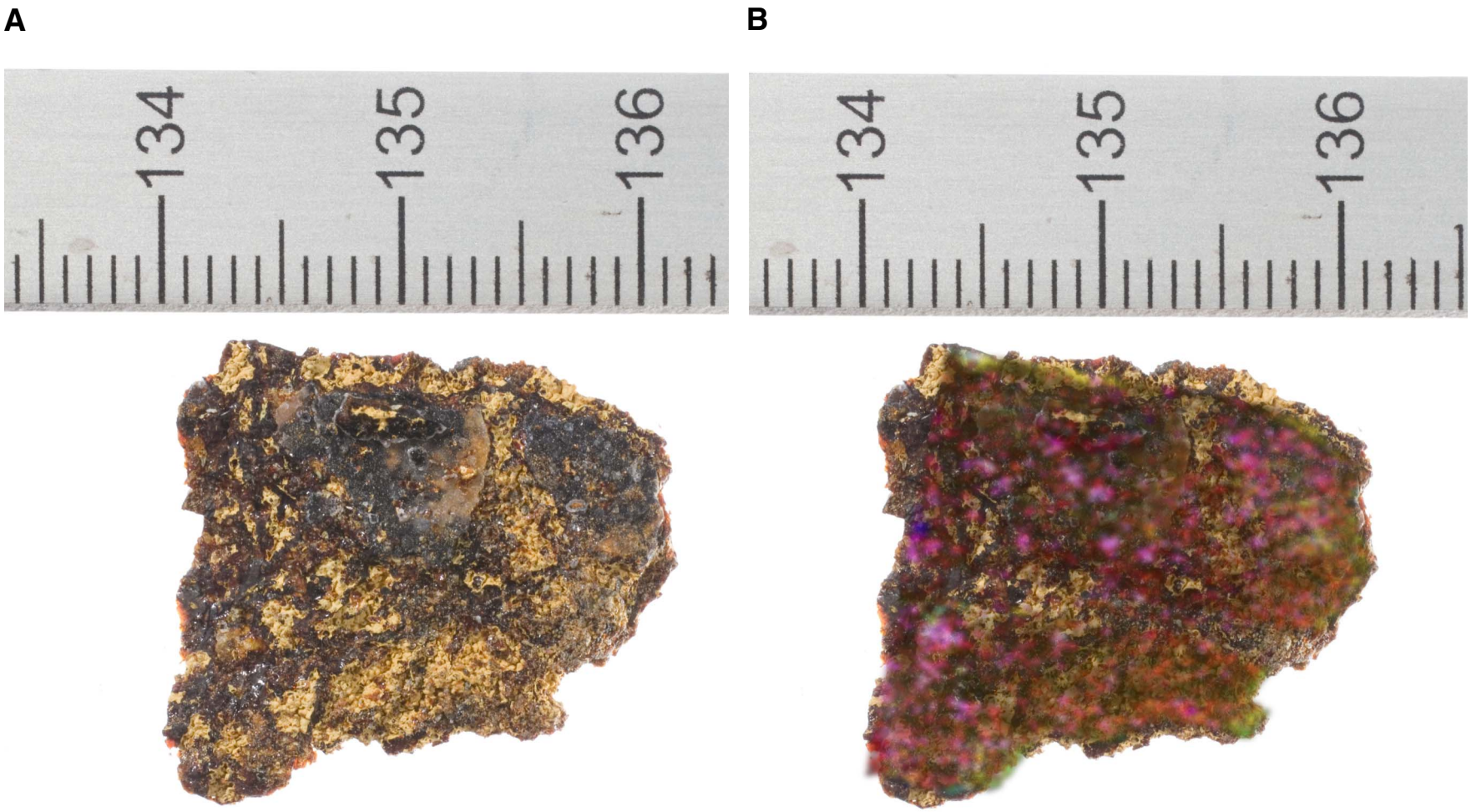

**Figure F29. A, B.** DEBI-pt scanning results for an aphyric variolitic basalt sample from whole-round Sample 336-U1383C-26R-1-MBIOA. Although mineral fluorescence (maroon) was detected throughout the sample, there were greater regions of organic fluorescence (yellow orange) compared to Sample 336-U1383C-6R-1-MBIOA (Fig. F28). The fluorescence from organics produced a large enough signal to obscure mineral fluorescence. Scale bar = 12 mm.

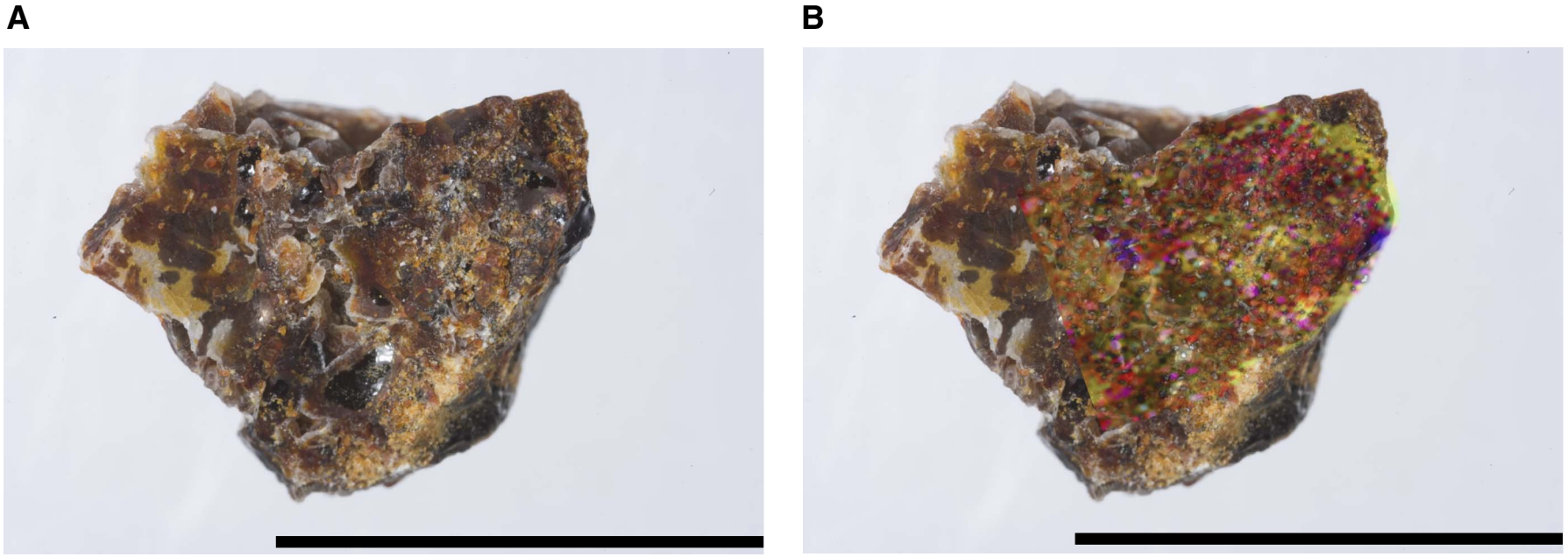

**Figure F30.** Gamma ray attenuation (GRA) density and moisture and density (MAD) measurements, Hole U1383C. **A.** GRA bulk density and density from discrete measurements. Gray intensity indicates more intense filtering. **B.** Bulk, dry, and grain densities calculated for discrete samples. **C.** Porosity. **D.** Void ratio.

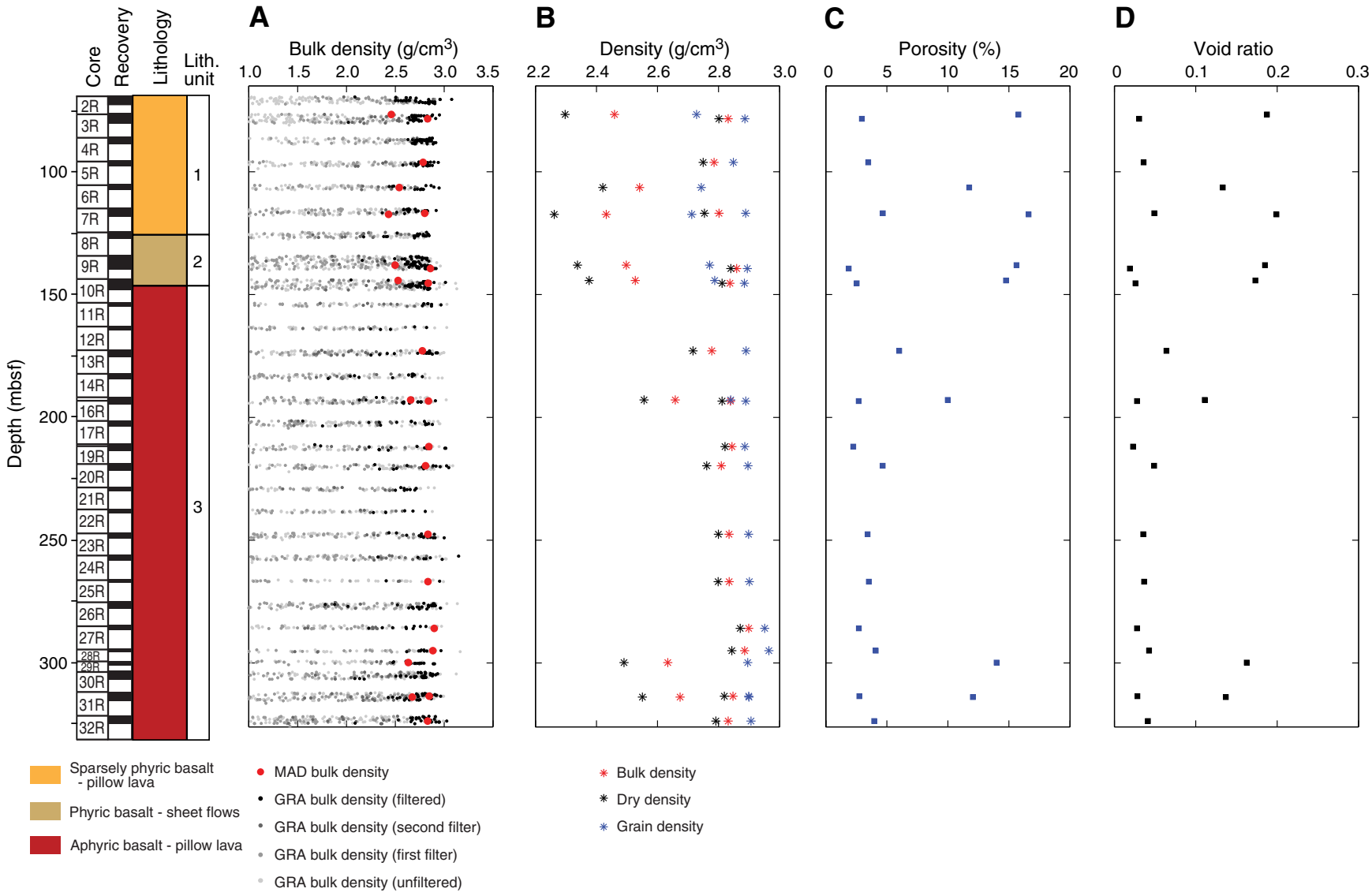

**Figure F31.** Whole-round and point magnetic susceptibility, Hole U1383C. Gray intensity indicates more intense filtering.

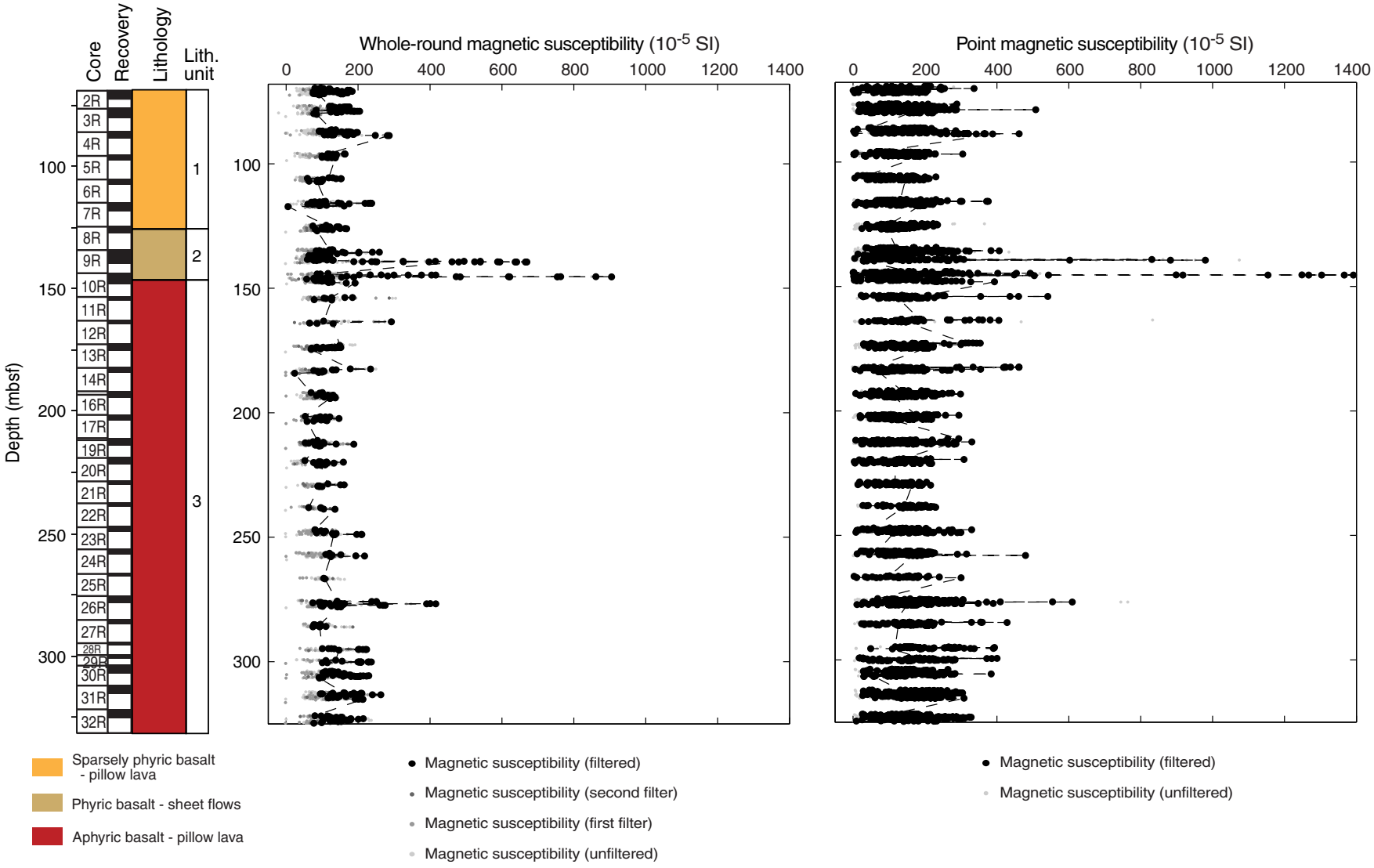

**Figure F32.** Natural gamma radiation (NGR) total counts per second (cps) and potassium percentage based on NGR and inductively coupled plasma–atomic emission spectrometry (ICP-AES) values, Hole U1383C.

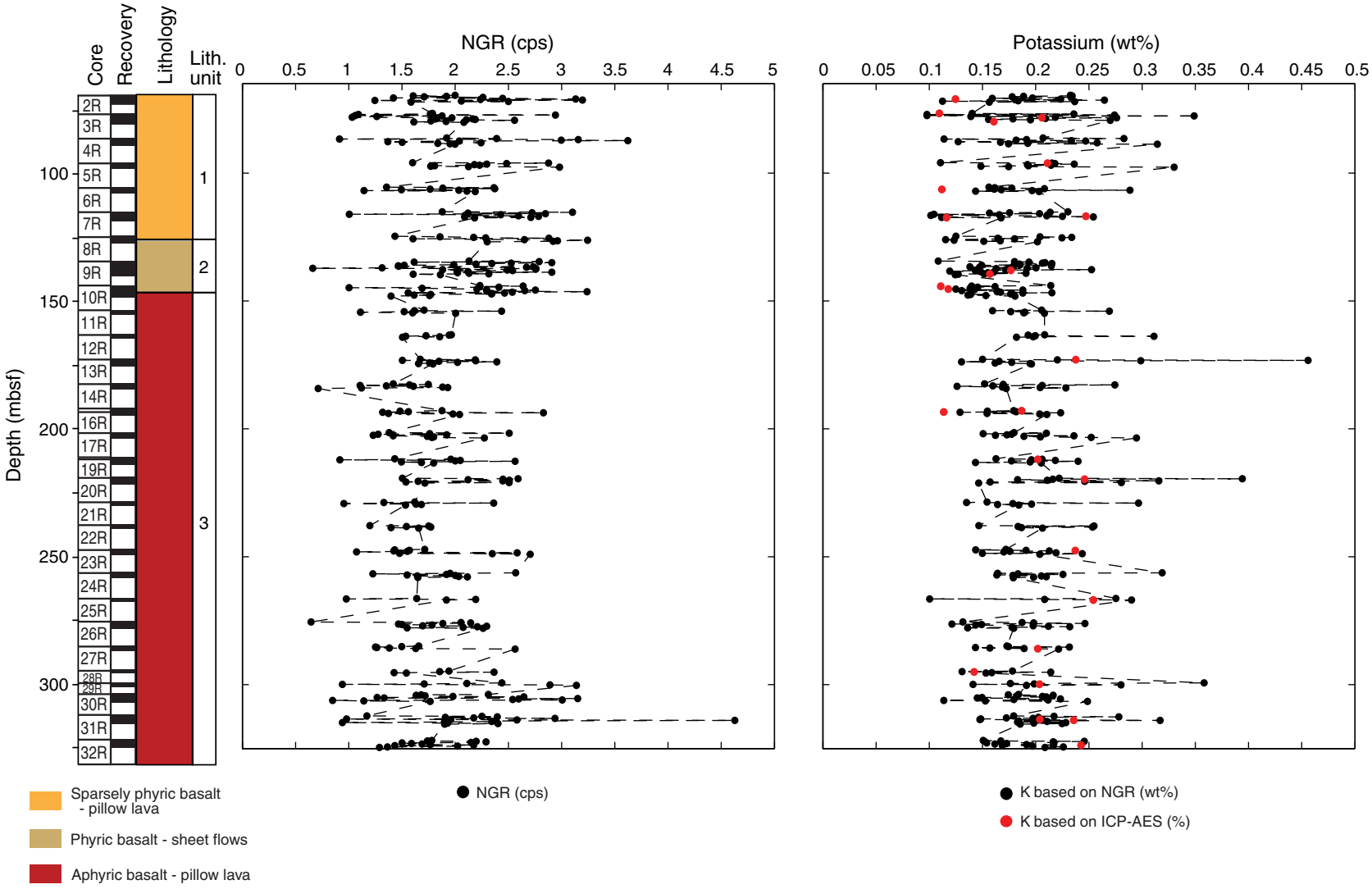

**Figure F33.** Summary of natural gamma ray log measurements, Hole U1383C. Note that downhole natural gamma radiation measurements are in gAPI (American Petroleum Institute gamma ray units). Measurements include total gamma ray (TGR), potassium abundance, thorium, and uranium. AMCII UL2 = adapted microbiology combination II (AMC II) Uplog 2, FMS p1 = Formation MicroScanner-sonic Pass 1, AMCII D1 = AMC II Downlog 1. K core = from NGR measured on the cores.

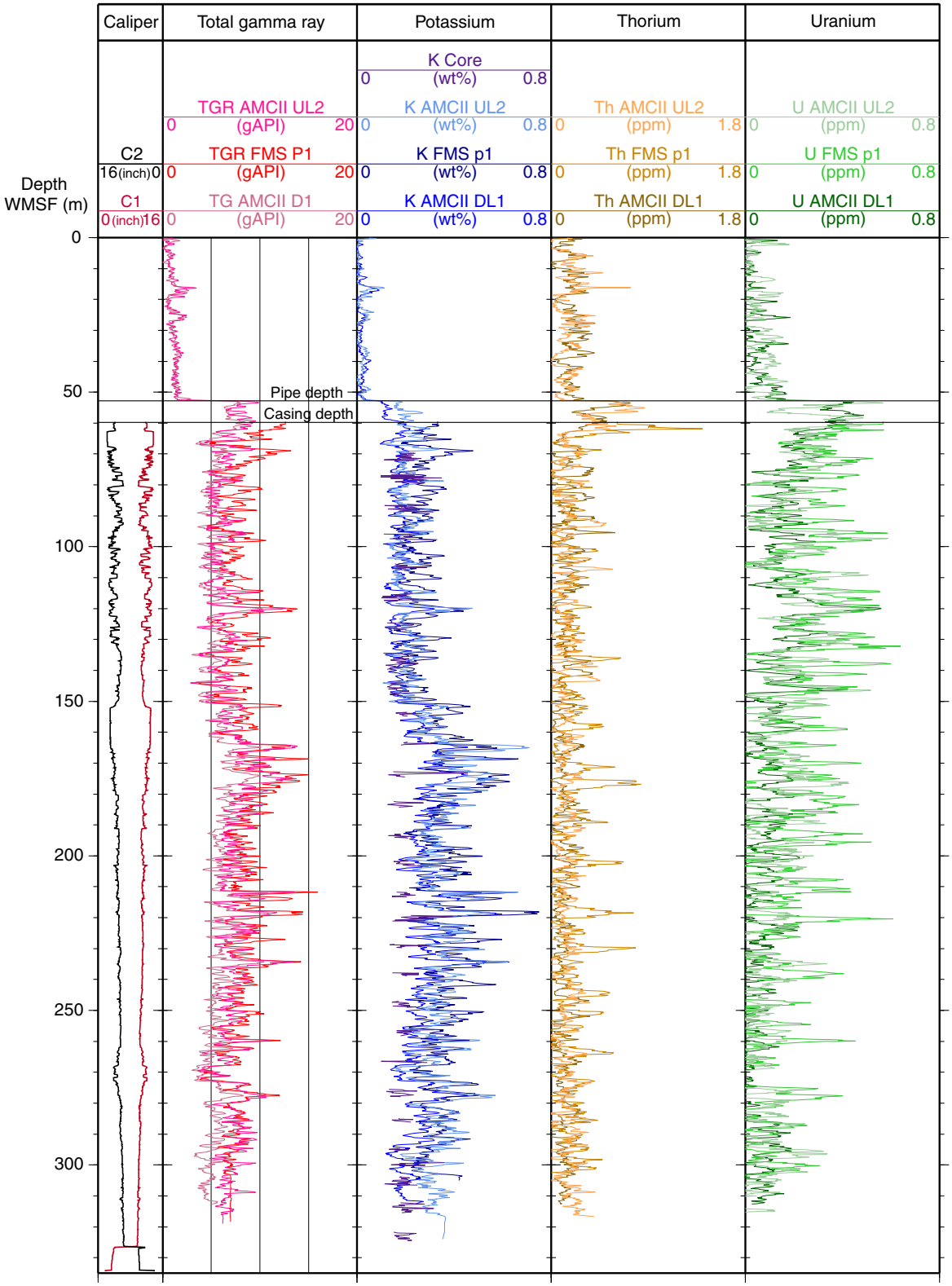

**Figure F34.** Porosity and bulk density correlation with *P*-wave velocity, Hole U1383C.

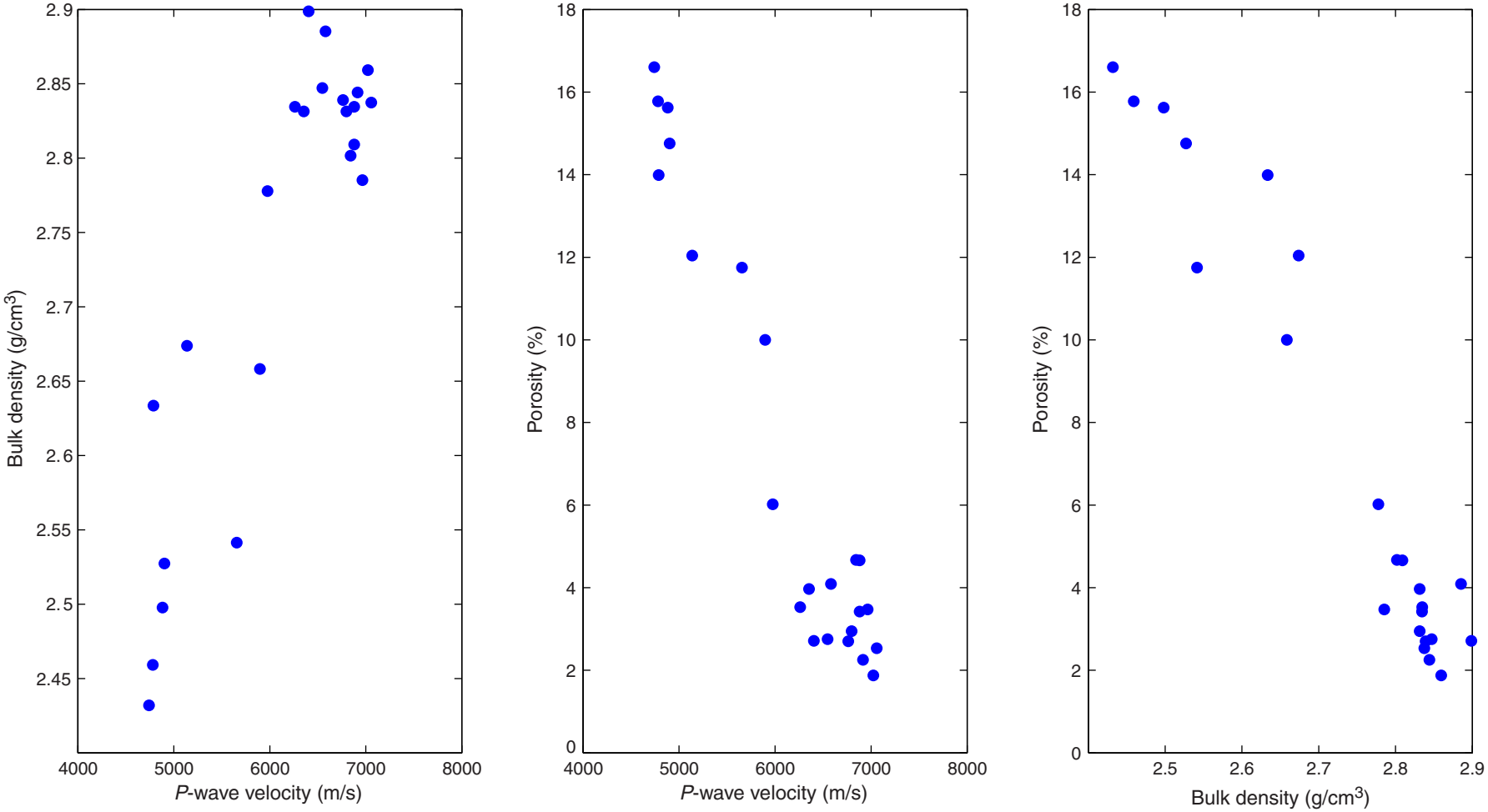

**Figure F35.** Porosity correlation with alteration and weight loss on ignition (LOI) values, Hole U1383C.

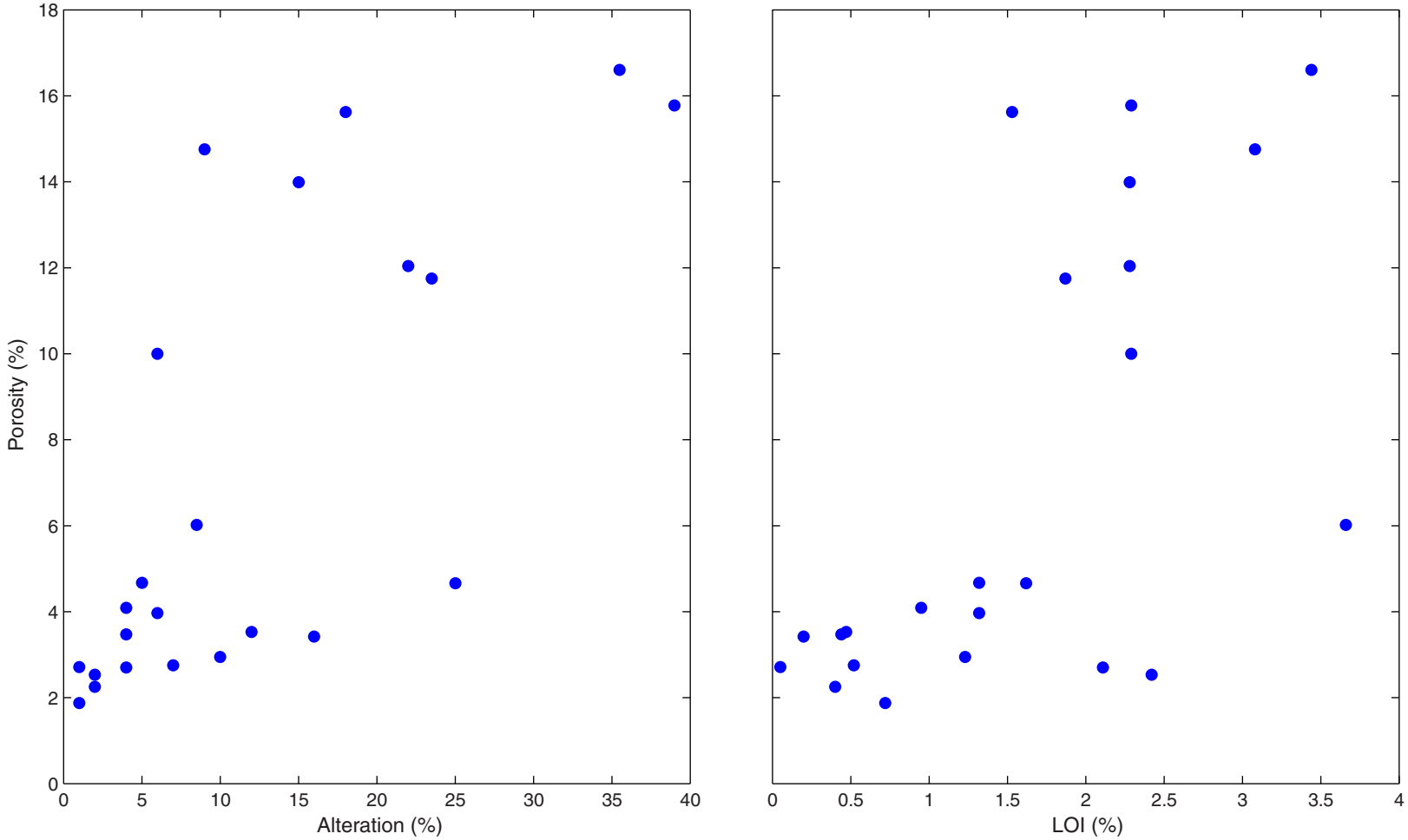

**Figure F36.** Compressional *P*-wave velocity measurements for *x*-, *y*-, and *z*-axes and percentage of alteration, Hole U1383C.

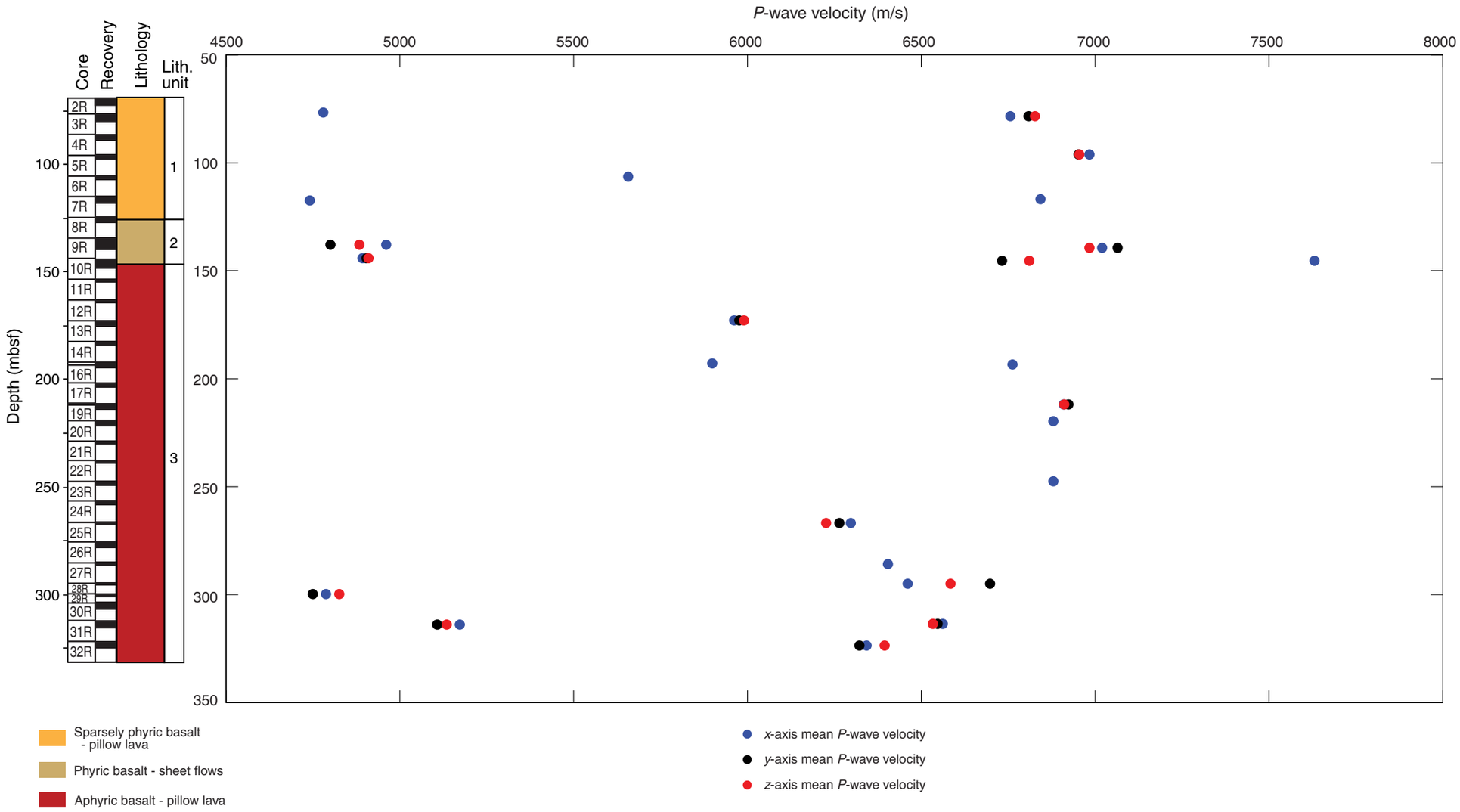

**Figure F37.** Thermal conductivity values for basalt core pieces longer than 6 cm, Hole U1383C. Gray indicates pieces with high presence of veins.

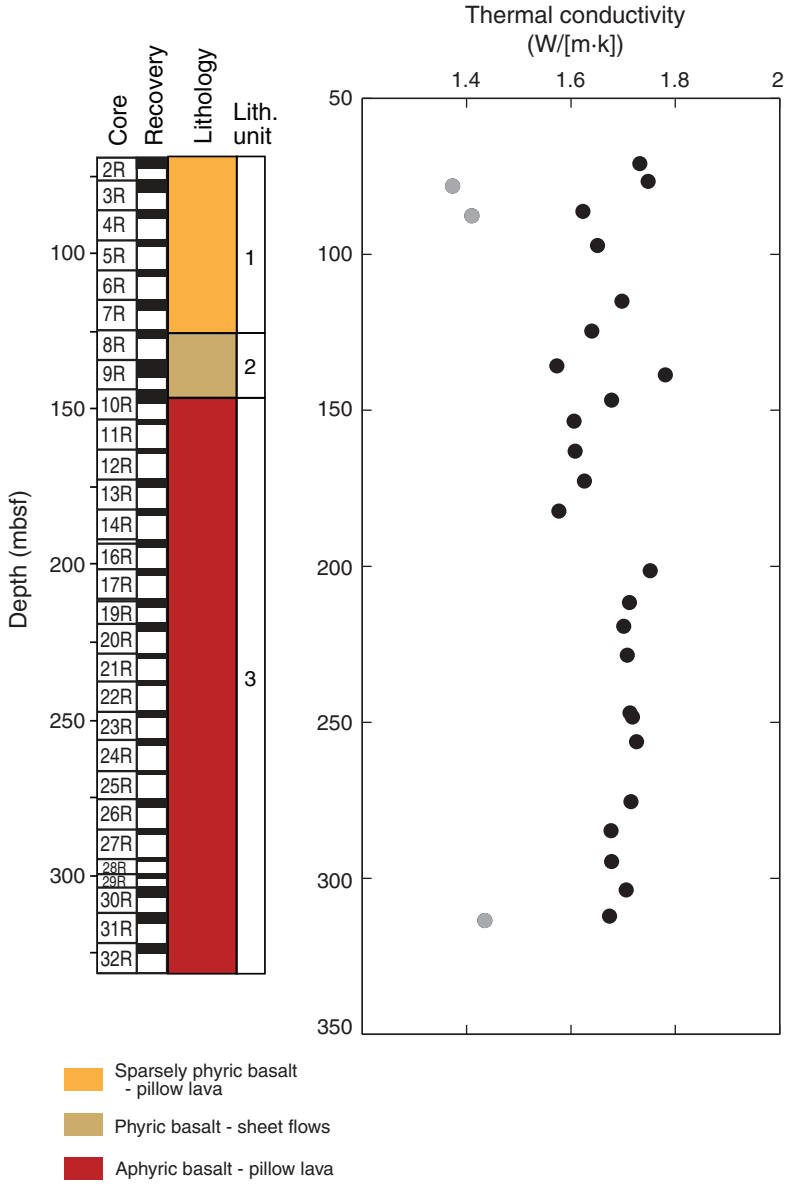

**Figure F38.** Plots of color reflectance and tristimulus axes values, Hole U1383C. L*, a* (green = negative, red = positive), b* (blue = negative, yellow = positive), and a*/b*.

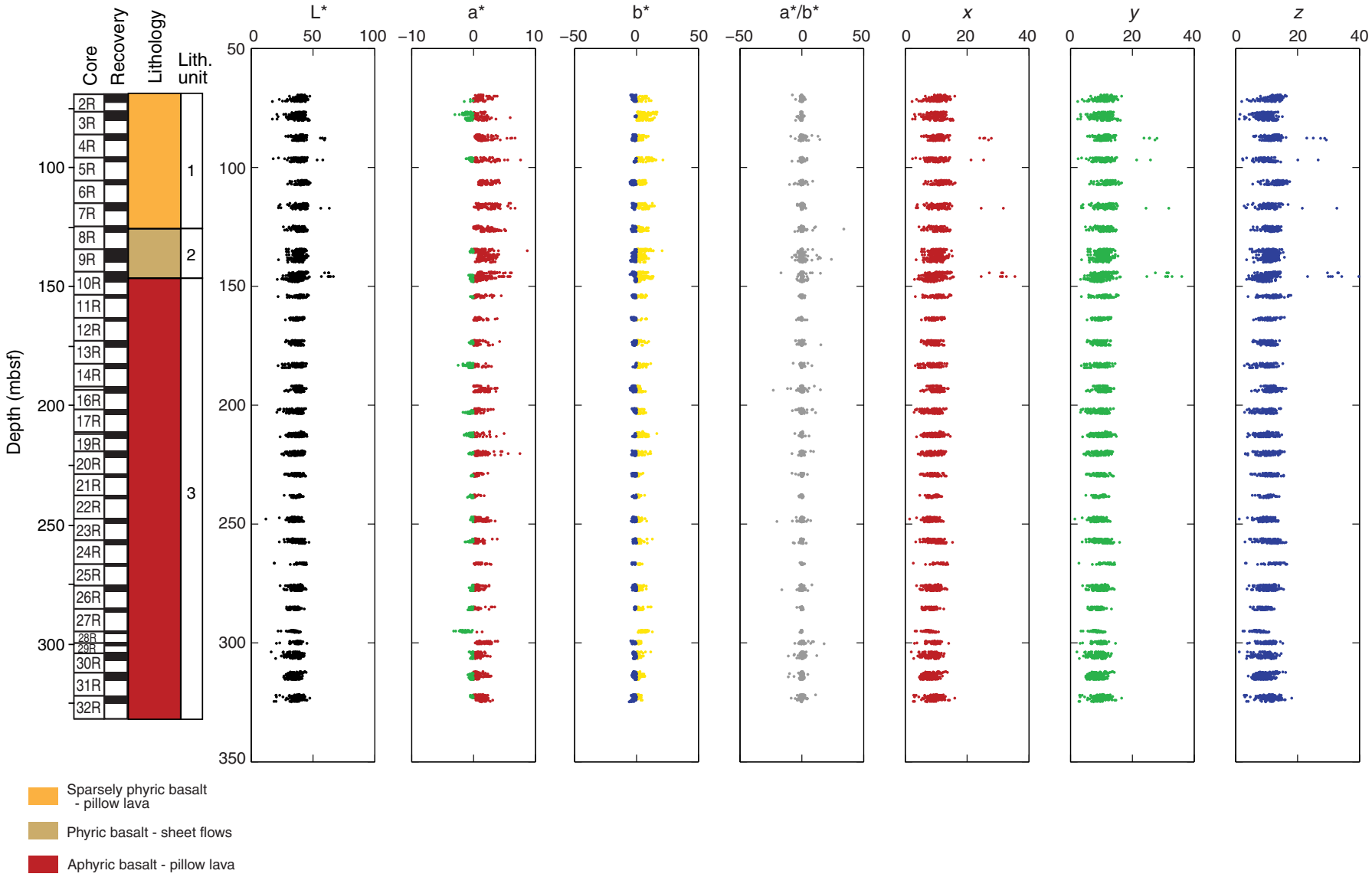

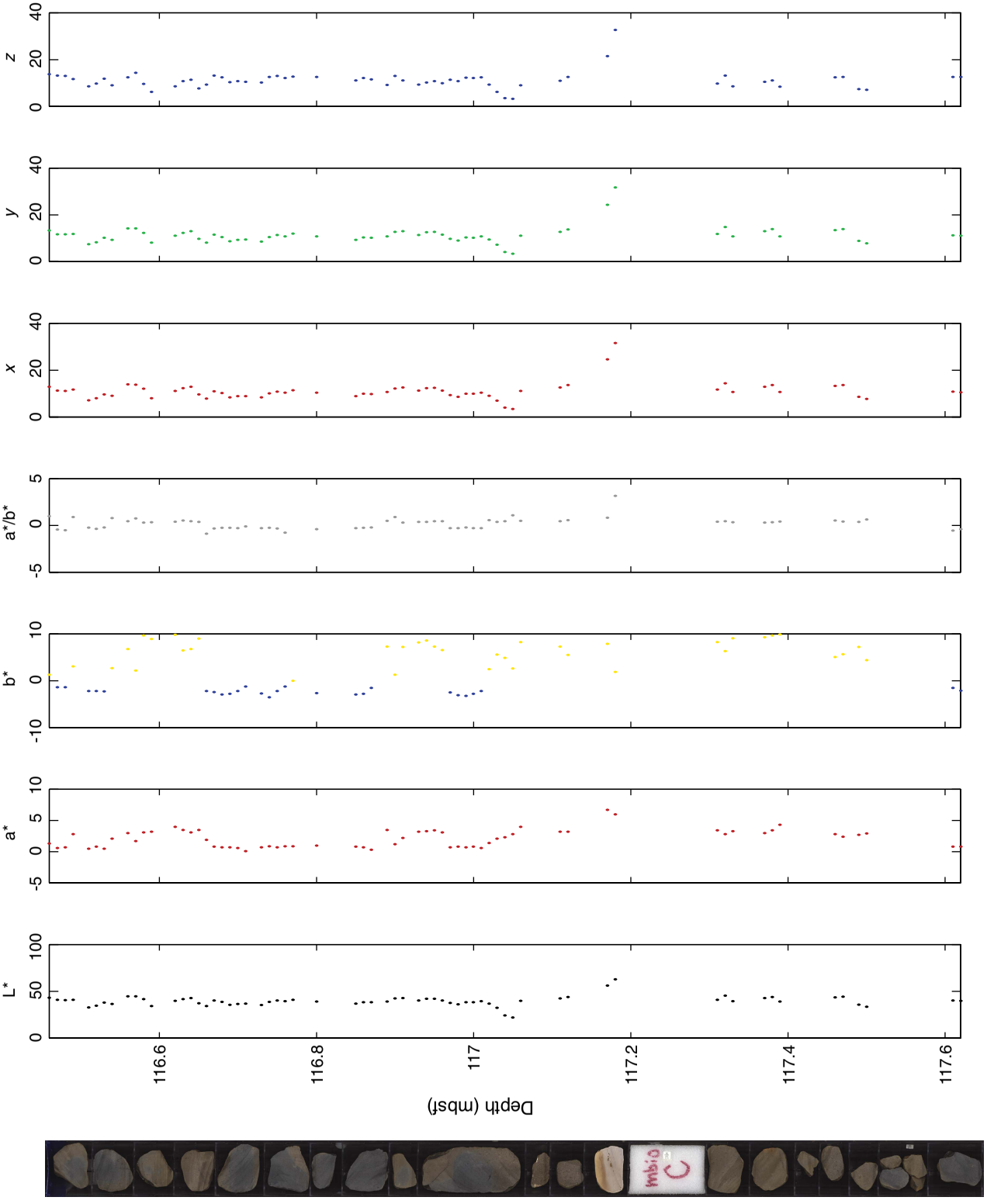


**Figure F39.** Detailed color reflectance values and scanned image of Section 336-U1383C-7R-2.

**Figure F40. A.** Adapted microbiology combination tool string II. LEH-QT = logging equipment head-q tension, EDTC = Enhanced Digital Telemetry Cartridge (gamma ray), HNGS = Hostile Environment Natural Gamma Ray Sonde, HLDS = Hostile Environment Litho-Density Sonde, ELIC = EFTB-Lamont Interface Cartridge, MFTM = Multifunction Telemetry Module, DEBI-t = Deep Exploration Biosphere Investigative tool. **B.** Schematic of Hole U1383C logging passes (two downlogs and two uplogs).

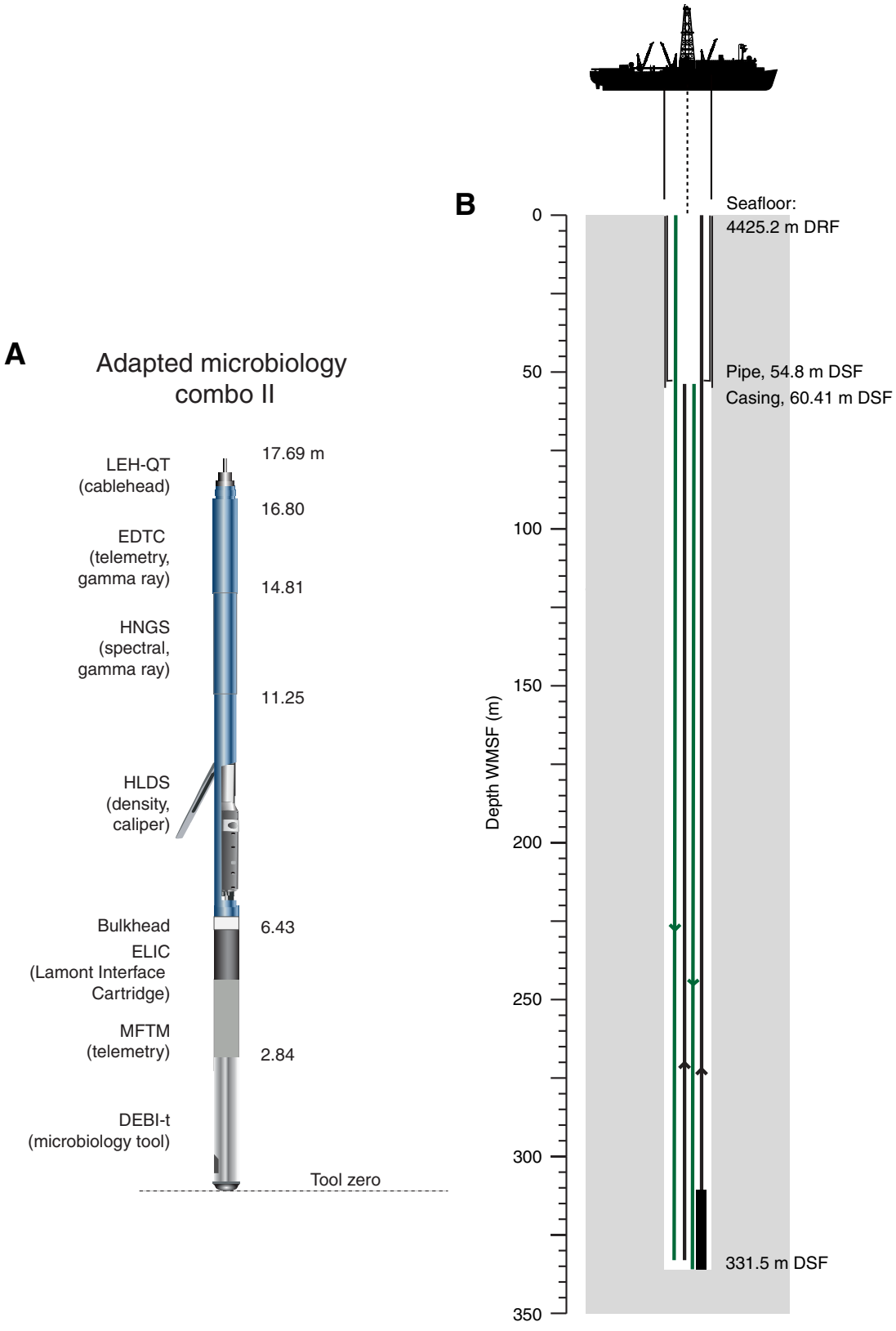

**Figure F41. A.** Formation MicroScanner (FMS)-sonic tool string. LEH-QT = logging equipment head-q tension, HNGS = Hostile Environment Natural Gamma Ray Sonde, DSI = Dipole Shear Sonic Imager, GPIT = General Purpose Inclinometry Tool. **B.** Schematic of Hole U1383C logging passes (two uplog passes).

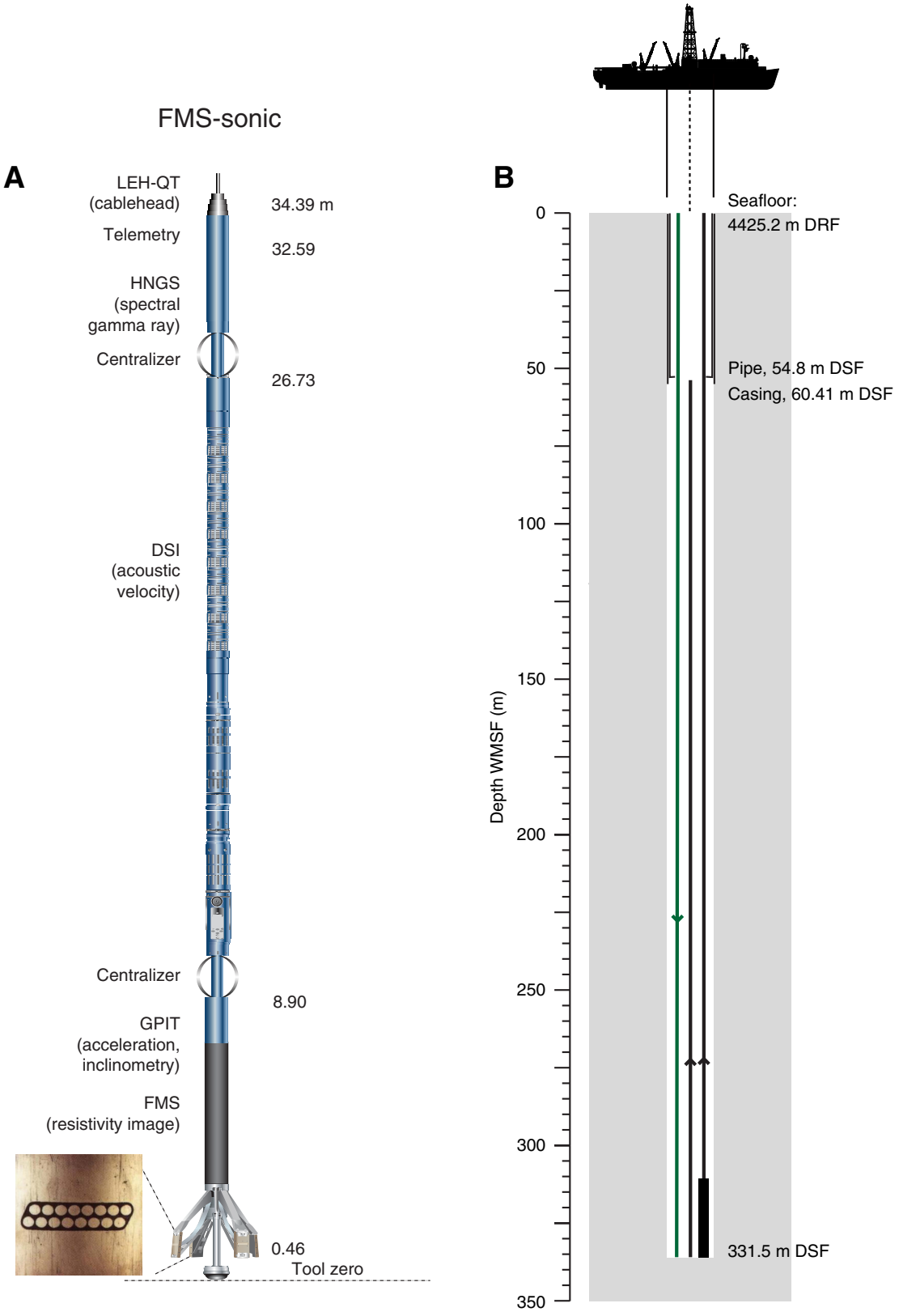

**Figure F42.** Summary of Hole U1383C logging results. Blue lines = log unit divisions, black lines = limits of pipe and casing. Measurements include borehole diameter (CALI = adapted microbiology combination II (AMC II) Uplog 1; FMS C1, C2 = Formation MicroScanner (FMS) Pass 1), total gamma ray (TGR) (AMCII UL2 = AMC II Uplog 2, FMS P1 = FMS-sonic Pass 1, FMS P2 = FMS-sonic Pass 2, AMCII D1 = AMC II Downlog 1), density (bulk density = AMC II Uplogs 1 and 2; MAD = moisture and density testing on discrete core samples), apparent resistivity (FMS P2 = FMS pad average from Pass 1, FMS P1 = FMS pad average from Pass 2), compressional velocity ($V_P$ core = from discrete core cube samples, $V_P$ P1 = FMS-sonic Pass 1, P2 = FMS-sonic Pass 2). A summary of core recovery and lithologic units is provided at the far left (see Fig. F4 for full explanation), and on the far right is electrical stratigraphy based on FMS electrical images.

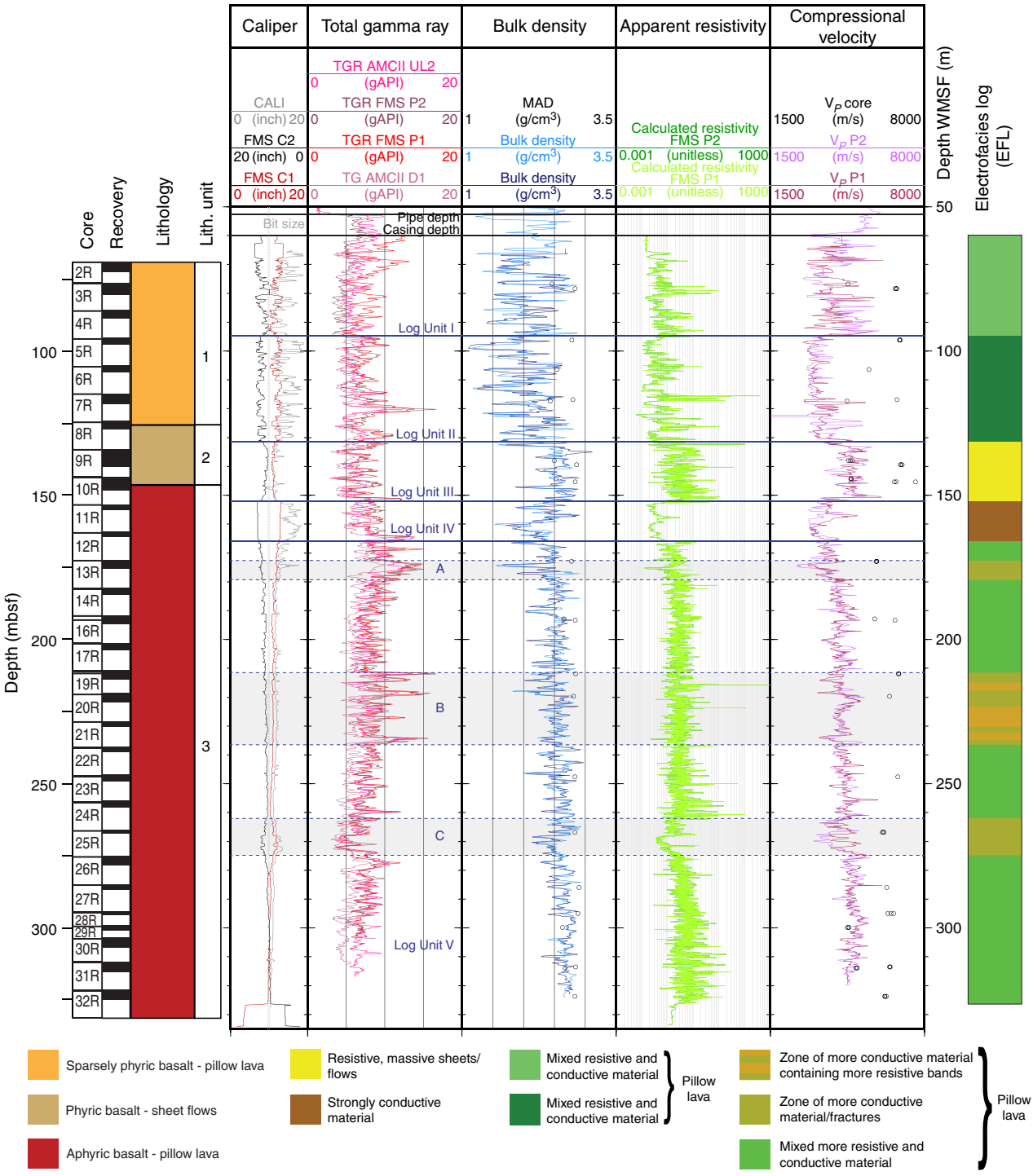

**Figure F43.** Summary comparing DEBI-t photon intensity data, Holes 395A, U1382A, and U1383C. The depth to which any pipe or casing was present is represented by a black line, and the shaded gray areas highlight the open-hole section.

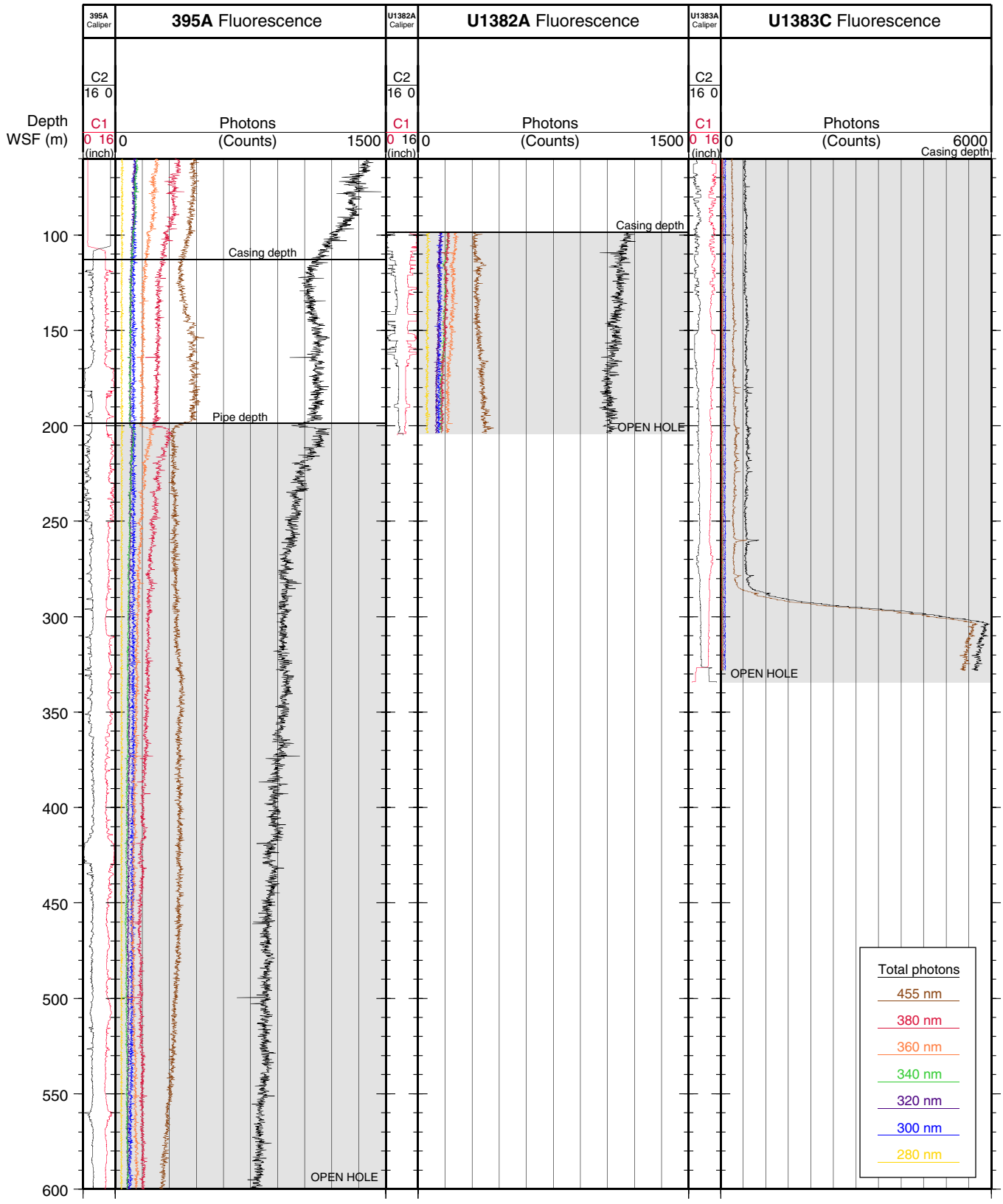

**Figure F44.** DEBI-t photon intensity data, Hole U1383C downlog.

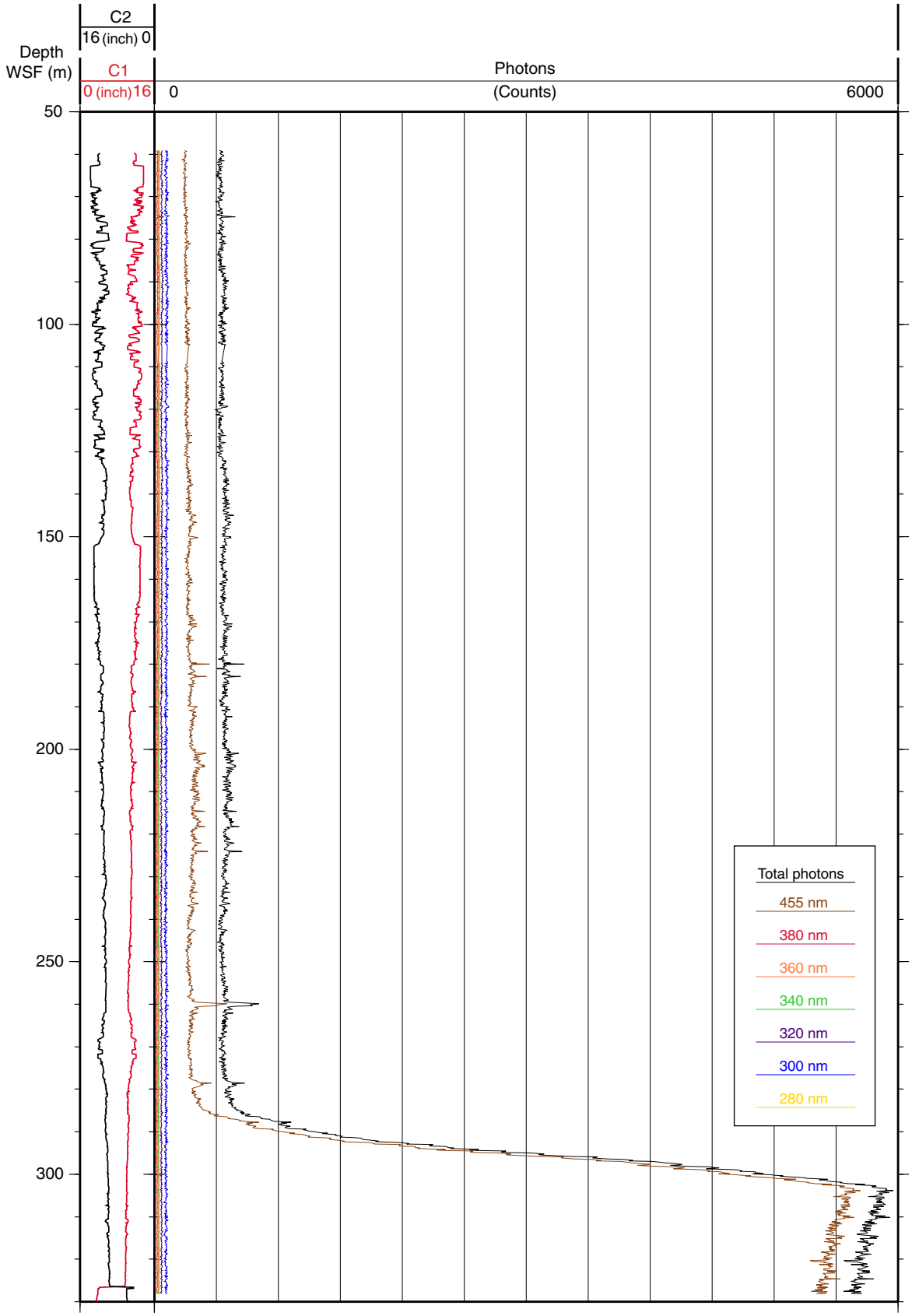

**Figure F45.** DEBI-t photon intensity data, Hole U1383C uplog.

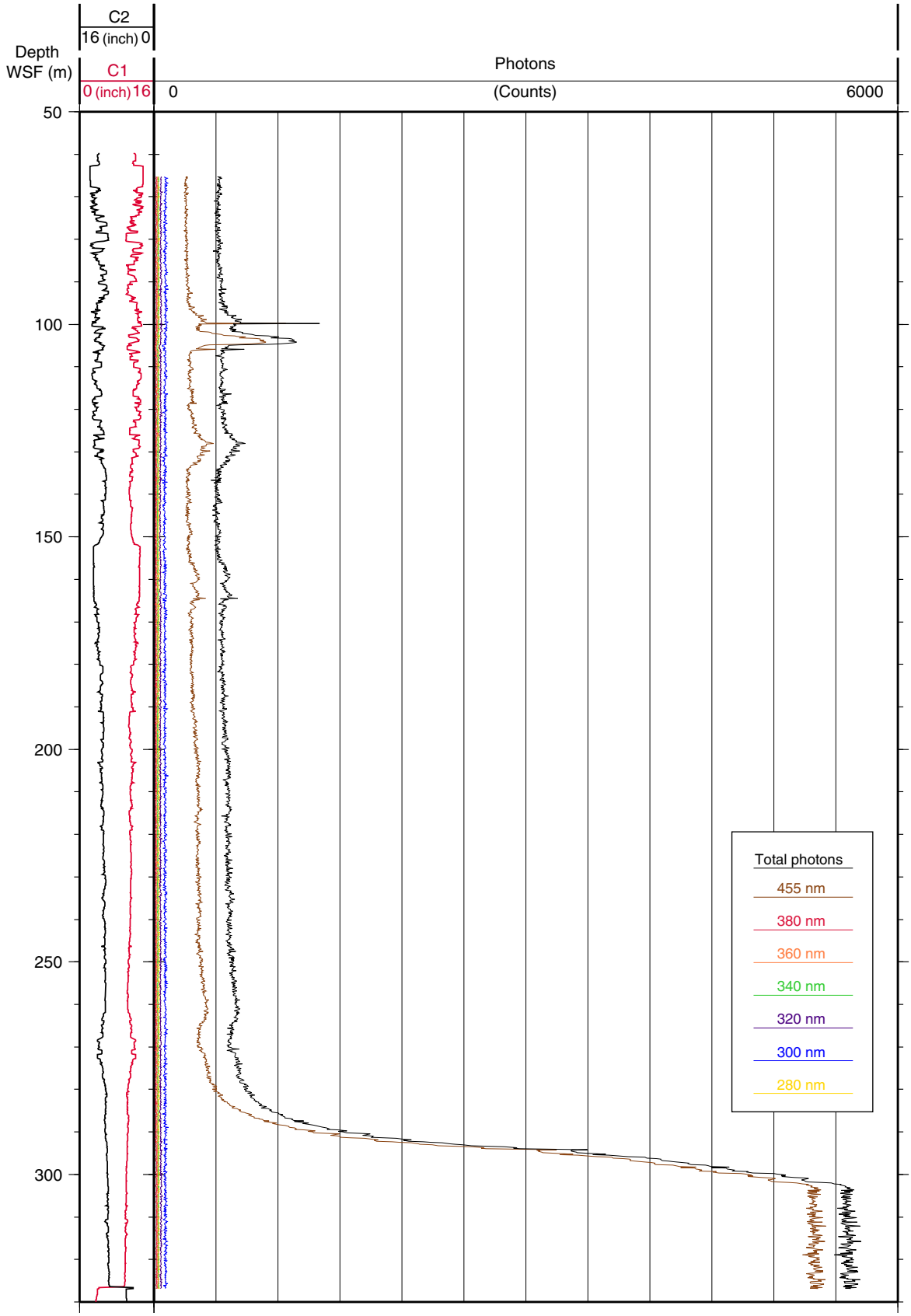

**Figure F46.** Composite of features imaged by the Formation MicroScanner (FMS), Hole U1383C. Note that images here are shown from Pass 1 of the FMS-sonic tool string. **A.** Boundary between log Units I and II, moving from more a resistive to more conductive region. **B.** Typical section in log Unit II. **C.** Nature of boundary between log Units III and IV. **D.** Zone of typical pillow lavas visible in log Unit IV. A high-resolution bulk density curve (in blue) is shown to the right of each FMS image for information.

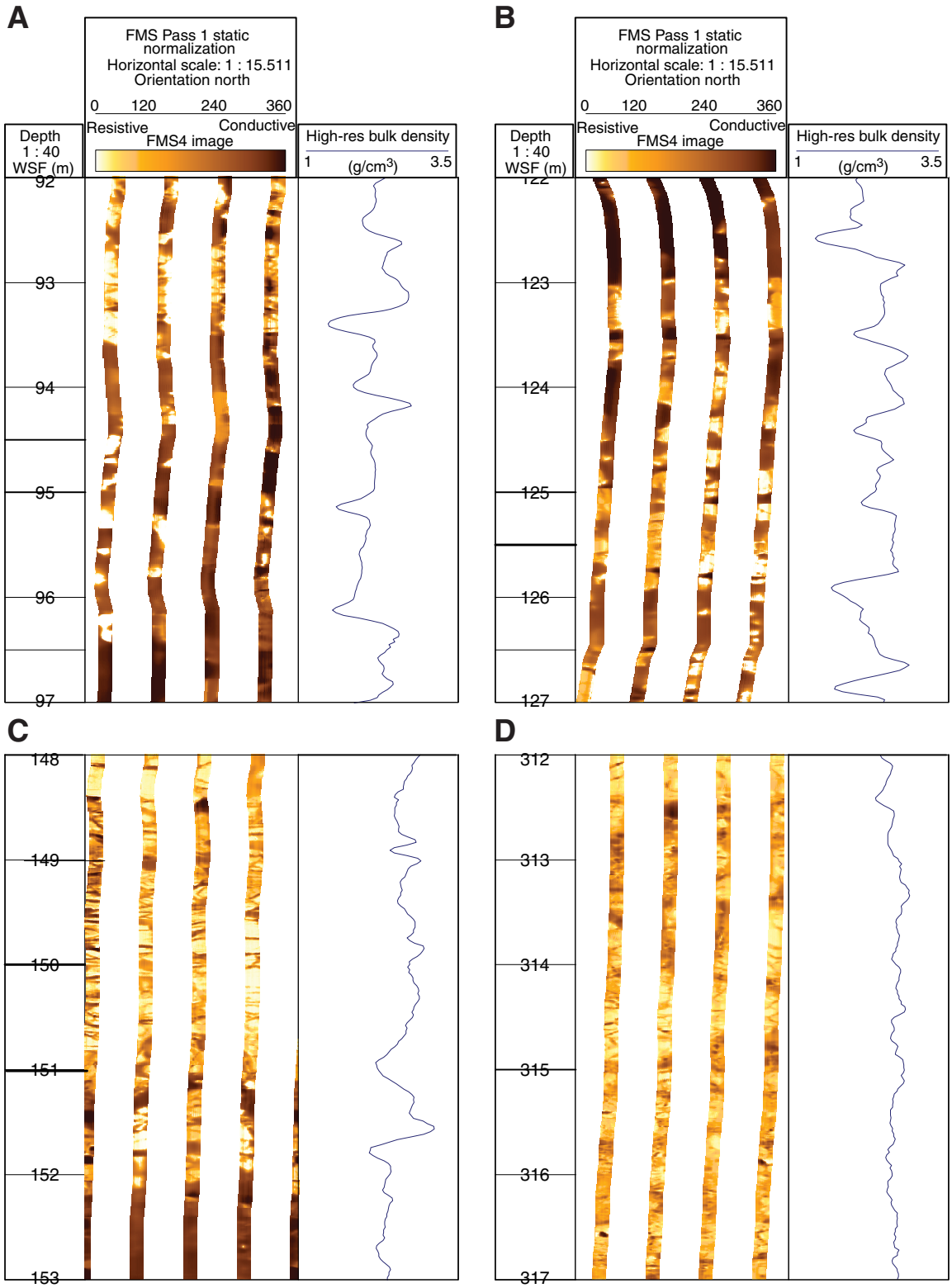

**Figure F47.** Pressure and temperature records collected with Micro-Smart downhole electronic Gauge 4986 during attempted packer experiments, Hole U1383C.

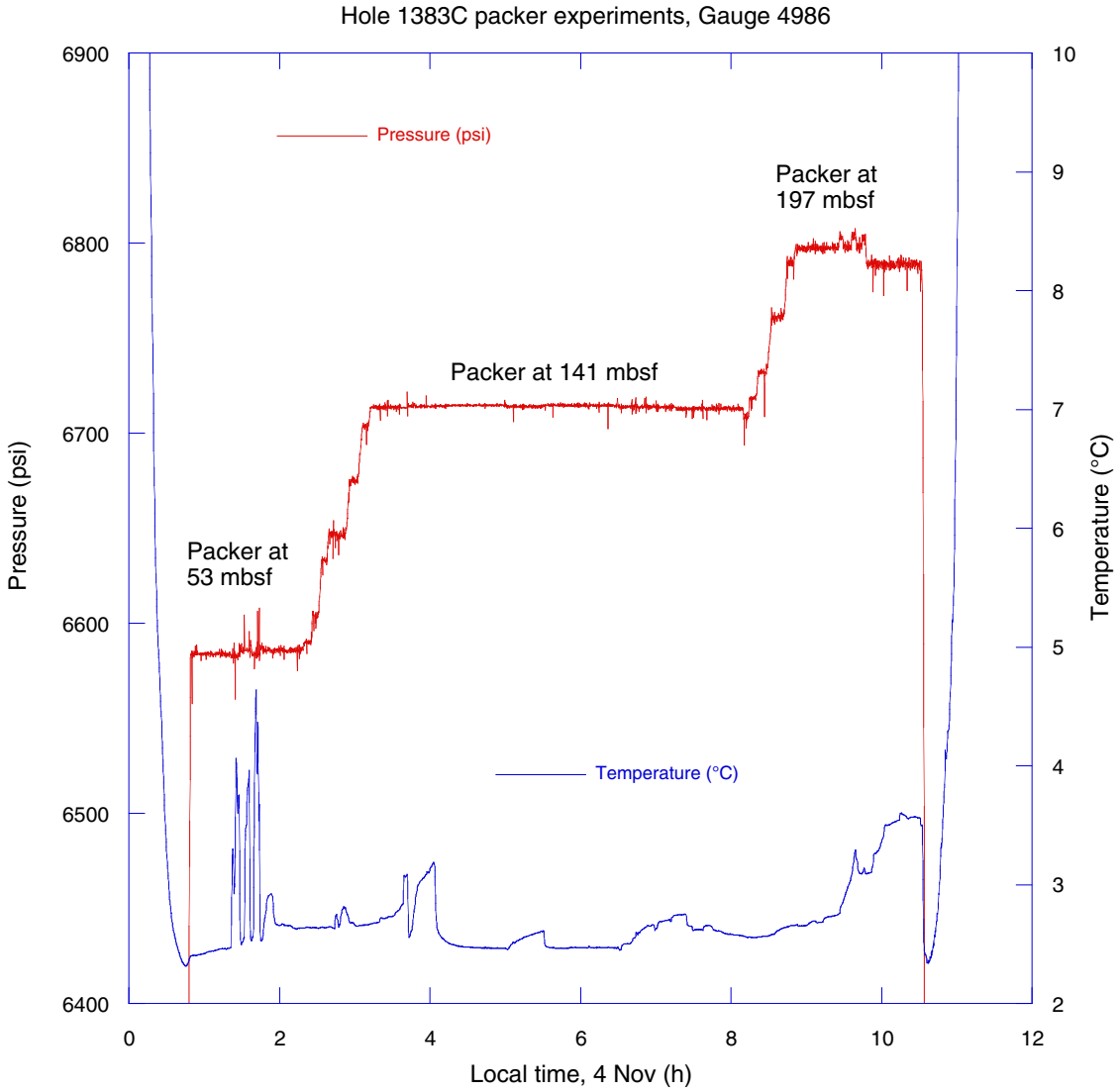

**Table T1.** Summary of basement operations completed at Site U1383. Operations included (A) a jet-in test in Hole U1383A; (B) installing a reentry cone with 16 inch casing, installing 10.75 inch casing, drilling a 14.75 inch hole below the casing with a bit failure, and installing a remotely operated vehicle (ROV) platform in Hole U1383B; and (C) installing a reentry cone and two casing strings, rotary core barrel (RCB) coring to 331.5 mbsf, downhole logging and packer experiments, and installing a multilevel subseafloor borehole observatory (CORK) in Hole U1383C. (Continued on next five pages.)

| Operational task | Start Date (2011) | Start Time (h) | End Date (2011) | End Time (h) | Task time Hours | Task time Days |
|---|---|---|---|---|---|---|
| **(A) Hole U1383A: jet-in test at proposed Site NP-2** | | | | | | |
| Make up 18.5 inch tricone bit | | | | | | |
| Handle BHA (will take 1 h) | 12 Oct | 1230 | 12 Oct | 1400 | 1.50 | 0.06 |
| Trip: surface to mudline, ±1 h in 4425 m of water | 12 Oct | 1400 | 12 Oct | 2045 | 6.75 | 0.28 |
| Handle camera (will take 0.5 h) | 12 Oct | 2045 | 12 Oct | 2100 | 0.25 | 0.01 |
| Pick up top drive and space out drill pipe (will take 0.75 h) | 12 Oct | 2100 | 12 Oct | 2145 | 0.75 | 0.03 |
| Drill string tag (will take 0.5 h) | 12 Oct | 2145 | 12 Oct | 2215 | 0.50 | 0.02 |
| Begin to recover camera frame | | | | | | |
| Record SCRs and space out for jet-in test (will take 0.25 h); spud Hole U1383A at 2240 h | 12 Oct | 2215 | 12 Oct | 2245 | 0.50 | 0.02 |
| Jet-in test (will take 6 h) to 4461 mbrf (36 mbsf); very firm with max weight down and 120 spm (ROP ~1.0 m/h) | 12 Oct | 2245 | 13 Oct | 0200 | 3.25 | 0.14 |
| Pull out of hole (will take 0.5 h); top drive clears seafloor at 0221 h | 13 Oct | 0200 | 13 Oct | 0245 | 0.75 | 0.03 |
| Set back top drive (will take 0.25 h) | 13 Oct | 0245 | 13 Oct | 0300 | 0.25 | 0.01 |
| Trip: depth to surface: from (mudline) 0 mbsf to surface, plus 0 h in 4425 m of water | 13 Oct | 0300 | 13 Oct | 0900 | 6.00 | 0.25 |
| Handle BHA (will take 1 h) | 13 Oct | 0900 | 13 Oct | 0930 | 0.50 | 0.02 |
| Bit clears rig floor at 0931 h; end of Hole U1383A | | | | | | |
| **Hole U1383A totals:** | 12 Oct | 1230 | 13 Oct | 0930 | 21.00 | 0.88 |
| **(B) Hole U1383B: install reentry cone and 20 inch casing** | | | | | | |
| Reentry cone (will take 2 h) | 13 Oct | 0930 | 13 Oct | 1015 | 0.75 | 0.03 |
| Run 20 inch casing | | | | | | |
| Rig up/down for casing (will take 1 h) | 13 Oct | 1015 | 13 Oct | 1030 | 0.25 | 0.01 |
| Assemble 20 inch casing | 13 Oct | 1030 | 13 Oct | 1245 | 2.25 | 0.09 |
| Rig up/down for casing (will take 0.25 h) | 13 Oct | 1245 | 13 Oct | 1315 | 0.50 | 0.02 |
| Make up casing running tool (will take 0.5 h) | 13 Oct | 1315 | 13 Oct | 1315 | 0.00 | 0.00 |
| Lower 20 inch casing and latch into reentry funnel (will take 0.5 h) | 13 Oct | 1315 | 13 Oct | 1345 | 0.50 | 0.02 |
| Release running tool, pull back to rig floor, and RIH with bottom section of BHA (will take 0.5 h) | 13 Oct | 1345 | 13 Oct | 1415 | 0.50 | 0.02 |
| RIH and latch running tool into reentry cone (will take 0.5 h) | 13 Oct | 1415 | 13 Oct | 1500 | 0.75 | 0.03 |
| Pick up reentry cone and open moonpool doors/lower reentry cone (will take 0.25 h) | 13 Oct | 1500 | 13 Oct | 1515 | 0.25 | 0.01 |
| Reentry funnel in water at 1522 h | | | | | | |
| Handle BHA (will take 1 h) | 13 Oct | 1515 | 13 Oct | 1545 | 0.50 | 0.02 |
| Trip: surface to mudline, plus 0 h in 4425 m of water | 13 Oct | 1545 | 13 Oct | 2330 | 7.75 | 0.32 |
| Deploy camera (will take 0.5 h) | 13 Oct | 2330 | 14 Oct | 0000 | 0.50 | 0.02 |
| Pick up top drive and space out drill pipe (will take 1 h) | 14 Oct | 0000 | 14 Oct | 0100 | 1.00 | 0.04 |
| Spud Hole U1383B at 0100 h | | | | | | |
| Jet-in casing (will take 5 h) | 14 Oct | 0100 | 14 Oct | 0500 | 4.00 | 0.17 |
| Repair mud pump #2; sheared pin in the pony rod (will take 0.5 h) | 14 Oct | 0500 | 14 Oct | 0530 | 0.50 | 0.02 |
| Resume jetting-in casing (will take 1 h) | 14 Oct | 0530 | 14 Oct | 0730 | 2.00 | 0.08 |
| POOH with 20 inch casing to clear seafloor, and move 50 m at 045° (will take 0.75 h) | 14 Oct | 0730 | 14 Oct | 0815 | 0.75 | 0.03 |
| Stop jet-in of 20 inch casing at 0728 h; clear seafloor at 0730 h | | | | | | |
| Resume jet-in of 20 inch casing (will take 2 h); spud at 0810 h | 14 Oct | 0815 | 14 Oct | 1015 | 2.00 | 0.08 |
| Release running tool (will take 1 h); release at 1035 h | 14 Oct | 1015 | 14 Oct | 1030 | 0.25 | 0.01 |
| Set back top drive (will take 0.5 h) | 14 Oct | 1030 | 14 Oct | 1100 | 0.50 | 0.02 |
| Trip: mudline to surface, ±1 h in 4425 m of water | 14 Oct | 1100 | 14 Oct | 1715 | 6.25 | 0.26 |
| Recover camera (will take 0.5 h) | 14 Oct | 1715 | 14 Oct | 1730 | 0.25 | 0.01 |
| Handle BHA (will take 1 h) | 14 Oct | 1730 | 14 Oct | 1815 | 0.75 | 0.03 |
| De-torque and lay out casing running tool and lay out drill collars pups (will take 1 h) | 14 Oct | 1815 | 14 Oct | 1915 | 1.00 | 0.04 |
| **Hole U1383B: drill out 18.5 inch hole for 16 inch casing** | | | | | | |
| Change out bit jets in 18.5 inch tricone bit (will take 0.5 h) | 14 Oct | 1915 | 14 Oct | 1945 | 0.50 | 0.02 |
| Handle BHA (will take 0.75 h) | 14 Oct | 1945 | 14 Oct | 2015 | 0.50 | 0.02 |
| Trip: surface to 2978 mbrf (will take 5 h) | 14 Oct | 2015 | 15 Oct | 0115 | 5.00 | 0.21 |
| Deploy camera (will take 0.5 h) | 15 Oct | 0115 | 15 Oct | 0130 | 0.25 | 0.01 |
| Slip/Cut drill line at 100 stands (will take 1.5 h) | 15 Oct | 0130 | 15 Oct | 0245 | 1.25 | 0.05 |
| Trip from 2978 mbrf to mudline (will take 2 h) | 15 Oct | 0245 | 15 Oct | 0515 | 2.50 | 0.10 |
| Maneuver ship for reentry (will take 0.5 h); reenter Hole U1383B at 0518 h | 15 Oct | 0515 | 15 Oct | 0515 | 0.00 | 0.00 |
| Recover camera from seafloor | 15 Oct | 0515 | 15 Oct | 0645 | 1.50 | 0.06 |
| Trip to casing shoe and pick up top drive while recovering camera frame | | | | | | |
| Trip: depth to depth: from (mudline) 0 to 40 mbsf, plus 0 h in 4425 m of water | 15 Oct | 0645 | 15 Oct | 0645 | 0.00 | 0.00 |
| Pick up top drive and space out drill pipe (will take 0 h) | 15 Oct | 0645 | 15 Oct | 0645 | 0.00 | 0.00 |
| RIH and tag bottom at 0704 h (will take 0.25 h) | 15 Oct | 0645 | 15 Oct | 0700 | 0.25 | 0.01 |
| Drill ahead 18.5 inch hole in sediment: from 40 to 53 mbsf at 15 m/h | 15 Oct | 0700 | 15 Oct | 0730 | 0.50 | 0.02 |
| Basement contact at 53 mbsf at 0723 h | | | | | | |

**Table T1 (continued).** (Continued on next page.)

| Operational task | Start Date (2011) | Start Time (h) | End Date (2011) | End Time (h) | Task time Hours | Task time Days |
|---|---|---|---|---|---|---|
| Drill ahead 18.5 inch hole in basement: from 53 to 68 mbsf at 2 m/h | 15 Oct | 0730 | 15 Oct | 1630 | 9.00 | 0.38 |
| Circulation (will take 1 h) | 15 Oct | 1630 | 15 Oct | 1700 | 0.50 | 0.02 |
| Wiper trip: from 68 mbsf to 35 mbsf and back | 15 Oct | 1700 | 15 Oct | 2045 | 3.75 | 0.16 |
| Wiper trip 1: 4 m soft fill on bottom; circulate mud sweep | | | | | | |
| Wiper trip 2: 2 m soft fill; circulate mud sweep | | | | | | |
| Wiper trip 3: 2 m soft fill again; circulate mud sweep | | | | | | |
| End of hole conditioning: 1 m soft fill—easily washed | | | | | | |
| Trip: depth to depth: from 68 to 35 mbsf, plus 0 h in 4425 m of water | 15 Oct | 2045 | 15 Oct | 2100 | 0.25 | 0.01 |
| Set back top drive (will take 0.5 h) | 15 Oct | 2100 | 15 Oct | 2115 | 0.25 | 0.01 |
| Trip: depth to surface: from 35 mbsf to surface, ±0.5 h in 4425 m of water | 15 Oct | 2115 | 16 Oct | 0430 | 7.25 | 0.30 |
| Handle BHA (will take 1 h) | 16 Oct | 0430 | 16 Oct | 0500 | 0.50 | 0.02 |
| **Hole U1383B: install 16 inch casing** | | | | | | |
| Lay out bit sub/float valve, make up casing running tool with drill collars, rack back stand (will take 0.5 h) | 16 Oct | 0500 | 16 Oct | 0530 | 0.50 | 0.02 |
| Rig up/down for casing (will take 2 h) | 16 Oct | 0530 | 16 Oct | 0615 | 0.75 | 0.03 |
| Assemble 16 inch casing | 16 Oct | 0615 | 16 Oct | 0745 | 1.50 | 0.06 |
| Make up casing running tool with 16 inch casing hanger and replace master bushings (will take 1 h) | 16 Oct | 0745 | 16 Oct | 0815 | 0.50 | 0.02 |
| Handle BHA (will take 0.5 h) | 16 Oct | 0815 | 16 Oct | 0830 | 0.25 | 0.01 |
| Trip: surface to mudline, plus 0 h in 4425 m of water | 16 Oct | 0830 | 16 Oct | 1445 | 6.25 | 0.26 |
| Deploy camera (will take 0.25 h) | 16 Oct | 1445 | 16 Oct | 1500 | 0.25 | 0.01 |
| Maneuver ship for reentry (will take 0.5 h); reenter at 1524 h | 16 Oct | 1500 | 16 Oct | 1530 | 0.50 | 0.02 |
| Trip: mudline to depth: from 0 to 50 mbsf, plus 0.5 h | 16 Oct | 1530 | 16 Oct | 1600 | 0.50 | 0.02 |
| Unable to pass basement contact; work drill string/offset ship (will take 3 h) | 16 Oct | 1600 | 16 Oct | 1945 | 3.75 | 0.16 |
| Work casing shoe to ~3.0 m into basement; hole apparently slightly deviated | | | | | | |
| Decision made to POOH and shorten casing length by 5.0 m, placing 16 inch casing shoe ~1.0 m into basement (original target was 5–6 m into basement) | | | | | | |
| Trip: depth to surface: from 50 mbsf to surface, ±1.5 h in 4425 m of water | 16 Oct | 1945 | 17 Oct | 0300 | 7.25 | 0.30 |
| Handle BHA and remove casing running tool from casing hanger (will take 0.5 h) | 17 Oct | 0300 | 17 Oct | 0330 | 0.50 | 0.02 |
| Break out and lay out hanger joint (will take 1 h) | 17 Oct | 0330 | 17 Oct | 0515 | 1.75 | 0.07 |
| Break out and lay out 2 additional joints of casing (will take 1.25 h) | 17 Oct | 0515 | 17 Oct | 0630 | 1.25 | 0.05 |
| Shorten casing shoe joint by 5.0 m and weld on new casing shoe (will take 1.5 h) | 17 Oct | 0630 | 17 Oct | 0800 | 1.50 | 0.06 |
| Make up remaining casing joints (will take 1.5 h) | 17 Oct | 0800 | 17 Oct | 0930 | 1.50 | 0.06 |
| Make up casing running tool with 16 inch casing hanger (will take 0.5 h) | 17 Oct | 0930 | 17 Oct | 0945 | 0.25 | 0.01 |
| Handle BHA (will take 0.25 h) | 17 Oct | 0945 | 17 Oct | 1000 | 0.25 | 0.01 |
| Trip: surface to mudline, ±1.5 h in 4425 m of water | 17 Oct | 1000 | 17 Oct | 1500 | 5.00 | 0.21 |
| Handle camera (will take 0.5 h) | 17 Oct | 1500 | 17 Oct | 1530 | 0.50 | 0.02 |
| Maneuver ship for reentry (will take 0.5 h); reenter at 1537 h | 17 Oct | 1530 | 17 Oct | 1545 | 0.25 | 0.01 |
| Trip: mudline to depth: from 0 to 50 mbsf, plus 0.5 h | 17 Oct | 1545 | 17 Oct | 1600 | 0.25 | 0.01 |
| Pick up top drive and space out drill pipe (will take 0.5 h) | 17 Oct | 1600 | 17 Oct | 1615 | 0.25 | 0.01 |
| Land casing (will take 1 h) | 17 Oct | 1615 | 17 Oct | 1630 | 0.25 | 0.01 |
| Cement casing shoe (will take 2 h) | 17 Oct | 1630 | 17 Oct | 1745 | 1.25 | 0.05 |
| Release cone/casing hanger (will take 0.5 h); release casing at 1743 h | 17 Oct | 1745 | 17 Oct | 1745 | 0.00 | 0.00 |
| Circulation (will take 1 h) | 17 Oct | 1745 | 17 Oct | 1845 | 1.00 | 0.04 |
| Set back top drive (will take 0.5 h) | 17 Oct | 1845 | 17 Oct | 1915 | 0.50 | 0.02 |
| Recover camera (will take 0.5 h) | 17 Oct | 1915 | 17 Oct | 1945 | 0.50 | 0.02 |
| Trip: mudline to surface, plus 0 h in 4425 m of water | 17 Oct | 1945 | 18 Oct | 0115 | 5.50 | 0.23 |
| Handle BHA (will take 1 h) | 18 Oct | 0115 | 18 Oct | 0145 | 0.50 | 0.02 |
| De-torque casing running tool and lay out to rig floor (will take 0.5 h) | 18 Oct | 0145 | 18 Oct | 0200 | 0.25 | 0.01 |
| **Hole U1383B: drill 14.75 inch hole for 10.75 inch tricone bit and drill out for 10.75 inch casing** | | | | | | |
| Handle BHA (will take 1 h) | 18 Oct | 0200 | 18 Oct | 0330 | 1.50 | 0.06 |
| Deploy camera (will take 0.5 h) | 18 Oct | 0330 | 18 Oct | 0400 | 0.50 | 0.02 |
| Trip: surface to mudline, ±1.25 h in 4425 m of water | 18 Oct | 0400 | 18 Oct | 1015 | 6.25 | 0.26 |
| Slip/Cut drill line (will take 1.5 h) | 18 Oct | 1015 | 18 Oct | 1200 | 1.75 | 0.07 |
| Maneuver ship for reentry (will take 0.5 h); reenter at 1210 h | 18 Oct | 1200 | 18 Oct | 1215 | 0.25 | 0.01 |
| Trip: mudline to depth: from 0 to 59 mbsf, plus 1 h | 18 Oct | 1215 | 18 Oct | 1300 | 0.75 | 0.03 |
| Recover camera (will take 0.5 h) | 18 Oct | 1300 | 18 Oct | 1330 | 0.50 | 0.02 |
| Tag cement at 49 mbsf | | | | | | |
| Pick up top drive and space out drill pipe (will take 1 h) | 18 Oct | 1330 | 18 Oct | 1345 | 0.25 | 0.01 |
| Take slow circulating rates (will take 0.75 h) | 18 Oct | 1345 | 18 Oct | 1415 | 0.50 | 0.02 |
| Drill ahead (drill out cement/shoe): from 59 to 69 mbsf at 3 m/h | 18 Oct | 1415 | 18 Oct | 1500 | 0.75 | 0.03 |
| Break though at 1502 h at 57 mbsf | | | | | | |
| On-bottom drilling at 1520 h | | | | | | |
| Drill ahead: from 69 to 84 mbsf at 1.4 m/h (adjusted ROP to reflect actual time required during first drilled interval of 15 m) | 18 Oct | 1500 | 19 Oct | 0145 | 10.75 | 0.45 |
| Drill ahead: from 84 to 89 mbsf at 1.4 m/h | 19 Oct | 0145 | 19 Oct | 0515 | 3.50 | 0.15 |
| Wiper trip: from 89 mbsf to 54 mbsf and back | 19 Oct | 0515 | 19 Oct | 0715 | 2.00 | 0.08 |
| Hole problems; bit not advancing (will take 2.75 h) | 19 Oct | 0715 | 19 Oct | 1000 | 2.75 | 0.11 |
| Set back top drive (will take 0.5 h) | 19 Oct | 1000 | 19 Oct | 1030 | 0.50 | 0.02 |
| Trip: depth to surface: from 89 mbsf to surface, ±1.5 h in 4425 m of water | 19 Oct | 1030 | 19 Oct | 1700 | 6.50 | 0.27 |

**Table T1 (continued).** (Continued on next page.)

| Operational task | Start Date (2011) | Start Time (h) | End Date (2011) | End Time (h) | Task time Hours | Task time Days |
|---|---|---|---|---|---|---|
| Clear seafloor at 1050 h | | | | | | |
| Handle BHA (will take 1 h) | 19 Oct | 1700 | 19 Oct | 1745 | 0.75 | 0.03 |
| Damaged bit cleared rig floor at 1750 h, ending Hole U1383B | | | | | | |
| **Hole U1383B totals:** | 13 Oct | 0930 | 19 Oct | 1745 | 152.25 | 6.34 |
| **(C) Hole U1383C: re-start deep CORK observatory installation; install reentry cone with 16 inch casing** | | | | | | |
| Inspect bit; found 2 of 3 bit shanks/cutters missing and third damaged (will take 0.25 h) | 19 Oct | 1745 | 19 Oct | 1800 | 0.25 | 0.01 |
| Hold meeting to discuss operational options (will take 0.5 h) | 19 Oct | 1800 | 19 Oct | 1830 | 0.50 | 0.02 |
| Determine low likelihood that hole can be salvaged; decision made to restart hole with new reentry installation | | | | | | |
| Assemble new reentry cone and prepare new 16 inch conductor casing shoe joint (will take 12 h) | 19 Oct | 1830 | 20 Oct | 0630 | 12.00 | 0.50 |
| Deploy reentry cone and 16 inch conductor casing | | | | | | |
| Reentry cone (will take 0 h) | 20 Oct | 0630 | 20 Oct | 0630 | 0.00 | 0.00 |
| Handle BHA (will take 0 h) | 20 Oct | 0630 | 20 Oct | 0630 | 0.00 | 0.00 |
| Rig up/down for casing (will take 0.75 h) | 20 Oct | 0630 | 20 Oct | 0700 | 0.50 | 0.02 |
| Assemble 16 inch casing | 20 Oct | 0700 | 20 Oct | 0800 | 1.00 | 0.04 |
| Rig up/down for casing (will take 0 h) | 20 Oct | 0800 | 20 Oct | 0800 | 0.00 | 0.00 |
| Make up casing running tool (will take 0.5 h) | 20 Oct | 0800 | 20 Oct | 0830 | 0.50 | 0.02 |
| Lower 16 inch casing and latch into reentry funnel (will take 0.25 h) | 20 Oct | 0830 | 20 Oct | 0845 | 0.25 | 0.01 |
| Release running tool from reentry cone (will take 0.25 h) | 20 Oct | 0845 | 20 Oct | 0900 | 0.25 | 0.01 |
| Make up BHA below running tool (will take 1 h) | 20 Oct | 0900 | 20 Oct | 1000 | 1.00 | 0.04 |
| Lower and make up running tool in reentry cone (will take 0.5 h) | 20 Oct | 1000 | 20 Oct | 1015 | 0.25 | 0.01 |
| Pick up reentry cone and open moonpool doors/lower reentry cone (will take 0.75 h) | 20 Oct | 1015 | 20 Oct | 1030 | 0.25 | 0.01 |
| Pick up tapered drill collar and 2 stands of 5.5 inch transition drill pipe (will take 0.75 h) | 20 Oct | 1030 | 20 Oct | 1100 | 0.50 | 0.02 |
| Fill pipe as required/deploy camera at 70 stands during pipe trip (will take 0.5 h) | 20 Oct | 1100 | 20 Oct | 1130 | 0.50 | 0.02 |
| Trip: surface to mudline, ±1.25 h in 4425 m of water | 20 Oct | 1130 | 20 Oct | 1815 | 6.75 | 0.28 |
| Pick up top drive and space out drill pipe (will take 0.75 h) | 20 Oct | 1815 | 20 Oct | 1900 | 0.75 | 0.03 |
| Spud Hole U1383C at 1900 h | | | | | | |
| Jet-in casing (will take 2.75 h) | 20 Oct | 1900 | 20 Oct | 2130 | 2.50 | 0.10 |
| Release running tool (will take 0.25 h); release at 2130 h | 20 Oct | 2130 | 20 Oct | 2130 | 0.00 | 0.00 |
| POOH with top drive (will take 0.25 h) | 20 Oct | 2130 | 20 Oct | 2145 | 0.25 | 0.01 |
| Set back top drive (will take 0.5 h) | 20 Oct | 2145 | 20 Oct | 2215 | 0.50 | 0.02 |
| Trip: mudline to surface, ±1.75 h in 4425 m of water | 20 Oct | 2215 | 21 Oct | 0415 | 6.00 | 0.25 |
| Recover camera (will take 0.25 h) | 21 Oct | 0415 | 21 Oct | 0430 | 0.25 | 0.01 |
| Handle BHA, de-torque and lay out casing running tool, and lay out drill collars pups (will take 1 h) | 21 Oct | 0430 | 21 Oct | 0600 | 1.50 | 0.06 |
| **Hole U1383C: drill out 14.75 inch hole for 10.75 inch casing** | | | | | | |
| Make up 14.75 inch triton bit (will take 0.5 h) | 21 Oct | 0600 | 21 Oct | 0630 | 0.50 | 0.02 |
| Handle BHA (will take 0.5 h) | 21 Oct | 0630 | 21 Oct | 0700 | 0.50 | 0.02 |
| Trip: surface to mudline, ±1 h in 4425 m of water | 21 Oct | 0700 | 21 Oct | 1345 | 6.75 | 0.28 |
| Deploy camera (will take 0.5 h) | 21 Oct | 1345 | 21 Oct | 1415 | 0.50 | 0.02 |
| Maneuver ship for reentry (will take 0.5 h); reenter Hole U1383C at 1444 h | 21 Oct | 1415 | 21 Oct | 1445 | 0.50 | 0.02 |
| Pick up top drive and space out drill pipe (will take 0.5 h) | 21 Oct | 1445 | 21 Oct | 1515 | 0.50 | 0.02 |
| Move bit from (mudline) 0 to 35 mbsf (will take 0.5 h) | 21 Oct | 1515 | 21 Oct | 1545 | 0.50 | 0.02 |
| Handle camera (will take 0.75 h) | 21 Oct | 1545 | 21 Oct | 1630 | 0.75 | 0.03 |
| Drill ahead 14.75 inch hole in sediment: from 35 to 38 mbsf at 30 m/h | 21 Oct | 1630 | 21 Oct | 1645 | 0.25 | 0.01 |
| Basement contact at 38 mbsf at 1645 h | | | | | 0.00 | 0.00 |
| Drill ahead 14.75 inch hole in basement: from 38 to 69.5 mbsf at 1.3 m/h | 21 Oct | 1645 | 22 Oct | 1845 | 26.00 | 1.08 |
| Circulation (will take 1 h) | 22 Oct | 1845 | 22 Oct | 1915 | 0.50 | 0.02 |
| Wiper trip: from 69.5 mbsf to 80 mbsf and back | 22 Oct | 1915 | 22 Oct | 2345 | 4.50 | 0.19 |
| Wiper trip 1: ledge(?) at 100 m, 10 m fill on bottom; circulate to TD and pump 50 bbl mud sweep | | | | | | |
| Wiper trip 2: no ledge and 3 m(??) fill on bottom; circulate to TD and pump 50 bbl sweep | | | | | | |
| Wiper trip 3: apparent 7 m fill; circulate to TD and pump 80 bbl mud sweep | | | | | | |
| Wiper trip 4: 5 m fill; circulate 80 bbl sweep | | | | | | |
| Wiper trip 5: 2.7 m fill; POOH | | | | | | |
| Trip: depth to mudline: 69.5 mbsf to mudline, plus 0.25 h | 22 Oct | 2345 | 23 Oct | 0000 | 0.25 | 0.01 |
| Set back top drive (will take 0.25 h) | 23 Oct | 0000 | 23 Oct | 0015 | 0.25 | 0.01 |
| Clear seafloor at 0025 h | | | | | | |
| Trip: mudline to surface, ±1.5 h in 4425 m of water | 23 Oct | 0015 | 23 Oct | 0630 | 6.25 | 0.26 |
| Handle BHA (will take 0.75 h) | 23 Oct | 0630 | 23 Oct | 0700 | 0.50 | 0.02 |
| Bit clears rotary table at 0702 h | | | | | | |
| **Hole U1383C: install 10.75 inch casing** | | | | | | |
| Make up stand with casing running tool and stand back in derrick (will take 0.5 h) | 23 Oct | 0700 | 23 Oct | 0730 | 0.50 | 0.02 |
| Rig up/down for casing (will take 0.75 h) | 23 Oct | 0730 | 23 Oct | 0815 | 0.75 | 0.03 |
| Case with 10.75 inch casing from 0 to 65 mbsf at 4 joints/h, plus 0 h | 23 Oct | 0815 | 23 Oct | 0930 | 1.25 | 0.05 |
| Make up 10.75 inch casing hanger and weld coupling (will take 0.25 h)/weld all casing couplings | 23 Oct | 0930 | 23 Oct | 0945 | 0.25 | 0.01 |
| Make up casing running tool to casing hanger/pull bushings/lower through rotary table (will take 0.5 h) | 23 Oct | 0945 | 23 Oct | 1015 | 0.50 | 0.02 |
| Make up 1 stand of 8.25 inch drill collars (will take 0.25 h) | 23 Oct | 1015 | 23 Oct | 1030 | 0.25 | 0.01 |
| Deploy camera (will take 0.5 h) | 23 Oct | 1030 | 23 Oct | 1100 | 0.50 | 0.02 |
| Trip: surface to mudline, ±1 h in 4425 m of water | 23 Oct | 1100 | 23 Oct | 1600 | 5.00 | 0.21 |

**Table T1 (continued).** (Continued on next page.)

| Operational task | Start Date (2011) | Start Time (h) | End Date (2011) | End Time (h) | Task time Hours | Task time Days |
|---|---|---|---|---|---|---|
| Maneuver ship for reentry (will take 0.5 h); reenter at 1626 h | 23 Oct | 1600 | 23 Oct | 1630 | 0.50 | 0.02 |
| RIH with 10.75 inch casing | | | | | | |
| Pick up top drive and space out drill pipe (will take 0.5 h) | 23 Oct | 1630 | 23 Oct | 1700 | 0.50 | 0.02 |
| Trip: mudline to depth: from 0 to 65 mbsf, plus 0.5 h | 23 Oct | 1700 | 23 Oct | 1715 | 0.25 | 0.01 |
| Land 10.75 inch casing hanger at 1720 h | | | | | | |
| Work on cement pump (will take 0.5 h) | 23 Oct | 1715 | 23 Oct | 1845 | 1.50 | 0.06 |
| Cement casing shoe (will take 1.75 h); pump 20 bbl cement; attempt to leave cement 15 m above casing shoe | 23 Oct | 1845 | 23 Oct | 1930 | 0.75 | 0.03 |
| Cementing took longer than planned because of lumps in cement line; pumped 5 extra bbl | | | | | | |
| Release cone/casing hanger (will take 0.25 h) | 23 Oct | 1930 | 23 Oct | 1945 | 0.25 | 0.01 |
| Flush drill pipe (will take 1 h) | 23 Oct | 1945 | 23 Oct | 2030 | 0.75 | 0.03 |
| Set back top drive (will take 0.5 h) | 23 Oct | 2030 | 23 Oct | 2100 | 0.50 | 0.02 |
| POOH with drill string (will take 4 h) | 23 Oct | 2100 | 24 Oct | 0015 | 3.25 | 0.14 |
| Handle camera (will take 0.5 h) | 24 Oct | 0015 | 24 Oct | 0015 | 0.00 | 0.00 |
| Slip/Cut originally scheduled at 70 stands but conducted at 82 stands because of racker breakdown | | | | | | |
| Problem: spool valve manifold smoking; removed for repair or replacement | | | | | | |
| Slip/Cut drill line (will take 1.5 h) | 24 Oct | 0015 | 24 Oct | 0145 | 1.50 | 0.06 |
| Racker still broke down | | | | | | |
| Service rig and prepare core barrels | 24 Oct | 0145 | 24 Oct | 0445 | 3.00 | 0.13 |
| Spooler replaced, but now another hydraulic hose leaking and had to be replaced | | | | | | |
| Racker repaired and operational | | | | | | |
| POOH with drill string (will take 3 h) | 24 Oct | 0445 | 24 Oct | 0800 | 3.25 | 0.14 |
| Running tool cleared rotary table at 0825 h | | | | | | |
| Handle BHA, de-torque and lay out casing running tool, and lay out drill collars pups (will take 1.5 h) | 24 Oct | 0800 | 24 Oct | 0845 | 0.75 | 0.03 |
| **Hole U1383C: RCB coring, Bit 1** | | | | | | |
| Make up RCB core barrel/center bit assembly (will take 1 h) | 24 Oct | 0845 | 24 Oct | 0915 | 0.50 | 0.02 |
| Make up RCB C-7 core bit and outer core barrel assembly (will take 1 h) | 24 Oct | 0915 | 24 Oct | 0930 | 0.25 | 0.01 |
| Space out core barrels (will take 0.5 h) | 24 Oct | 0930 | 24 Oct | 0945 | 0.25 | 0.01 |
| Install center bit (will take 0.5 h) | 24 Oct | 0945 | 24 Oct | 1000 | 0.25 | 0.01 |
| Handle BHA (will take 1 h) | 24 Oct | 1000 | 24 Oct | 1030 | 0.50 | 0.02 |
| Deploy camera (will take 0.5 h) | 24 Oct | 1030 | 24 Oct | 1100 | 0.50 | 0.02 |
| Trip: surface to mudline, ±1.5 h in 4425 m of water | 24 Oct | 1100 | 24 Oct | 1600 | 5.00 | 0.21 |
| Maneuver ship for reentry (will take 0.5 h); reenter at 1605 h (reentry lasted ~10 min) | 24 Oct | 1600 | 24 Oct | 1600 | 0.00 | 0.00 |
| Recover camera (will take 1 h) | 24 Oct | 1600 | 24 Oct | 1730 | 1.50 | 0.06 |
| Trip: mudline to depth: from 0 to 60 mbsf, plus 0 h | 24 Oct | 1730 | 24 Oct | 1730 | 0.00 | 0.00 |
| Pick up top drive and space out drill pipe (will take 0.5 h) | 24 Oct | 1730 | 24 Oct | 1815 | 0.75 | 0.03 |
| Tag cement at 1820 h; 4469.0 mbrf/43.8 mbsf (1 m higher than calculated) | | | | | | |
| Drill out cement using RCB center bit (will take 2.25 h) | 24 Oct | 1815 | 24 Oct | 2115 | 3.00 | 0.13 |
| Broke out of cement at 4490 mbrf (64.8 mbsf), or 4.4 m below casing shoe | | | | | | |
| Clean out rathole to total depth (will take 0.25 h) | 24 Oct | 2115 | 24 Oct | 2130 | 0.25 | 0.01 |
| Circulation (will take 1.25 h) | 24 Oct | 2130 | 24 Oct | 2215 | 0.75 | 0.03 |
| Aft core line hanging up in oil saver/switch to forward line (will take 0.75 h) | 24 Oct | 2215 | 24 Oct | 2300 | 0.75 | 0.03 |
| Change to forward core line | | | | | | |
| Recover RCB center bit (will take 1.25 h) | 24 Oct | 2300 | 25 Oct | 0000 | 1.00 | 0.04 |
| Deploy RCB core barrel (will take 0.5 h) | 25 Oct | 0000 | 25 Oct | 0030 | 0.50 | 0.02 |
| SCR (will take 0.25 h) | 25 Oct | 0030 | 25 Oct | 0030 | 0.00 | 0.00 |
| Clean out hole to total depth at 70 mbsf (will take 1 h) | 25 Oct | 0030 | 25 Oct | 0130 | 1.00 | 0.04 |
| Move bit from 60 to 70 mbsf (will take 0 h) | 25 Oct | 0130 | 25 Oct | 0130 | 0.00 | 0.00 |
| RCB bit Run 1 (195 m; 58 bit rotating hours) | | | | | | |
| ROP taken from Site U1382 rate for RCB to 200 mbsf | | | | | | |
| Cut RCB Core 336-U1383C-2R (will take 4 h) | 25 Oct | 0130 | 25 Oct | 0300 | 1.50 | 0.06 |
| Problem stabbing sinker bars (will take 0.5 h) | 25 Oct | 0300 | 25 Oct | 0330 | 0.50 | 0.02 |
| RIH and recover Core 2R (will take 1.25 h); Core 336-U1383C-2R on deck at 0430 h, 20 Oct | 25 Oct | 0330 | 25 Oct | 0430 | 1.00 | 0.04 |
| Move bit from 70 to 76.6 mbsf (will take 0 h) | 25 Oct | 0430 | 25 Oct | 0430 | 0.00 | 0.00 |
| RCB core basement: 76.6–86.2 mbsf at 2.1 m/h; Core 336-U1383C-3R on deck at 1030 h | 25 Oct | 0430 | 25 Oct | 1030 | 6.00 | 0.25 |
| RCB core basement: 86.2–95.8 mbsf at 2.2 m/h; Core 336-U1383C-4R on deck at 1635 h | 25 Oct | 1030 | 25 Oct | 1630 | 6.00 | 0.25 |
| RCB core sediment: 95.8–105.4 mbsf at 2.2 m/h; Core 336-U1383C-5R on deck at 2230 h | 25 Oct | 1630 | 25 Oct | 2230 | 6.00 | 0.25 |
| RCB core basement: 105.4–115 mbsf at 2.2 m/h; Core 336-U1383C-6R on deck at 0310 h, 26 Oct | 25 Oct | 2230 | 26 Oct | 0315 | 4.75 | 0.20 |
| RCB core basement: 115–124.6 mbsf at 2.8 m/h; Core 336-U1383C-7R on deck at 0650 h | 26 Oct | 0315 | 26 Oct | 0645 | 3.50 | 0.15 |
| RCB core basement: 124.6–134.2 mbsf at 2.8 m/h; Core 336-U1383C-8R on deck at 1210 h | 26 Oct | 0645 | 26 Oct | 1215 | 5.50 | 0.23 |
| RCB core basement: 134.2–143.8 mbsf at 2.8 m/h; Core 336-U1383C-9R on deck at 1710 h | 26 Oct | 1215 | 26 Oct | 1715 | 5.00 | 0.21 |
| RCB core basement: 143.8–153.4 mbsf at 2.8 m/h; Core 336-U1383C-10R on deck at 2330 h | 26 Oct | 1715 | 26 Oct | 2330 | 6.25 | 0.26 |
| RCB core basement: 153.4–163.1 mbsf at 2.8 m/h; Core 336-U1383C-11R on deck at 0240 h, 27 Oct | 26 Oct | 2330 | 27 Oct | 0245 | 3.25 | 0.14 |
| RCB core basement: 163.1–172.7 mbsf at 2.8 m/h; Core 336-U1383C-12R on deck at 0610 h | 27 Oct | 0245 | 27 Oct | 0615 | 3.50 | 0.15 |
| RCB core basement: 172.7–182.3 mbsf at 2.8 m/h; Core 336-U1383C-13R on deck at 0950 h | 27 Oct | 0615 | 27 Oct | 0945 | 3.50 | 0.15 |
| RCB core basement: 182.3–191.9 mbsf at 4 m/h; Core 336-U1383C-14R on deck at 1335 h | 27 Oct | 0945 | 27 Oct | 1330 | 3.75 | 0.16 |
| RCB core basement: 191.9–192.8 mbsf at 4 m/h; Core 336-U1383C-15R on deck at 1605 h | 27 Oct | 1330 | 27 Oct | 1600 | 2.50 | 0.10 |
| Wiper trip: 192.8 mbsf to 60 mbsf and back | 27 Oct | 1600 | 27 Oct | 2130 | 5.50 | 0.23 |
| Deploy RCB core barrel and circulate mud sweep on bottom (will take 1 h) | 27 Oct | 2130 | 27 Oct | 2230 | 1.00 | 0.04 |

**Table T1 (continued).** (Continued on next page.)

| Operational task | Start Date (2011) | Start Time (h) | End Date (2011) | End Time (h) | Task time Hours | Task time Days |
|---|---|---|---|---|---|---|
| RCB core basement: 192.8–201.4 mbsf at 3 m/h; Core 336-U1383C-16R on deck at 0605 h, 28 Oct | 27 Oct | 2230 | 28 Oct | 0300 | 4.50 | 0.19 |
| RCB core basement: 201.4–211.1 mbsf at 3 m/h; Core 336-U1383C-17R on deck at 0710 h | 28 Oct | 0300 | 28 Oct | 0715 | 4.25 | 0.18 |
| RCB core basement: 211.1–211.6 mbsf at 3 m/h; Core 336-U1383C-18R on deck at 0920 h | 28 Oct | 0715 | 28 Oct | 0915 | 2.00 | 0.08 |
| Circulation (will take 1 h) | 28 Oct | 0915 | 28 Oct | 0945 | 0.50 | 0.02 |
| Trip with top drive from 211.6 to 60 mbsf at 4 stands/h | 28 Oct | 0945 | 28 Oct | 1000 | 0.25 | 0.01 |
| Set back top drive (will take 0.5 h) | 28 Oct | 1000 | 28 Oct | 1030 | 0.50 | 0.02 |
| Clear seafloor at 1052 h | | | | | | |
| Trip: depth to surface: from 60 mbsf to surface, ±1.5 h in 4425 m of water | 28 Oct | 1030 | 28 Oct | 1630 | 6.00 | 0.25 |
| Handle BHA (will take 1 h) | 28 Oct | 1630 | 28 Oct | 1715 | 0.75 | 0.03 |
| Bit clears rotary table at 1720 h | | | | | | |
| **Hole U1383C: RCB coring, Bit 2** | | | | | | |
| Penetration rate taken from DSDP rates in 1976 for similar depths with RCB | | | | | | |
| Inspect bit/float valve/support bearing and make up new RCB bit (will take 1 h) | 28 Oct | 1715 | 28 Oct | 1815 | 1.00 | 0.04 |
| Rig service/maintenance (will take 1 h) | 28 Oct | 1815 | 28 Oct | 1915 | 1.00 | 0.04 |
| Remove and repair hydraulic actuator assembly (air leak) (will take 8 h) | 28 Oct | 1915 | 29 Oct | 0315 | 8.00 | 0.33 |
| Make up new RCB bit assembly, space out core barrels, and pick up 3 drill collars; make up BHA (will take 2.25 h) | 29 Oct | 0315 | 29 Oct | 0530 | 2.25 | 0.09 |
| Reinstall repaired hydraulic actuator cylinder (will take 1 h) | 29 Oct | 0530 | 29 Oct | 0630 | 1.00 | 0.04 |
| Deploy camera (will take 0.5 h) | 29 Oct | 0630 | 29 Oct | 0700 | 0.50 | 0.02 |
| Trip: surface to mudline, ±1 h in 4425 m of water | 29 Oct | 0700 | 29 Oct | 1230 | 5.50 | 0.23 |
| Maneuver ship for reentry (will take 0.5 h); reenter at 1231 h | 29 Oct | 1230 | 29 Oct | 1230 | 0.00 | 0.00 |
| Trip: mudline to depth: from 0 to 60 mbsf, plus 0 h | 29 Oct | 1230 | 29 Oct | 1330 | 1.00 | 0.04 |
| Recover camera (will take 0.5 h) | 29 Oct | 1330 | 29 Oct | 1415 | 0.75 | 0.03 |
| Pick up top drive and space out drill pipe (will take 1 h) | 29 Oct | 1415 | 29 Oct | 1515 | 1.00 | 0.04 |
| Trip with top drive from 60 to 211.6 mbsf at 4 stands/h | 29 Oct | 1515 | 29 Oct | 1715 | 2.00 | 0.08 |
| Circulation (will take 1.25 h) | 29 Oct | 1715 | 29 Oct | 1830 | 1.25 | 0.05 |
| Deploy RCB core barrel and record SCRs (will take 0.75 h) | 29 Oct | 1830 | 29 Oct | 1900 | 0.50 | 0.02 |
| Core with 30 ft knobbies because of water depth, sea state, and slow ROP | | | | | | |
| RCB core basement: 211.6–219.2 mbsf at 3 m/h; Core 336-U1383C-19R on deck at 2330 h | 29 Oct | 1900 | 29 Oct | 2330 | 4.50 | 0.19 |
| RCB core basement: 219.2–228.5 mbsf at 2.75 m/h; Core 336-U1383C-20R on deck at 0425 h, 30 Oct | 29 Oct | 2330 | 30 Oct | 0430 | 5.00 | 0.21 |
| RCB core basement: 228.5–237.7 mbsf at 2.75 m/h; Core 336-U1383C-21R on deck at 0800 h | 30 Oct | 0430 | 30 Oct | 0800 | 3.50 | 0.15 |
| RCB core basement: 237.7–247 mbsf at 2.75 m/h; Core 336-U1383C-22R on deck at 1130 h | 30 Oct | 0800 | 30 Oct | 1130 | 3.50 | 0.15 |
| RCB core basement: 247–256.2 mbsf at 2.75 m/h; Core 336-U1383C-23R on deck at 1915 h | 30 Oct | 1130 | 30 Oct | 1615 | 4.75 | 0.20 |
| Remove three knobbies, replace with drill pipe (will take 2 h) | 30 Oct | 1615 | 30 Oct | 1815 | 2.00 | 0.08 |
| Work pipe on bottom of hole/make connection/deploy core barrel (will take 1 h) | 30 Oct | 1815 | 30 Oct | 1845 | 0.50 | 0.02 |
| RCB core basement: 256.2–266.2 mbsf at 2.75 m/h; Core 336-U1383C-24R on deck at 2330 h | 30 Oct | 1845 | 30 Oct | 2330 | 4.75 | 0.20 |
| RCB core basement: 266.2–275.4 mbsf at 5.5 m/h; Core 336-U1383C-25R on deck at 0245 h, 31 Oct | 30 Oct | 2330 | 31 Oct | 0245 | 3.25 | 0.14 |
| RCB core basement: 275.4–284.7 mbsf at 3.5 m/h; Core 336-U1383C-26R on deck at 0645 h | 31 Oct | 0245 | 31 Oct | 0645 | 4.00 | 0.17 |
| RCB core basement: 284.7–294 mbsf at 2.75 m/h; Core 336-U1383C-27R on deck at 1135 h | 31 Oct | 0645 | 31 Oct | 1130 | 4.75 | 0.20 |
| RCB core basement: 294–299.2 mbsf at 1.3 m/h; Core 336-U1383C-28R on deck at 1630 h | 31 Oct | 1130 | 31 Oct | 1630 | 5.00 | 0.21 |
| RCB core basement: 299.2–303.7 mbsf at 2.5 m/h; Core 336-U1383C-29R on deck at 2005 h | 31 Oct | 1630 | 31 Oct | 2000 | 3.50 | 0.15 |
| RCB core basement: 303.7–312.1 mbsf at 1.9 m/h; Core 336-U1383C-30R on deck at 0230 h, 1 Nov | 31 Oct | 2000 | 1 Nov | 0230 | 6.50 | 0.27 |
| RCB core basement: 312.1–321.7 mbsf at 2 m/h; Core 336-U1373C-31R on deck at 0845 h | 1 Nov | 0230 | 1 Nov | 0845 | 6.25 | 0.26 |
| RCB core basement: 321.7–331.5 mbsf at 2.75 m/h; Core 336-U1383C-32R on deck at 1355 h | 1 Nov | 0845 | 1 Nov | 1400 | 5.25 | 0.22 |
| Circulation (will take 1 h) | 1 Nov | 1400 | 1 Nov | 1400 | 0.00 | 0.00 |
| Pump 30 bbl while cutting last meter of core | | | | | | |
| Wiper trip 1: 331.5–60 mbsf and back; numerous ledges and tight spots required reaming with top drive plus circulation; 4 m of fill on bottom; 70 bbl high-vis mud sweep | 1 Nov | 1400 | 2 Nov | 0130 | 11.50 | 0.48 |
| Circulation (will take 0.75 h) | 2 Nov | 0130 | 2 Nov | 0215 | 0.75 | 0.03 |
| Wiper trip 2: 331.5–60 mbsf and back; pull to casing shoe (no problems); RIH using motion compensator but no top drive; no hang-ups and no fill on bottom | 2 Nov | 0215 | 2 Nov | 0430 | 2.25 | 0.09 |
| Circulation (will take 0 h) | 2 Nov | 0430 | 2 Nov | 0430 | 0.00 | 0.00 |
| Wiper trip 3: 331.5–80 mbsf and back; same result as wiper trip 2 | 2 Nov | 0430 | 2 Nov | 0545 | 1.25 | 0.05 |
| Circulation (will take 0 h) | 2 Nov | 0545 | 2 Nov | 0545 | 0.00 | 0.00 |
| Trip: depth to surface: from 331.5 mbsf to surface, ±1 h in 4425 m of water | 2 Nov | 0545 | 2 Nov | 1245 | 7.00 | 0.29 |
| Clear seafloor at 0625 h | | | | | | |
| Handle BHA (will take 1 h) | 2 Nov | 1245 | 2 Nov | 1315 | 0.50 | 0.02 |
| Bit clears rotary table at 1315 h | | | | | | |
| **Hole U1383C: downhole logging, hydrologic packer experiments, and depth check** | | | | | | |
| Make up stand of 6.75 inch drill collars for CORK (will take 1 h) | 2 Nov | 1315 | 2 Nov | 1530 | 2.25 | 0.09 |
| Handle BHA (will take 2 h) | 2 Nov | 1530 | 2 Nov | 1645 | 1.25 | 0.05 |
| Deploy camera (will take 0.5 h) | 2 Nov | 1645 | 2 Nov | 1715 | 0.50 | 0.02 |
| Trip: surface to mudline, ±1 h in 4425 m of water | 2 Nov | 1715 | 2 Nov | 2345 | 6.50 | 0.27 |
| Maneuver ship for reentry (will take 0 h); reenter at 2342 h (3 min reentry) | 2 Nov | 2345 | 2 Nov | 2345 | 0.00 | 0.00 |
| Trip: mudline to depth: from 0 to 55 mbsf, plus 0.25 h | 2 Nov | 2345 | 3 Nov | 0000 | 0.25 | 0.01 |
| Rig up (will take 1 h) | 3 Nov | 0000 | 3 Nov | 0100 | 1.00 | 0.04 |
| Triple combination: log from 55 to 331.5 mbsf at 275 m/h | 3 Nov | 0100 | 3 Nov | 1245 | 11.75 | 0.49 |
| FMS-sonic: log from 55 to 331.5 mbsf at 275 m/h | 3 Nov | 1245 | 3 Nov | 2245 | 10.00 | 0.42 |
| Rig down (will take 1 h) | 3 Nov | 2245 | 3 Nov | 2315 | 0.50 | 0.02 |

**Table T1 (continued).**

| Operational task | Start Date (2011) | Start Time (h) | End Date (2011) | End Time (h) | Task time Hours | Task time Days |
|---|---|---|---|---|---|---|
| Pick up top drive and space out drill pipe (will take 0.75 h) | 3 Nov | 2315 | 4 Nov | 0015 | 1.00 | 0.04 |
| Packer testing: based on 2 injection tests per packer seat, reduced time allocated from 36 to 26 h | | | | | | |
| Packer: from 60 to 290 mbsf doing 3 tests (will take 11 h) | 4 Nov | 0015 | 4 Nov | 1100 | 10.75 | 0.45 |
| Packer Set 1 inside casing; 3 failed attempts (using up to 2200 psi); heave too high; packer slipping or deflating | | | | | | |
| Packer Set 2 in open hole at ~141 mbsf | | | | | | |
| Packer Set 3 in open hole at ~196 mbsf; couldn't get packer to seat; test canceled | | | | | | |
| Set back top drive (will take 0.5 h) | 4 Nov | 1100 | 4 Nov | 1130 | 0.50 | 0.02 |
| RIH for depth check (will take 0.5 h) | 4 Nov | 1130 | 4 Nov | 1200 | 0.50 | 0.02 |
| Move bit from 55 to 331.5 mbsf (will take 0 h) | 4 Nov | 1200 | 4 Nov | 1200 | 0.00 | 0.00 |
| Handle camera (will take 0.5 h) | 4 Nov | 1200 | 4 Nov | 1215 | 0.25 | 0.01 |
| Trip: depth to mudline: from 331.5 mbsf to mudline, plus 0 h | 4 Nov | 1215 | 4 Nov | 1315 | 1.00 | 0.04 |
| Clear seafloor at 1310 h | | | | | | |
| Hole U1383B: free-fall deployment of ROV platform; drill pipe vessel over to Hole U1383B | 4 Nov | 1315 | 4 Nov | 1330 | 0.25 | 0.01 |
| Maneuver ship for reentry (will take 0.5 h); reenter at 1350 h | 4 Nov | 1330 | 4 Nov | 1345 | 0.25 | 0.01 |
| Recover camera from seafloor | 4 Nov | 1345 | 4 Nov | 1515 | 1.50 | 0.06 |
| Make up and drop ROV platform from surface (will take 2 h) | 4 Nov | 1515 | 4 Nov | 1645 | 1.50 | 0.06 |
| Deploy camera to seafloor | 4 Nov | 1645 | 4 Nov | 1815 | 1.50 | 0.06 |
| Observe ROV platform in reentry cone/pull clear of seafloor/prepare for slip and cut (will take 0.25 h) | 4 Nov | 1815 | 4 Nov | 1830 | 0.25 | 0.01 |
| Clear seafloor at 1818 h | | | | | | |
| Slip/cut drill line (will take 1.5 h) | 4 Nov | 1830 | 4 Nov | 2015 | 1.75 | 0.07 |
| Recover camera during slip and cut | | | | | | |
| Rig up CORK umbilicals in moonpool while POOH with drill string | | | | | 0.00 | 0.00 |
| Trip: depth to surface: from (mudline) 0 mbsf to surface, ±1 h in 4425 m of water | 4 Nov | 2015 | 5 Nov | 0200 | 5.75 | 0.24 |
| Handle BHA (will take 1 h) | 5 Nov | 0200 | 5 Nov | 0300 | 1.00 | 0.04 |
| **Hole U1383C: assemble/install CORK and OsmoSampler string** | | | | | | |
| Make up CORK plumb bob with ten 15 ft long, 6.75 inch drill collars (will take 2 h) | 5 Nov | 0300 | 5 Nov | 0500 | 2.00 | 0.08 |
| Rig up for casing (will take 1 h) | 5 Nov | 0500 | 5 Nov | 0600 | 1.00 | 0.04 |
| Install crossovers, 5.5 inch casing pup, landing seat, and packer (will take 2 h) | 5 Nov | 0600 | 5 Nov | 0800 | 2.00 | 0.08 |
| Make up packer connections (will take 1 h) | 5 Nov | 0800 | 5 Nov | 0845 | 0.75 | 0.03 |
| Run 38.2 m of 4.5 inch fiberglass casing (will take 2 h) | 5 Nov | 0845 | 5 Nov | 1015 | 1.50 | 0.06 |
| Install second packer and make up hydraulic connections at both ends (will take 2 h) | 5 Nov | 1015 | 5 Nov | 1215 | 2.00 | 0.08 |
| Install 80 m of 4.5 inch fiberglass casing per plan (will take 2 h) | 5 Nov | 1215 | 5 Nov | 1415 | 2.00 | 0.08 |
| Install third packer and make up hydraulic connections (will take 2 h) | 5 Nov | 1415 | 5 Nov | 1630 | 2.25 | 0.09 |
| Install 48 m of 4.5 inch steel casing (will take 2 h) | 5 Nov | 1630 | 5 Nov | 1715 | 0.75 | 0.03 |
| Make up final umbilical terminations to CORK head (will take 2 h) | 5 Nov | 1715 | 5 Nov | 1915 | 2.00 | 0.08 |
| Hang-off CORK head on moonpool C-plates and remove CORK running tool (will take 1 h) | 5 Nov | 1915 | 5 Nov | 1945 | 0.50 | 0.02 |
| Make up and deploy instrument string (will take 1.5 h) | 5 Nov | 1945 | 5 Nov | 2115 | 1.50 | 0.06 |
| Make up CORK running tool and rig-up packer inflate line (will take 0.5 h) | 5 Nov | 2115 | 5 Nov | 2145 | 0.50 | 0.02 |
| Replace bushings. Pick up one stand of drill collars and lower CORK head below keel to equalize pressure. Raise head back to moonpool | 5 Nov | 2145 | 5 Nov | 2230 | 0.75 | 0.03 |
| Install OsmoSampler pump and close all valves (will take 0.75 h) | 5 Nov | 2230 | 5 Nov | 2315 | 0.75 | 0.03 |
| Remove moonpool grating and test-fit camera frame over CORK head (will take 0.75 h) | 5 Nov | 2315 | 6 Nov | 0000 | 0.75 | 0.03 |
| Handle BHA (will take 0.5 h) | 6 Nov | 0000 | 6 Nov | 0030 | 0.50 | 0.02 |
| Deploy camera (will take 0.5 h) | 6 Nov | 0030 | 6 Nov | 0100 | 0.50 | 0.02 |
| Trip: surface to mudline, plus 2 h in 4425 m of water | 6 Nov | 0100 | 6 Nov | 0915 | 8.25 | 0.34 |
| Maneuver ship for reentry (will take 0.5 h); reenter at 0941 h | 6 Nov | 0915 | 6 Nov | 0945 | 0.50 | 0.02 |
| RIH slowly, pick up top drive, space out and land CORK (will take 1.75 h); CORK lands at 1127 h | 6 Nov | 0945 | 6 Nov | 1130 | 1.75 | 0.07 |
| Recover camera frame and pressure up drill string to inflate CORK packers (will take 2.25 h) | 6 Nov | 1130 | 6 Nov | 1315 | 1.75 | 0.07 |
| Assemble ROV platform and make up with deployment tool and camera frame (will take 1.25 h) | 6 Nov | 1315 | 6 Nov | 1415 | 1.00 | 0.04 |
| Deploy camera with ROV platform (will take 3 h) | 6 Nov | 1415 | 6 Nov | 1630 | 2.25 | 0.09 |
| Monitor ROV release (will take 0.25 h) | 6 Nov | 1630 | 6 Nov | 1645 | 0.25 | 0.01 |
| Recover camera from seafloor | 6 Nov | 1645 | 6 Nov | 1800 | 1.25 | 0.05 |
| Remove slings from camera at surface | | | | | | |
| Remove ROV deployment slings and assembly (will take 0.5 h) | 6 Nov | 1800 | 6 Nov | 1830 | 0.50 | 0.02 |
| Deploy camera to seafloor | 6 Nov | 1830 | 6 Nov | 2015 | 1.75 | 0.07 |
| Release CORK (will take 0.25 h) | 6 Nov | 2015 | 6 Nov | 2015 | 0.00 | 0.00 |
| Survey CORK (will take 0.25 h) | 6 Nov | 2015 | 6 Nov | 2015 | 0.00 | 0.00 |
| Set back top drive (will take 0.5 h) | 6 Nov | 2015 | 6 Nov | 2045 | 0.50 | 0.02 |
| Trip: mudline to surface, ±1.5 h in 4425 m of water | 6 Nov | 2045 | 7 Nov | 0300 | 6.25 | 0.26 |
| Recover camera (will take 0.25 h) | 7 Nov | 0300 | 7 Nov | 0245 | –0.25 | –0.01 |
| Set back BHA and lay out CORK running tool (will take 0.25 h) | 7 Nov | 0245 | 7 Nov | 0315 | 0.50 | 0.02 |
| **Hole U1383C totals:** | 19 Oct | 1745 | 7 Nov | 0315 | 441.50 | 18.40 |

Times are given as local ship time, which is Universal Time Coordinated (UTC) – 3 h for all on-site operations. BHA = bottom-hole assembly. SCR = slow circulation rate. spm = strokes per minute, ROP = rate of penetration. POOH = pull out of hole, RIH = run in hole. TD = total depth. DSDP = Deep Sea Drilling Project. FMS = Formation MicroScanner.

**Table T2.** Basement coring summary, Site U1383. (Continued on next page.)

**Hole U1383A**
Latitude: 22°48.1229′N
Longitude: 46°03.1661′W
Time on site (h): 21.75 (1145 h, 12 October to 0930 h, 13 October 2011; ship local)
Seafloor (drill pipe measurement below rig floor in meters; DRF): 4425.2
Distance between rig floor and sea level (m): 11.28
Water depth (drill pipe measurement from sea level in meters): 4413.92
Total penetration (drilling depth below seafloor in meters; DSF): 36.0
Total depth (drill pipe measurement from rig floor in meters; DRF): 4461.2
Total length of cored section (m): 0
Total core recovered (m): 0
Core recovery (%): 0
Total number of cores: 0

**Hole U1383B**
Latitude: 22°48.1328′N
Longitude: 46°03.1556′W
Time on site (h): 152.25 (0930 h, 13 October to 1745 h, 19 October 2011; ship local)
Seafloor (drill pipe measurement below rig floor in meters; DRF): 4425.2
Distance between rig floor and sea level (m): 11.28
Water depth (drill pipe measurement from sea level in meters): 4413.92
Total penetration (drilling depth below seafloor in meters; DSF): 89.64
Total depth (drill pipe measurement from rig floor in meters; DRF): 4514.84
Total length of cored section (m): 0
Total core recovered (m): 0
Core recovery (%): 0
Total number of cores: 0

**Hole U1383C**
Latitude: 22°48.1241′N
Longitude: 46°03.1662′E
Time on site (h): 441.5 (1745 h, 19 October to 0315 h, 7 November 2011; ship local)
Seafloor (drill pipe measurement below rig floor in meters; DRF): 4425.2
Distance between rig floor and sea level (m): 11.28
Water depth (drill pipe measurement from sea level in meters): 4413.92
Total penetration (drilling depth below seafloor in meters; DSF): 331.5
Total depth (drill pipe measurement from rig floor in meters; DRF): 4756.7
Total length of cored section (m): 262.0
Total core recovered (m): 50.31
Core recovery (%): 19
Total number of cores: 31

| Core | Date (2011) | Local time (h) | Depth DSF (m) Top of cored interval | Depth DSF (m) Bottom of cored interval | Interval cored (m) | Length of core recovered (m) | Curated length (m) | Recovery (%) |
|---|---|---|---|---|---|---|---|---|
| 336-U1382C- | | | | | | | | |
| 1-1 | | | *****Drilled from 0.0 to 34.7 m DSF***** | | | | | |
| 1-2 | | | *****Drilled from 34.7 to 69.5 m DSF***** | | | | | |
| 2R | 25 Oct | 0730 | 69.5 | 76.6 | 7.1 | 2.19 | 2.93 | 31 |
| 3R | 25 Oct | 1320 | 76.6 | 86.2 | 9.6 | 2.17 | 3.69 | 23 |
| 4R | 25 Oct | 1935 | 86.2 | 95.8 | 9.6 | 2.08 | 2.56 | 22 |
| 5R | 26 Oct | 0130 | 95.8 | 105.4 | 9.6 | 1.56 | 1.93 | 16 |
| 6R | 26 Oct | 0610 | 105.4 | 115.0 | 9.6 | 1.47 | 1.93 | 15 |
| 7R | 26 Oct | 0950 | 115.0 | 124.6 | 9.6 | 1.80 | 2.65 | 19 |
| 8R | 26 Oct | 1510 | 124.6 | 134.3 | 9.7 | 1.97 | 2.43 | 20 |
| 9R | 26 Oct | 2010 | 134.3 | 143.9 | 9.6 | 4.13 | 5.50 | 43 |
| 10R | 27 Oct | 0230 | 143.9 | 153.5 | 9.6 | 3.24 | 4.24 | 34 |
| 11R | 27 Oct | 0540 | 153.5 | 163.1 | 9.6 | 1.06 | 1.35 | 11 |
| 12R | 27 Oct | 0910 | 163.1 | 172.7 | 9.6 | 0.88 | 1.32 | 9 |
| 13R | 27 Oct | 1250 | 172.7 | 182.3 | 9.6 | 1.43 | 2.13 | 15 |
| 14R | 27 Oct | 1635 | 182.3 | 191.8 | 9.5 | 1.40 | 1.96 | 15 |
| 15R | 27 Oct | 1905 | 191.8 | 192.8 | 1.0 | 0.37 | 0.42 | 37 |
| 16R | 28 Oct | 0605 | 192.8 | 201.4 | 8.6 | 1.10 | 1.68 | 13 |
| 17R | 28 Oct | 1010 | 201.4 | 211.1 | 9.7 | 1.60 | 2.16 | 16 |
| 18R | 28 Oct | 1220 | 211.1 | 211.6 | 0.5 | 0.10 | 0.12 | 20 |
| 19R | 30 Oct | 0235 | 211.6 | 219.2 | 7.6 | 1.38 | 1.77 | 18 |
| 20R | 30 Oct | 0725 | 219.2 | 228.5 | 9.3 | 1.48 | 1.98 | 16 |
| 21R | 30 Oct | 1100 | 228.5 | 237.7 | 9.2 | 1.09 | 1.40 | 12 |
| 22R | 30 Oct | 1430 | 237.7 | 247.0 | 9.3 | 0.99 | 1.24 | 11 |
| 23R | 30 Oct | 1915 | 247.0 | 256.2 | 9.2 | 1.62 | 2.15 | 18 |

**Table T2 (continued).**

| Core | Date (2011) | Local time (h) | Depth DSF (m) Top of cored interval | Depth DSF (m) Bottom of cored interval | Interval cored (m) | Length of core recovered (m) | Curated length (m) | Recovery (%) |
|---|---|---|---|---|---|---|---|---|
| 24R | 31 Oct | 0230 | 256.2 | 266.2 | 10.0 | 1.63 | 1.95 | 16 |
| 25R | 31 Oct | 0545 | 266.2 | 275.4 | 9.2 | 0.75 | 0.83 | 8 |
| 26R | 31 Oct | 0945 | 275.4 | 284.8 | 9.4 | 1.85 | 2.68 | 20 |
| 27R | 31 Oct | 1435 | 284.8 | 294.6 | 9.8 | 1.18 | 1.35 | 12 |
| 28R | 31 Oct | 1930 | 294.6 | 299.2 | 4.6 | 0.94 | 0.98 | 20 |
| 29R | 31 Oct | 2305 | 299.2 | 303.7 | 4.5 | 1.03 | 1.21 | 23 |
| 30R | 1 Nov | 0530 | 303.7 | 312.1 | 8.4 | 2.76 | 2.95 | 33 |
| 31R | 1 Nov | 1145 | 312.1 | 321.7 | 9.6 | 2.71 | 3.32 | 28 |
| 32R | 1 Nov | 1655 | 321.7 | 331.5 | 9.8 | 2.35 | 3.06 | 24 |
| | | | | Totals: | 262.0 | 50.31 | 65.87 | 19 |

Local time is Universal Time Coordinated (UTC) – 3 h. DRF = drilling depth below rig floor, DSF = drilling depth below seafloor. R = rotary core barrel core, numeric core type = drilled interval.

**Table T3.** Configuration of new CORK completion hardware deployed in Hole U1383C. (Continued on next page).

| Part Number | Description | Diameter (inch) | | Connection | | Measured length (m) | Cumulative bottom depth (mbsf) | Comments |
|---|---|---|---|---|---|---|---|---|
| | | Outside | Inside | Up | Down | | | |
| | CORK | 5.00 | 4.05 | | 4.50 8RD STC pin | 1.34 | 1.3 | 1.18 m CORK + 0.16 mbsf |
| 24 | Casing, 4.5 inch, 10.5 lb | 5.00 | 4.05 | 4.50 8RD cplg box | 4.50 8RD STC pin | 13.73 | 15.1 | |
| 25 | Casing, 4.5 inch, 10.5 lb | 5.00 | 4.05 | 4.50 8RD cplg box | 4.50 8RD STC pin | 13.75 | 28.9 | |
| 26 | Casing, 4.5 inch, 10.5 lb | 5.00 | 4.05 | 4.50 8RD cplg box | 4.50 8RD STC pin | 11.23 | 40.1 | |
| OH5073 | Casing pup, 4.5 inch, 10.5 lb | 5.00 | 4.05 | 4.50 8RD cplg box | 4.50 8RD STC pin | 6.00 | 46.1 | |
| OH5072 | Casing pup, 4.5 inch, 10.5 lb | 5.00 | 4.05 | 4.50 8RD cplg box | 4.50 8RD STC pin | 3.00 | 49.1 | |
| D1 | Packer, combo, 4.5 inch, coated | 10.50 | 4.05 | 4.50 8RD cplg box | 4.50 8RD STC pin | 9.07 | 58.2 | 10.75 inch, 54 lb casing to 60 mbsf |
| OJ3221 | Landing seat, 3.375 inch, coated | 5.00 | 3.375 | 4.50 8RD STC box | 4.50 8RD STC pin | 0.19 | 58.4 | |
| OJ3225 | Crossover, 4-1/2 LTC × 4-1/2 EUE | 5.00 | 4.00 | 4.50 8RD LTC box | 4.50 8RD EUE pin | 0.18 | 58.6 | |
| 72 | Casing, 4.5 inch, fiberglass - red | 5.00 | 3.91 | 4.50 8RD EUE box | 4.50 8RD EUE pin | 8.86 | 67.4 | |
| 74 | Casing, 4.5 inch, fiberglass - red | 5.00 | 3.91 | 4.50 8RD EUE box | 4.50 8RD EUE pin | 8.87 | 76.3 | |
| 119 | Casing, 4.5 inch, fiberglass, slotted - blue | 5.00 | 3.91 | 4.50 8RD EUE box | 4.50 8RD EUE pin | 8.88 | 85.2 | |
| 120 | Casing, 4.5 inch, fiberglass, slotted - blue | 5.00 | 3.91 | 4.50 8RD EUE box | 4.50 8RD EUE pin | 8.87 | 94.1 | |
| 121 | Casing, 4.5 inch, fiberglass, slotted - blue | 5.00 | 3.91 | 4.50 8RD EUE box | 4.50 8RD EUE pin | 8.79 | 102.9 | Miniscreens at 100 mbsf* |
| 122 | Casing, 4.5 inch, fiberglass, slotted - blue | 5.00 | 3.91 | 4.50 8RD EUE box | 4.50 8RD EUE pin | 8.88 | 111.8 | |
| 123 | Casing, 4.5 inch, fiberglass, slotted - blue | 5.00 | 3.91 | 4.50 8RD EUE box | 4.50 8RD EUE pin | 8.85 | 120.6 | |
| 124 | Casing, 4.5 inch, fiberglass, slotted - blue | 5.00 | 3.91 | 4.50 8RD EUE box | 4.50 8RD EUE pin | 8.82 | 129.4 | |
| 73 | Casing, 4.5 inch, fiberglass - red | 5.00 | 3.91 | 4.50 8RD EUE box | 4.50 8RD EUE pin | 8.76 | 138.2 | |
| | Casing pup, 4.5 inch, fiberglass | 5.00 | 3.91 | 4.50 8RD EUE box | 4.50 8RD EUE pin | 0.52 | 138.7 | |
| OJ3226 | Crossover, 4-1/2 EUE × 4-1/2 STC | 5.50 | 4.00 | 4.50 8RD EUE box | 4.50 8RD STC pin | 0.19 | 138.9 | |
| B4 | Packer, inflate, 4.5, coated | 8.08 | 4.052 | 4.50 8RD cplg box | 4.50 8RD STC pin | 6.60 | 145.5 | |
| OJ3222 | Landing seat, 3.125, coated | 5.00 | 3.125 | 4.50 8RD STC box | 4.50 8RD STC pin | 0.19 | 145.7 | |
| OJ3225 | Crossover, 4-1/2 LTC × 4-1/2 EUE | 5.00 | 4.00 | 4.50 8RD LTC box | 4.50 8RD EUE pin | 0.18 | 145.9 | |
| 118 | Casing, 4.5 inch, fiberglass, slotted - blue | 5.00 | 3.91 | 4.50 8RD EUE box | 4.50 8RD EUE pin | 8.87 | 154.8 | |
| 125 | Casing, 4.5 inch, fiberglass, slotted - blue | 5.00 | 3.91 | 4.50 8RD EUE box | 4.50 8RD EUE pin | 8.63 | 163.4 | Miniscreens at 162 mbsf† |
| 126 | Casing, 4.5 inch, fiberglass, slotted - blue | 5.00 | 3.91 | 4.50 8RD EUE box | 4.50 8RD EUE pin | 8.86 | 172.3 | |
| 127 | Casing, 4.5 inch, fiberglass, slotted - blue | 5.00 | 3.91 | 4.50 8RD EUE box | 4.50 8RD EUE pin | 8.83 | 181.1 | |
| 75 | Casing, 4.5 inch, fiberglass - red | 5.00 | 3.91 | 4.50 8RD EUE box | 4.50 8RD EUE pin | 8.85 | 190.0 | |
| | Casing pup, 4.5 inch, fiberglass | 5.00 | 3.91 | 4.50 8RD EUE box | 4.50 8RD EUE pin | 2.96 | 192.9 | |
| OJ3226 | Crossover, 4-1/2 EUE × 4-1/2 STC | 5.50 | 4.00 | 4.50 8RD EUE box | 4.50 8RD STC pin | 0.19 | 193.1 | |
| B3 | Packer, inflate, 4.5 inch, coated | 8.08 | 4.052 | 4.50 8RD cplg box | 4.50 8RD STC pin | 6.60 | 199.7 | |
| OJ3223 | Landing seat, 2.875 inch, coated | 5.00 | 2.875 | 4.50 8RD STC box | 4.50 8RD STC pin | 0.19 | 199.9 | |
| OJ3282 | Crossover, 4.5 × 5.5 inch, coated | 5.50 | 4.05 | 4.50 8RD LTC box | 5.50 8RD LTC pin | 0.19 | 200.1 | |
| OJ3283 | Casing, 5.5 inch, perforated, coated, 14 lb | 6.05 | 5.01 | 5.50 8RD LTC cplg | 5.50 8RD STC pin | 3.12 | 203.2 | Miniscreens at 203 mbsf‡ |
| OJ3281 | Crossover, 5.5 × 6.75 inch, coated | 6.75 | 4.13 | 5.50 8RD LTC box | 5.5 FH pin | 0.48 | 203.7 | |
| OJ3285 | Drill collar, perforated, coated | 6.75 | 4.13 | 5.50 FHM box | 5.5 FHM pin | 4.29 | 208.0 | |
| OJ3285 | Drill collar, perforated, coated | 6.75 | 4.13 | 5.50 FHM box | 5.5 FHM pin | 4.29 | 212.3 | |
| OJ3285 | Drill collar, perforated, coated | 6.75 | 4.13 | 5.50 FHM box | 5.5 FHM pin | 4.29 | 216.6 | |
| OJ3285 | Drill collar, perforated, coated | 6.75 | 4.13 | 5.50 FHM box | 5.5 FHM pin | 4.29 | 220.9 | |
| OJ3285 | Drill collar, perforated, coated | 6.75 | 4.13 | 5.50 FHM box | 5.5 FHM pin | 4.29 | 225.2 | |
| OJ3285 | Drill collar, perforated, coated | 6.75 | 4.13 | 5.50 FHM box | 5.5 FHM pin | 4.29 | 229.5 | |
| OJ3285 | Drill collar, perforated, coated | 6.75 | 4.13 | 5.50 FHM box | 5.5 FHM pin | 4.29 | 233.8 | |
| OJ3285 | Drill collar, perforated, coated | 6.75 | 4.13 | 5.50 FHM box | 5.5 FHM pin | 4.29 | 238.1 | |
| OJ3285 | Drill collar, perforated, coated | 6.75 | 4.13 | 5.50 FHM box | 5.5 FHM pin | 4.29 | 242.3 | |
| OJ3285 | Drill collar, perforated, coated | 6.75 | 4.13 | 5.50 FHM box | 5.5 FHM pin | 4.29 | 246.6 | |
| OJ3286 | Bullnose, coated | 6.75 | 4.13 | 5.50 FHM box | Bullnose | 0.91 | 247.6 | |

## Table T3 (continued).

* = 102.9 m microbiology umbilical (0.5 inch ID Tefzel), Spool A. † = 172.1 m microbiology umbilical (0.5 inch ID Tefzel), Spool B. ‡ = 203.0 m each, microbiology umbilical (0.5 inch ID Tefzel), Spool C, stainless steel pressure and packer inflation umbilicals (1 × 0.5 inch OD and 3 × 0.25 inch OD), and stainless steel geochemistry umbilicals (3 × 0.25 inch OD and 3 × 0.125 inch OD). Part numbers beginning with "OJ" designate USIO engineering part numbers; numbers 24–107 are identification numbers assigned when casing was loaded and measured; D1, B3, and B4 identify the three packers used. ID = inside diameter, OD = outside diameter. 8RD = size of threaded tubing connection, STC = short thread coupling, cplg = coupling, LTC = long thread coupling, EUE = external upset ends connection, FH = full hole threaded tool joint, FHM = full hole modified tool joint, box = female threaded connection, pin = male threaded connection.

**Table T4.** Downhole instrument string deployed in Hole U1383A CORK during IODP Expedition 336.

| Item | Length (m) | Connector length (m)* | Depth (mbsf) | FLOCS or $O_2$ probe ID | Temperature probe† |
|---|---|---|---|---|---|
| Bottom of top plug | | | –6.45 | | |
| Spectra with hose | 1 (1.02) | | –5.43 | | |
| Small sinker bar - 10 lb | 0.3 | | –5.13 | | |
| Spectra‡ (lifts at 12.5 m, 25 m) | 33.6 (34.10) | | 28.97 | | |
| Middle sinker bar - 100 lb | 1.524 | | 30.49 | | |
| Spectra (lifts at 3.9 m, 16.4 m) | 28.9 (29.33) | | | | |
| Landing seat, 3.375, coated | | | 58.40 | | |
| Spectra (lifts at 3.4 m, 15.9 m) | 24.5 (24.87) | | 83.27 | | |
| MBIO OS | 5.73 | 0.16 | 89.16 | 100/101 | A 1857015 |
| Enrichment OS | 5.2 | 0.16 | 94.52 | 96/97 | |
| Standard OS | 2.63 | 0.16 | 97.31 | | |
| Acid-addition OS | 5.2 | 0.16 | 102.67 | | |
| BOSS OS | 5.2 | 0.16 | 108.03 | | |
| Oxygen probe | 0.58 | 0.16 | 108.77 | 22022 | |
| Copper OS - Gas | 2.63 | 0.16 | 111.56 | | O 9944910 |
| Spectra (lifts at 2.4 m, 14.9 m, 27.4 m) | 35.0 (35.53) | | | | |
| Landing Seat, 3.125, coated | | | 145.70 | | |
| MBIO OS | 5.73 | 0.16 | 151.59 | 102/103 | A 1857006 |
| Enrichment OS | 5.2 | 0.16 | 156.95 | 98/99 | |
| Standard OS | 2.63 | 0.16 | 159.74 | | |
| Acid-addition OS | 5.2 | 0.16 | 165.10 | | |
| BOSS OS | 5.2 | 0.16 | 170.46 | | |
| Oxygen probe | 0.58 | 0.16 | 171.20 | 22021 | |
| Copper OS - Gas | 2.63 | 0.16 | 173.99 | | O 9944709 |
| Spectra (lifts at 2.6 m, 15.1 m) | 26.4 (26.80) | | | | |
| Landing Seat, 2.874, coated | | | 199.90 | | |
| Spectra | 4.0 (4.06) | | 203.96 | | |
| MBIO OS | 7.61 | 0.16 | 211.73 | 104/105 | A 185710 |
| Enrichment OS | 6.8 | 0.16 | 218.69 | 95/94 | |
| Standard OS | 3.43 | 0.16 | 222.28 | | |
| Acid-addition OS | 6.8 | 0.16 | 229.24 | | |
| BOSS OS | 6.8 | 0.16 | 236.20 | | |
| Copper OS - Gas | 3.43 | 0.16 | 239.79 | | O 9944711 |
| Sinker bar - 150 lb | 3.19 | 0.16 | 243.14 | | |

* = a stainless steel coupler was used to join two packages and join packages to the sinker bar and landing seat. † = temperature probes were purchased from Onset (O) and Antares (A); probes are located 53 cm from the top of the OsmoSampler packages except for A 185710 which was positioned 15 cm from the bottom of the OsmoSampler package. ‡ = Spectra lengths are given in measured units and expected lengths based on stretch within the hole (in parentheses); some downhole depths for Spectra are not given because additional line was used to ensure that the plugs could seat at the correct depths. Lifting loops were weaved at 10.5, 23, and 35.5 m for the 43.4 m long rope; 14.3, 26.8, 39.3, 51.8, and 64.3 m for the 66.2 m long rope; and 2, 14.5, and 27.5 for the 39.5 m long rope. FLOCS = Flow-through Osmo Colonization System. MBIO = microbiology, OS = OsmoSampler, BOSS = BioOsmoSampling System.

**Table T5.** Summary of basement stratigraphy and subunits recovered in Hole 1383C. (Continued on next two pages.)

| Lith. unit | Subunit | Depth (m) Top | Depth (m) Bottom | Core, section (Piece) Top | Core, section (Piece) Bottom | Pieces in subunit (*N*) | Lithology | Unit interpretation | Vesicularity | Groundmass alteration (%) | Veins Average density (vein/m) | Veins Average width (mm) | Halos Color | Halos Average width (mm) |
|---|---|---|---|---|---|---|---|---|---|---|---|---|---|---|
| 1 | 1-1 | 69.51 | 87.53 | 336-U1383C-2R-1 (1) | 336-U1383C-4R-1 (15) | 105 | Aphyric to sparsely phyric | Pillow lava | Nonvesicular–sparsely vesicular (mean = 0.8%: max = 4%; size: 0.1–1 mm) | 1–40 (mean = 8) | 18 | 0.5 (max = 2) | Dark brown–grayish brown | ~10 |
| 1 | 1-2 | 87.54 | 87.56 | 4R-1 (16) | 4R-1 (16) | 2 | Limestone | Interflow sediment | | | | | | |
| 1 | 1-3 | 87.78 | 88.47 | 4R-2 (3) | 4R-2 (10) | 7 | Sparsely phyric | Pillow lava | Nonvesicular–sparsely vesicular (mean = 0.5%: max = 2.7%; size: 0.1–1 mm) | 3–15 (mean = 8) | 24 | 0.5 (max = 1) | Dark brown–grayish brown | ~8 |
| 1 | 1-4 | 88.48 | 88.54 | 4R-2A (11) | 4R-2A (11) | 1 | Limestone | Interflow sediment | | | | | | |
| 1 | 1-5 | 88.54 | 96.89 | 4R-2 (12) | 5R-1 (17) | 18 | Aphyric to sparsely phyric | Pillow lava | Nonvesicular–sparsely vesicular (mean = 0.5%: max = 3%; size: 0.1–1 mm) | 1–20 (mean = 8) | 16 | 0.4 (max = 1) | Mainly grayish brown | ~12 |
| 1 | 1-6 | 96.90 | 96.93 | 5R-1A (18) | 5R-1A (18) | 1 | Limestone | Interflow sediment | | | | | | |
| 1 | 1-7 | 96.94 | 117.13 | 5R-1 (19) | 7R-2 (12) | 70 | Aphyric to sparsely phyric | Pillow lava | Nonvesicular–sparsely vesicular (mean = 0.5%: max = 4%; size: 0.1–0.8 mm) | 1–40 (mean = 8) | 24 | 0.5 (max = 5) | Mainly grayish brown | ~15 |
| 1 | 1-8 | 117.14 | 117.30 | 7R-2A (13) | 7R-2A (14) | 2 | Sedimentary breccia | Interflow sediment | | | | | | |
| 1 | 1-9 | 117.30 | 126.52 | 7R-2 (15) | 8R-2 (6) | 37 | Aphyric to sparsely phyric | Pillow lava | Nonvesicular–sparsely vesicular (mean = 0.5%: max = 2%; size: 0.1–0.8 mm) | 3–40 (mean = 10) | 18 | 0.7 (max = 3) | Mainly grayish brown with several composite dark and brown | ~15 |
| 1 | 1-10 | 126.52 | 126.55 | 8R-2A (7) | 8R-2A (7) | 1 | Sedimentary breccia | Interflow sediment | | | | | | |
| 1 | 1-11 | 126.55 | 126.72 | 8R-2 (8) | 8R-2 (10) | 3 | Aphyric to sparsely phyric | Pillow lava | Nonvesicular vesicular (<0.1%) | 25–30 | | | | |
| 2 | 2-1 | 126.73 | 144.27 | 8R-2 (11) | 10R-1 (7) | 80 | Sparsely to highly phyric | Basalt flow/sheet flow | Nonvesicular–sparsely vesicular (mean = 0.7%: max = 4%; size: 0.1–1 mm) | 1–70 (mean = 8) | 15 | 0.2 (max = 1) | Dark brown–grayish brown | ~13 |
| 2 | 2-2 | 144.28 | 144.38 | 10R-1A (8) | 10R-1A (9) | 2 | Sedimentary breccia | Interflow sediment | | | | | | |
| 2 | 2-3 | 144.38 | 145.89 | 10R-1 (10) | 10R-2 (8) | 20 | Sparsely to highly phyric | Basalt flow/sheet flow | Nonvesicular–sparsely vesicular (mean = 1.1%; max = 5%; size: 0.1–1 mm) | 2–20 (mean = 9) | 17 | 0.2 (max = 1) | Dark brown–grayish brown | ~22 |
| 2 | 2-4 | 145.90 | 145.97 | 10R-2A (9) | 10R-2A (9) | 1 | Sedimentary breccia | Interflow sediment | | | | | | |
| 2 | 2-5 | 145.90 | 146.59 | 10R-2 (9) | 10R-2 (18) | 8 | Sparsely to highly phyric | Basalt flow/sheet flow | Nonvesicular–sparsely vesicular (mean = 0.7%: max = 3%; size: 0.1–1 mm) | 12–18 (mean = 15) | 27 | 0.5 (max = 2) | Mainly grayish brown | ~33 |
| 2 | 2-6 | 146.61 | 146.62 | 10R-2A (19) | 10R-2A (19) | 1 | Sedimentary breccia | Interflow sediment | | | | | | |
| 2 | 2-7 | 146.63 | 153.96 | 10R-2 (20) | 11R-1 (8) | 33 | Sparsely to highly phyric | Basalt flow/sheet flow | Nonvesicular–sparsely vesicular (mean = 1%: max = 2%; size: 0.1–1 mm) | 2–25 (mean = 9) | 19 | 0.2 (max = 0.8) | Mainly dark brown/green overlapping grayish brown | ~13 |

**Table T5 (continued).** (Continued on next page.)

| Lith. unit | Subunit | Depth (m) Top | Depth (m) Bottom | Core, section (Piece) Top | Core, section (Piece) Bottom | Pieces in subunit (*N*) | Lithology | Unit interpretation | Vesicularity | Groundmass alteration (%) | Veins Average density (vein/m) | Veins Average width (mm) | Halos Color | Halos Average width (mm) |
|---|---|---|---|---|---|---|---|---|---|---|---|---|---|---|
| 2 | 2-8 | 153.96 | 163.69 | 11R-1 (9) | 12R-1 (10) | 20 | Sparsely to highly phyric | Basalt flow/ sheet flow | Nonvesicular–sparsely vesicular (mean = 0.9%: max = 3%; size: 0.1–1 mm) | 1–20 (mean = 7) | 18 | 0.3 (max = 2) | Mainly dark green with minor grayish brown | ~20 |
| 2 | 2-9 | 163.69 | 163.72 | 12R-1A (11) | 12R-1A (11) | 1 | Sedimentary breccia | Interflow sediment | | | | | | |
| 3 | 3-1 | 163.72 | 163.80 | 12R-1A (12) | 12R-1A (13) | 2 | Brecciated glassy basalt | Hyaloclastite | | | | | | |
| 3 | 3-2 | 163.80 | 164.26 | 12R-1A (14) | 12R-1A (24) | 10 | Aphyric | Pillow lava | Nonvesicular vesicular (<0.5%) | 2–4 (mean = 3) | 25 | 0.2 (max = 0.3) | Mainly grayish brown | ~6 |
| 3 | 3-3 | 164.26 | 164.29 | 12R-1A (24) | 12R-1A (24) | 1 | Brecciated glassy basalt | Hyaloclastite | | | | | | |
| 3 | 3-4 | 164.29 | 173.08 | 12R-1A (25) | 13R-1A (7) | 8 | Aphyric–sparsely phyric | Basalt flow/ sheet flow | Nonvesicular vesicular (<0.5%) | 1–6 (mean = 3) | 45 | 0.2 (max = 0.5) | Mainly dark brown–grayish brown | ~9 |
| 3 | 3-5 | 173.08 | 173.32 | 13R-1A (8) | 13R-1A (12) | 5 | Brecciated glassy basalt | Hyaloclastite | | | | | | |
| 3 | 3-6 | 173.32 | 212.26 | 13R-1 (13) | 19R-1 (13) | 135 | Aphyric–sparsely/ moderately phyric | Pillow lava | Nonvesicular–sparsely vesicular (mean = 0.6%: max = 3%; size: 0.1–0.8 mm) | 1–15 (mean = 5) | 27 | 0.2 (max = 0.6) | Mainly grayish brown | ~11 |
| 3 | 3-7 | 212.26 | 212.30 | 19R-1A (14) | 19R-1A (14) | 1 | Brecciated glassy basalt | Hyaloclastite | | | | | | |
| 3 | 3-8 | 212.30 | 219.35 | 19R-1 (15) | 20R-1 (3) | 21 | Aphyric | Pillow lava | Nonvesicular–sparsely vesicular (mean <0.5%: max = 3%; size: 0.1–0.8 mm) | 1–5 (mean = 3) | 27 | 0.2 (max 1) | Mainly grayish brown | ~9 |
| 3 | 3-9 | 219.35 | 219.47 | 20R-1A (4) | 20R-1A (5) | 2 | Brecciated glassy basalt | Hyaloclastite | | | | | | |
| 3 | 3-10 | 219.47 | 220.31 | 20R-1 (6) | 20R-1 (20) | 15 | Aphyric | Pillow lava | Nonvesicular (<0.5%) | 1–5 (mean = 3) | 25 | 0.15 (max = 0.2) | Mainly grayish brown | ~4 |
| 3 | 3-11 | 220.31 | 220.35 | 20R-1-A (21) | 20R-1A (21) | 1 | Brecciated glassy basalt | Hyaloclastite | | | | | | |
| 3 | 3-12 | 220.35 | 220.38 | 20R-1-A (22) | 20R-1A (22) | 1 | Aphyric | Pillow lava | Nonvesicular (<0.5%) | 2–5 (mean = 3) | | | | |
| 3 | 3-13 | 220.38 | 220.47 | 20R-1-A (23) | 20R-1A (24) | 2 | Brecciated glassy basalt | | | | | | | |
| 3 | 3-14 | 220.47 | 220.58 | 20R-1-A (25) | 20R-1A (26) | 2 | Aphyric | Pillow lava | Mainly nonvesicular (<0.5%) except with vugs up–2.8 mm | 2–5 (mean = 3) | | | | |
| 3 | 3-15 | 220.58 | 220.66 | 20R-1-A (27) | 20R-1A (28) | 2 | Brecciated glassy basalt | Hyaloclastite | | | | | | |
| 3 | 3-16 | 220.74 | 220.94 | 20R-2 (2) | 20R-2 (5) | 4 | Aphyric | Pillow lava | Nonvesicular (<0.5%) | (mean = 3) | 45 | 0.2 (max = 0.5) | None | NA |
| 3 | 3-17 | 220.94 | 220.99 | 20R-2-A (6) | 20R-2A (6) | 1 | Brecciated glassy basalt | Hyaloclastite | | | | | | |
| 3 | 3-18 | 220.99 | 229.45 | 20R-2 (7) | 21R-1 (16) | 17 | Aphyric | Basalt flow/ sheet flow | Nonvesicular–sparsely vesicular (mean <0.5%: max = 2%; size: 0.2–0.8 mm) | 1–4 (mean = 2) | 30 | 0.6 (max = 3) | Mainly grayish brown | ~7 |
| 3 | 3-19 | 229.45 | 229.48 | 21R-1-A (17) | 21R-1A (17) | 1 | Brecciated glassy basalt | Hyaloclastite | | | | | | |
| 3 | 3-20 | 229.48 | 237.93 | 21R-1 (18) | 22R-1 (5) | 13 | Aphyric | Pillow lava | Nonvesicular (<0.5%) | 1–3 (mean = 2) | 40–50 | 0.2 (max = 0.6) | None | NA |

**Table T5 (continued).**

| Lith. unit | Subunit | Depth (m) Top | Depth (m) Bottom | Core, section (Piece) Top | Core, section (Piece) Bottom | Pieces in subunit (*N*) | Lithology | Unit interpretation | Vesicularity | Groundmass alteration (%) | Veins: Average density (vein/m) | Veins: Average width (mm) | Halos: Color | Halos: Average width (mm) |
|---|---|---|---|---|---|---|---|---|---|---|---|---|---|---|
| 3 | 3-21 | 237.93 | 237.98 | 22R-1-A (6) | 22R-1A (6) | 1 | Brecciated glassy basalt | Hyaloclastite | | | | | | |
| 3 | 3-22 | 237.98 | 256.25 | 22R-1 (7) | 24R-1 (1) | 48 | Aphyric | Pillow lava | Nonvesicular–sparsely vesicular (mean <0.5%: max = 4%; size: 0.1–0.6 mm) | 1–10 (mean = 4) | 35 | 0.2 (max = 1) | Mainly grayish brown | ~7 |
| 3 | 3-23 | 256.25 | 256.30 | 24R-1A (2) | 24R-1A (2) | 1 | Brecciated glassy basalt | Hyaloclastite | | | | | | |
| 3 | 3-24 | 256.30 | 299.25 | 24R-1 (3) | 29R-1 (1) | 125 | Aphyric | Pillow lava | Nonvesicular–sparsely vesicular (mean <0.5%: max = 3%; size: 0.1–0.5 mm) | 1–15 (mean = 4) | 33 | 0.2 (max = 1) | Mainly dark to grayish brown | ~7 |
| 3 | 3-25 | 299.25 | 299.29 | 29R-1A (2) | 29R-1A (2) | 1 | Brecciated glassy basalt | Hyaloclastite | | | | | | |
| 3 | 3-26 | 299.29 | 312.18 | 29R-1 (3) | 31R-1 (2) | 58 | Aphyric | Pillow lava | Nonvesicular (<0.5%) | 1–20 (mean = 5) | 38 | 0.3 (max = 1.5) | Mainly dark to grayish brown | ~9 |
| 3 | 3-27 | 312.18 | 312.24 | 31R-1A (3) | 31R-1A (3) | 1 | Brecciated glassy basalt | Hyaloclastite | | | | | | |
| 3 | 3-28 | 312.24 | 324.12 | 31R-1 (4) | 32R-2 (17) | 79 | Aphyric | Pillow lava | Nonvesicular (<0.5%) | 1–20 (mean = 5) | 33 | 0.3 (max = 3) | Mainly dark to grayish brown | ~7 |
| 3 | 3-29 | 324.27 | 324.35 | 32R-3A (1) | 32R-3A (1) | 1 | Breccia | Pseudobreccia? | | | | | | |
| 3 | 3-30 | 324.35 | 324.76 | 32R-3 (2) | 32R-3 (9) | 8 | Aphyric | Pillow lava | Nonvesicular (<0.5%) | 1–5 (mean = 3) | | | | NA |

NA = not applicable.

**Table T6.** Summary of primary and secondary mineralogy determined by thin section microscopy observation and XRD. (Continued on next two pages.)

| Core, section (Piece) | Lith. unit | Thin section | Rock name | Grain size | Texture | Thin section | | XRD | | Total alteration (%) |
|---|---|---|---|---|---|---|---|---|---|---|
| | | | | | | Primary minerals | Secondary minerals | Primary minerals | Secondary minerals | |
| 336-U1383C- | | | | | | | | | | |
| 2R-1 (7) | 1-1 | | | | | | | | Phillipsite (Na)<br>Calcite | |
| 2R-2 (3) | 1-1 | 28 | Sparsely plagioclase-olivine-phyric basalt, avesicular | Glassy to microcrystalline | Hyalophytic | Olivine<br>Plagioclase<br>Clinopyroxene<br>Fe-Ti oxide<br>Glass | Zeolite<br>Palagonite | Mixed plagioclase, diopside/augite | | 15 |
| 3R-3 (7) | 1-1 | 29 | Sparsely plagioclase-olivine-phyric basalt | Microcrystalline to fine grained | Hyalophytic to fine grained | Olivine<br>Plagioclase<br>Clinopyroxene<br>Fe-Ti oxide | Clay<br>Carbonate<br>Zeolite | Mixed plagioclase, diopside/augite | | 7.2 |
| 3R-1 (2) | 1-1 | 30 | Avesicular sparsely plagioclase-phyric basalt | Microcrystalline | Hyalophytic | Olivine<br>Plagioclase<br>Clinopyroxene | Clay<br>FeOOH<br>Zeolite | Mixed plagioclase, diopside/augite | | 39 |
| 3R-2 (5) | 1-1 | 31 | Sparsely plagioclase-olivine-phyric basalt | Microcrystalline | Porphyritic | Olivine<br>Plagioclase<br>Clinopyroxene<br>Fe-Ti oxide | Clay<br>FeOOH | Mixed plagioclase, diopside/augite, olivine | | 10 |
| 5R-1 (6) | 1-5 | 32 | Sparsely plagioclase-olivine-phyric basalt | Cryptocrystalline to microcrystalline | Hyalophytic to trachytic | Olivine<br>Plagioclase<br>Clinopyroxene<br>Fe-Ti oxide<br>Sulfide | Clay | Mixed plagioclase, diopside/augite, olivine | | 4 |
| 5R-1 (11) | 1-5 | 33 | Sparsely plagioclase-olivine-phyric basalt | Microcrystalline | Hyalophytic to trachytic | Olivine<br>Plagioclase<br>Clinopyroxene<br>Fe-Ti oxide<br>Sulfide | Clay<br>Zeolite | | | 10 |
| 6R-1 (17) | 1-7 | 34 | Sparsely plagioclase-olivine-phyric avesicular basalt (chilled margin) | Glassy to microcrystalline | Hyalophitic to aphanitic to intersertal | Plagioclase<br>Clinopyroxene<br>Fe-Ti oxide<br>Sulfide<br>Glass | Clay<br>Zeolite | Mixed plagioclase, diopside/augite | | 23.5 |
| 6R-1 (7) | 1-7 | 35 | Sparsely plagioclase-olivine-phyric avesicular basalt (chilled margin) | Glassy to microcrystalline | Hyalophitic to aphanitic to intersertal | Plagioclase<br>Fe-Ti oxide<br>Sulfide<br>Glass | Clay | | | 5 |
| 7R-2 (8) | 1-7 | 36 | Sparsely plagioclase-olivine-phyric sparsely vesicular basalt | Micro- to cryptocrystalline | Intersertal | Plagioclase<br>Clinopyroxene<br>Fe-Ti oxide<br>Sulfide | Clay<br>FeOOH | Mixed plagioclase, diopside/augite, olivine | | 5 |
| 7R-2 (16) | 1-9 | 38 | Moderately plagioclase-olivine-phyric sparsely vesicular basalt | Micro- to cryptocrystalline | Intersertal | Plagioclase<br>Clinopyroxene<br>Fe-Ti oxide<br>Sulfide | Clay<br>Zeolite | Mixed plagioclase, diopside/augite | | 35.5 |
| 9R-3 (10) | 2-1 | 39 | Moderately plagioclase-olivine-phyric sparsely vesicular basalt | Microcrystalline | Intersertal | Plagioclase<br>Clinopyroxene<br>Fe-Ti oxide<br>Sulfide | Clay<br>Zeolite | Mixed plagioclase, diopside/augite | | 18 |

**Table T6 (continued).** (Continued on next page.)

| Core, section (Piece) | Lith. unit | Thin section | Rock name | Grain size | Texture | Thin section | | XRD | | Total alteration (%) |
|---|---|---|---|---|---|---|---|---|---|---|
| | | | | | | Primary minerals | Secondary minerals | Primary minerals | Secondary minerals | |
| 9R-4 (9) | 2-1 | 40 | Highly plagioclase-olivine-phyric sparsely vesicular basalt | Microcrystalline | Intersertal | Plagioclase<br>Clinopyroxene<br>Fe-Ti oxide<br>Sulfide | Clay | Mixed plagioclase, diopside/augite, olivine | | 1 |
| 10R-1 (7) | 2-1 | 41 | Plagioclase-olivine-phyric basalt | Microcrystalline | Porphyritic | Olivine<br>Plagioclase<br>Clinopyroxene<br>Fe-Ti oxide | Clay<br>Zeolite | Mixed plagioclase, diopside/augite | | 3–15? |
| 10R-2 (1b) | 2-3 | 43 | Avesicular, plagioclase-olivine-phyric basalt | Fine grained | Porphyritic, intersertal groundmass | Olivine<br>Plagioclase<br>Clinopyroxene<br>Fe-Ti oxide<br>Sulfide | Clay | Mixed plagioclase, diopside/augite, olivine | | 2 |
| 13R-1 (5) | 3-4 | 44 | Aphyric sparsely vesicular basalt | Microcrystalline | Intersertal | Olivine<br>Plagioclase<br>Clinopyroxene<br>Fe-Ti oxide<br>Sulfide | Clay<br>FeOOH | Mixed plagioclase, diopside/augite | Clay | 8.5 |
| 16R-1 (3) | 3-6 | 45 | Aphyric sparsely vesicular basalt | Microcrystalline | Intersertal | Olivine<br>Plagioclase<br>Clinopyroxene<br>Fe-Ti oxide<br>Sulfide | Clay<br>FeOOH<br>Carbonate | Mixed plagioclase, diopside/augite, olivine | | 6 |
| 16R-1 (14) | 3-6 | 46 | Aphyric basalt with blotchy alteration | Crypto- to microcrystalline | Hyalophitic | Olivine<br>Plagioclase<br>Clinopyroxene<br>Fe-Ti oxide | Clay | Mixed plagioclase, diopside/augite, olivine | | 4 |
| 16R-2 (6) | 3-6 | 47 | Sparsely vesicular aphyric basalt | Crypto- to microcrystalline | Aphanitic | Olivine<br>Plagioclase | Clay<br>Carbonate<br>Zeolite | Mixed plagioclase, diopside/augite, olivine | | 3 |
| 16R-2 (7) | 3-6 | 48 | Aphyric sparsely vesicular basalt | Microcrystalline | Intersertal | Olivine<br>Plagioclase<br>Clinopyroxene<br>Fe-Ti oxide | Clay<br>Zeolite | | | 23 |
| 19R-1 (6b) | 3-6 | 49 | Aphyric basalt with blotchy alteration | Cryptocrystalline | Hyalophitic | Olivine<br>Plagioclase<br>Clinopyroxene<br>Fe-Ti oxide | Clay<br>Palagonite | | | 2 |
| 20R-1 (28) | 3-13 | 50 | Hyaloclastite | | | Olivine<br>Plagioclase<br>Glass | FeOOH<br>Zeolite<br>Palagonite<br>Calcedony | | | 50 |
| 20R-1 (9) | 3-10 | 51 | Aphyric sparsely vesicular basalt | Microcrystalline | Intersertal | Olivine<br>Plagioclase<br>Clinopyroxene<br>Fe-Ti oxide | Clay<br>FeOOH<br>Pyrite<br>Zeolite | Mixed plagioclase, diopside/augite | | 25 |
| 23R-1 (10) | 3-20 | 52 | Aphyric sparsely vesicular basalt | Microcrystalline | Intersertal | Olivine<br>Plagioclase<br>Clinopyroxene<br>Fe-Ti oxide<br>Sulfide | Clay<br>FeOOH | Mixed plagioclase, diopside/augite, olivine | | 16 |

**Table T6 (continued).**

| Core, section (Piece) | Lith. unit | Thin section | Rock name | Grain size | Texture | Thin section | | XRD | | Total alteration (%) |
|---|---|---|---|---|---|---|---|---|---|---|
| | | | | | | Primary minerals | Secondary minerals | Primary minerals | Secondary minerals | |
| 25R-1 (14) | 3-22 | 53 | Aphyric basalt with blotchy alteration | Microcrystalline | Aphanitic to hyalophytic | Olivine<br>Plagioclase<br>Clinopyroxene<br>Fe-Ti oxide | Clay<br>Zeolite | Mixed plagioclase, diopside/augite, olivine | | 12 |
| 27R-1 (19) | 3-22 | | | | | | | Mixed plagioclase, diopside/augite, olivine | | |
| 28R-1 (7) | 3-22 | 54 | Aphyric basalt | Microcrystalline | Intersertal | Olivine<br>Plagioclase<br>Clinopyroxene<br>Fe-Ti oxide | Clay | Mixed plagioclase, diopside/augite, olivine | | 4 |
| 29R-1 (14) | 3-24 | 55 | Aphyric sparsely vesicular basalt | Microcrystalline | Intersertal | Olivine<br>Plagioclase<br>Clinopyroxene<br>Fe-Ti oxide | Clay<br>FeOOH<br>Pyrite<br>Carbonate | Mixed plagioclase, diopside/augite, olivine | Phillipsite (Na) | 15 |
| 31R-2 (1) | 3-26 | 56 | Aphyric sparsely vesicular basalt | Microcrystalline | Intersertal | Olivine<br>Plagioclase<br>Clinopyroxene<br>Fe-Ti oxide | Clay<br>FeOOH<br>Pyrite | Mixed plagioclase, diopside/augite, olivine | | 7 |
| 31R-2 (6) | 3-26 | 57 | Aphyric sparsely vesicular basalt | Crypto- to microcrystalline | Intersertal | Olivine<br>Plagioclase<br>Clinopyroxene<br>Fe-Ti oxide | Clay<br>FeOOH<br>Carbonate<br>Zeolite | Mixed plagioclase, diopside/augite | Phillipsite (Na) | 22 |
| 32R-2 (9) | 3-26 | 58 | Aphyric basalt | Fine grained | Intersertal | Olivine<br>Plagioclase<br>Clinopyroxene<br>Fe-Ti oxide<br>Sulfide | Clay | Mixed plagioclase, diopside/augite | | 6 |

**Table T7.** Shipboard geochemical analysis, Hole U1383C.

| | 336-U1383C- | | | | | | | | | | | | | |
|---|---|---|---|---|---|---|---|---|---|---|---|---|---|---|
| Core, section: | 2R-2 | 3R-1 | 3R-2 | 3R-3 | 5R-1 | 6R-1 | 7R-2 | 7R-2 | 9R-3 | 9R-4 | 10R-1 | 10R-2 | 13R-1 | 16R-1 |
| Top depth (mbsf): | 71.08 | 76.63 | 78.36 | 79.87 | 96.14 | 106.40 | 116.85 | 117.39 | 138.01 | 139.43 | 144.23 | 145.34 | 172.94 | 192.91 |
| Bottom depth (mbsf): | 71.11 | 76.66 | 78.39 | 79.90 | 96.17 | 106.44 | 116.88 | 117.41 | 138.04 | 139.45 | 144.26 | 145.37 | 172.96 | 192.94 |
| Major element oxide (wt%): | | | | | | | | | | | | | | |
| $SiO_2$ | 47.64 | 46.90 | 49.76 | 47.61 | 49.78 | 47.72 | 49.40 | 46.63 | 48.13 | 49.84 | 48.12 | 50.12 | 50.19 | 49.57 |
| $TiO_2$ | 1.97 | 2.02 | 1.71 | 1.94 | 1.70 | 1.97 | 1.74 | 2.15 | 1.72 | 1.50 | 1.69 | 1.51 | 1.78 | 1.76 |
| $Al_2O_3$ | 17.96 | 18.21 | 15.51 | 17.56 | 15.38 | 17.65 | 16.00 | 19.18 | 18.51 | 16.60 | 18.17 | 16.20 | 15.49 | 15.08 |
| $Fe_2O_3^T$ | 12.57 | 13.02 | 10.67 | 12.26 | 10.86 | 12.64 | 11.00 | 13.83 | 11.38 | 9.78 | 11.12 | 9.92 | 10.95 | 11.37 |
| MgO | 4.01 | 3.34 | 7.72 | 3.91 | 7.74 | 4.24 | 6.92 | 3.31 | 3.85 | 7.43 | 4.88 | 7.59 | 7.07 | 8.29 |
| CaO | 12.02 | 12.83 | 11.22 | 12.99 | 11.21 | 12.18 | 11.44 | 10.90 | 12.65 | 11.61 | 12.57 | 11.46 | 10.90 | 10.63 |
| $Na_2O$ | 3.36 | 3.21 | 3.01 | 3.29 | 2.89 | 3.19 | 3.01 | 3.51 | 3.31 | 2.91 | 3.11 | 2.90 | 3.17 | 2.92 |
| $K_2O$ | 0.15 | 0.13 | 0.25 | 0.19 | 0.25 | 0.13 | 0.30 | 0.14 | 0.21 | 0.19 | 0.13 | 0.14 | 0.29 | 0.23 |
| $P_2O_5$ | 0.32 | 0.34 | 0.16 | 0.25 | 0.17 | 0.27 | 0.18 | 0.34 | 0.24 | 0.14 | 0.22 | 0.15 | 0.16 | 0.17 |
| Trace element (ppm): | | | | | | | | | | | | | | |
| Ba | 16.22 | 12.65 | 6.6 | 14.1 | 6.9 | 12.62 | 6.9 | 24.30 | 13.17 | 5.7 | 13.30 | 5.4 | 3.9 | 3.77 |
| Co | 61.0 | 102.2 | 69.5 | 105.5 | 81.7 | 62.4 | 62.6 | 67.3 | 50.8 | 58.5 | 56.4 | 49.5 | 53.5 | 73.7 |
| Cr | 311 | 326 | 281 | 313 | 282 | 313 | 279 | 295 | 279 | 249 | 273 | 260 | 308 | 306 |
| Cu | 74.2 | 54.2 | 69.6 | 65.5 | 70.7 | 64.7 | 68.0 | 81.7 | 77.6 | 69.9 | 69.2 | 78.1 | 75.8 | 74.4 |
| Ni | 106 | 71 | 117 | 106 | 120 | 102 | 109 | 126 | 79 | 91 | 84 | 94 | 167 | 190 |
| Sc | 46.8 | 49.0 | 40.0 | 45.6 | 39.4 | 46.3 | 39.7 | 47.8 | 42.5 | 37.0 | 41.6 | 37.0 | 38.8 | 38.9 |
| Sr | 197 | 195 | 169 | 186 | 158 | 194 | 160 | 219 | 189 | 161 | 190 | 156 | 156 | 151 |
| V | 363 | 403 | 304 | 363 | 302 | 364 | 304 | 329 | 331 | 266 | 321 | 265 | 284 | 283 |
| Y | 42.4 | 47.0 | 36.7 | 42.9 | 36.8 | 43.8 | 37.2 | 42.6 | 37.9 | 32.7 | 37.5 | 32.7 | 37.5 | 37.8 |
| Zr | 137.5 | 133.9 | 121 | 138 | 120 | 139 | 119 | 152 | 118 | 105 | 114 | 104 | 114.5 | 113.0 |
| Volatile element (wt%): | | | | | | | | | | | | | | |
| LOI | 2.09 | 2.29 | 1.23 | 2.16 | 0.44 | 1.87 | 1.32 | 3.44 | 1.53 | 0.72 | 3.08 | 2.42 | 3.66 | 2.29 |

LOI = loss on ignition.

**Table T7 (continued).**

| | 336-U1383C- | | | | | | | | | | |
|---|---|---|---|---|---|---|---|---|---|---|---|
| Core, section: | 16R-1 | 19R-1 | 20R-1 | 23R-1 | 25R-1 | 27R-1 | 28R-1 | 29R-1 | 31R-2 | 31R-2 | 32R-2 |
| Top depth (mbsf): | 193.39 | 211.90 | 219.67 | 247.57 | 266.87 | 285.93 | 295.00 | 299.80 | 313.55 | 313.89 | 323.68 |
| Bottom depth (mbsf): | 193.41 | 211.92 | 219.70 | 247.61 | 266.93 | 285.96 | 295.02 | 299.82 | 313.58 | 313.91 | 323.70 |
| Major element oxide (wt%): | | | | | | | | | | | |
| $SiO_2$ | 49.05 | 48.99 | 49.00 | 49.11 | 49.03 | 49.44 | 50.02 | 48.11 | 49.51 | 48.57 | 49.13 |
| $TiO_2$ | 1.76 | 1.74 | 1.79 | 1.69 | 1.73 | 1.71 | 1.69 | 1.81 | 1.70 | 1.82 | 1.70 |
| $Al_2O_3$ | 15.35 | 15.24 | 16.10 | 15.01 | 15.21 | 15.03 | 14.94 | 15.87 | 14.92 | 16.29 | 14.96 |
| $Fe_2O_3^T$ | 11.92 | 12.08 | 12.46 | 11.84 | 12.13 | 11.54 | 11.28 | 12.32 | 11.66 | 12.53 | 12.34 |
| MgO | 7.92 | 7.80 | 6.03 | 8.60 | 7.65 | 8.32 | 8.25 | 6.51 | 8.43 | 5.42 | 7.94 |
| CaO | 10.73 | 10.76 | 10.91 | 10.45 | 10.62 | 10.51 | 10.43 | 11.72 | 10.39 | 11.54 | 10.54 |
| $Na_2O$ | 2.98 | 3.00 | 3.24 | 2.85 | 3.17 | 3.04 | 3.06 | 3.24 | 2.99 | 3.36 | 2.94 |
| $K_2O$ | 0.14 | 0.24 | 0.30 | 0.29 | 0.31 | 0.24 | 0.17 | 0.25 | 0.25 | 0.28 | 0.29 |
| $P_2O_5$ | 0.16 | 0.15 | 0.18 | 0.15 | 0.16 | 0.15 | 0.15 | 0.18 | 0.15 | 0.19 | 0.16 |
| Trace element (ppm): | | | | | | | | | | | |
| Ba | 5.60 | 4.98 | 7.09 | 3.95 | 5.12 | 4.65 | 2.51 | 7.52 | 2.89 | 9.84 | 3.41 |
| Co | 58.3 | 54.6 | 53.9 | 58.7 | 52.4 | 51.8 | 53.3 | 61.9 | 56.3 | 53.9 | 65.5 |
| Cr | 301 | 290 | 295 | 290 | 291 | 292 | 287 | 300 | 290 | 295 | 294 |
| Cu | 73.7 | 72.5 | 73.1 | 74.5 | 73.0 | 74.4 | 73.9 | 69.0 | 72.4 | 74.2 | 73.8 |
| Ni | 164.6 | 161.2 | 167 | 176 | 157.0 | 177 | 181 | 164 | 173 | 167 | 164 |
| Sc | 38.9 | 37.4 | 39.9 | 37.0 | 37.5 | 37.1 | 36.7 | 39.6 | 36.7 | 40.3 | 37.9 |
| Sr | 154 | 158 | 151 | 142 | 149 | 150 | 148 | 163 | 143 | 166 | 149 |
| V | 286 | 273 | 296 | 268 | 271 | 264 | 263 | 301 | 261 | 319 | 270 |
| Y | 38.3 | 36.2 | 38.0 | 35.2 | 36.3 | 35.7 | 35.2 | 38.7 | 35.8 | 39.8 | 36.2 |
| Zr | 111 | 108.0 | 112 | 107 | 107 | 106.1 | 106.7 | 109.6 | 105.8 | 109.5 | 105.9 |
| Volatile element (wt%): | | | | | | | | | | | |
| LOI | 2.11 | 0.40 | 1.62 | 0.20 | 0.47 | 0.05 | 0.95 | 2.28 | 0.52 | 2.28 | 1.32 |

**Table T8.** List of whole-round cores collected for microbiological analysis from Hole U1383C, along with subsamples collected and results of microsphere contamination checks. (Continued on next page.)

| Label identifier | Depth (mbsf) | | Description | DNA/RNA | Isotopes | Archive | DEBI-pt | Geochem pooled | Microspheres | |
|---|---|---|---|---|---|---|---|---|---|---|
| | Top | Bottom | | | | | | | First wash | Final wash |
| 336-U1383C-2R-1-MBIOA | 69.85 | 69.95 | Aphyric basalt, brown oxidation halo, red alteration in veins, altered chilled margin on one end, clays on other end | x | x | x | x | | Yes | No |
| 336-U1383C-2R-1-MBIOC | 70.57 | 70.64 | Aphyric basalt, slight alteration with brown oxidation halos, some orange alteration on one end | x | x | x | x | | Yes | Yes (1) |
| 336-U1383C-2R-1-MBIOB | 70.69 | 70.73 | Aphyric basalt, brown oxidation, altered chilled margin on one end | x | | | x | | Yes | Yes (2) |
| 336-U1383C-2R-2-MBIOD | 71.61 | 71.70 | Aphyric basalt, extensive brown oxidation halo, thin veins with carbonate, trace glass | x | x | | | x | Yes | No |
| 336-U1383C-2R-2-MBIOE | 72.11 | 72.19 | Aphyric basalt, highly altered, 2 mm thick vein with red alteration, light brown alteration on one end with black crust | x | x | | x | x | Yes | Yes (1) |
| 336-U1383C-3R-1-MBIOA | 77.08 | 77.18 | Aphyric basalt, moderate brown oxidation halo with intersecting 1 mm thick veins | x | x | x | | | No | ND |
| 336-U1383C-3R-1-MBIOB | 77.50 | 77.58 | Aphyric basalt, slight alteration, tan alteration deposits | x | | x | | | Yes | No |
| 336-U1383C-3R-1-MBIOC | 77.84 | 77.90 | Aphyric basalt, moderate alteration, some orange and green alteration | x | | | | | No | ND |
| 336-U1383C-3R-2-MBIOD | 78.16 | 78.27 | Aphyric basalt, extensive alteration, large vein with light orange-brown-green alteration | x | x | x | x | | No | ND |
| 336-U1383C-3R-3-MBIOE | 79.56 | 79.59 | Mottled light tan and carmel colored micrite with red and white alteration, some glassy clasts with alteration | x | x | x | x | | Yes | Yes (2) |
| 336-U1383C-4R-1-MBIOA | 86.61 | 86.73 | Aphyric basalt, extensive alteration, significant orange alteration rind | x | x | x | | | Yes (2) | No |
| 336-U1383C-4R-1-MBIOB | 87.57 | 87.64 | Light tan micrite breccia (?) with altered glass clasts | x | x | x | x | | Yes (5) | No |
| 336-U1383C-4R-2-MBIOC | 87.72 | 87.78 | Aphyric basalt with extensive alteration, altered chilled margin at one end | x | x | x | | | Yes | Yes (1) |
| 336-U1383C-4R-2-MBIOD | 87.98 | 88.09 | Aphyric basalt, extensive alteration, with mm-thick white veins (some chilled margin?) | x | x | x | x | | Yes | No |
| 336-U1383C-5R-1-MBIOA | 96.40 | 96.45 | Aphyric basalt, extensive alteration, multiple thin carbonate veins | x | x | | x | | Yes (2) | No |
| 336-U1383C-5R-1-MBIOD | 96.59 | 96.64 | Aphyric basalt, slight alteration, some dark brown and ochre alteration | x | | | | | Yes (15) | Yes (1) |
| 336-U1383C-5R-1-MBIOB | 96.93 | 97.01 | Aphyric basalt, moderately altered, 1 mm thick vein with red alteration, trace ochre alteration | x | x | x | x | | Yes (15) | No |
| 336-U1383C-5R-2-MBIOC | 97.20 | 97.24 | Aphyric basalt, extensive alteration, thin intersecting veins, possible $MnO_2$ crust or micrite, trace carbonate | x | | | | | Yes (1) | No |
| 336-U1383C-6R-1-MBIOA | 105.41 | 105.49 | Aphyric basalt, slight alteration, altered chilled margin, ochre alteration | x | x | | x | | No | ND |
| 336-U1383C-6R-2-MBIOB | 106.75 | 106.84 | Aphyric basalt, moderate alteration, thin carbonate veins, altered chilled margin | x | | | | | Yes (1) | No |
| 336-U1383C-7R-1-MBIOA | 115.10 | 115.17 | Aphyric basalt | x | x | x | | | Yes (8) | Yes (2) |
| 336-U1383C-7R-1-MBIOB | 115.20 | 115.29 | Aphyric basalt with chilled margin | x | | x | | | No | ND |
| 336-U1383C-7R-2-MBIOC | 116.54 | 116.64 | Aphyric altered basalt and light tan micrite pieces with glass clasts | x | x | x | | | Yes (1) | No |
| 336-U1383C-8R-1-MBIOA | 124.70 | 124.79 | Aphyric basalt, extensive alteration with veins, fused with micrite (?) | x | x | x | x | | Yes (7) | Yes (2) |
| 336-U1383C-8R-1-MBIOB | 125.88 | 125.96 | Aphyric basalt, moderate alteration with altered chilled margin | x | x | x | x | | No | ND |
| 336-U1383C-9R-1-MBIOA | 134.72 | 134.78 | Aphyric basalt, extensive alteration with chilled margin | x | x | x | | | Yes (100) | Yes (42) |
| 336-U1383C-9R-2-MBIOB | 136.02 | 136.09 | Phyric basalt, extensive alteration, with white vein | x | x | x | x | | No | ND |
| 336-U1383C-9R-2-MBIOC | 136.61 | 136.73 | Phyric basalt, extensive alteration | x | | x | | | Yes (3) | No |
| 336-U1383C-9R-3-MBIOD | 137.35 | 137.45 | Phyric basalt with red and black alteration in vein | x | x | x | x | | Yes (2) | Yes (3) |
| 336-U1383C-10R-1-MBIOA | 144.28 | 144.34 | Light tan micrite with large clasts of altered glass | x | x | | x | | Yes (40) | Yes (1) |
| 336-U1383C-10R-1-MBIOB | 144.76 | 144.86 | Phyric basalt, highly altered, exposed ochre vein-filling material | x | x | x | x | x | Yes (5) | No |
| 336-U1383C-10R-1-MBIOD | 145.18 | 145.27 | Phyric basalt, moderately altered, multiple veins, slight red alteration | x | x | x | | | Yes (30) | Yes (1) |
| 336-U1383C-10R-2-MBIOC | 146.19 | 146.27 | Phyric basalt, highly oxidized, red and slight ochre alteration, chilled margin | x | | | | x | Yes (5) | No |
| 336-U1383C-11R-1-MBIOA | 153.75 | 153.80 | Aphyric basalt, highly altered, sparse orange alteration | x | | | | | Yes (9) | No |
| 336-U1383C-11R-1-MBIOB | 154.21 | 154.28 | Phyric basalt, highly altered, some light brown breccia matrix with basalt clasts up to 1 cm | x | x | x | x | | Yes (3) | Yes (2) |
| 336-U1383C-11R-1-MBIOC | 154.40 | 154.50 | Phyric basalt, extensive alteration, orange and olive alteration | x | x | | | | Yes (5) | No |
| 336-U1383C-12R-1-MBIOA | 163.72 | 163.77 | Aphyric basalt with glassy rim | x | x | x | x | | Yes (3) | Yes (1) |
| 336-U1383C-12R-1-MBIOB | 164.34 | 164.42 | Massive | x | x | x | | | Yes (3) | Yes (11) |
| 336-U1383C-13R-1-MBIOA | 173.16 | 173.25 | Variolitic with altered chilled margin | x | x | x | x | x | Yes (3) | No |
| 336-U1383C-13R-1-MBIOB | 174.09 | 174.15 | Relatively unaltered basalt glass | x | x | | x | x | No | ND |
| 336-U1383C-13R-2-MBIOC | 174.54 | 174.59 | Massive basalt | x | x | x | | | No | ND |
| 336-U1383C-14R-1-MBIOB | 182.83 | 182.94 | Aphyric variolitic basalt | x | x | x | | x | Yes (4) | No |
| 336-U1383C-14R-1-MBIOA | 183.44 | 183.53 | Aphyric variolitic basalt | x | x | x | | x | Yes (3) | No |

**Table T8 (continued).**

| Label identifier | Depth (mbsf) Top | Depth (mbsf) Bottom | Description | DNA/RNA | Isotopes | Archive | DEBI-pt | Geochem pooled | Microspheres First wash | Microspheres Final wash |
|---|---|---|---|---|---|---|---|---|---|---|
| 336-U1383C-14R-2-MBIOC | 184.03 | 184.12 | Aphyric, variolitic altered basalt with chilled margin | x | x | x | x | | Yes (15) | Yes (3) |
| 336-U1383C-14R-2-MBIOD | 184.12 | 184.18 | Aphyric basalt with chilled margin, core catcher pure glass | x | x | | | x | Yes (5) | No |
| 336-U1383C-16R-1-MBIOA | 193.59 | 193.64 | Aphyric basalt, moderately altered, gray-green-tan alteration | x | x | | | | No | ND |
| 336-U1383C-16R-2-MBIOB | 193.92 | 193.97 | Aphyric basalt, highly altered, thin vein, oxidation halo | x | x | | | | Yes (1) | No |
| 336-U1383C-17R-1-MBIOA | 202.12 | 202.17 | Aphyric basalt, variolitic | x | x | x | x | | No | ND |
| 336-U1383C-17R-1-MBIOB | 202.47 | 202.53 | Aphyric basalt, glassy rim | x | x | x | x | x | No | ND |
| 336-U1383C-17R-1-MBIOC | 202.73 | 202.81 | Aphyric basalt, variolitic, fractured | x | x | x | x | x | No | ND |
| 336-U1383C-17R-2-MBIOD | 203.01 | 203.10 | Aphyric basalt, glassy rim | x | x | x | x | x | Yes (2) | No |
| 336-U1383C-19R-1-MBIOA | 212.06 | 212.11 | Two small pieces, mostly glass, rust alteration | x | x | | x | | Yes (1) | Yes (2) |
| 336-U1383C-19R-1-MBIOB | 212.15 | 212.22 | Aphyric basalt, highly oxidized, multiple fractures, light brown alteration, relatively brittle | x | x | x | x | | Yes (2) | Yes (2) |
| 336-U1383C-19R-1-MBIOC | 212.51 | 212.57 | Aphyric basalt, highly oxidized, fewer fractures and less alteration than 19R-1-MBIOB | x | | | | | Yes (3) | Yes (1) |
| 336-U1383C-20R-1-MBIOA | 219.35 | 219.42 | All basalt glass, rust alteration | x | x | | x | x | Yes (4) | No |
| 336-U1383C-20R-1-MBIOB | 220.38 | 220.44 | All basalt glass, rust alteration | x | | x | x | x | Yes (4) | Yes (1) |
| 336-U1383C-20R-2-MBIOC | 220.66 | 220.74 | Aphyric basalt, variolitic, blue-gray-brown-green alteration, extremely hard | x | x | x | | x | Yes (3) | Yes (1) |
| 336-U1383C-21R-1-MBIOA | 228.74 | 228.83 | Aphyric basalt, glassy rim, vein | x | x | x | | | Yes (3) | No |
| 336-U1383C-21R-1-MBIOB | 229.10 | 229.17 | Aphyric basalt, glass, variolitic, palagonite | x | | | | | Yes (7) | Yes (2) |
| 336-U1383C-22R-1-MBIOA | 237.84 | 237.89 | Aphyric basalt, glass, variolitic | x | x | x | x | x | No | ND |
| 336-U1383C-22R-1-MBIOB | 238.22 | 238.27 | Aphyric basalt, white vein | x | x | x | | | Yes (7) | No |
| 336-U1383C-23R-1-MBIOA | 248.09 | 248.19 | Phyric, massive basalt | x | x | x | | | Yes (1) | No |
| 336-U1383C-23R-1-MBIOB | 248.29 | 248.34 | Aphyric basalt, glass, variolitic | x | x | | x | x | No | ND |
| 336-U1383C-24R-1-MBIOA | 256.64 | 256.69 | Aphyric basalt glass with rust alteration, vesicles, maybe some breccia or hyaloclastite, white gooey material on inside | x | x | | x | | Yes (7) | Yes (1) |
| 336-U1383C-24R-1-MBIOB | 257.04 | 257.11 | Aphyric basalt, oxidized, dark orange-brown alteration, fractured | x | x | | x | | Yes (11) | No |
| 336-U1383C-25R-1-MBIOA | 266.48 | 266.53 | Aphyric basalt, mild oxidation, dark red-black alteration, vugs | x | x | | | | Yes (1) | No |
| 336-U1383C-26R-1-MBIOA | 275.46 | 275.55 | Aphyric basalt glass, variolitic | x | x | | x | | Yes (4) | Yes (1) |
| 336-U1383C-26R-1-MBIOB | 276.54 | 276.62 | Aphyric massive basalt, oxidized | x | x | x | x | | No | ND |
| 336-U1383C-27R-1-MBIOA | 285.15 | 285.20 | Aphyric massive basalt, alteration | x | x | x | x | | Yes (2) | Yes (3) |
| 336-U1383C-27R-1-MBIOB | 285.34 | 285.45 | Aphyric massive basalt, alteration, some fractures | x | x | | | | No | ND |
| 336-U1383C-28R-1-MBIOA | 294.60 | 294.67 | Aphyric massive basalt, variolitic, glassy margin | x | x | x | | | Yes (4) | Yes (2) |
| 336-U1383C-29R-1-MBIOA | 299.86 | 300.02 | Aphyric basalt, highly oxidized, thin carbonate veins | x | x | x | x | | Yes (2) | Yes (1) |
| 336-U1383C-30R-1-MBIOA | 304.00 | 304.09 | Aphyric basalt, oxidized, some fractures, dark orange alteration | x | x | x | | | Yes (4) | Yes (2) |
| 336-U1383C-30R-2-MBIOB | 305.11 | 305.20 | Aphyric massive basalt, highly oxidized, variolitic, one thin carbonate vein, orange-ochre alteration | x | | x | | | No | ND |
| 336-U1383C-30R-3-MBIOC | 306.16 | 306.27 | Aphyric massive basalt, variolitic, carbonate vein, split in two pieces | x | x | | | | Yes (1) | Yes (1) |
| 336-U1383C-31R-1-MBIOA | 312.18 | 312.24 | Glassy basalt | x | x | x | x | x | Yes (7) | Yes (8) |
| 336-U1383C-31R-1-MBIOB | 313.35 | 313.45 | Aphyric massive basalt, fractured | x | x | x | | | No | ND |
| 336-U1383C-31R-2-MBIOC | 314.74 | 314.83 | Aphyric massive basalt, variolitic | x | x | x | | | Yes (1) | No |
| 336-U1383C-32R-2-MBIOA | 324.12 | 324.27 | Phyric basalt with veins | x | x | x | x | | Yes (2) | No |
| | | | Totals: | 79 | 65 | 51 | 40 | 18 | | |

Number in parentheses indicates abundance of microspheres observed in sample wash. DEBI-pt = Deep Exploration Biosphere Investigative portable tool. ND = not determined.

**Table T9.** Moisture and density, *P*-wave velocity measurements, degree of alteration, LOI values, and thin section number for discrete samples, Hole U1383C.

| Core, section, interval (cm) | Depth (mbsf) | | MAD | | | | | P-wave velocity (m/s) | | | | | Geochemistry | Petrology | |
|---|---|---|---|---|---|---|---|---|---|---|---|---|---|---|---|
| | | | | | | | | | | | All axes | | | | |
| | Top | Bottom | Bulk density (g/cm$^3$) | Dry density (g/cm$^3$) | Grain density (g/cm$^3$) | Porosity (%) | Void ratio | *x* | *y* | *z* | Mean | SD | LOI (wt%) | Alteration (%) | Thin section |
| 336-U1383C- | | | | | | | | | | | | | | | |
| 3R-1W, 6–9 | 76.66 | 76.69 | 2.46 | 2.30 | 2.73 | 15.78 | 0.19 | 4780 | — | — | 4780 | — | 2.29 | 39 | 30 |
| 3R-2W, 28–31 | 78.38 | 78.41 | 2.83 | 2.80 | 2.89 | 2.95 | 0.03 | 6756 | 6808 | 6827 | 6797 | 37 | 1.23 | 10 | 31 |
| 5R-1W, 37–40 | 96.17 | 96.2 | 2.79 | 2.75 | 2.85 | 3.47 | 0.04 | 6984 | 6952 | 6955 | 6963 | 18 | 0.44 | 4 | 32 |
| 6R-1W, 100–104 | 106.4 | 106.44 | 2.54 | 2.42 | 2.74 | 11.75 | 0.13 | 5657 | — | — | 5657 | — | 1.87 | 23.5 | 34 |
| 7R-2W, 41–44 | 116.85 | 116.88 | 2.80 | 2.75 | 2.89 | 4.67 | 0.05 | 6843 | — | — | 6843 | — | 1.32 | 5 | 36 |
| 7R-2W, 91–94 | 117.35 | 117.38 | 2.43 | 2.26 | 2.71 | 16.61 | 0.20 | 4741 | — | — | 4741 | — | 3.44 | 35.5 | 38 |
| 9R-3W, 74–78 | 137.98 | 138.02 | 2.50 | 2.34 | 2.77 | 15.62 | 0.19 | 4961 | 4800 | 4884 | 4882 | 80 | 1.53 | 18 | 39 |
| 9R-4W, 76–78 | 139.41 | 139.43 | 2.86 | 2.84 | 2.89 | 1.87 | 0.02 | 7020 | 7064 | 6984 | 7023 | 40 | 0.72 | 1 | 40 |
| 10R-1W, 33–36 | 144.23 | 144.26 | 2.53 | 2.38 | 2.79 | 14.76 | 0.17 | 4893 | 4905 | 4910 | 4902 | 9 | 3.08 | 9* | 41 |
| 10R-2W, 10–12 | 145.37 | 145.39 | 2.84 | 2.81 | 2.88 | 2.53 | 0.03 | 7631 | 6732 | 6810 | 7058 | 498 | 2.42 | 2 | 42 |
| 13R-1W, 21–24 | 172.91 | 172.94 | 2.78 | 2.72 | 2.89 | 6.02 | 0.06 | 5962 | 5976 | 5990 | 5976 | 14 | 3.66 | 8.5 | 43 |
| 16R-1W, 10–13 | 192.9 | 192.93 | 2.66 | 2.56 | 2.84 | 9.99 | 0.11 | 5899 | — | — | 5899 | — | 2.29 | 6 | 44 |
| 16R-1W, 58–60 | 193.38 | 193.4 | 2.84 | 2.81 | 2.89 | 2.70 | 0.03 | 6762 | — | — | 6762 | — | 2.11 | 4 | 45 |
| 19R-1W, 30–32 | 211.9 | 211.92 | 2.84 | 2.82 | 2.89 | 2.25 | 0.02 | 6909 | 6923 | 6911 | 6914 | 8 | 0.4 | 2 | 46 |
| 20R-1W, 47–50 | 219.67 | 219.7 | 2.81 | 2.76 | 2.90 | 4.66 | 0.05 | 6880 | — | — | 6880 | — | 1.62 | 25 | 49 |
| 23R-1W, 57–61 | 247.57 | 247.61 | 2.83 | 2.80 | 2.90 | 3.42 | 0.04 | 6880 | — | — | 6880 | — | 0.2 | 16 | 51 |
| 25R-1W, 68–72 | 266.88 | 266.92 | 2.83 | 2.80 | 2.90 | 3.52 | 0.04 | 6298 | 6265 | 6227 | 6263 | 36 | 0.47 | 12 | 52 |
| 27R-1W, 110–113 | 285.9 | 285.93 | 2.90 | 2.87 | 2.95 | 2.71 | 0.03 | 6404 | — | — | 6404 | — | 0.05 | 1* | 53 |
| 28R-1W, 40–42 | 295 | 295.02 | 2.89 | 2.84 | 2.96 | 4.09 | 0.04 | 6461 | 6698 | 6584 | 6581 | 119 | 0.95 | 4 | — |
| 29R-1W, 62–64 | 299.82 | 299.84 | 2.63 | 2.49 | 2.90 | 13.99 | 0.16 | 4788 | 4750 | 4825 | 4788 | 38 | 2.28 | 15 | 54 |
| 31R-2W, 3.5–5.5 | 313.535 | 313.555 | 2.85 | 2.82 | 2.90 | 2.75 | 0.03 | 6562 | 6547 | 6534 | 6548 | 14 | 0.52 | 7 | 55 |
| 31R-2W, 37–39 | 313.87 | 313.89 | 2.67 | 2.55 | 2.90 | 12.04 | 0.14 | 5172 | 5108 | 5135 | 5138 | 32 | 2.28 | 22 | 56 |
| 32R-2W, 53–55 | 323.66 | 323.68 | 2.83 | 2.79 | 2.91 | 3.96 | 0.04 | 6343 | 6322 | 6395 | 6353 | 37 | 1.32 | 6 | 58 |

* = no thin section available to estimate alteration. MAD = moisture and density. SD = standard deviation. LOI = loss on ignition.

**Table T10.** Summary of color reflectance values (minimum, maximum, mean, and standard deviation [SD]), Hole U1383C.

| | L* | a* | b* | *x*-tristimulus | *y*-tristimulus | *z*-tristimulus |
|---|---|---|---|---|---|---|
| Minimum | 11.90 | –3.20 | –6.00 | 1.40 | 1.40 | 1.20 |
| Maximum | 66.50 | 8.70 | 21.40 | 35.50 | 36.00 | 39.80 |
| Mean | 37.48 | 0.84 | 0.93 | 9.61 | 10.02 | 10.47 |
| SD | 4.59 | 1.24 | 3.56 | 2.57 | 2.60 | 2.83 |

**Table T11.** Logging operations summary, Hole U1383C.

| Date (2011) | Time (h) | Activity |
|---|---|---|
| 3 Nov | 0025 | Downhole logging operations start |
| 3 Nov | 0120 | On power up the tools string encountered a communications issue. The problem was located around the resistivity sonde (HRLA). Following some trouble-shooting, the HRLA sonde was removed from the tool string. |
| 3 Nov | 0255 | AMC II tool string run into hole and a downlog was started from surface to monitor the DEBI-t |
| 3 Nov | 0504 | Begin "true" downlog at 4400.5 m WRF |
| 3 Nov | 0536 | Wireline heave compensator optimization performed |
| 3 Nov | 0705 | Reach total depth of 4750.1 m WRF (bottom of hole not tagged on this down pass) |
| 3 Nov | 0706 | Begin uplog |
| 3 Nov | 0806 | Begin second downlog (from 4486.5 m WRF) |
| 3 Nov | 0906 | Begin second uplog (from 4752.4 m WRF; tagged bottom) |
| 3 Nov | 1012 | Second uplog finished at 4412.8 m WRF after logging through the seafloor |
| 3 Nov | 1310 | AMC II tool string rigged down |
| 3 Nov | 1344 | FMS-sonic tool string rigged up |
| 3 Nov | 1410 | FMS-sonic run into hole |
| 3 Nov | 1634 | Begin logging downward from 4400.1 m WRF; WHC was assessed briefly and was completed at 1710 h |
| 3 Nov | 1746 | Tool string reached total depth 4757.2 m WRF |
| 3 Nov | 1748 | Begin first pass |
| 3 Nov | 1835 | End of first pass (ran calipers just into casing) |
| 3 Nov | 1836 | Run tool string back down to total depth |
| 3 Nov | 1901 | Begin second pass |
| 3 Nov | 1952 | End of second pass |
| 3 Nov | 2220 | Tool string back to the surface |
| 3 Nov | 2245 | FMS-sonic rigged down and logging operations concluded |

HRLA = High-Resolution Laterolog Array, AMC II = adapted microbiology combination II, FMS = Formation MicroScanner. DEBI-t = Deep Exploration Biosphere Investigative tool. WHC = wireline heave compensator. Time is reported as ship local (UTC – 3 h).

# Appendix

Photographs of whole-round samples taken for microbiology are shown in Figures AF1, AF2, AF3, AF4, AF5, AF6, AF7, AF8, AF9, AF10, AF11, AF12, AF13, AF14, AF15, AF16, AF17, AF18, AF19, AF20, AF21, AF22, AF23, AF24, AF25, AF26, AF27, AF28, AF29, AF30, AF31, AF32, AF33, AF34, AF35, AF36, AF37, AF38, AF39, AF40, AF41, AF42, AF43, AF44, AF45, AF46, AF47, AF48, AF49, AF50, AF51, AF52, AF53, AF54, AF55, AF56, AF57, AF58, AF59, AF60, AF61, AF62, AF63, AF64, AF65, AF66, AF67, AF68, AF69, AF70, AF71, AF72, AF73, AF74, AF75, AF76, AF77, AF78, and AF79.

**Figure AF1.** Photograph of microbiology whole-round Sample 336-U1383C-2R-1-MBIOA. DEBI-pt = Deep Exploration Biosphere Investigative portable tool.

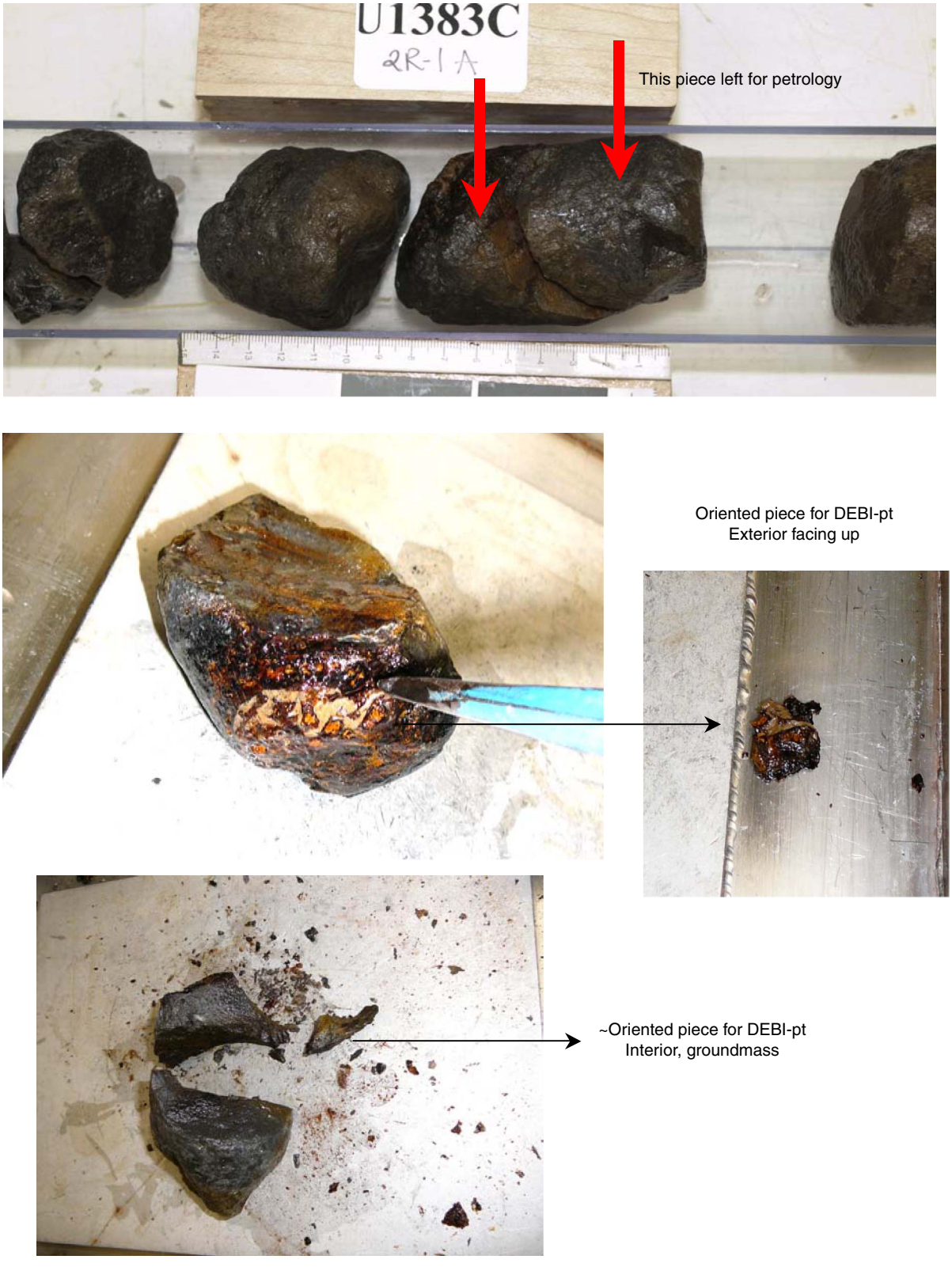

**Figure AF2.** Photograph of microbiology whole-round Sample 336-U1383C-2R-1-MBIOB. DEBI-pt = Deep Exploration Biosphere Investigative portable tool.

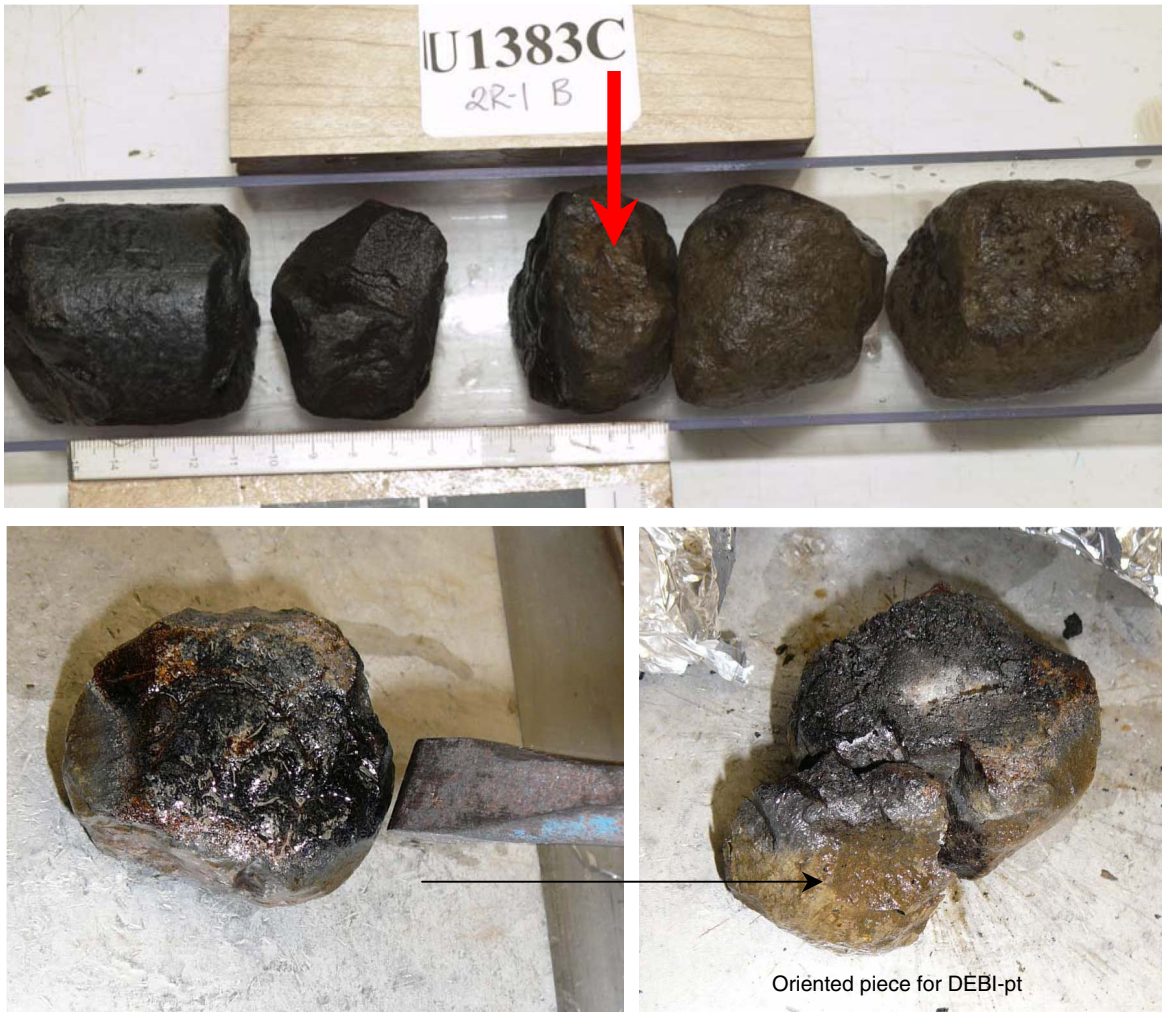

**Figure AF3.** Photograph of microbiology whole-round Sample 336-U1383C-2R-1-MBIOC. DEBI-pt = Deep Exploration Biosphere Investigative portable tool.

**Figure AF4.** Photograph of microbiology whole-round Sample 336-U1383C-2R-2-MBIOD.

**Figure AF5.** Photograph of microbiology whole-round Sample 336-U1383C-2R-2-MBIOE. DEBI-pt = Deep Exploration Biosphere Investigative portable tool.

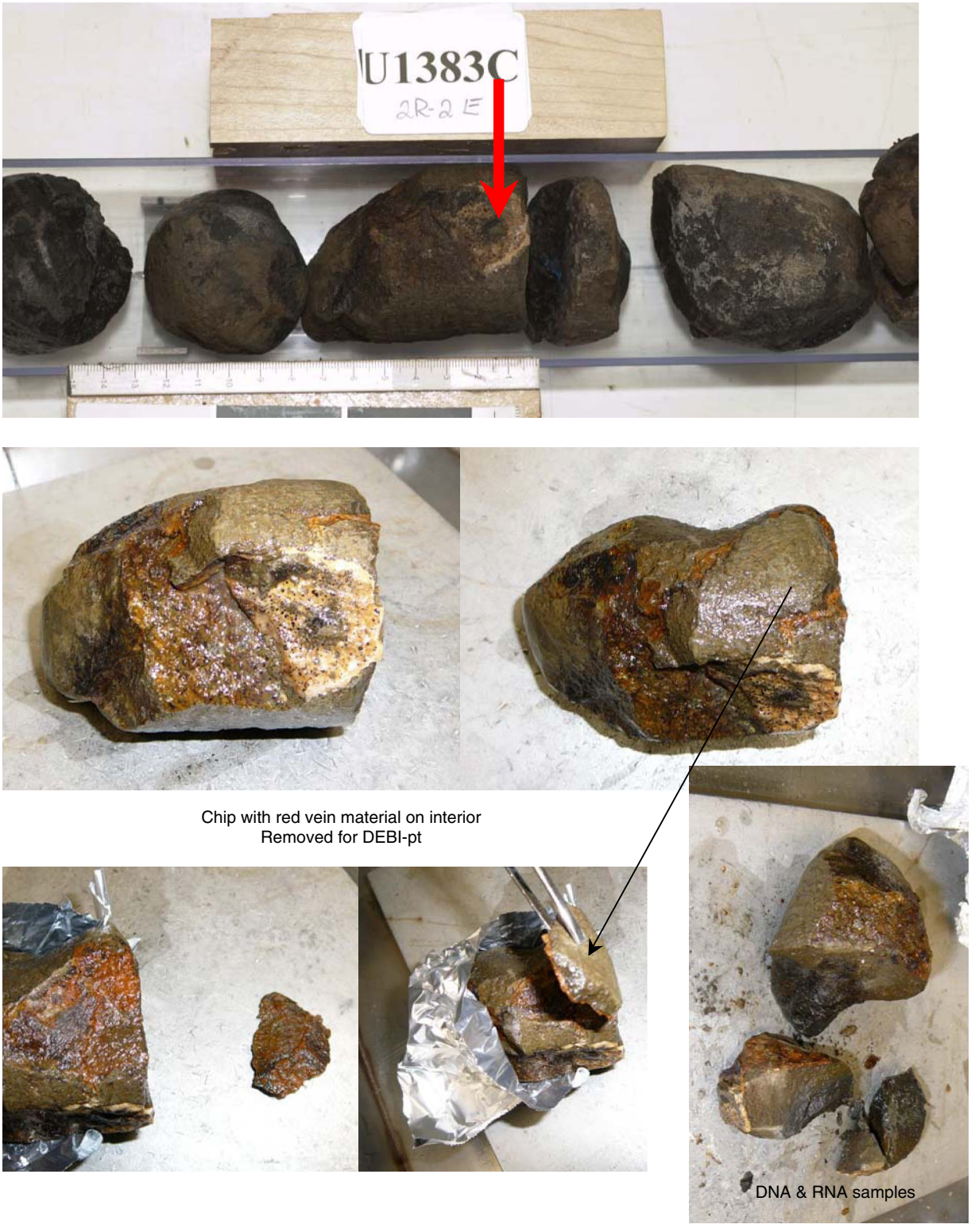

**Figure AF6.** Photograph of microbiology whole-round Sample 336-U1383C-3R-1-MBIOA.

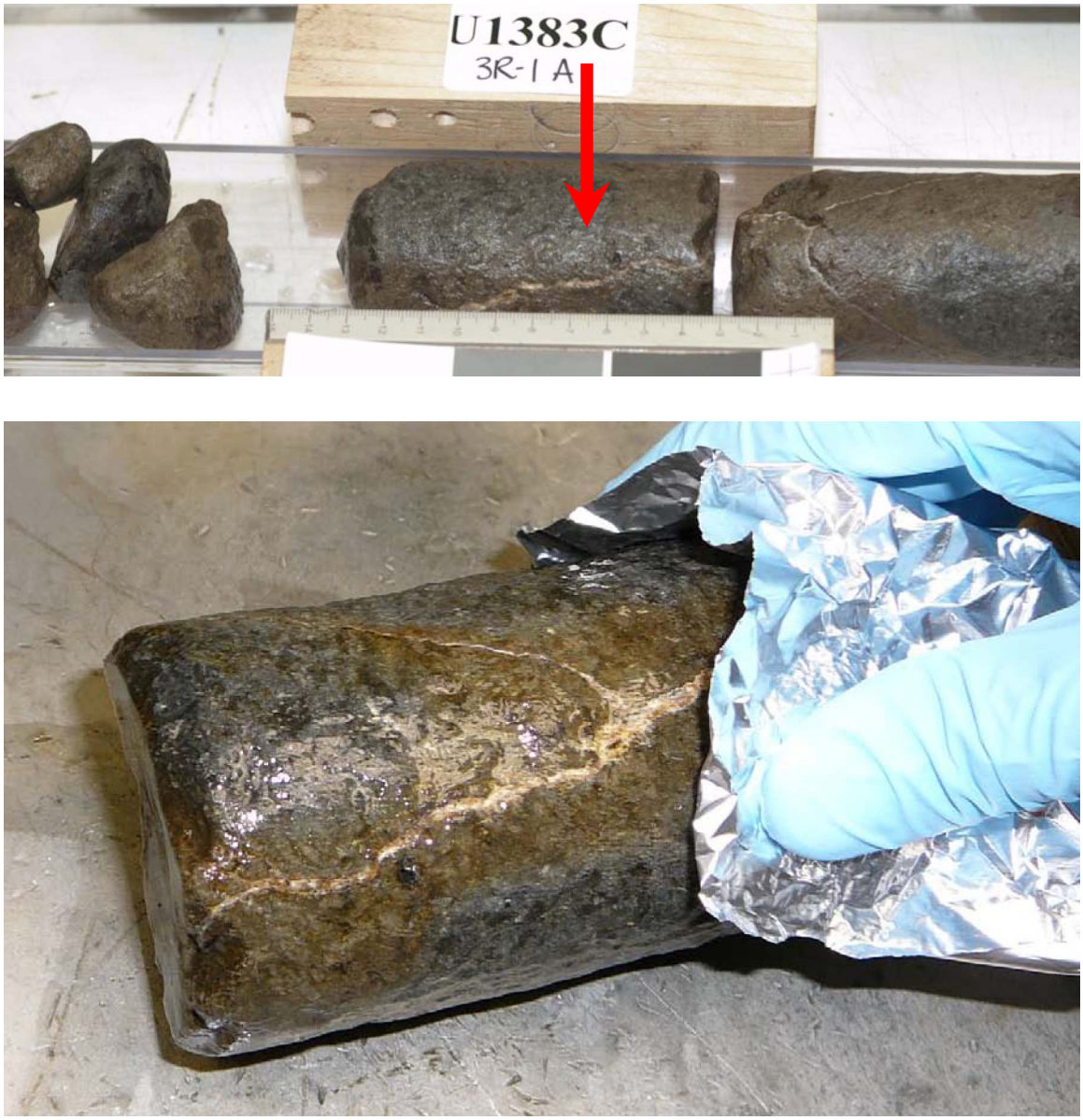

**Figure AF7.** Photograph of microbiology whole-round Sample 336-U1383C-3R-1-MBIOB.

**Figure AF8.** Photograph of microbiology whole-round Sample 336-U1383C-3R-1-MBIOC.

**Figure AF9.** Photograph of microbiology whole-round Sample 336-U1383C-3R-2-MBIOD.


**Figure AF10.** Photograph of microbiology whole-round Sample 336-U1383C-3R-2-MBIOE.

**Figure AF11.** Photograph of microbiology whole-round Sample 336-U1383C-4R-1-MBIOA.

**Figure AF12.** Photograph of microbiology whole-round Sample 336-U1383C-4R-1-MBIOB.

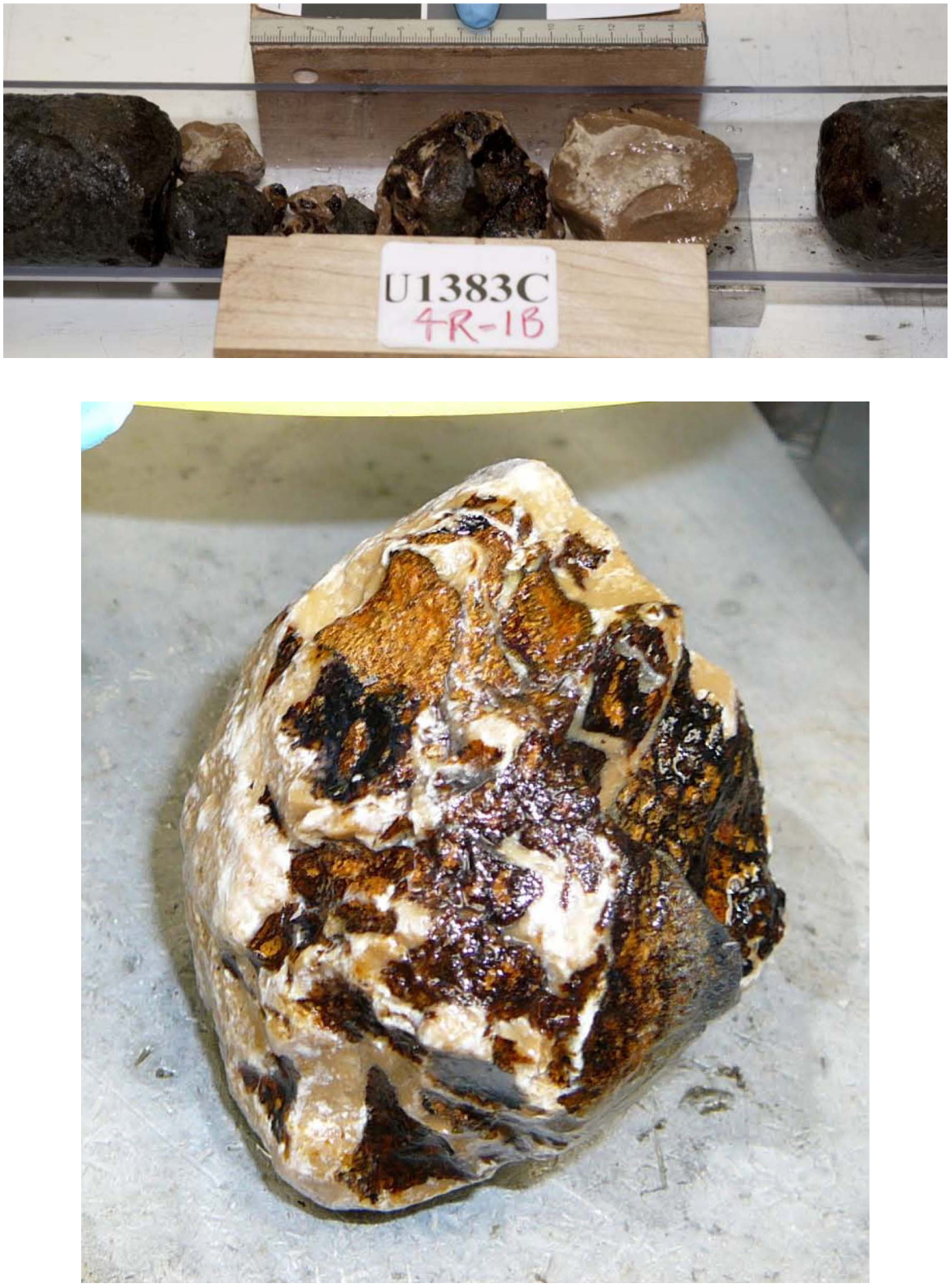

**Figure AF13.** Photograph of microbiology whole-round Sample 336-U1383C-4R-2-MBIOC.


**Figure AF14.** Photograph of microbiology whole-round Sample 336-U1383C-4R-2-MBIOD.

**Figure AF15.** Photograph of microbiology whole-round Sample 336-U1383C-5R-1-MBIOA. DEBI-pt = Deep Exploration Biosphere Investigative portable tool.

**Figure AF16.** Photograph of microbiology whole-round Sample 336-U1383C-5R-1-MBIOB. DEBI-pt = Deep Exploration Biosphere Investigative portable tool.

**Figure AF17.** Photograph of microbiology whole-round Sample 336-U1383C-5R-2-MBIOC.

**Figure AF18.** Photograph of microbiology whole-round Sample 336-U1383C-5R-1-MBIOD.

**Figure AF19.** Photograph of microbiology whole-round Sample 336-U1383C-6R-1-MBIOA. DEBI-pt = Deep Exploration Biosphere Investigative portable tool.


Oriented piece for DEBI-pt
Alteration interior facing up

**Figure AF20.** Photograph of microbiology whole-round Sample 336-U1383C-6R-2-MBIOB (originally 6R-1-MBIOB).

**Figure AF21.** Photograph of microbiology whole-round Sample 336-U1383C-7R-1-MBIOA.

**Figure AF22.** Photograph of microbiology whole-round Sample 336-U1383C-7R-1-MBIOB.

**Figure AF23.** Photograph of microbiology whole-round Sample 336-U1383C-7R-2-MBIOC.

**Figure AF24.** Photograph of microbiology whole-round Sample 336-U1383C-8R-1-MBIOA.


**Figure AF25.** Photograph of microbiology whole-round Sample 336-U1383C-8R-1-MBIOB (originally 8R-2-MBIOB).


**Figure AF26.** Photograph of microbiology whole-round Sample 336-U1383C-9R-1-MBIOA.


**Figure AF27.** Photograph of microbiology whole-round Sample 336-U1383C-9R-2-MBIOB.

**Figure AF28.** Photograph of microbiology whole-round Sample 336-U1383C-9R-2-MBIOC.

**Figure AF29.** Photograph of microbiology whole-round Sample 336-U1383C-9R-3-MBIOD.

**Figure AF30.** Photograph of microbiology whole-round Sample 336-U1383C-10R-1-MBIOA. DEBI-pt = Deep Exploration Biosphere Investigative portable tool.

**Figure AF31.** Photograph of microbiology whole-round Sample 336-U1383C-10R-1-MBIOB. DEBI-pt = Deep Exploration Biosphere Investigative portable tool.


Oriented pieces for DEBI-pt
Alteration rind exterior facing tweezers
Two pieces

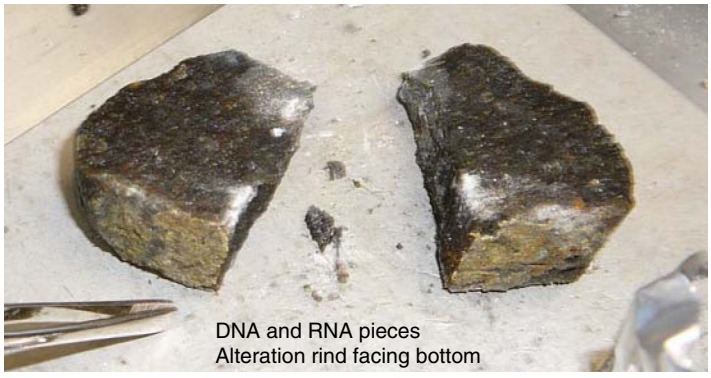

DNA and RNA pieces
Alteration rind facing bottom

**Figure AF32.** Photograph of microbiology whole-round Sample 336-U1383C-10R-1-MBIOD.


**Figure AF33.** Photograph of microbiology whole-round Sample 336-U1383C-10R-2-MBIOC.

**Figure AF34.** Photograph of microbiology whole-round Sample 336-U1383C-11R-1-MBIOA.

**Figure AF35.** Photograph of microbiology whole-round Sample 336-U1383C-11R-1-MBIOB. DEBI-pt = Deep Exploration Biosphere Investigative portable tool.

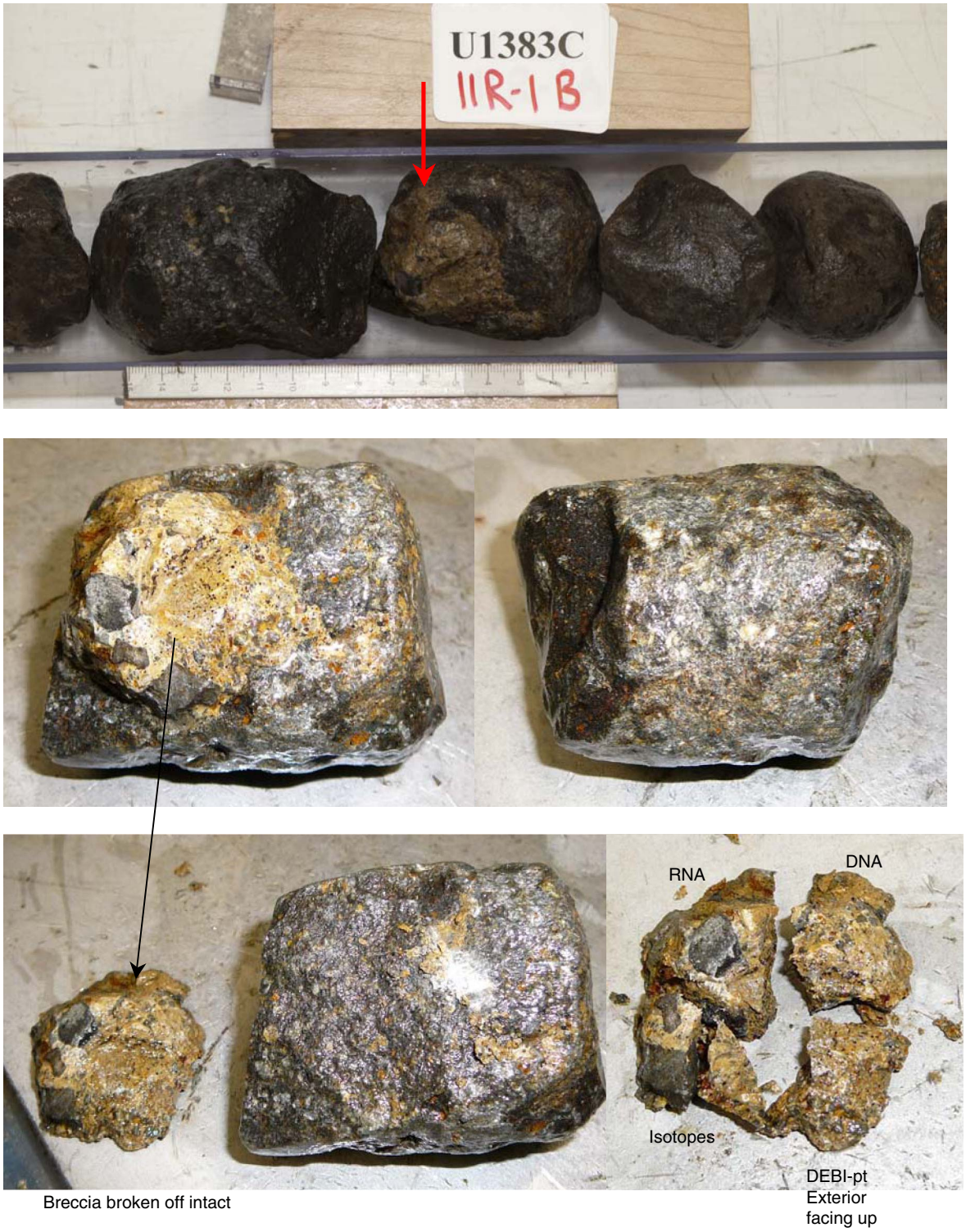

**Figure AF36.** Photograph of microbiology whole-round Sample 336-U1383C-11R-1-MBIOC.


**Figure AF37.** Photograph of microbiology whole-round Sample 336-U1383C-12R-1-MBIOA.

**Figure AF38.** Photograph of microbiology whole-round Sample 336-U1383C-12R-1-MBIOB.

**Figure AF39.** Photograph of microbiology whole-round Sample 336-U1383C-13R-1-MBIOA.

**Figure AF40.** Photograph of microbiology whole-round Sample 336-U1383C-13R-1-MBIOB (originally 13R-2-MBIOB).

**Figure AF41.** Photograph of microbiology whole-round Sample 336-U1383C-13R-2-MBIOC.

**Figure AF42.** Photograph of microbiology whole-round Sample 336-U1383C-14R-1-MBIOA.

**Figure AF43.** Photograph of microbiology whole-round Sample 336-U1383C-14R-1-MBIOB.

**Figure AF44.** Photograph of microbiology whole-round Sample 336-U1383C-14R-2-MBIOC.

**Figure AF45.** Photograph of microbiology whole-round Sample 336-U1383C-14R-2-MBIOD.

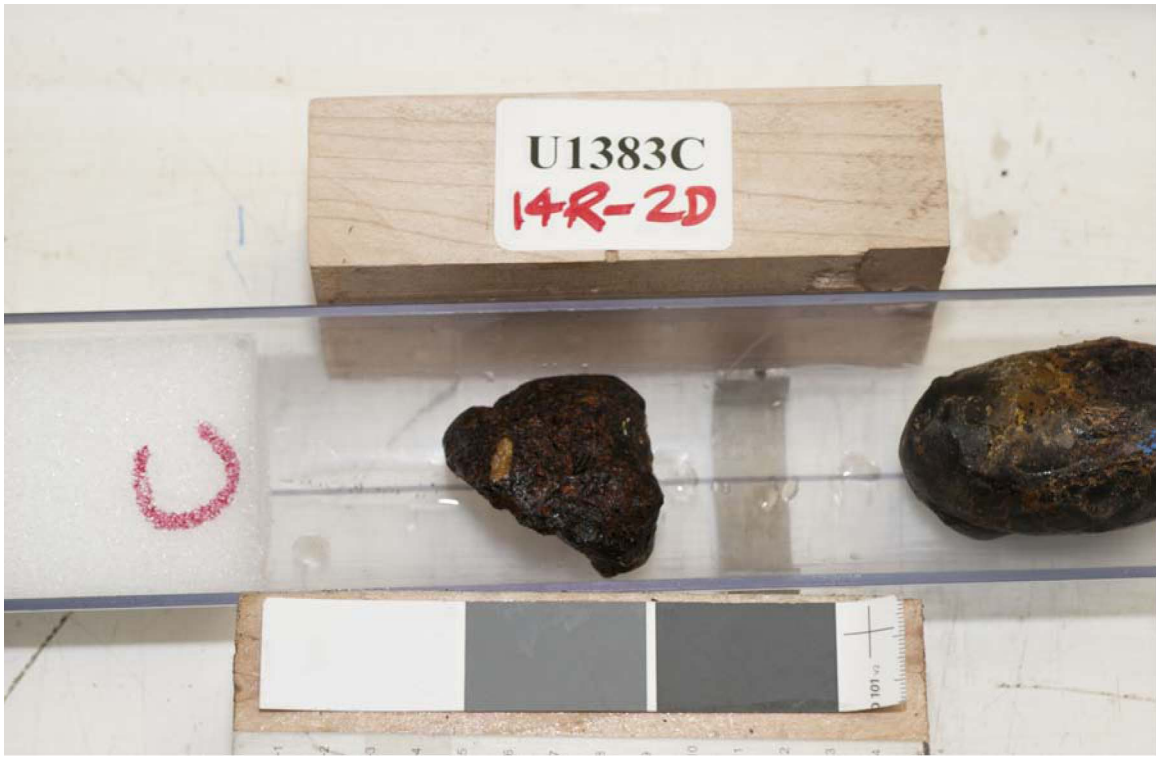

**Figure AF46.** Photograph of microbiology whole-round Sample 336-U1383C-16R-1-MBIOA.

**Figure AF47.** Photograph of microbiology whole-round Sample 336-U1383C-16R-2-MBIOB (originally 16R-1-MBIOB).

**Figure AF48.** Photograph of microbiology whole-round Sample 336-U1383C-17R-1-MBIOA.

**Figure AF49.** Photograph of microbiology whole-round Sample 336-U1383C-17R-1-MBIOB.

**Figure AF50.** Photograph of microbiology whole-round Sample 336-U1383C-17R-1-MBIOC (originally 17R-2-MBIOC).

**Figure AF51.** Photograph of microbiology whole-round Sample 336-U1383C-17R-2-MBIOD.

**Figure AF52.** Photograph of microbiology whole-round Sample 336-U1383C-19R-1-MBIOA. DEBI-pt = Deep Exploration Biosphere Investigative portable tool.

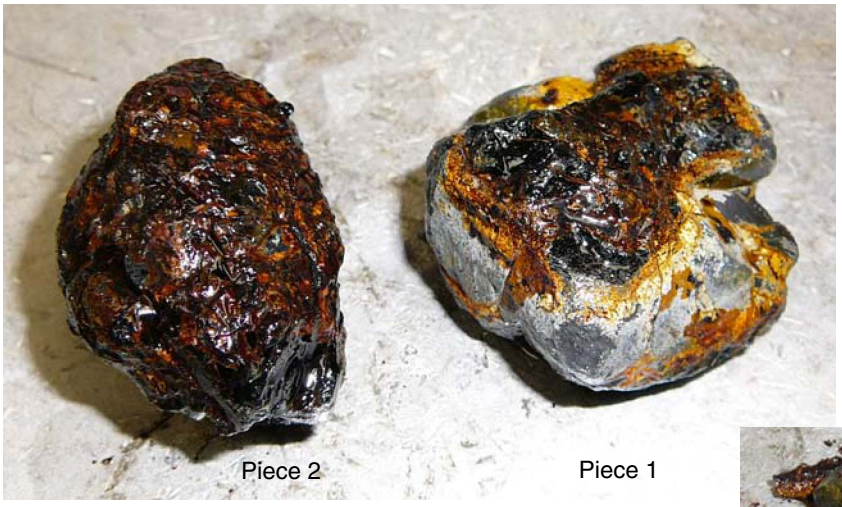





Cross-section piece for DEBI-pt. Ends touching tweezer and away from tweezers are exterior

**Figure AF53.** Photograph of microbiology whole-round Sample 336-U1383C-19R-1-MBIOB.

**Figure AF54.** Photograph of microbiology whole-round Sample 336-U1383C-19R-1-MBIOC.


**Figure AF55.** Photograph of microbiology whole-round Sample 336-U1383C-20R-1-MBIOA. DEBI-pt = Deep Exploration Biosphere Investigative portable tool.


Pieces for DEBI-pt from interior of rock

**Figure AF56.** Photograph of microbiology whole-round Sample 336-U1383C-20R-1-MBIOB (originally 20R-2-MBIOB). DEBI-pt = Deep Exploration Biosphere Investigative portable tool.

**Figure AF57.** Photograph of microbiology whole-round Sample 336-U1383C-20R-2-MBIOC.

**Figure AF58.** Photograph of microbiology whole-round Sample 336-U1383C-21R-1-MBIOA.

**Figure AF59.** Photograph of microbiology whole-round Sample 336-U1383C-21R-1-MBIOB.

**Figure AF60.** Photograph of microbiology whole-round Sample 336-U1383C-22R-1-MBIOA.


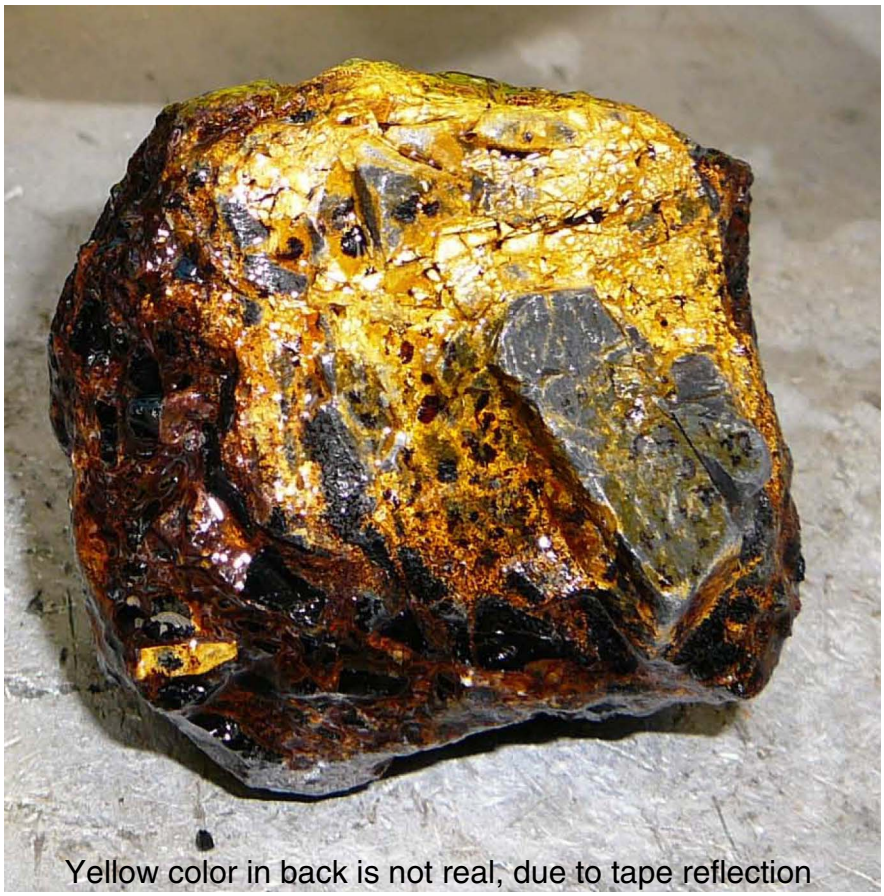

**Figure AF61.** Photograph of microbiology whole-round Sample 336-U1383C-22R-1-MBIOB.

**Figure AF62.** Photograph of microbiology whole-round Sample 336-U1383C-23R-1-MBIOA.

**Figure AF63.** Photograph of microbiology whole-round Sample 336-U1383C-23R-1-MBIOB.

**Figure AF64.** Photograph of microbiology whole-round Sample 336-U1383C-24R-1-MBIOA. DEBI-pt = Deep Exploration Biosphere Investigative portable tool.

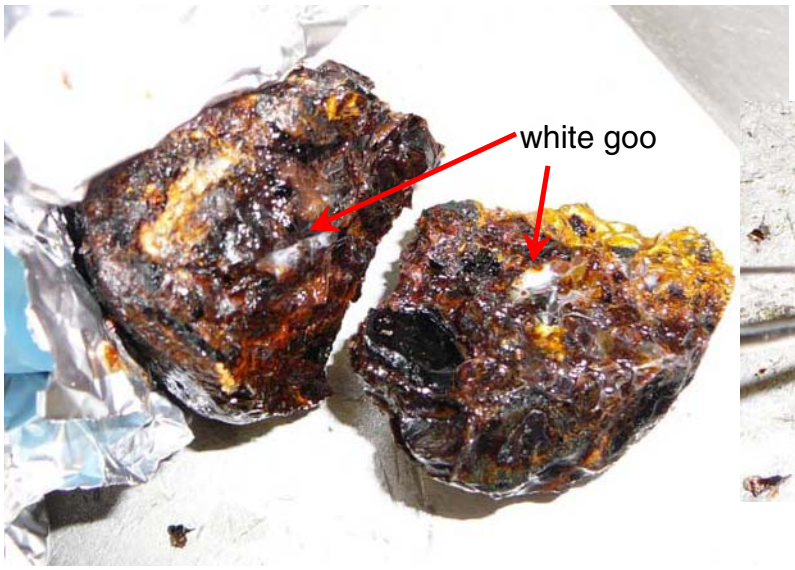


Piece for DEBI-pt, interior up, tweezers pointing to white goo

**Figure AF65.** Photograph of microbiology whole-round Sample 336-U1383C-24R-1-MBIOB. DEBI-pt = Deep Exploration Biosphere Investigative portable tool.


Two pieces for DEBI-pt, all interior

**Figure AF66.** Photograph of microbiology whole-round Sample 336-U1383C-25R-1-MBIOA.


**Figure AF67.** Photograph of microbiology whole-round Sample 336-U1383C-26R-1-MBIOA.

**Figure AF68.** Photograph of microbiology whole-round Sample 336-U1383C-26R-1-MBIOB.

**Figure AF69.** Photograph of microbiology whole-round Sample 336-U1383C-27R-1-MBIOA.

**Figure AF70.** Photograph of microbiology whole-round Sample 336-U1383C-27R-1-MBIOB.

**Figure AF71.** Photograph of microbiology whole-round Sample 336-U1383C-28R-1-MBIOA.

**Figure AF72.** Photograph of microbiology whole-round Sample 336-U1383C-29R-1-MBIOA. DEBI-pt = Deep Exploration Biosphere Investigative portable tool.

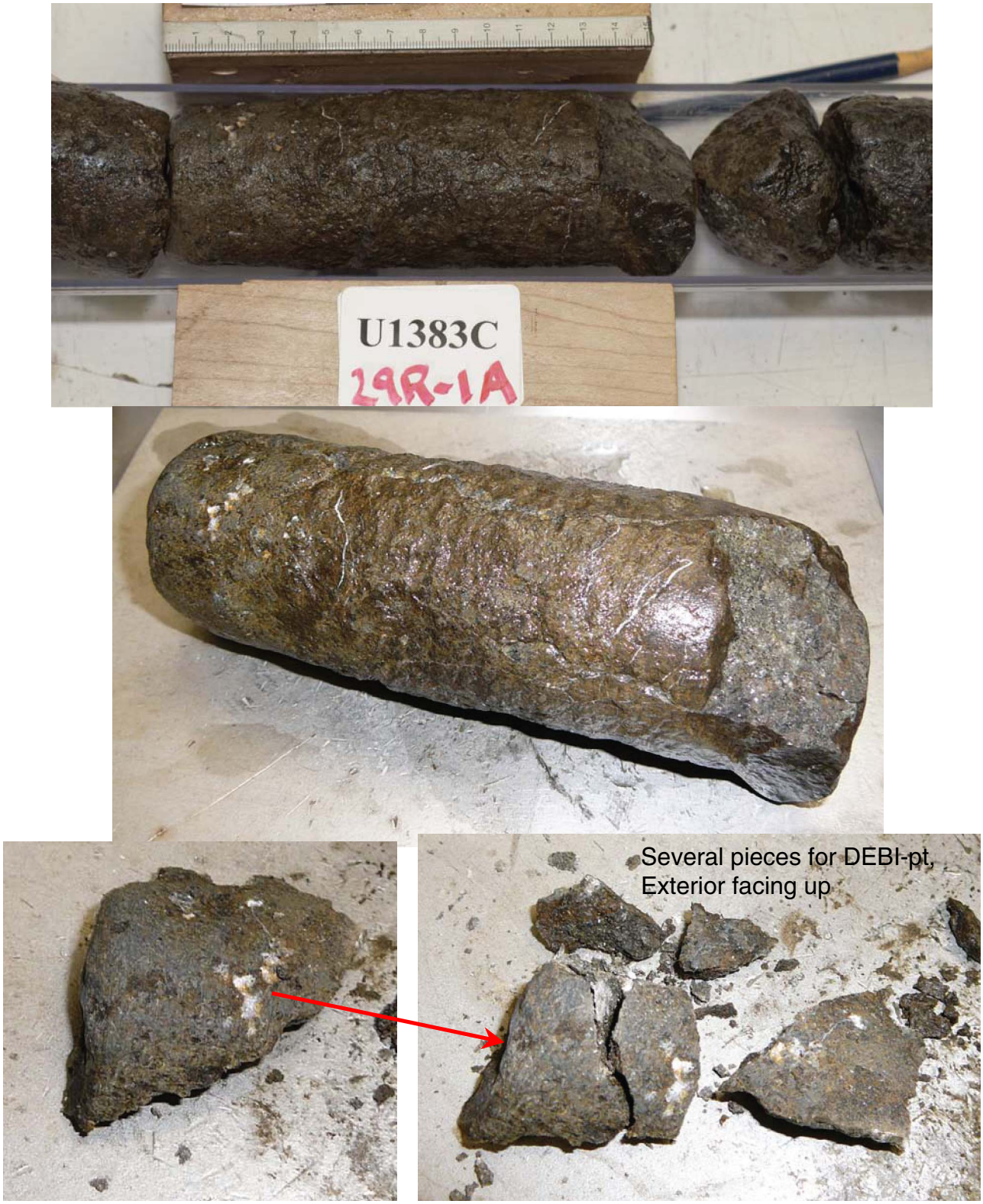

**Figure AF73.** Photograph of microbiology whole-round Sample 336-U1383C-30R-1-MBIOA.


**Figure AF74.** Photograph of microbiology whole-round Sample 336-U1383C-30R-2-MBIOB.

**Figure AF75.** Photograph of microbiology whole-round Sample 336-U1383C-30R-3-MBIOC.


**Figure AF76.** Photograph of microbiology whole-round Sample 336-U1383C-31R-1-MBIOA.

**Figure AF77.** Photograph of microbiology whole-round Sample 336-U1383C-31R-1-MBIOB (was 31R-2-MBIOB).


**Figure AF78.** Photograph of microbiology whole-round Sample 336-U1383C-31R-2-MBIOC (originally 31R-3-MBIOC).

**Figure AF79.** Photograph of microbiology whole-round Sample 336-U1383C-32R-2-MBIOA.